CHEMOSTRATIGRAPHY OF THE EARLY PALEOPROTEROZOIC CARBONATE SUCCESSIONS (KAAPVAAL AND WYOMING CRATONS)

by

Andrey Bekker

Dissertation submitted to the Faculty of the
Virginia Polytechnic Institute and State University
in partial fulfillment of the requirements for the degree of

Doctor of Phylosophy
in
Geological Sciences

Kenneth A. Eriksson (Chair)
Richard K. Bambach
Juha A. Karhu
A. Jay Kaufman
J. Fred Read
J. Donald Rimstidt

August, 24, 2001
Blacksburg, Virginia

Keywords: Paleoproterozoic, chemostratigraphy, carbonates, climate change, glacials, biogeochemical cycling of carbon

CHEMOSTRATIGRAPHY OF THE EARLY PALEOPROTEROZOIC CARBONATE SUCCESSIONS (KAAPVAAL AND WYOMING CRATONS)

by

Andrey Bekker

K. A. Eriksson, Chairman

Department of Geological Sciences, Virginia Tech

(ABSTRACT)

Evidence of three glaciations in Paleoproterozoic successions of North America and at least one on three other continents, suggests that these glaciations were of global extent. In common with the Neoproterozoic record, carbonates cap the glacials. However, the relationship between biogeochemical cycling of carbon and ice ages has not been fully appreciated. This research involved the sedimentology and isotope stratigraphy of carbonates and shales in Paleoproterozoic glacially-influenced successions of Wyoming and South Africa. Carbonates of the Vagner Formation cap the middle of three diamictites in the Snowy Pass Supergroup, Medicine Bow Mountains, WY. The Duitschland Formation occurs between two glacial horizons in South Africa. Limestones retain negative $\delta^{13}C$ values for over 60 m in the Vagner Formation, and for over 100 m in the lower part of the Duitschland Formation. Isotope compositions of TOC from the lower part of the Duitschland Formation reveal pronounced enrichment resulting in

significantly lower fractionation between organic and inorganic carbon. This is similar to enrichment noted in Neoproterozoic cap carbonates. Combined with strongly positive carbon isotope compositions in upper Duitschland carbonates, the data from the Vagner Formation underscores strongly positive-to-negative carbon isotope trends bracketing Paleoproterozoic glaciations. These trends mimic those noted in Neoproterozoic glacial successions and possibly indicate a recurrence of global glaciations.

The Slaughterhouse and Nash Fork formations significantly postdate the glacial epoch. Both the lower part of the Nash Fork Formation, Medicine Bow Mountains and the Slaughterhouse Formation, Sierra Madre contains carbonates with ^{13}C-enrichment >+6‰ and locally up to +28‰, whereas carbonates higher in the Nash Fork Formation have $\delta^{13}C$ values between 0 and 2.5‰. This dramatic change in the composition of the Paleoproterozoic ocean is constrained at ca. 2.1 Ga (Karhu, 1993). Carbonates in the Rawhide Canyon section of the Whalen Group in the Hartville Uplift (the easternmost exposure of the Wyoming Craton) display $\delta^{13}C$ values up to +8.2‰ suggesting correlation with the Slaughterhouse and Nash Fork formations and their deposition on continuous carbonate platform along the margin of the Wyoming Craton. These data support an open-marine, and therefore a global origin for the ca. 2.2-2.1 Ga carbon isotope excursion.

ACKNOWLEDGMENTS

I would like to thank Dr. Kenneth A. Eriksson for serving as the chairman of my committee. His help in interpreting the data and editing my writing during the later stages of this project is most appreciated. This project would not have started without the advice, help and support provided by Dr. Juha A. Karhu, formerly with the Finnish Geological Survey and now with the Department of Geology, University of Helsinki. Dr. Karhu and his technical staff helped to analyze many samples for this project. Dr. A. Jay Kaufman's work on the Neoproterozoic successions inspired my interest in the relationship between biogeochemical cycling of carbon and climatic changes. He provided lab facilities, a place to stay, and funding for analytical work in his lab. Discussions with Fred Read, Don Rimstidt and Richard Bambach helped to shape my understanding of Paleoproterozoic environmental changes. I also appreciate the support the rest of the faculty in the department offered me over the years. Thank you to the paleo- and structure people for their help and tolerance towards a stranger in their quarters.

I offer thanks to the Department of Geological Sciences for their continuous support in the form of graduate teaching assistantships for the last five years, as well as for the fellowships to carry out analytical and fieldwork over the summers. The funding from the GSA, the Southeastern Section of GSA and the Colorado Scientific Society is greatly appreciated. I would also like to thank the departmental staff for all their help.

The project on the global survey of Paleoproterozoic successions would not have been possible without selfless contributions of local geologists who shared their data and knowledge. I greatly appreciate their guidance in the field and help with the literature search. I would like to mention a few names: Jack Redden, Ed DeWitt, Kevin Chamberlain, Paul Sims, Paul Graff, Warren Day, Bryan Krapez, Nic Beukes, Pavel Medvedev, Darrel Long, Dhiraj Banerjee, Kath Grey, Richard Ojakangas, Victor Melezhik, Vasiliy Gulii, Daniel Pineyro and Gerry Bennett. Special thanks to my family

for their love and support. It was an incredible learning experience. I am grateful for the opportunity to pursue what I thought was important and for the help from everyone along the way.

TABLE OF CONTENTS

LIST OF FIGURES

LIST OF TABLES

INTRODUCTION

This dissertation is comprised of four chapters that independantly present and discuss the sedimentology and chemostratigraphy of Paleoproterozoic successions on the Wyoming and Kaapvaal cratons.

Chapter 1 presents a study of carbonates and shales of the early Paleoproterozoic Duitschland Formation, South Africa that is sandwiched between two glacial diamictites. Carbonates in the lower part of the Duitschland Formation record negative carbon isotope values whereas organic carbon from carbonates and shales have ^{13}C-enriched values and, consequently, fractionation between organic and carbonate carbon is remarkably reduced. The upper part of the Duitschland Formation contains carbonates with highly ^{13}C-enriched values up to +10‰ and fractionation between organic and carbonate carbon is close to 30‰. This negative-to-positive trend in carbon isotope composition of carbonates sandwiched between glacials and decreased fractionation immediately above glacial deposits mimics the Neoproterozoic record of isotopic and climatic changes. Based on this similarity, coupling between biogeochemical cycling of carbon and climatic changes can be inferred for the Paleoproterozoic glacial epoch.

Chapter 2 presents a sedimentologic study of the Nash Fork Formation in the upper part of the Snowy Pass Supergroup, Medicine Bow Mountains, Wyoming. Based on detailed mapping and logging of sections, a new lithostratigraphy is proposed for the Nash Fork Formation. Two prominent drowning events expressed by organic-rich black shales divide the formation into three parts. Further subdivision into twelve members is based on recognition and mapping along strike of characteristic facies associations. Facies associations as well as their stacking patterns in the Nash Fork Formation suggest an open-marine depositional environment on the southern margin of the Wyoming Craton.

Chapter 3 presents a chemostratigraphic study of the Vagner and Nash Fork formations of the Snowy Pass Supergroup, Medicine Bow Mountains, Wyoming. Carbonates of the Vagner Formation overlie the middle of three glacial diamictites in the Snowy Pass Supergroup and have negative carbon isotope compositions. They are interpreted as cap carbonates deposited in response to high carbonate alkalinity fluxes into the post-glacial ocean either from the deeper part of the ocean or from the continent. In constrast, the Nash Fork Formation that is present stratigraphically well above glacial

diamictites and likely significantly younger that the end of the Paleoproterozoic glacial epoch, straddles the change in composition of the Paleoproterozoic ocean from highly positive carbon isotope values to those near to 0‰. This change was constrained on the Fennoscandian Shield to ca. 2.1 Ga and a similar age is inferred for the Nash Fork Formation. Consequently, the upper part of the Snowy Pass Supergroup was deposited on an open-marine passive margin and is unrelated to and significantly older then the 1.78-1.74 Ga Medicine Bow Orogeny.

Chapter 4 presents a chemostratigraphic study of carbonate units from supracrustal belts around the Archean Wyoming Craton. The age of these supracrustal belts is poorly constrained geochronologically and their lithostratigraphic correlation is complicated by the large distances that separates them. The Slaughterhouse Formation from the upper part of the Snowy Pass Group, Sierra Madre is considered to be deep-water time equivalent of the Nash Fork Formation from the adjacent Medicine Bow Mountains. Carbonates of the Slaughterhouse Formation show remarkable ^{13}C-enrichment similar to that found in carbonates from the lower part of the Nash Fork Formation. Carbonates of the Whalen Group from the Rawhide section of the Hartville Uplift, WY that is the easternmost exposure along the southern margin of the Wyoming Craton are ^{13}C-enriched up to +8.2‰. Combined, the chemostratigraphic and lithostratigraphic data suggest that all these units are correlatable and were deposited on a continuous carbonate platform along the southern margin of the Wyoming Craton. Consequently, this study supports an open-marine, and therefore a global origin for the ca. 2.2-2.1 Ga carbon isotope excursion. Carbonates from the Boxelder, Estes, and Roberts Draw formations of the Black Hills, SD exposed along the eastern margin of the Wyoming Craton have carbon isotope values close to 0‰. These chemostratigraphic data combined with geochronologic data suggest that the final rifting and breakup on the eastern margin of the Wyoming Craton occurred between 2.1 and 2.0 Ga and succeeded the carbon isotope excursion. The two drowning events within the Nash Fork Formation deposited on the southern margin of the Wyoming Craton are related to reactivation of the mature passive margin in response to these tectonic events along the eastern margin.

CHAPTER 1

CHEMOSTRATIGRAPHY OF THE PALEOPROTEROZOIC DUITSCHLAND FORMATION, SOUTH AFRICA: IMPLICATIONS FOR COUPLED CLIMATE CHANGE AND CARBON CYCLING

ABSTRACT. The Paleoproterozoic Duitschland Formation lies stratigraphically beneath the Timeball Hill Formation, which contains the only unequivocal glacial unit of this era in the Transvaal Basin, South Africa. Lithologic evidence in Paleoproterozoic successions of North America, however, indicates the existence of three discrete and potentially global ice ages within this 300 my interval. Carbonates of the Duitschland Formation are significantly enriched in ^{13}C up to +10.1 permil in the upper part of the succession above a notable sequence boundary. In contrast, the lower part of this unit contains carbonates with consistently negative $\delta^{13}C$ values. Trace and major element compositions of these carbonates as well as carbon-isotopic compositions of coexisting organic matter support a primary origin for the markedly positive carbon isotope anomaly. The stratigraphic constraints indicate that ^{13}C-enriched carbonates were deposited prior to Paleoproterozoic glaciation in southern Africa, similar to carbonates stratigraphically beneath Neoproterozoic glacial diamictites worldwide. Also mirroring the Neoproterozoic record are strongly negative $\delta^{13}C$ values in cap carbonates atop glacial diamictites in Paleoproterozoic strata of Wyoming and Ontario. The litho- and chemostratigraphic constraints indicate that the interval of negative carbon isotope values in well-preserved carbonates of the lower Duitschland Formation may reflect a second Paleoproterozoic ice age in the Transvaal succession. This interpretation is further supported by recently discovered bullet-shaped clasts with striations in diamictite from the basal part of the succession. Thus, the emerging temporal pattern of carbon isotope variations and glaciation in the Paleoproterozoic has a close analogue to Neoproterozoic events, suggesting a coupling of climatic and biogeochemical changes at both ends of the eon.

INTRODUCTION

The Paleoproterozoic Era (1.6-2.5 Ga) is a distinct interval in Earth history characterized by inter-related tectonic, evolutionary, climatic, and biogeochemical events resulting in broad changes of Earth's surface environments. The detailed relationship between key transitions is poorly understood, however, due to uncertainties in correlation and the age of sedimentary successions where critical events

are preserved, as well as stratigraphic omissions and post-depositional insults that obscure the true nature of temporal trends. For example, in North America, three discrete levels of Paleoproterozoic glacial diamictites are recognized in the Huronian and Snowy Pass supergroups of Ontario and Wyoming (Young, 1973, 1988; Ojakangas, 1985), respectively; on other continents only a single unequivocal diamictite of glacial origin has thus far been recognized (Ojakangas, 1985). In North America, these ice ages are radiometrically constrained to have occurred over a 230 my interval between 2.22 and 2.45 Ga (Fig. 1.1; Krogh, Davis, and Corfu, 1984; Corfu and Andrews, 1986).

Karhu and Holland (1996) suggest that following the last of the Paleoproterozoic ice ages is a positive carbon isotope excursion whose extreme magnitude (> +12 permil; Fig. 1.1) finds a match only in a narrow interval of Neoproterozoic time (0.545-1.0 Ga; Iyer and others, 1995; Misi and Veizer, 1998). This carbon isotope anomaly is best documented in 2.1 to 2.2 Ga old sedimentary sequences from Baltica (Baker and Fallick, 1989; Karhu, 1993; Melezhik and others, 1996) where only one stratigraphic level of glacial diamictite is recognized; notably, it lies below the biogeochemical anomaly.

Both ends of the Proterozoic Eon are characterized by (1) protracted intervals of tectonic assembly (resulting in the formation of the supercontinents known as Kenoraland and Rodinia) and breakup; (2) oscillations between greenhouse and icehouse conditions; and (3) significant changes in the composition of the atmosphere and ocean, and, in particular, strong carbon isotope excursions. However, in contrast with the known Paleoproterozoic record of isotopes and ice ages (with the biogeochemical anomaly following the last known ice age), the high resolution Neoproterozoic record reveals that strongly positive-to-negative $\delta^{13}C$ of seawater proxies bracket at least two (Kennedy and others, 1998) and perhaps as many as four or more (Kaufman, Knoll, and Narbonne, 1997; Corsetti and Kaufman, 1999) discrete glaciations. In particular, strongly positive $\delta^{13}C$ in carbonates characterize pre-glacial successions while negative $\delta^{13}C$ anomalies occur in all "cap carbonates" atop Neoproterozoic diamictites. These enigmatic biogeochemical and climatic events are viewed as a response to extreme modulations in atmospheric CO_2 concentrations (Kaufman, Knoll, and Narbonne, 1997; Hoffman, Kaufman, and Halverson, 1998; Hoffman and others, 1998) at a time when 6.5 percent less radiant energy was reaching the planet's surface relative to today (Kasting, 1987). Lowering of CO_2 below threshold concentrations plausibly plunged the planet into a runaway glaciation that resulted in high albedo "Snowball Earth" conditions, where the oceans were blanketed in a thick cover of sea ice for

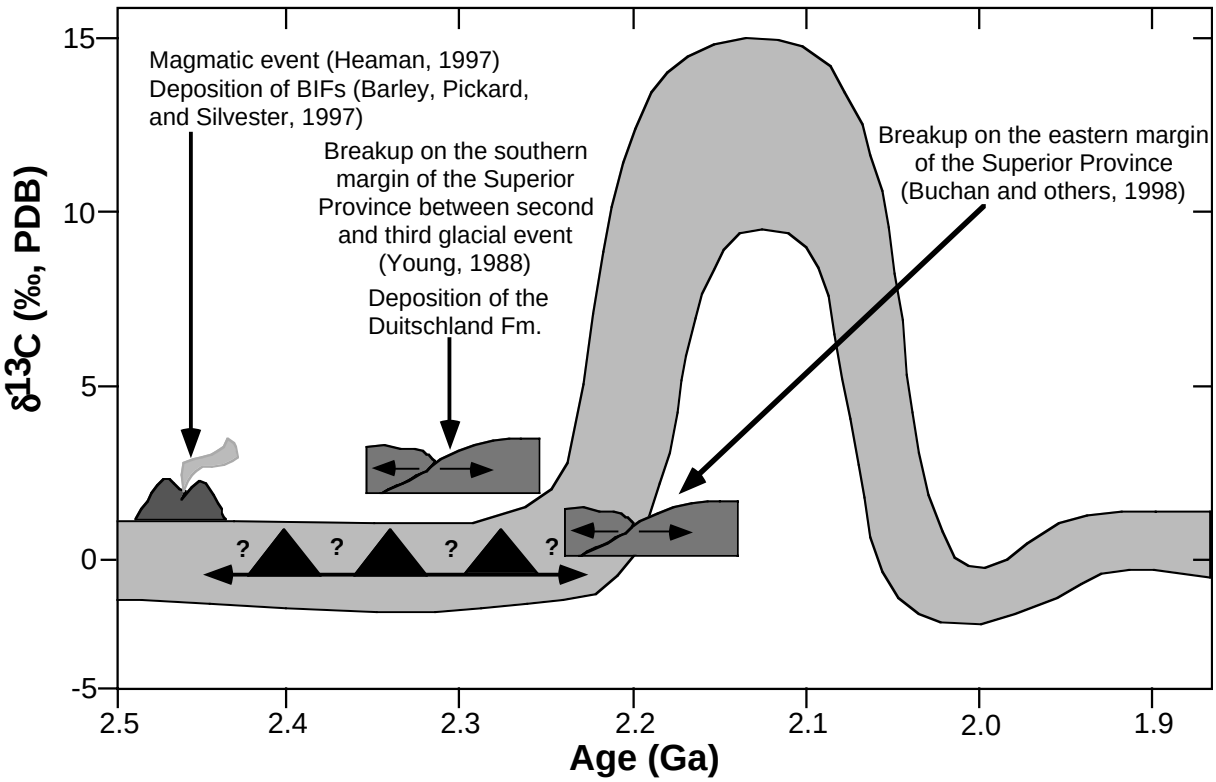

Fig. 1.1. Schematic representation of Paleoproterozoic $\delta^{13}C$ variations presented by Karhu and Holland (1996) and timing of key geological events through this interval. Black triangles and question marks between them represent three glacial events of the Paleoproterozoic in North America and their age uncertainty.

millions of years (Kirschvink, 1992; Hoffman and others, 1998). This hypothesis is consistent with paleomagnetic data for equatorial glaciation at sealevel in the Neoproterozoic of Australia (Schmidt, Williams, and Embleton, 1991; Sohl, Christie-Blick, and Kent, 1999) and arctic Canada (Park and others, 1997).

In the early Paleoproterozoic, when the solar output is estimated to be only 82 percent of the modern (Kasting, 1987), paleomagnetic studies in South Africa and Canada also point to the probability of low latitude glaciation (Evans, Beukes, and Kirschvink, 1997; Williams and Schmidt, 1997; Buchan and others, 1998; Schmidt and Williams, 1999; see also Mertanen and others, 1999 for a potential low

latitude position of Baltica). If Snowball Earth-like conditions punctuated surface environments in both intervals, why is the temporal relationship between ice ages and extreme carbon isotope excursions different at the beginning and end of the Proterozoic Eon?

To investigate this question, in particular whether extreme ^{13}C enrichments characterize carbonates beneath glacial strata of Paleoproterozoic age, we chose to study well-preserved carbonates of the Duitschland Formation in South Africa. This succession lies stratigraphically below the glaciogenic Timeball Hill Formation (Visser, 1971-1972). Highly positive carbon isotope values have been reported previously in carbonates altered by contact metamorphism from the upper Duitschland Formation (Buick and others, 1998). Insofar as samples of this study were collected at high resolution within a sequence stratigraphic framework and diagenetic tests were conducted to evaluate the degree of sample alteration, this research differs considerably from all previous chemostratigraphic studies of Paleoproterozoic strata. In addition, carbon isotope compositions of coexisting organic matter were determined to further evaluate the primary nature of carbon isotope variations.

REGIONAL GEOLOGY AND STRATIGRAPHY

Paleoproterozoic successions in South Africa are preserved in the Transvaal and Griqualand West basins. The Vryburg Rise (Fig. 1.2; Button, 1986) presently separates these once contiguous deposits. Lithostratigraphic correlation between the structural sub-basins is supported by available chronostratigraphic data and based on several marker-beds including: (1) thick stromatolitic carbonate platform facies (Campbellrand and Malmani subgroups); (2) banded iron-formation (Griquatown, Kuruman, and Penge IFs); (3) glacial diamictite and associated units (Makganyene Diamictite and upper part of the Timeball Hill Formation); and (4) thick volcanics of intermediate composition (Ongeluk andesite and Hekpoort Formation). A glaciomarine environment of deposition was inferred for the upper part of the Timeball Hill Formation (Visser, 1971-1972) and the equivalent Makganyene Diamictite (Visser, 1981) based on the presence of striated, pock-marked, and faceted pebbles, as well as laminated shales. Based on paleomagnetic data from the Ongeluk andesite, a unit overlying the glacial diamictite, a low latitude position for the Kaapvaal Craton during this ice age was inferred (Evans, Beukes, and Kirschvink, 1997).

The Duitschland Formation sits at the base of the Pretoria Group in the Transvaal Basin (Fig. 1.3) and is a time equivalent of the Rooihoogte Formation (Swart, ms). A maximum age constraint for the Duitschland Formation is based on 2480 ± 6 Ma U-Pb SHRIMP age for the underlying Penge Iron-Formation (A.F. Trendall, unpublished data in Nelson, Trendall, and Altermann, 1999). A tentative minimum age limit for the Chuniespoort Group including the Duitschland Formation is based on Pb-Pb whole rock dating of the Ongeluk andesites in the lithostratigraphically equivalent Ghaap Group of the Griqualand West Basin at 2222 ± 13 Ma (Cornell and others, 1996). This age, however, was not confirmed by U-Pb SHRIMP zircon study and is likely related to a heterogeneous initial Pb isotopic composition (Bau and others, 1999). In addition, the Moodraai Dolomite, stratigraphically above the Ongeluk andesite in the Griqualand West Basin, has a Pb-Pb isotopic carbonate age of 2394 ± 26 Ma (Bau and others, 1999). When combined, these ages with their uncertainties constrain the Timeball Hill glaciation and deposition of the Duitschland Formation between 2486 and 2368 Ma.

The Duitschland Formation is exposed in two areas near Potgietersrus in the northern part of the Olifants River Valley (Figs. 1.2 and 1.4; Martini, 1979). In these areas an unconformity at the base of the Duitschland Formation separates this unit from ~50 m thick laminated, ferruginous dolomite rhythmites of the underlying Tongwane Formation (Fig. 1.3). These dolomites are considered to be conformable with the underlying Penge Iron Formation (Martini, 1979). In the eastern Transvaal Basin, erosional unconformity separates the Duitschland Formation from the overlying Timeball Hill Formation. Regionally, however, a paraconformable contact between the Duitschland and Timeball Hill formations has been observed (Swart, ms). Accordingly, the Duitschland Formation is included in the basal part of the Pretoria Group. Martini (1979) recognized several stratigraphic levels of diamictite in the Duitschland Formation (Fig. 1.5), but evidence linking these to glacial activity was not presented. Recently, the basal diamictite of the Duitschland Formation has been interpreted as glacial in origin based on its (1) basin wide distribution, (2) heterogeneous composition of clast types (including basement rocks and BIF), and (3) presence of clear striations on *in situ* bullet shaped quartzite pebbles and cobbles (Fig. 1.6A; Coetzee, ms; Beukes and others, 2001).

The Duitschland Formation was studied in the type area 20-km southeast of Potgietersrus on Duitschland Farm as well as exposures on DeHoop and Langbaken farms (Fig. 1.4). This succession

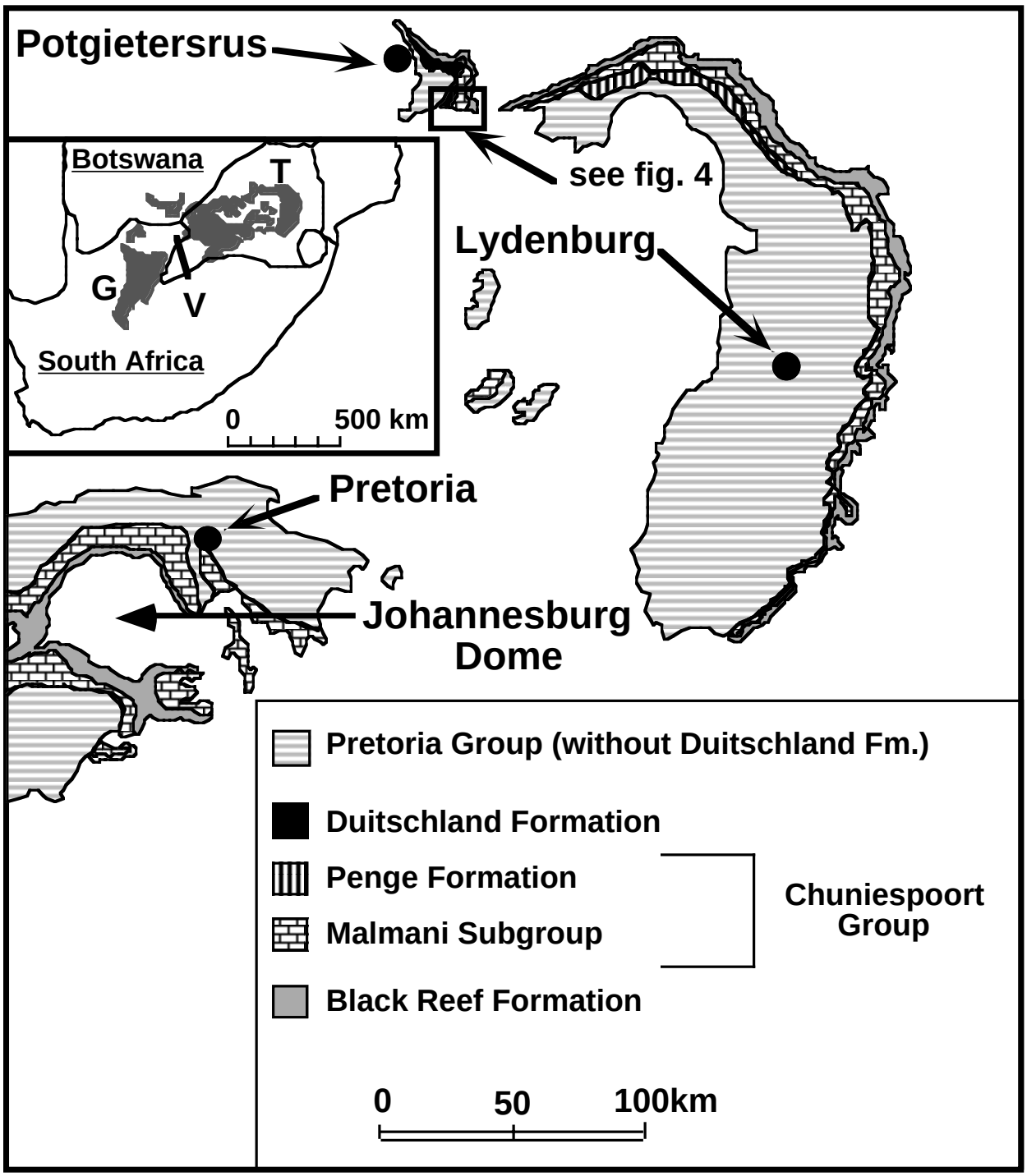

Fig. 1.2. Simplified geological map showing Potgietersus area where sections of the Duitschland Formation were studied. Inset shows the Griqualand West (G) and Transvaal (T) basins and Vryburg (V) rise. See Fig. 1.4 for the detailed map of the Potgietersus area.

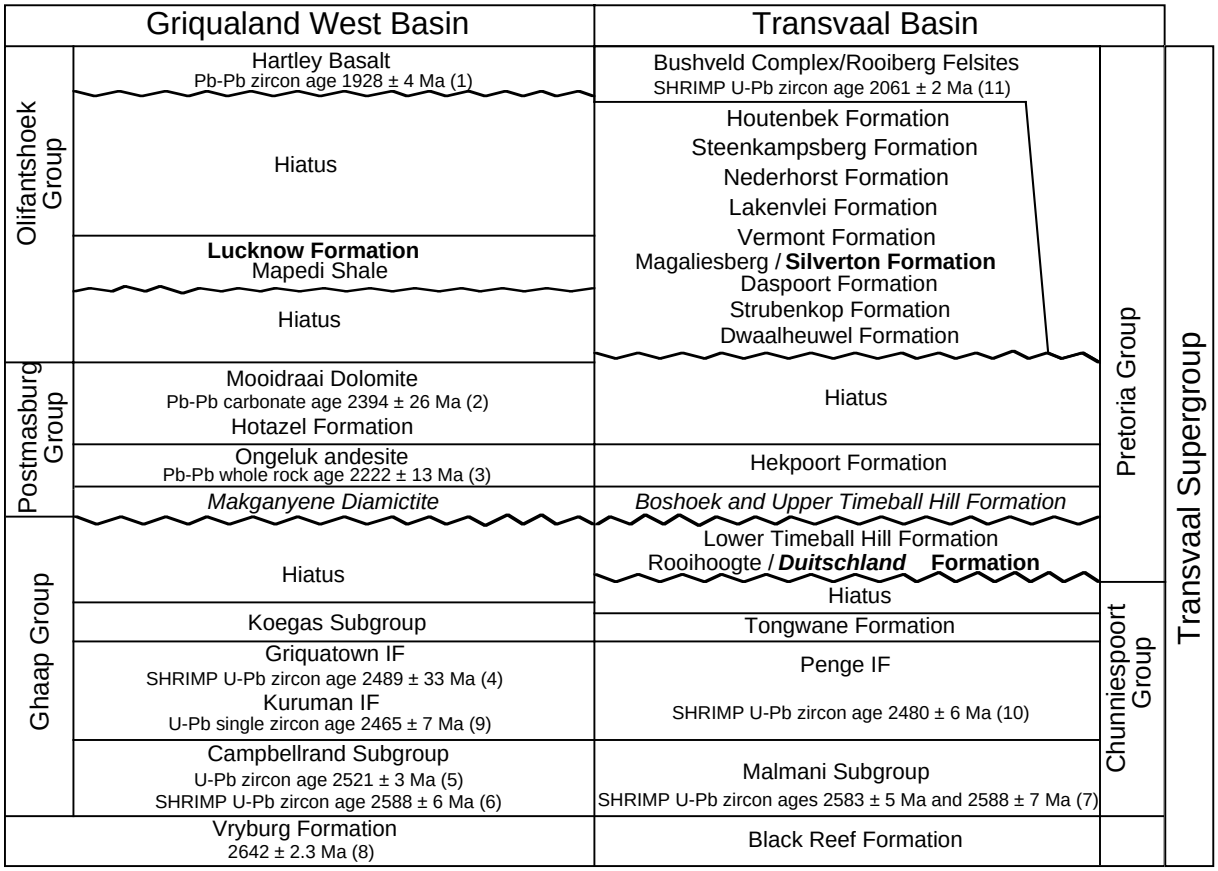

Fig. 1.3. Correlation chart for the lower part of the Transvaal Supergroup in the Griqualand West and Transvaal structural basins, South Africa (after Swart, ms and Dorland, ms). Sources of ages: 1 – Cornell, Armstrong, and Walraven, 1998; 2 –Bau and others, 1999; 3 – Cornell, Schütte, and Englinton, 1996; 4 – Trendall unpubl. data in Nelson, Trendall, and Altermann, 1999; 5 – Sumner and Bowring, 1996; 6 – Altermann and Nelson, 1998; 7 – Martin and others, 1998; 8 – Walraven and others, in press, in Nelson, Trendall, and Altermann, 1999; 9 – Armstrong, pers. com., 1996, in Martin and others, 1998; 10 – Trendall unpubl. data in Nelson, Trendall, and Altermann, 1999; 11 – Walraven, Armstrong, and Kruger, 1990; McNaughton and Pollard, 1993; Walraven, 1997. Units in bold type contain ^{13}C-enriched carbonates and units in italics contain diamictites.

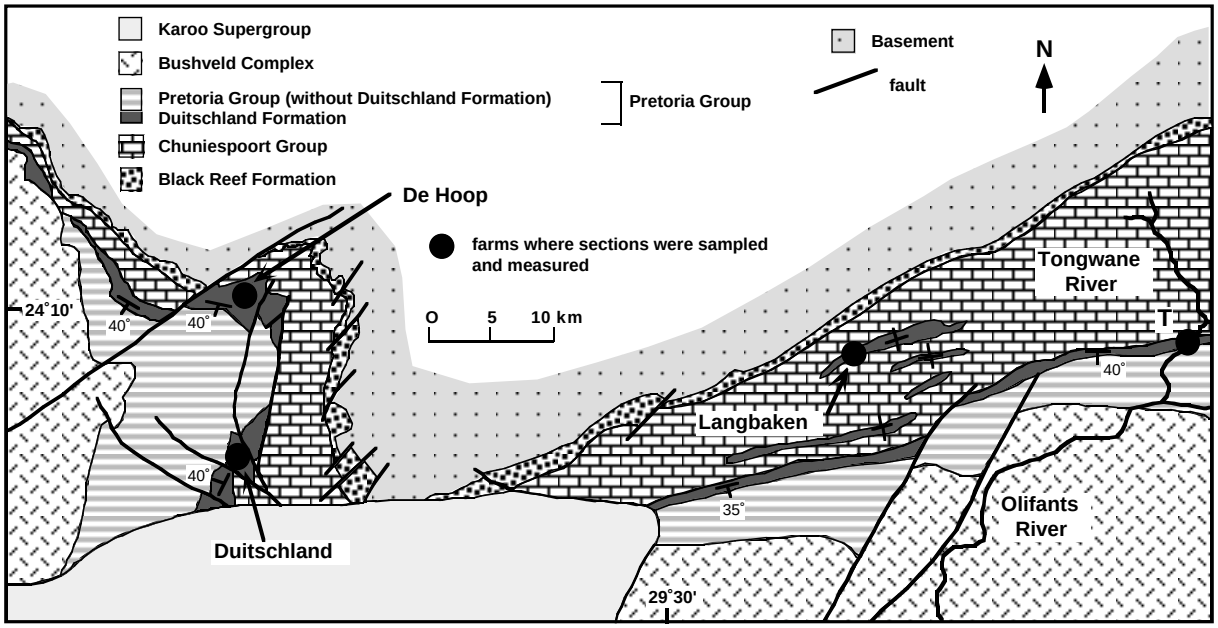

Fig. 1.4. Detailed map of the Potgietersus area with locations of sampled sections of the Duitschland and Tongwane formations. T is location where Tongwane Formation was sampled.

has a thickness of about 1000 m and is clearly divided into two parts by a notable sequence boundary marked by conglomerate at the base of the quartzite unit (Fig. 1.5; Swart, ms). The lower half begins with chert edge-wise conglomerate and the glacial diamictite overlain by thick, finely-laminated carbonaceous shale, which is in turn overlain by interbedded layers of limestone, marl, and breccia. Carbonate layers are thin and composed of gray, finely laminated limestone rhythmites, likely deposited in deep water below storm wave base. Chert and limestone breccias in the lower part of the succession are interpreted as a gravity flow slope deposit (Swart, ms). Quartzite and dolomite dominate near the top of this upward-shallowing succession.

The upper half of the formation starts with fine- to coarse-grained quartzite and conglomerates that fine upward into shale. The shale then forms the base of two upward-shallowing shale-carbonate cycles (Fig. 1.5). Above the basal conglomeritic quartzite, the cycles consist of shale with minor quartzite, carbonate, and breccia. An up section decrease in the abundance of shale and the presence of ripple marks in fine-grained quartzite at the top of the first cycle suggest that deposition occurred in shallow water environments. The first thick carbonate is limestone composed of isopachous sheet

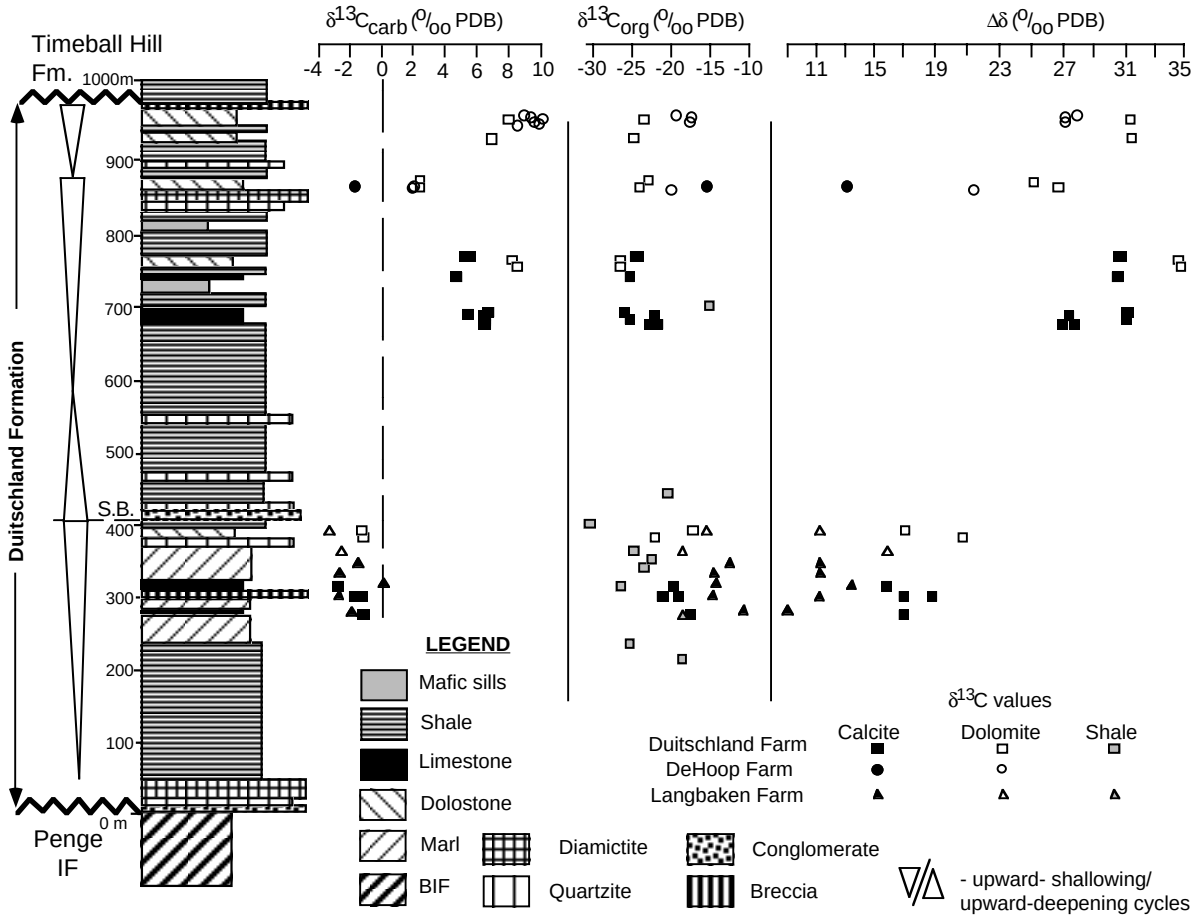

Fig. 1.5. Generalized stratigraphic column of the Duitschland Formation with measured variations in $\delta^{13}C_{carb}$, $\delta^{13}C_{org}$ and $\Delta\delta$ from Duitschland, DeHoop, and Langbaken farms.

cements (= laminated tufa) likely formed as synsedimentary cements on the seafloor (Fig. 1.6B; Hoffman, 1975; Grotzinger, 1994; Kah and Knoll, 1996). The overlying shale and carbonate are intruded by two sills emanating from the nearby Bushveld Complex, which produced contact metamorphism of some carbonates in this part of the section (Fig. 1.5; Buick and others, 1998). The carbonate bed above the first sill is a light-colored ivory and pink shallow-water limestone with nodules and large stromatolitic domes (Martini, 1979). The overlying dolomite layer in the same cycle is also

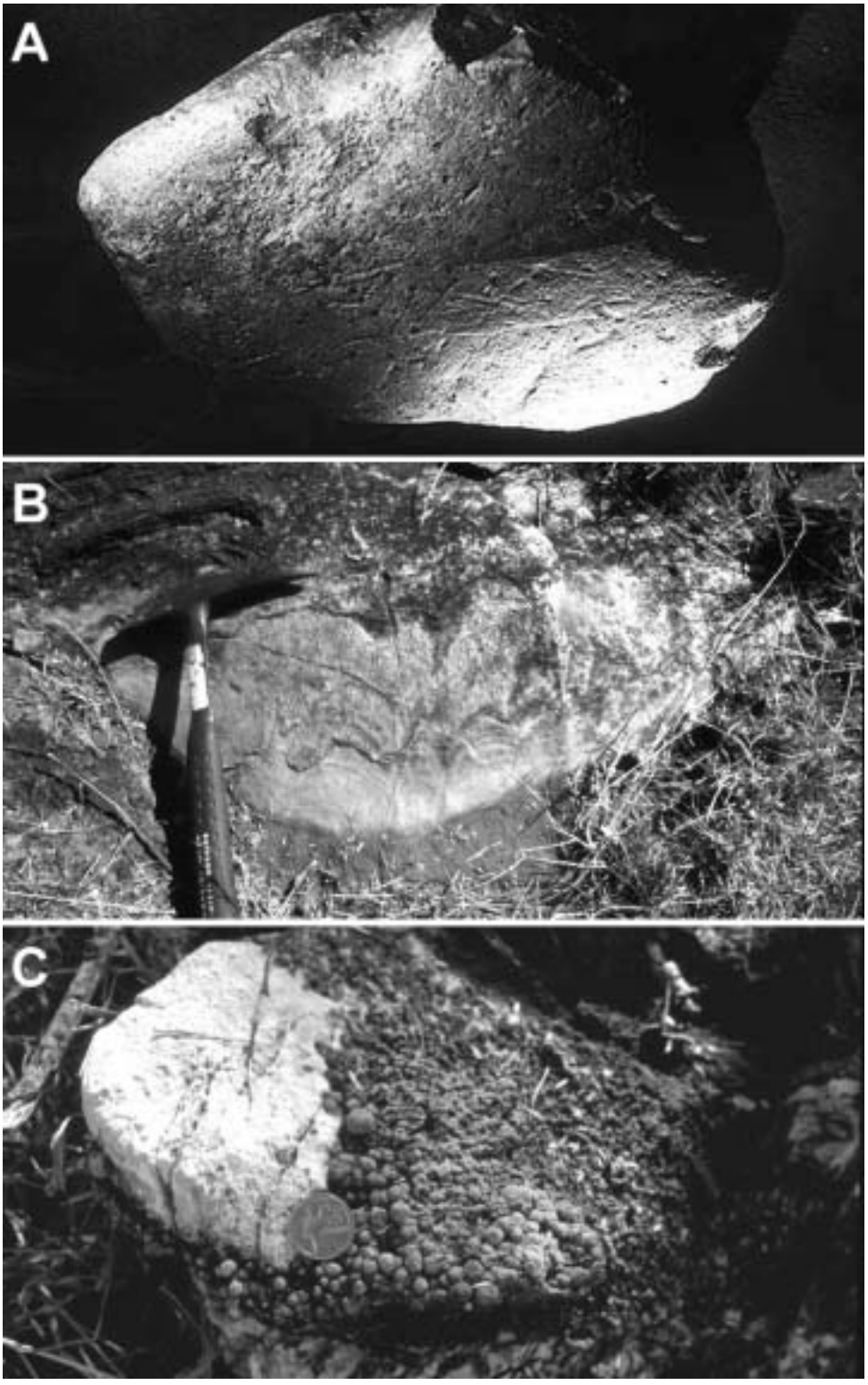

Fig. 1.6. A – striated quartzite cobble plucked from the lower Duitschland puddingstone diamictite; B – isopachous sheet cements from the upper Duitschland Formation; C – giant ooids and grapestones from the upper part of the Duitschland Formation.

stromatolitic near its base but contains oolites and fan-shaped chert nodules as well as ripple-marked red to yellow dolomite with flaser muddy laminations above.

A chert breccia with a muddy matrix at the top of the second upward shallowing cycle is interpreted as a mudflow deposit (Swart, ms). The uppermost upward-shallowing cycle includes three ivory-colored dolomite beds with domal stromatolites, as well as silicified giant ooids (up to 0.5 cm) and grapestones (Fig. 1.6C). These large, spherical coated grains must have required considerable wave energy to form (Sumner and Grotzinger, 1993) and are therefore most-likely marine in origin. These coated grains differ from vadose zone pisolites insofar as they are perfectly round, well sorted, and locally abundant. The final cycle terminates with a stromatolitic, cherty dolomite and a karstic chert breccia at the very top (Swart, ms), overlain sharply by black carbonaceous shale of the Timeball Hill Formation (Fig. 1.5).

Although the Duitschland Formation is only locally preserved in the northeastern part of the Transvaal Basin**,** we infer a marine depositional environment for this succession. This view is consistent with sedimentologic evidence in the paraconformably overlying Timeball Hill Formation, which includes deep-water contourites near the base and tidally influenced deltaic deposits (Eriksson and Reczko, 1998). In addition, the giant spherical ooids and grapestones of the upper Duitschland strongly resemble those found in dominantly marine Neoproterozoic successions in Svalbard (Swett and Knoll, 1989), Namibia (Hegenberger, 1993), and the Great Basin, United States of America (Tucker, 1986). Finally, the high Sr concentration in some samples and low $^{87}Sr/^{86}Sr$ of the isopachous cements (see below) strongly suggest an open marine setting and original aragonitic precursor (Veizer, 1983).

METHODS

Whole-rock powders were prepared from samples collected from the measured sections. Major and trace element concentrations were determined through the dissolution of ~10 mg of carbonate in 5 ml of 0.5 M acetic acid and subsequent analysis by ICP-AES at the Geological Survey of Finland (Table 1.1). Uncertainties in the analytical data based on the measurement of multiple standard materials by this method are 5 percent for major elements and better than 10 percent for trace elements.

TABLE 1.1. Carbon, oxygen and strontium isotope values and trace and major element concentrations in South African carbonates

Sample	$\delta^{13}C$ (PDB)	$\delta^{18}O$ (PDB)	Mineral/ Rock	Ba ppm	Ca %	Fe %	Mg %	Mn %	Sr ppm	Mn/Sr	TOC mgC/g	$\delta^{13}C_{org}$ (PDB)	$\Delta\delta$ (PDB)	$^{87}Sr/^{86}Sr$
Tongwane Formation														
TON/4	2.9	-9.3	Dolomite	14	22.8	2.28	11.9	0.73	47	157	0.09	-28.2	31.1	
TON/5	2.8	-8.8	Dolomite	16	22.68	2.74	11.3	0.64	42	153	0.06	-25.8	28.6	
TON-6	1.9	-9.5	Dolomite					4.7	18	2517				
TON-7A	3.5	-7.1	Dolomite					0.3	24	143				
TON-7B	2.98	-8.26	Dolomite					0.3	29	103				
Duitschland Formation														
Duitschland Farm profile														
Duit/2	-1.3	-14.3	Calcite	< 7	40.17	0.54	0.28	0.14	488	3	0.46	-18.1	16.8	0.712179
Duit/3	-1.8	-14.7	Calcite	< 7	39.43	1.04	0.39	0.21	435	5	0.98	-21.0	19.2	0.713527
Duit/6	-3.1	-10.5	Calcite	< 7	39.91	0.51	0.37	0.10	969	1	1.71	-19.5	16.4	0.711412
Duit/9	-1.4	-12.9	Dolomite	< 7	22.25	4.03	11.2	0.20	127	16	0.31	-21.9	20.5	
Duit/10	-1.6	-11.8	Dolomite	< 7	22.09	3.81	10.8	0.29	137	21	0.27	-18.8	17.2	
Duit/15	6.0	-17.3	Calcite	11	37.27	0.79	0.26	0.18	387	5	0.48	-22.5	28.5	0.704334
Duit/16	6.0	-17.3	Calcite	14	38.25	0.40	0.43	0.19	749	3	0.43	-25.3	31.3	0.704518
Duit/17	5.2	-18.1	Calcite	81	38.07	0.07	1.17	0.25	320	8	0.92	-25.9	31.1	0.712039
Duit/18	4.4	-17.4	Calcite	65	38.37	0.82	0.49	0.29	789	4	0.36	-25.2	29.6	0.708079
Duit/19	8.1	-11.5	Dolomite	8	23.62	0.16	12.8	0.13	49	27	0.40	-26.7	34.8	
Duit/20	7.9	-12.3	Dolomite	37	22.92	0.16	12.9	0.11	39	28	0.35	-26.7	34.6	
Duit/21A	5.5	-18.7	Calcite	12	36.68	0.07	0.50	0.27	141	19	0.36	-24.3	29.8	
Duit/21B	5.6	-18.6	Calcite	22	36.86	0.05	0.50	0.24	137	18	0.31	-24.6	30.2	
Duit/24	2.3	-14.5	Dolomite	< 7	22.81	0.55	13.0	0.14	55	26	0.18	-24.1	26.4	
Duit/25	2.3	-12.2	Dolomite	18	22.83	0.49	13.1	0.09	48	19	0.45	-23.0	25.3	
Duit/26	6.8	-14.9	Dolomite	215	24.40	2.69	11.0	0.12	81	14	0.33	-24.8	31.6	
Duit/28	7.9	-10.7	Dolomite	28	22.97	0.74	12.9	0.12	52	23	0.22	-23.5	31.4	
KB99.3.A			Shale								4.82	-18.7		
KB99.3.B			Shale								3.45	-25.4		
KB99.3.C	-2.0	-14.4	Calcite					0.07	330	2	0.53	-19.0	17.0	
KB99.3.D			Shale								5.6	-26.2		
KB99.3.E			Shale								3.7	-23.5		
KB99.3.F			Shale								3.38	-22.6		
KB99.3.G			Shale								4.09	-24.7		
KB99.3.H			Shale								1.05	-30.6		
KB99.3.I			Shale								1.19	-20.4		
KB99.3.J	6.0	-16.8	Calcite					0.05	612	0.8	0.18	-21.0	27.0	
KB99.3.K	6.0	-16.6	Calcite					0.05	612	0.8	0.22	-22.0	28.0	
KB99.3.L			Shale								0.35	-15.0		
KB99.3.M	6.1	-16.5	Calcite					0.08	645	1.2				
Langbaken Farm profile														
KB99.1.0.5			Shale								3.3	-18.7		
KB99.1.5.0	-1.8	-12.7	Calcite					0.05	318	1.6	0.3	-10.8	9.0	
KB99.1.11.0	-3.0	-9.5	Calcite					0.04	280	1.4	0.4	-14.7	11.3	
KB99.1.19.5	0.1	-10.1	Calcite					0.02	457	0.5	0.5	-14	13.9	
KB99.1.27.5	-2.7	-10.2	Calcite					0.04	307	1.3	1.8	-14.3	11.6	
KB99.1.37.5	-1.8	-10.5	Calcite					0.04	172	2.1	1.4	-12.2	10.4	
KB99.1.60.5	-2.4	-9.1	Dolomite					0.16	44	37.4	0.08	-18.5	16.1	

KB99.1.83.0	-3.7	-9.4	Dolomite	0.24	52	45.7	0.2	-15.2	11.5	
DeHoop Farm profile										
KB99.2.0.5	8.7	-9.4	Dolomite	0.05	57	8.5	0.15	-19.3	28.0	
KB99.2.3.0	9.5	-8.5	Dolomite	0.03	54	4.8	0.08	-17.1	26.6	
KB99.2.4.0	10.1	-6.8	Dolomite	0.02	35	6.0				
KB99.2.9.0	8.9	-10.0	Dolomite	0.04	63	5.6	0.07	-17.7	26.6	
KB99.2.13.5	9.4	-10.9	Dolomite	0.04	95	3.7				
KB99.2.20.0	8.1	-12.1	Dolomite	0.04	70	5.6				
KB99.2.A	2.4	-11.2	Dolomite	0.04	53	7.2				
KB99.2.B	-2.0	-11.9	Calcite	0.03	57	5.2	0.13	-15.2	13.2	
KB99.2.C	2.0	-12.7	Dolomite	0.05	42	11.3	0.08	-19.9	21.9	
Lucknow Formation										
Venn/4	10.3	-8.3	Dolomite	0.02	8.9	21.2	0.33	-25.4	35.7	0.712606
Venn/6	10.5	-7.8	Dolomite	0.02	11.9	19.7	0.22	-24.3	34.8	0.707873

Carbon dioxide was extracted at the Geological Survey of Finland from whole-rock powders by closed tube reaction with anhydrous phosphoric acid (ρ > 1.89 g/cc; 16+ hours) at a temperature of 25ºC for limestone and for 1 hr at 100ºC for dolomite; resulting CO_2 was isolated by cryogenic distillation for mass spectrometric analysis on a Finnigan MAT 251. The fractionation factors used for mineral correction of oxygen isotopes in calcite prepared at 25ºC and dolomite at 100ºC were 1.00913 and 1.01025, respectively. A second set of carbonate samples (KB99 series) was micro-drilled, and the powders reacted with anhydrous phosphoric acid at 90ºC in a Micromass Multiprep carbonate device; the resulting carbon dioxide was then measured with a Micromass Optima mass spectrometer at Rutgers University. The fractionation factors used for mineral correction of oxygen isotopes in calcite and dolomite prepared at 90ºC were 1.00798 and 1.00895, respectively. For both techniques, the external precision based onmultiple standard measurements of NBS-19 was better than 0.1 permil versus V-PDB for both carbon and oxygen.

Total organic carbon (TOC) was isolated from the carbonate samples by repeated acidification and centrifugation with concentrated HCl followed by washing until the sample reached neutral pH (Kaufman and Knoll, 1995). Dried samples in Vycor tubes were then mixed with CuO as an oxidant, evacuated, sealed, and combusted at 850ºC for 12 hrs. The volume of CO_2 quantified during cryogenic distillation was used to calculate organic carbon concentrations in the samples. Carbon isotope abundance in extracted and purified CO_2 was measured with a VG PRISM mass spectrometer at Mountain Mass Spectrometry. To test for the uncertainty of abundance and isotopic composition measurements on TOC, organic-rich and organic-poor standard powders were chosen for replicate (n =

4) analysis. For analyses of the organic-rich sample uncertainties were ± 0.26 mgC/g for abundance (5.57 mgC/g average) and ± 0.03 permil for carbon-isotopic composition (-34.47 permil average); for the organic-poor sample uncertainties were ± 0.06 mgC/g (0.18 mgC/g average) and ± 1.3 permil (-24.1 permil average) for abundance and carbon-isotopic composition, respectively.

Samples chosen for Sr isotopic analysis were treated repeatedly with 0.4 M ammonium acetate (3 times; pH = 8.2) prior to dissolution with 0.5 M acetic acid in order to remove diagenetic components (Gorokhov and others, 1995; Montañez and others, 1996). Strontium was eluted from solution by ion exchange chromatography using ElChrom Sr spec resin and weak 0.05 M nitric acid and measured on a VG Sector 54 multi-collector thermal ionization mass spectrometer at the University of Maryland. Repeated analysis of NBS-987 over a period of 3 months when these samples were analyzed gave a value of 0.710248 +/- 0.000005.

RESULTS

Table 1.1 and Appendix 1 includes sample numbers, stratigraphic positions, sample descriptions and analytical results for all samples analyzed in this study. Carbonates in the lower half of the Duitschland Formation are composed of limestone with the exception of dolomite beds immediately below the sequence boundary. Carbonates above this boundary consist of both limestone and dolomite with the latter increasing upsection. Calculations based on yields of carbon dioxide from reaction with phosphoric acid indicated that the carbonate content in most samples exceeded 70 percent.

Elemental analyses reveal that limestone samples are significantly enriched in strontium (up to 969 ppm) relative to dolomites in the Duitschland Formation (Table 1.1; see also Martini, 1979). Manganese concentration in the Duitschland carbonates is quite variable. This results in Mn/Sr (a common diagenetic indicator for marine carbonates; for example, Veizer, 1983; Derry, Kaufman, and Jacobsen, 1992; Kaufman, Knoll, and Awramik, 1992) ranging from 1 to 28, with the highest values in limestone samples adjacent to the two mafic sills, as well as in all dolomites.

Oxygen isotope values for Duitschland carbonates from the type section at Duitschland Farm are notably lower than -10 permil, suggesting exchange of the oxygen in primary carbonates with hot fluids, likely associated with Bushveld intrusion (Valley, 1986). Sampled localities that are farther away from

this large igneous province (Langbaken and DeHoop) contain equivalent carbonates less depleted in ^{18}O (Table 1.1).

All carbonates in the lower part of the Duitschland Formation are depleted in ^{13}C with a minimum value of -3.7 permil. In strong contrast, most carbonates above the sequence boundary are systematically enriched in ^{13}C with a maximum value of +10.1 permil. However, in the upper part of the formation above a second diamictite level $\delta^{13}C$ values are consistently lower; on DeHoop Farm a single sample of flat laminated cherty limestone has a value of -2 permil. Notably, limestone samples adjacent to the mafic sills are 2 to 4 permil less enriched in ^{13}C relative to nearby dolomites.

Total organic carbon (TOC) isolated from shale and carbonate samples range in abundance between 0.06 and 5.6 mgC/g sample. These organic isolates have variable $\delta^{13}C$ values (ranging between -30.6 to -10.8 permil), with carbonates being consistently more ^{13}C enriched than interbedded shales. The $\delta^{13}C$ values of organic isolates from carbonates of the upper Duitschland range between -26.7 to -15.0 permil.

Six samples were selected for Sr isotope analysis based on their Sr abundances (>300 ppm) and Mn/Sr ratios (< 5; Table 1.1). Two closely spaced samples from the level of the isopachous sheet cements in the upper half of the Duitschland Formation yielded similarly low $^{87}Sr/^{86}Sr$ values (about 0.7043-0.7045); other analyzed samples were considerably more radiogenic.

EFFECTS OF DIAGENESIS AND METAMORPHISM

In any geochemical consideration of sedimentary rocks, post-depositional effects on primary elemental and isotopic compositions must be considered. Post-depositional processes may result in the alteration of marine carbonates, which can be recognized through a detailed study of elemental and isotopic trends (Veizer, 1983; Fairchild, Marshall, and Bertrand-Sarfati, 1990; Banner and Hanson, 1990; Derry, Kaufman, and Jacobsen, 1992; Jacobsen and Kaufman, 1999). Superimposed on regional insults, the diagenetic picture for the Duitschland Formation is complicated by the intrusion in the type area of mafic sills into the upper part of the formation.

Because of the predominance of oxygen in all fluids, the oxygen isotopic compositions of carbonates are substantially altered long before carbon isotope values under the influence of meteoric or hydrothermal solutions. Lower $\delta^{18}O$ values commonly indicate a higher degree of exchange between post-depositional fluids and carbonates. Oxygen isotope values of studied carbonates are approx -10 permil or less in most samples, with a greater degree of ^{18}O depletion noted at Duitschland Farm. It is clear that the oxygen isotope composition of all samples has been altered to some degree, although the most enriched values (up to -6.8 permil) are consistent with those found in well-preserved Paleoproterozoic successions worldwide (Veizer, Clayton, and Hinton, 1992; Veizer and others, 1992; Melezhik, Fallick, and Clark, 1997; and our own unpublished data). In the upper half of the formation, limestones adjacent to the mafic sills have the most ^{18}O depleted compositions (see Valley, 1986 for the effects of contact metamorphism on both O and C isotopes in carbonates); however, nearby dolomites are notably more enriched in ^{18}O, similar to carbonates in the lower half of the formation. Carbonates analyzed by Buick and others (1998) were specifically collected near these mafic sills.

Mn/Sr elemental ratios are also used as an indicator of postdepositional alteration in carbonates (Veizer, 1983), where higher Mn and lower Sr abundance are typically related to meteoric diagenesis. Application of these criteria is rather ambiguous to Paleoproterozoic carbonates that may have formed in an anoxic ocean enriched in Fe^{2+} and Mn^{2+}. As expected due to crystal lattice effects, Sr contents are higher and Mn/Sr ratios are much lower in calcites than in dolomites (Table 1.1). Low Sr concentrations in dolomites (up to 140 ppm) may be localized in fluid or mineral inclusions (Veizer, 1983).

Because Sr is a trace element in carbonate, $^{87}Sr/^{86}Sr$ ratios are easily altered through exchange with radiogenic fluids of continental derivation or the *in situ* decay of ^{87}Rb to ^{87}Sr in clay and clastic minerals within the carbonates. Strontium isotope ratios were measured in samples with low Mn/Sr and high Sr concentrations. All analyzed samples from the lower part of succession, regardless of their present Sr contents, have highly radiogenic Sr isotope values (Table 1.1). This is likely the consequence of the interbedding of these relatively thin limestone horizons in a predominantly shaley interval. On the other hand, two closely spaced samples from thick carbonates with isopachous cements and relatively high Sr contents in the upper part of the succession (Duit/15 and Duit/16) had virtually the same $^{87}Sr/^{86}Sr$ value. We tentatively interpret these low values (about 0.7045) as reflecting ocean $^{87}Sr/^{86}Sr$ values around 2.4 Ga ago.

Carbon isotope exchange between co-existing organic matter and carbonates during metamorphism may lead to a depletion of ^{13}C in carbonates and enrichment of ^{13}C in organic C (Valley, 1986), resulting in lower fractionation between Corg and Ccarb ($\Delta\delta$). In this study, however, we note no relationship between TOC contents and $\delta^{13}C$ values of organic matter that might result from regional metamorphism (Hayes, Kaplan, and Wedeking, 1983). The degree of carbon isotope fractionation varies throughout the succession with an apparent bimodal stratigraphic distribution of values. In the underlying Tongwane Formation and all but one Duitschland sample above the sequence boundary, $\Delta\delta$ values range between 21.9 and 34.8 permil with an average of about 30 permil. These values are comparable with those found in 2.2 to 2.1 Ga carbonates of the Fennoscandian Shield (Karhu, 1993), and with the long-term average of around 30 permil for the last 800 Ma (Hayes, Strauss, and Kaufman, 1999). These values are consistent with maximal carbon isotope fractionations by primary producers in the ocean and further suggest that the upper Duitschland carbonates were not strongly affected by post-depositional processes, including contact metamorphism.

On the other hand, samples below the sequence boundary have negative $\delta^{13}C$ in carbonates containing organic matter significantly enriched in ^{13}C (resulting in smaller $\Delta\delta$ values) ranging between 9.0 and 20.5 permil. A similarly low $\Delta\delta$ value is recorded in the single anomalous limestone sample above the sequence boundary, which notably lies immediately above a diamictite of unknown origin at ~850 m (Fig. 1.5). Both negative $\delta^{13}C$ values and a smaller magnitude of carbon isotope fractionation might be explained by metamorphic equilibration. This interpretation, however, conflicts with a similarity in $\delta^{18}O$ values throughout the succession. The higher abundance of TOC in the lower part of the formation as well as the larger $\Delta\delta$ in the contact metamorphosed upper part of the formation is also inconsistent with a higher metamorphic grade for lower Duitschland sedimentary rocks. Analyses of organic-rich Neoproterozoic “cap carbonates” in Namibia and the United States of America also show significantly reduced $\Delta\delta$ values (Kaufman, Hoffman, and Halverson, 1997; Hayes, Strauss, and Kaufman, 1999) similar to those reported here from the lower Duitschland carbonates. If the smaller $\Delta\delta$ values are not a post-depositional phenomenon, then it is conceivable that the reduced fractionation is due to carbon limitation to growing cells in shallow seawater. Two environmental options seem viable: (1) either carbon dioxide was limiting because of low concentrations in the atmosphere (Jasper and Hayes, 1990; Freeman and Hayes, 1991), or (2) high growth rates resulted in a depletion of intracellular

CO_2 available for fixation (Bidigare and others, 1997, 1999; Popp and others, 1998). Based on experience from the Neoproterozoic record, the combined organic and inorganic carbon isotope results from the organic-rich lower Duitschland sedimentary rocks suggest deposition in the immediate aftermath of a global glaciation (see discussion below).

In conclusion, most of the samples in this study appear to record near to primary carbon isotope compositions in both organic and inorganic phases. While two closely spaced samples also appear to preserve unaltered $^{87}Sr/^{86}Sr$ values, most are likely reset. All oxygen isotope compositions of Duitschland carbonates appear to be reset to variable degrees.

THE RELATIONSHIP OF ISOTOPE ANOMALIES AND ICE AGES IN THE TRANSVAAL BASIN

Assuming that little-altered carbon isotope compositions are preserved in the Duitschland Formation carbonates, we can now ask about the stratigraphic relationship of carbon isotope anomalies and glacial phenomena. The only unequivocal glacial horizon previously recognized in the Transvaal basin occurs within the upper Timeball Hill Formation (Fig. 1.3). The notable ^{13}C enrichment of upper Duitschland carbonates (along with co-existing organic matter) stratigraphically beneath the glacial deposits supports the view that at least one Paleoproterozoic ice age was preceded by a positive carbon isotope anomaly. Lacking absolute age constraints, however, the time between deposition of upper Duitschland carbonates and the Timeball Hill diamictite is unknown.

Above the Makganyene Diamictite, the equivalent of the upper Timeball Hill diamictite in the Griqualand West basin, are finely-laminated carbonate-bearing manganese ores of the Hotazel Formation (Beukes, 1983; Tsikos and Moore, 1997). This sedimentary ore deposit is suggested to have accumulated in the aftermath of a widespread and potentially global glaciation (Kirschvink and others, 2000). During this ice age Fe and Mn apparently built up to high concentrations in an anoxic ocean dominated by hydrothermal inputs. These deep water manganese-rich carbonates have highly negative $\delta^{13}C$ values (ranging between -12 to -15 permil), which Kirschvink and others (2000) interpret as a syn-sedimentary overprint of recycled organic matter on primary ocean compositions nearer to -5 permil (Calver, 2000). Notable accumulations of carbonate hosted Mn ore are known in ^{13}C-depleted

Neoproterozoic cap rocks from China (Li and others, 1999), Brazil (Urban, Stribrny, and Lippolt, 1993), and Namibia (Bühn, Stanistreet, and Okrusch, 1992).

Above the diamictite and the Hotazel cap rock are dolomites of the Mooidraai Formation, which have $\delta^{13}C$ values near to 0 permil (Bau and others, 1999; Kirschvink and others, 2000). Unconformably overlying the Mooidraai Formation is the Mapedi Shale and the Lucknow Formation of the Olifantshoek Group (Fig. 1.3). Highly ^{13}C-enriched carbonates of the Lucknow Formation have been considered as evidence for a post-2.1 Ga carbon isotope excursion, based on the 1928±4 Ma Pb-Pb zircon age of the overlying Hartley Basalt (Buick and others, 1998; Melezhik and others, 1999). This interpretation, however, is inconsistent with field observations of unconformity between the Lucknow Formation and Hartley basalts (Fig. 1.3; Swart, ms; Dorland, ms), as well as new litho- and chemo-stratigraphic correlations between the lower part of the Olifantshoek Group and the upper part of the Pretoria Group, which is intruded by the ~2.06 Ga old Bushveld Complex (Beukes and others, 2001). The Lucknow and equivalent Silverton formations in South Africa and the Lomugundi Formation in Zimbabwe all contain carbonates highly enriched in ^{13}C (> +10 permil; Schidlowski, Eichmann, and Junge, 1976; Master and others, 1993; Buick and others, 1998; see additional data in Table 1.1). Given their stratigraphic position above glacial strata and beneath the 2.06 Ga Bushveld felsites, the biogeochemical anomaly preserved at this stratigraphic level may be equivalent to the ca. 2.1 to 2.2 Ga event described by Karhu and Holland (1996).

As discussed above, carbonates in the lower Duitschland Formation have negative $\delta^{13}C$ values, and lie above a diamictite recently established to be glacial in origin (Coetzee, ms; Beukes and others, 2001). Lower Duitschland carbonates occur within a 400 m sequence beginning with deep-water facies and shallowing upward to the first clear sequence boundary at approx 400 m (Fig. 1.5). This stratigraphic framework is strikingly similar to post-glacial carbonate-dominated sequences in the Neoproterozoic of Namibia (Hoffman, Kaufman, and Halverson, 1998; Hoffman and others, 1998). These thick (up to 500 m) finely-laminated and stromatolitic cap carbonates, which conformably overlie diamictites, were deposited below the storm-wave base, lack exposure surfaces, and shallow to sea level only in their upper parts (Kaufman, Knoll, and Narbonne, 1997; Hoffman, Kaufman, and Halverson, 1998; Hoffman and others, 1998). Due to the lack of exposure surfaces in both Neoproterozoic and Paleoproterozoic examples, it is conceivable that the accommodation space – later filled by several

hundred meters of sediment – was created by subsidence on continental margins during extended glaciation and little sedimentary input (Hoffman, Kaufman, and Halverson, 1998).

Unconformably below the lower Duitschland diamictite are carbonates of the Tongwane Formation, which have only moderately enriched carbon isotope values (about +3.5 permil, Table 1.1), and the Penge Iron Formation. At present there are no known carbonates beneath this diamictite with strongly positive $\delta^{13}C$ values. This might be due to missing stratigraphy beneath the unconformity surface, but we note that carbonates sandwiched between early Paleoproterozoic glacial strata and banded iron-formations worldwide are not significantly enriched in ^{13}C. Beneath the Penge Iron Formation, platform carbonates of the Malmani Subgroup and equivalents have $\delta^{13}C$ values very close to 0 permil (Beukes and others, 1990; Veizer, Clayton, and Hinton, 1992).

Summarizing data from the Transvaal Basin and equivalents, there now appears to be compelling lithologic and biogeochemical evidence for at least two Paleoproterozoic ice ages in South Africa. Given this discovery, we then ask how might these two events correlate with the three known levels glaciations preserved in the Huronian Supergroup of North America?

CORRELATION WITH THE HURONIAN SUPERGROUP

The three levels of Paleoproterozoic glacial deposits in North America include, from youngest to oldest, the Gowganda, Bruce, and Ramsay Lake formations. Carbonates, however, only occur at two levels in the Huronian stratigraphy. The Gordon Lake Formation, which is stratigraphically above the youngest diamictite but older than the 2.22 Ga Nipissing sills that intrude the whole succession, has carbonates with highly positive $\delta^{13}C$ (up to +8 permil) values (Bekker, Karhu, and Bennett, 1996). The Espanola Formation rhythmites, which sit immediately above the Bruce diamictite, are characterized by negative $\delta^{13}C$ values (Veizer, Clayton, and Hinton, 1992) and are interpreted here as a cap carbonate. Negative $\delta^{13}C$ values are also noted in equivalent carbonates atop the middle of three diamictite horizons in the Paleoproterozoic Snowy Pass Supergroup (Bekker and Karhu, 1996; Bekker and others, 1999).

Clearly the lack of carbonate lithologies complicates chemostratigraphic correlation with units in South Africa. Nonetheless, it seems plausible that the uppermost Huronian glacial unit is correlative with the Upper Timeball Hill Formation diamictite and equivalents. This tentative correlation is based

on the position of these glacial deposits beneath highly ^{13}C enriched carbonates (the Gordon Lake and Silverton/Lucknow formations in Canada and South Africa, respectively) and oxygenated paleosols, aluminous shales, and mature quartzites (Young, 1973; Rainbird, Nesbitt, and Donaldson, 1990; Beukes, Gutzmer, and Dorland, 1999; Gutzmer and Beukes, 1996; Schreiber and Eriksson, 1992).

Correlation of lower Duitschland cap carbonate facies with Espanola rhythmites is tempting, but lacking independent chronostratigraphic constraints it remains uncertain whether the lower Duitschland diamictite is equivalent to the Bruce or Ramsay Lake formations in the Huronian succession.

A PALEOPROTEROZOIC SNOWBALL EARTH?

The Neoproterozoic Snowball Earth hypothesis suggests that the planet was blanketed by continental glaciers and sea ice, extending to equatorial latitudes, for several million years (Hoffman and others, 1998). During such a catastrophic event the photosynthetic, hydrologic, and weathering cycles would have been shut down while the ocean quickly became anoxic and dominated by hydrothermal inputs. To escape from the extreme albedo of an ice-covered planet, CO_2 concentrations must have built up to phenomenal levels through millions of years of volcanic inputs (Caldiera and Kasting, 1992). The drawdown of atmospheric CO_2 levels resulting in an icehouse climate has been plausibly linked to the fragmentation of the Rodinia. By increasing the length of continental margins, breakup of the supercontinent resulted in the creation of a larger repository for organic matter. Enhanced biological productivity and an increase in the proportional burial of organic carbon over these passive margins, stimulated by higher concentrations of key nutrients in the Proterozoic oceans, is expressed in the highly positive $\delta^{13}C$ values of carbonate deposited prior to the glacial diamictites (Kaufman and Knoll, 1995; Kaufman, Knoll, and Narbonne, 1997).

Given that recent paleomagnetic results suggest equatorial glaciation in the Paleoproterozoic, we now ask whether tectonic and environmental changes similar to the Neoproterozoic bracket these Paleoproterozoic ice ages? Tectonic reconstruction and available age constraints indicate that the Paleoproterozoic supercontinent Kenoraland began rifting around 2.45 Ga (Williams and others, 1991; Heaman, 1997) prior to the ice ages. It is believed that rifting resulted in a high hydrothermal flux of Fe to the oceans and the deposition of BIFs worldwide (Beukes and others, 1990; Barley, Pickard, and Silvester, 1997). Subsidence over millions of years of global glaciation during which time was no

sedimentary input may created of large accommodation space that became filled up by lower Duitschland sediments in the aftermath of global glaciation. A buildup of Fe and Mn concentrations in the deep anoxic ocean beneath the global ice pack over millions of years is also inferred from the deposition of the manganiferous Hotazel Formation above the equivalent of Timeball Hill glacial strata (Kirschvink and others, 2000).

The hypothesis that the anoxic glacial oceans were dominated by hydrothermal inputs, which included key biolimiting nutrients like iron (Coale and others, 1996; Falkowski, Barber, and Smetacek, 1998) and phosphorous (van Cappellan and Ingall, 1994), may provide a clue to the reduced $\Delta\delta$ values measured in the organic-rich rocks of the lower Duitschland Formation. Since low pCO_2 is unlikely in the aftermath of a Snowball Earth (Caldiera and Kasting, 1992), carbon limitation through extreme growth rates of photoautotrophs is the most likely process resulting in the markedly decreased carbon isotope fractionations (Kaufman, Hoffman, and Halverson, 1997). Under conditions where nutrients are readily available, the rate of carbon fixation within cells can be faster than the rate of diffusion of dissolved CO_2 into the cells (Berry, 1988; Riebesell, Wolf-Gladrow, and Smetacek, 1993; Bidigare and others, 1997), which in part may be related to cell geometry (Popp and others, 1998). This would result in less isotopic discrimination and enrichment of ^{13}C in biomass. This view is strongly supported by recent experiments conducted during the IronEx II iron fertilization of the low productivity equatorial Pacific Ocean (Bidigare and others, 1999). These authors report up to a 7 permil carbon isotopic enrichment in algal biomass, which is largely the result of elevated growth rates. In addition to the carbon isotopic enrichment and significantly reduced $\Delta\delta$, stimulation of growth rate was accompanied by a seven-fold increase in the export of particulate organic carbon to sediments.

Finally, if high pCO_2 lasted for some time after the ice age, it is likely that high temperature and high weathering rates in stable tectonic environment would have resulted in lateritic paleosols and mature quartzites in overlying units. Evidence for these lithologies, unusual in the context of successions otherwise dominated by immature siliciclastics, are preserved immediately above the youngest Paleoproterozoic diamictites in North America, Fennoscandia, and South Africa (Young, 1973; Gutzmer and Beukes, 1996; Schreiber and Eriksson, 1992; Marmo, 1992).

SPECULATION ON THE TIMING OF PALEOPROTEROZOIC ATMOSPHERIC OXYGEN RISE

The composition of Earth's Archean and Paleoproterozoic atmosphere is at the heart of a heated controversy between researchers who maintain that surface environments were either oxidizing from the origin of oxygenic photosynthesis onward (Ohmoto, 1997), or were near-neutral until a critical oxygenation event around 2 by ago (Holland, 1994; Rye and Holland, 1998). In the latter model, atmospheric pO_2 was likely below 0.1 percent PAL until tectonic and biological forces resulted in an oxygen buildup to 15 percent or greater. In the rock record, evidence of this event is marked by (1) the retention of iron in fossil soil horizons; (2) the apparent cessation of detrital uraninite and pyrite deposits as well as banded iron-formations; and (3) the sudden appearance of sedimentary red beds. Recently, the late Paleoproterozoic oxidation event was tied to extraordinary changes in the carbon isotope composition of marine carbonates (Karhu and Holland, 1996) and organic matter (Des Marais and others, 1992; Des Marais, 1997), potentially linked to the enhanced proportional burial of organic matter in sediments deposited between 2.2 to 2.1 Ga.

Following the interpretation of strong positive $\delta^{13}C$ anomalies as markers of oxidation events (Broecker, 1970; Hayes, 1983; Derry, Kaufman, and Jacobsen, 1992; Kaufman and Knoll, 1995; Karhu and Holland, 1996; Kaufman, Knoll, and Narbonne, 1997; but see Kump and others, 1999 for contrary view) suggests that the Paleoproterozoic oxygen buildup may have started up to 200 my earlier during deposition of the upper Duitschland beds. Of the factors believed to result in the enhanced burial of organic carbon and extreme ^{13}C enrichment of surfical seawater, those that appear to be most important are (1) high sedimentation rates, (2) bottom water anoxia, and (3) high biological productivity (Pedersen and Calvert, 1990). Unfortunately, the lack of a continuous record of Sr isotope changes in Paleoproterozoic oceans makes it difficult to estimate rates of continental erosion and sedimentation.

Support for an earlier oxygenation event comes from new field evidence for an oxidized 2.4 Ga paleosol and red beds of similar age in South Africa (Beukes, Gutzmer, and Dorland, 1999). In contrast, geochemical analyses of incomplete sections of the Hekpoort basalt were previously used to infer anoxic environment during their formation (Holland, 1994; Rye and Holland, 1998). Red beds were recently discovered in the basal part of the Timeball Hill Formation below the diamictite (Beukes, Gutzmer, and Dorland, 1999). Timeball Hill beds are also unique because they contain the oldest sulfide minerals

whose range of S-isotopic compositions suggests a buildup of oxidants in the ocean used by sulfate-reducing microbial communities (Cameron, 1982). Additionally, a strong negative Ce anomaly is preserved in Timeball Hill shales (Reczko, Eriksson, and Snyman, 1995) as well as the broadly equivalent manganiferous carbonates of the Hotazel Formation (Bau and others, 1999). It is significant that no Ce anomaly is present in older metalliferous sedimentary rocks of the Penge Iron-Formation and equivalents in the Griqualand West Basin (Bau and others, 1999). Notably, in Botswana equivalents of the Rooihoogte Formation, presently considered to be time-equivalent to the upper Duitschland Formation (Swart, ms; Fig. 1.4), contain manganese-rich stromatolitic dolomite and banded ironstone (Steyn, Gardyne, and Klop, 1986). These may represent the oldest Mn-rich deposits associated with the oxygenation of Earth's surface environment in the aftermath of one of the oldest ice ages.

In Canada, the oldest red and variegated beds occur in the pre-2.22 Ga Gowganda Formation of the Huronian Supergroup (Wood, 1979; Rainbird and Donaldson, 1988), again closely associated with glacial deposits and oxidized paleosols (Rainbird, Nesbitt, and Donaldson, 1990). The initial increase in sulfur isotope fractionation is recorded in beds immediately overlying the Gowganda Formation (Hattori, Krouse, and Campbell, 1983).

In Paleoproterozoic sedimentary rocks of Australia and elsewhere, paleontological and biomarker studies indicate the presence of oxygenic photoautotrophs as well as eukaryotes as old as 2.7 Ga (Summons and others, 1999; Brocks and others, 1999). It is possible, however, that these microorganisms evolved in local environments before the atmosphere and hydrosphere became fully oxygenated. Lastly, the discovery of mass-independent sulfur isotope fractionations in early Paleoproterozoic sedimentary sulfates and sulfides – theoretically linked to photochemical reactions in an ozone-depleted atmosphere (Farquhar and others, 2000) – support the view of an earlier, approx 2.4 Ga ago, rise in oxygen.

It is likely that atmospheric oxygen levels continued to rise from the time of upper Duitschland deposition through the extreme biogeochemical anomaly around 2.1 to 2.2 Ga (Karhu and Holland, 1996). However, if surface oxidation was tied to modulation in the organic carbon burial flux (Des Marais and others, 1992; Derry, Kaufman, and Jacobsen, 1992; Kaufman, Jacobsen, and Knoll, 1993; Des Marais, 1997) atmospheric oxygen contents may have similarly oscillated through this interval. The

reappearance of a large province of 2.1 to 1.9 Ga sedimentary iron formation in strata above equivalents of Huronian beds (Isley, 1995; Simonson and Hassler, 1996) suggests that the deep ocean was not irreversibly oxidized, even after the carbon isotope event described by Karhu and Holland (1996). In sum, the lithologic and geochemical data tied to new age constraints from South Africa suggest that the oxygen content of the Paleoproterozoic atmosphere oscillated accordingly to changes in the carbon cycle, perhaps closely associated with biological and tectonic events.

CONCLUSIONS

As demonstrated here, the emerging temporal pattern of Paleoproterozoic carbon isotope variations and glaciation has a close analogue to Neoproterozoic events, suggesting a coupling of climatic and biogeochemical changes at either end of the eon. In both intervals a marked decrease in atmospheric CO_2 levels, either through high productivity and burial of organic carbon (Kaufman, Knoll, and Narbonne, 1997) or by intense weathering (Hoffman and Schrag, 2000), may have resulted in global glaciation (Hoffman and others, 1998). In the context of the Proterozoic Eon as a whole however, it is notable that the intervening Mesoproterozoic (1.0-1.7 Ga) interval lacks evidence of glaciation or of extreme $\delta^{13}C$ excursions (Buick, Des Marais, and Knoll, 1995; Knoll, Kaufman, and Semikhatov, 1995; Brasier and Lindsay, 1998; Kah and others, 1999). Furthermore, there are some unresolved differences between Neoproterozoic and Paleoproterozoic $\delta^{13}C$ excursions and environmental perturbations. Contrary to prediction (Kaufman, 1997), there is no known significant ^{13}C enrichment in carbonate unit below the Duitschland diamictite and above the Penge Iron Formation and potential equivalents worldwide. Similarly, the end of the Paleoproterozoic carbon isotope excursion at approx 2.1 Ga is not marked by recognized glacial phenomenon. While these discrepancies might be the result of omissions in these truly ancient stratigraphic records, they might also be real. In either case they warrant further investigation.

REFERENCES

Altermann, W., and Nelson, D. R., 1998, Sedimentation rates, basin analyses, and regional correlations of three Neoarchaean and Paleoproterozoic sub-basins of the Kaapvaal Craton as implied by precise SHRIMP U-Pb zircon ages from volcanic sediments: Journal of Sedimentary Geology, v. 120, p. 225-256.

Baker, A. J., and Fallick, A. E., 1989, Evidence from Lewisian limestones for isotopically heavy carbon in two-thousand-million-year-old sea water: Nature, v. 337, p. 352-354.

Banner, J. L., and Hanson, G. N., 1990, Calculation of simultaneous isotopic and trace element variations during water-rock interaction with application to carbonate diagenesis: Geochimica et Cosmochimica Acta, v. 54, p. 3123-3137.

Barley, M. E., Pickard, A. L., and Silvester, P. J., 1997, Emplacement of a large igneous province as a possible cause of banded iron formation 2.45 billion years ago: Nature, v. 385, p. 55-58.

Bau, M., Romer, R. L., Lüders, V., and Beukes, N. J., 1999, Pb, O, and C isotopes in silicified Mooidraai dolomite (Transvaal Supergroup, South Africa): implications for the composition of Paleoproterozoic seawater and 'dating' the increase of oxygen in the Precambrian atmosphere: Earth and Planetary Science Letters, v. 174, p. 43-57.

Bekker, A., Eriksson, K. A., Kaufman, A. J., Karhu, J. A., and Beukes, N. J., 1999, Paleoproterozoic record of biogeochemical events and ice ages: Geological Society of America, Annual Meeting, Abstracts with Programs, v. 31, no. 7, p. A-487.

Bekker, A., and Karhu, J. A., 1996, Study of carbon isotope ratios in carbonates of the Early Proterozoic Snowy Pass Supergroup, WY and its application for correlation with the Chocolay Group, MI and Huronian Supergroup, ON [abstract]: Institute on Lake Superior Geology, 42nd Annual Meeting, Cable, Wisconsin, 1996, Proceedings, v. 42, part 1, p. 4-5.

Bekker, A., Karhu, J. A., and Bennett, G., 1996, Lomagundi event in North America: application for stratigraphic correlation: Geological Society of America, Annual Meeting, Abstracts with Programs, v. 28, no. 7, p. A-229.

Berry, J. A., 1988, Studies of mechanisms affecting the fractionation of carbon isotopes in photosynthesis, *in* Ehleringer, J. R., and Nagy, K. A., editors, Stable isotopes in Ecological Research: New York, Springer-Verlag, p. 82-94.

Beukes, N. J., 1983, Paleoenvironmental setting of iron-formations in the depositional basin of the Transvaal Supergroup, South Africa, *in* Trendall, A. F., and Morris, R. C., editors, Iron-formations: Facts and problems: Amsterdam, Elsevier, p. 131-209.

Beukes, N. J., Bekker, A., Swart, Q., Dorland, H., Van Niekerk, H. S., Gutzmer, J., Karhu, J. A., and Kaufman, A. J., 2001, Implications of carbon isotope values of South African carbonates for the Paleoproterozoic secular carbon isotope curve: European Union of Geoscientists, Abstract Supplement, v. 13, no. 1, p. 88.

Beukes, N. J., Gutzmer, J., and Dorland, H., 1999, Paleoproterozoic laterites, supergene iron and manganese ores and atmospheric oxygen: Geological Society of Australia Abstracts, p. 20-23.

Beukes, N. J., Klein, C., Kaufman, A. J., and Hayes, J. M., 1990, Carbonate petrology, kerogen distribution, and carbon and oxygen isotope variations in an Early Proterozoic transition from limestone to iron-formation deposition, Transvaal Supergroup, South Africa: Economic Geology, v. 85, p. 663-690.

Bidigare, R. R., and 14 others, 1997, Consistent fractionation of ^{13}C in nature and in the laboratory: Growth rate effects in some haptophyte algae: Global Biogeochemical Cycles, v. 11, p. 279-292.

Bidigare, R. R., and 11 others, 1999, Iron-stimulated changes in ^{13}C fractionation and export by equatorial Pacific phytoplankton: Toward a paleogrowth rate proxy: Paleoceanography, v. 14, p. 589-595.

Brasier, M. D., and Lindsay, J. F., 1998, A billion years of environmental stability and the emergence of eukaryotes: New data from northern Australia: Geology, v. 26, p. 555-558.

Brocks, J. J., Logan, G. A., Buick, R., and Summons, R. E., 1999, Archean molecular fossils and the early rise of eukaryotes: Science, v. 285, p. 1033-1036.

Broecker, W. S., 1970, A boundary condition of the evolution of atmospheric oxygen: Journal of Geophysical Research, v. 75, p. 3553-3557.

Buchan, K. L., Mortensen, J. K., Card, K. D., and Percival, J. A., 1998, Paleomagnetism and U-Pb geochronology of diabase dyke swarms of Minto block, Superior Province, Quebec, Canada: Canadian Journal of Earth Sciences, v. 35, p. 1054-1069.

Bühn, B., Stanistreet, I. G., and Okrusch, M., 1992, Late Proterozoic outer shelf manganese and iron deposits at Otjosondu (Namibia) related to the Damaran oceanic opening: Economic Geology, v. 87, p. 1393-1411.

Buick, I. S., Uken, R., Gibson, R. L., and Wallmach, T., 1998, High-$\delta^{13}C$ Paleopoterozoic carbonates from the Transvaal Supergroup, South Africa: Geology, v. 26, p. 875-878.

Buick, R., Des Marais, D. J., and Knoll, A. H., 1995, Stable isotopic compositions of carbonates from the Mesoproterozoic Bangemall Group, northwestern Australia: Chemical Geology, v. 123, p. 153-171.

Button, A., 1986, The Transvaal sub-basin of the Transvaal sequence, *in* Anhaeusser, C. R., and Maske, S., editors, Mineral deposits of Southern Africa, v. 1: Johannesburg, Geological Society of South Africa, p. 811-817.

Caldeira, K., and Kasting, J. F., 1992, Susceptibility of the early Earth to irreversible glaciation caused by carbon dioxide clouds: Nature, v. 359, p. 226-228.

Calver, C. R., 2000, Isotope stratigraphy of the Ediacarian (Neoproterozoic III) of the Adelaide Rift Complex, Australia, and the overprint of water column stratification: Precambrian Research, v. 100, p. 121-150.

Cameron, E. M., 1982, Sulphate and sulphate reduction in early Precambrian oceans: Nature, v. 296, p. 145-148.

Cheney, E. S., and Twist, D., 1991, The conformable emplacement of the Bushveld mafic rocks along a regional unconformity in the Transvaal succession of South Africa: Precambrian Research, v. 52, p. 115-132.

Coale, K. H., and 18 others, 1996, A massive phytoplankton bloom induced by an ecosystem-scale iron fertilization experiment in the equatorial Pacific Ocean: Nature, v. 383, p. 495-501.

Coetzee, L.L., ms, 2001, Genetic stratigraphy of the Paleoproterozoic Pretoria Group in the western Transvaal: M.S. thesis, Rand Afrikaans University, Johannesburg, 195 p.

Corfu, F., and Andrews, A. J., 1986, A U-Pb age for mineralized Nipissing diabase, Gowganda, Ontario: Canadian Journal of Earth Sciences, v. 23, p. 107-109.

Cornell, D. H., Armstrong, R. A., and Walraven, F., 1998, Geochronology of the Proterozoic Hartley Basalt Formation, South Africa: constraints on the Kheis tectogenesis and the Kaapvaal Craton's earliest Wilson cycle: Journal of African Earth Sciences, v. 26, p. 5-27.

Cornell, D. H., Schütte, S. S., and Englinton, B. L., 1996, The Ongeluk basaltic andesite formation in Griqualand West, South Africa: submarine alteration in a 2222 Ma Proterozoic sea: Precambrian Research, v. 79, p. 101-123.

Corsetti, F. A., and Kaufman, A. J., 1999, Tossing Neoproterozoic snowballs between Death Valley, USA and Namibia: Geological Society of America, Annual Meeting, Abstracts with Programs, v. 31, no. 7, p. A-486.

Derry, L. A., Kaufman, A. J., and Jacobsen, S. B., 1992, Sedimentary cycling and environmental change in the Late Proterozoic: evidence from stable and radiogenic isotopes: Geochimica et Cosmochimica Acta, v. 56, p. 1317-1329.

Des Marais, D. J., 1997, Isotopic evolution of the biogeochemical carbon cycle during the Proterozoic Eon: Organic Geochemistry, v. 27, no. 5-6, p. 185-193.

Des Marais, D. J., Strauss, H., Summons, R. E., and Hayes, J. M., 1992, Carbon isotope evidence for the stepwise oxidation of the Proterozoic environment: Nature, v. 359, p. 605-609.

Dorland, H. C., ms, 1999, Paleoproterozoic laterites, red beds and ironstones of the Pretoria Group with reference to the history of atmospheric oxygen: M.S. thesis, Rand Afrikaans University, Johannesburg, 147 p.

Eriksson, P. G., and Reczko, B. F. F., 1998, Contourites associated with pelagic mudrocks and distal delta-fed turbidites in the Lower Proterozoic Timeball Hill Formation epeiric basin (Transvaal Supergroup), South Africa: Sedimentary Geology, v. 120, p. 319-335.

Evans, D. A., Beukes, N. J., and Kirschvink, J. L., 1997, Low-latitude glaciation in the Paleoproterozoic era: Nature, v. 386, p. 262-266.

Fairchild, I. J., Marshall, J. D., and Bertrand-Sarfati, J., 1990, Stratigraphic shifts in carbon isotopes from Proterozoic stromatolitic carbonates (Mauritania): influence of primary mineralogy and diagenesis: American Journal of Science, v. 290-A, p. 46-79.

Falkowski, P. G., Barber, R. T., and Smetacek, V., 1998, Biogeochemical controls and feedbacks on ocean primary productivity: Science, v. 281, p. 200-206.

Farquhar, J., Bao, H., and Thiemens, M., 2000, Atmospheric influence of Earth's earliest sulfur cycle: Science, v. 289, p. 756-758.

Freeman, K. H., and Hayes, J. M., 1992, Fractionation of carbon isotopes by phytoplankton and estimates of ancient CO_2 levels: Global Biogeochemical Cycles, v. 6, p. 185-198.

Gorokhov, I. M., Semikhatov, M. A., Baskakov, A. V., Kutyavin, E. P., Mel'nikov, N. N., Sochava, A. V., and Turchenko, T. L., 1995, Sr isotopic composition in Riphean, Vendian, and Lower Cambrian carbonates from Siberia: Stratigraphy and Geological Correlation, v. 3, p. 1-28.

Grotzinger, J. P., 1994, Trends in Precambrian carbonate sediments and their implication for understanding evolution, *in* Bengtson, S., editor, Early Life on Earth, Nobel Symposium no. 84: New York, Columbia University Press, p. 245-258.

Gutzmer, J., and Beukes, N. J., 1996, Karst-hosted fresh-water Paleoproterozoic Manganese deposits, Postmasburg, South Africa: Economic Geology, v. 91, p. 1435-1454.

Hattori, K., Krouse, H. R., and Campbell, F. A., 1983, The start of sulfur oxidation in continental environments: about 2.2 x 10^9 years ago: Science, v. 221, p. 549-551.

Hayes, J. M., 1983, Geochemical evidence earing on the origin of the aerobiosis; a speculative hypothesis, *in* Schopf, J. W., editor, Earth's Earliest Biosphere: Its origin and evolution: Princeton, New Jersey, Princeton University Press, p. 291-301.

Hayes, J. M., Kaplan, I. R., and Wedeking, K. W., 1983, Precambrian organic geochemistry, preservation of the record, *in* Schopf, J. W., editor, Earth's Earliest Biosphere: Its origin and evolution: Princeton, New Jersey, Princeton University Press, p. 93-134.

Hayes, J. M., Strauss, H., and Kaufman, A. J., 1999, The abundance of ^{13}C in marine organic matter and isotopic fractionation in the global biogeochemical cycle of carbon during the past 800 Ma: Chemical Geology, v. 161, p. 103-125.

Heaman, L. M., 1997, Global mafic magmatism at 2.45 Ga: Remnants of an ancient large igneous province?: Geology, v. 25, p. 299-302.

Hegenberger, W., 1993, Stratigraphy and sedimentology of the late Precambrian Witvlei and Nama groups, east of Windhoek: Geological Survey of Namibia, Memoir, 17, 82 p.

Hoffman, P. F., 1975, Shoaling-upward shale-to-dolomite cycles in the Rocknest Formation (lower Proterozoic), Northwest Territories, Canada, *in* Ginsburg, R. N., editor, Tidal deposits: New York, Springer-Verlag, p. 257-265.

Hoffman, P. F., Kaufman, A. J., Halverson, G. P., 1998, Comings and goings of global glaciations on a Neoproterozoic tropical platform in Namibia: GSA Today, v. 8, no. 5, p. 1-9.

Hoffman, P. F., Kaufman, A. J., Halverson, G. P., and Schrag, D. P., 1998, A Neoproterozoic Snowball Earth: Science, v. 281, p. 1342-1346.

Hoffman, P. F., and Schrag, D. P., 2000, Snowball Earth: Scientific American, no. 1, p. 68-75.

Holland, H. D., 1994, Early Proterozoic atmospheric change, *in* Bengston, S. editor, Early Proterozoic life on Earth, Nobel Symposium no. 84: New York, Columbia University Press, p. 237-241.

Isley, A. E., 1995, Hydrothermal plumes and the delivery of iron to banded iron formation: The Journal of Geology, v. 103, p. 169-185.

Iyer, S. S., Babinski, M., Krouse, H. R., and Chemale, F. Jr., 1995, Highly ^{13}C-enriched carbonate and organic matter in the Neoproterozoic sediments of the Bambuí Group, Brazil: Precambrian Research, v. 73, p. 271-282.

Jacobsen, S. B., and Kaufman, A. J., 1999, The Sr, C and O isotopic evolution of Neoproterozoic sea water: Chemical Geology, v. 161, p. 37-57.

Jasper, J. J., and Hayes, J. M., 1990, A carbon-isotopic record of CO_2 levels during the Late Quaternary: Nature, v. 347, p. 462-464.

Kah, L. C., and Knoll, A. H., 1996, Microbenthic distribution of Proterozoic tidal flats: envirnomental and taphonomic considerations: Geology, v. 24, p. 79-82.

Kah, L. C., Sherman, A. G., Narbonne, G. M., Knoll, A. H., and Kaufman, A. J., 1999, $\delta^{13}C$ stratigraphy of the Proterozoic Bylot Supergroup, Baffin Island, Canada: implications for regional lithostratigrpahic correlations: Canadian Journal of Earth Sciences, v. 36, p. 313-332.

Karhu, J. A., 1993, Paleoproterozoic evolution of the carbon isotope ratios of sedimentary carbonates in the Fennoscandian Shield: Geological Survey of Finland Bulletin 371, 87 p.

Karhu, J. A. and Holland, H. D., 1996, Carbon isotopes and the rise of atmospheric oxygen: Geology, v. 24, no. 10, p. 867-870.

Kasting, J. F., 1987, Theoretical constraints on oxygen and carbon dioxide concentrations in the Precambrian atmosphere: Precambrian Research, v. 34, p. 205-229.

Kaufman, A. J., 1997, An ice age in the tropics: Nature, v. 386, p. 227-228.

Kaufman, A. J., Hoffman, P. F., and Halverson, G. P., 1997, Comings and goings of Neoproterozoic ice ages in Namibia: Geological Society of America, Annual Meeting, Abstracts with Programs, v. 29, no. 7, p. A-196.

Kaufman, A. J., Jacobsen, S. B., and Knoll, A. H., 1993, The Vendian record of Sr and C isotopic variations in seawater: Implications for tectonics and paleoclimate: Earth and Planetary Science Letters, v. 120, p. 409-430.

Kaufman, A. J., and Knoll, A. H., 1995, Neoproterozoic variations in the C-isotopic composition of seawater: stratigraphic and biogeochemical implications: Precambrian Research, v. 73, p. 27-49.

Kaufman, A. J., Knoll, A. H., and Awramik, S. M., 1992, Biostratigraphic and chemostratigraphic correlation of Neoproterozoic sedimentary successions: Upper Tindir Group, northwestern Canada, as a test case: Geology, v. 20, p. 181-185.

Kaufman, A. J., Knoll, A. H., and Narbonne, G. M., 1997, Isotopes, ice ages, and terminal Proterozoic earth history: National Academy of Science, Proceedings, v. 94, p. 6600-6605.

Kennedy, M. J., Runnegar, B., Prave, A. R., Hoffmann, K.-H., Arthur, M. A., 1998, Two or four Neoproterozoic glaciations?: Geology, v. 26, p. 1059-1063.

Kirschvink, J. L., 1992, Late Proterozoic low-latitude global glaciation: the snowball Earth, *in* J. W. Schopf and C. Klein, editors, The Proterozoic biosphere: a multidisciplinary study: Cambridge, United Kingdom, Cambridge University Press, p. 51-52.

Kirschvink, J. L., Gaidos, E. J., Bertani, L. E., Beukes, N. J., Gutzmer, J., Maepa, L. N., and Steinberger, R. E., 2000, The Paleoproterozoic Snowball Earth: extreme climatic and geochemical global change and its biological consequences: National Academy of Science, Proceedings, v. 97, p. 1400-1405.

Knoll, A. H., Kaufman, A. J., and Semikhatov, M. A., 1995, The carbon isotopic composition of Proterozoic carbonates: Riphean successions from northwestern Siberia (Anabar Massif, Turukhansk Uplift): American Journal of Science, v. 295, p. 823-850.

Krogh, T. E., Davis, D. W., and Corfu, F., 1984, Precise U-Pb zircon and baddeleyite ages for the Sudbury area, *in* Pye, E. G., Naldrett, A. J., and Giblin, P. E., editors, The Geology and ore deposits of the Sudbury structure: Ontario Geological Survey, Special Volume 1, p. 431-446.

Kump, L. R., Arthur, M. A., Patzkowsky, M. E., Gibbs, M. T., Pinkus, D. S., and Sheehan, P. M., 1999, A weathering hypothesis for glaciation at high atmospheric pCO_2 during the Late Ordovician: Palaeogeography, Palaeoclimatology, Palaeoecology, v. 152, p. 173-187.

Li, R., Chen, J., Zhang, S., Lei, J., Shen, Y., and Chen, X., 1999, Spatial and temporal variations in carbon and sulfur isotopic compositions of Sinian sedimentary rocks in the Yangtze platform, South China: Precambrian Research, v. 97, pp. 59-75.

Marmo, J. S., 1992, The Lower Proterozoic Hokkalampi Paleosol in North Karelia, Eastern Finland, *in* Schidlowski, M., Golubic, M., Kimberley, M. M., McKirdy, D. M., and Trudinger, P. A., editors, Early Organic Evolution: Implications for Mineral and Energy Resources: Berlin, Germany, Springer-Verlag, p. 41-66.

Martin, D. McB., Clendenin, C. W., Krapez, B., and McNaughton, N. J., 1998, Tectonic and geochronological constraints on late Archaean and Palaeoproterozoic stratigraphic correlation within and between the Kaapvaal and Pilbara Cratons: Journal of the Geological Society, London, v. 155, p. 311-322.

Martini, J. E. J., 1979, A copper-bearing bed in the Pretoria Group in Northeastern Transvaal, in Geokongress '77: Geological Society of South Africa Special Publication 6, p. 65-72.

Master, S., Verhagen, B. H., Bassot, J. P., Beukes, N. J., and Lemoine, S., 1993, Stable isotopic signatures of Paleoproterozoic carbonate rocks from Guinea, Senegal, South Africa and

Zimbabwe: constraints on the timing of the ca. 2.0 Ga "Lomagundi" $\delta^{13}C$ excursion, Symposium: Early Proterozoic geochemical and structural constraints – metallogeny: Publication Occasionnelle 1993/23, p. 38-41.

McNaughton, N. J., and Pollard, P. J., 1993, Cassiterite: Potential for direct dating of mineral deposits and a precise age for the Bushveld Complex granites: comments and reply: Geology, v. 21, p. 285-286.

Melezhik, V. A., and Fallick, A. E., 1996, A widespread positive $\delta^{13}C_{carb}$ anomaly at around 2.33 - 2.06 Ga on the Fennoscandian Shield: a paradox?: Terra Nova, v. 8, p. 141-157.

Melezhik, V. A., Fallick, A. E., and Clark, T., 1997, Two billion year old isotopically heavy carbon: evidence from the Labrador Trough, Canada: Canadian Journal of Earth Sciences, v. 34, p. 271-285.

Melezhik, V. A., Fallick, A. E., Medvedev, P. V., and Makarikhin, V. V., 1999, Extreme $^{13}C_{carb}$ enrichment in ca. 2.0 Ga magnesite-stromatolite-dolomite- 'red beds' association in a global context: a case for the world-wide signal enhanced by a local environment: Earth-Science Reviews, v. 48, p. 71-120.

Mertanen, S., Halls, H. C., Vuollo, J. I., Pesonen, L. J., and Stepanov, V. S., 1999, Paleomagnetism of 2.44 Ga mafic dikes in Russian Karelia, eastern Fennoscandian Shield – implications for continental reconstructions: Precambrian Research, v. 98, p. 197-221.

Misi, A., and Veizer, J., 1998, Neoproterozoic carbonate sequences of the Una Group, Irece Basin, Brazil: chemostratigraphy, age and correlations: Precambrian Research, v. 89, p. 87-100.

Montañez, I. P., Banner, J. L., Osleger, D. A., Borg, L. E., Bosserman, P. J., 1995, Integrated Sr isotope variations and sea-level history of Middle to Upper Cambrian platform carbonates: Implications for the evolution of Cambrian seawater $^{87}Sr/^{86}Sr$: Geology, v. 24, p. 917-920.

Nelson, D. R., Trendall, A. F., and Altermann, W., 1999, Chronological correlations between the Pilbara and Kaapvaal cratons: Precambrian Research, v. 97, p. 165-189.

Ohmoto, H., 1997, When did the Earth's atmosphere become oxic?: The Geochemical News, no. 93, p. 12 - 13, 26-27.

Ojakangas, R. W., 1985, Evidence for Early Proterozoic glaciation: the dropstone unit - diamictite association: Geological Survey of Finland, Bulletin 331, p. 51-72.

Park, J. K., 1997, Paleomagnetic evidence for low-latitude glaciation during deposition of the Neoproterozoic Rapitan Group, Mackenzie Mountains, N.W.T., Canada: Canadian Journal of Earth Sciences, v. 34, p. 34-49.

Pedersen, T. F., and Calvert, S. E., 1990, Anoxia vs. productivity; what controls the formation of organic carbon rich sediments and sedimentary rocks: American Association of Petroleum Geologists Bulletin, v. 74, p. 454-466.

Popp, B. N., Laws, E. A., Bidigare, R. R., Dore, J. E., Hanson, K. L., and Wakeham, S. G., 1998, Effect of phytoplankton cell geometry on carbon isotope fractionation: Geochimica et Cosmochimica Acta, v. 62, p. 69-77.

Rainbird, R. H., and Donaldson, J. A., 1988, Nonglaciogenic deltaic deposits in the early Proterozoic Gowganda Formation, Cobalt Basin, Ontario: Canadian Journal of Earth Sciences, v. 25, p. 710-724.

Rainbird, R. H., Nesbitt, H. W., and Donaldson, J. A., 1990, Formation and diagenesis of sub-Huronian saprolith: comparison with a modern weathering profile: Journal of Geology, v. 98, p. 801-822.

Reczko, B. F. F., Eriksson, P. G., and Snyman, C. P., 1995, Some evidence for the base-metal potential of the Pretoria Group: stratigraphic targets, tectonic setting and REE patterns: Mineralum Deposita, v. 30, p. 162-167.

Riebesell, U., Wolf-Gladrow, D. A., and Smetacek, V., 1993, Carbon dioxide limitation of marine phytoplankton growth rates: Nature, v. 361, p. 249-251.

Rye, R., and Holland, H. D., 1998, Paleosols and the evolution of atmospheric oxygen: A critical review: American Journal of Science, v. 298, p. 621-672.

Schidlowski, M., Eichmann, R., and Junge, C., 1976, Carbon isotope geochemistry of the Precambrian Lomagundi carbonate province, Rhodesia: Geochimica et Cosmochimica Acta, v. 40, p. 449-455.

-------1975, Precambrian sedimentary carbonates: Carbon and oxygen isotope geochemistry and implications for the terrestrial oxygen budget: Precambrian Research, v. 2, p. 1-69.

Schmidt, P. W., and Williams, G. E., 1999, Paleomagnetism of the Paleoproterozoic hematitic breccia and paleosol at Ville-Marie, Québec: further evidence for the low paleolatitude of Huronian glaciation: Earth and Planetary Science Letters, v. 172, p. 273-285.

Schmidt, P. W., Williams, G. E., and Embleton, B. J. J., 1991, Low palaeolatitude of Late Proterozoic glaciation: early timing of remanence in haematite of the Elatina Formation, South Australia: Earth and Planetary Science Letters, v. 105, p. 355-367.

Schreiber, U. M., and Eriksson, P. G., 1992, An Early Paleoproterozoic braid-delta system in the Pretoria Group, Transvaal Sequence, South Africa: Journal of African Earth Sciences, v. 15, no. 1, p. 111- 125.

Simonson, B. M., and Hassler, S. W., 1996, Was the deposition of large Precambrian iron formations linked to major marine transgressions?: The Journal of Geology, v. 104, p. 665-676.

Sohl, L. E., Christie-Blick, N., and Kent, D. V., 1999, Paleomagnetic polarity reversals in Marinoan (ca. 600 Ma) glacial deposits of Australia: Implications for the duration of low-latitude glaciation in Neoproterozoic time: Geological Society of America Bulletin, v. 111, p. 1120-1139.

Steyn, M. v. R., Gardyne, W. N., and Klop, A. A. C., 1986, The Gopane manganese deposits, Bophuthatswana, *in* Anhaeusser, G. R., and Maske, S., editors: Mineral deposits of Southern Africa, v. 2, p. 985-989.

Summons, R. E., Jahnke, L. L., Hope, J. M., and Logan, G. A., 1999, 2-Methylhopanoids as biomarkers for cyanobacterial oxygenic photosynthesis: Nature, v. 400, p. 554-557.

Sumner, D. Y., and Bowring, S. A., 1996, U-Pb geochronologic constraints on deposition of the Campbellrand Subgroup, Transvaal Supergroup, South Africa: Precambrian Research, v. 79, p. 25-35.

Sumner, D. Y., and Grotzinger, J. P., 1993, Numerical modelling of ooid size and the problem of Neoproterozoic giant ooids: Journal of Sedimentary Petrology, v. 63, p. 974-982.

Swart, Q. D., M.S., 1999, Carbonate rocks of the Paleoproterozoic Pretoria and Postmasburg Groups, Transvaal Supergroup: M.S. thesis, Rand Afrikaans University, Johannesburg, South Africa, 126 p.

Swett, K., and Knoll, A. H., 1989, Marine pisolites from Upper Proterozoic carbonates of East Greenland and Spitsbergen: Sedimentology, v. 36, p. 75-93.

Tsikos, H., and Moore, J. M., 1997, Petrography and geochemistry of the Paleoproterozoic Hotazel Iron-Formation, Kalahari Manganese Field, South Africa: implications for Precambrian manganese metallogenesis: Economic Geology, v. 92, p. 87-97.

Tucker, M. E., 1986, Formerly aragonitic limestones associated with tillites in the Late Proterozoic of Death Valley, California: Journal of Sedimentary Petrology, v. 56, p. 818-830.

Urban, H., Stribrny, B., and Lippolt, H. J., 1992, Iron and manganese deposits of the Urucum District, mato Grosso do Sul, Brazil: Economic Geology, v. 87, p. 1375-1392.

Valley, J., 1986, Stable isotope geochemistry of metamophic rocks, *in* Valley, J. W., Taylor, H. P., and O'Neil, J. R., editors, Stable isotopes in high temperature geological processes: Mineralogical Society of America Reviews in Mineralogy, v. 26, p. 445-489.

Van Capellan, P., and Ingall, E. D., 1994, Benthic phosphorous regeneration, net primary production and ocean anoxia: A model for coupled marine biogeochemical cycles of carbon and phosphorous: Paleoceanography, v. 9, p. 677-692.

Veizer, J., 1983, Chemical diagenesis of carbonates: theory and application, *in* Arthur, M. A., Anderson, T. F., Kaplan, I. R., Veizer, J., and Land, L. S., editors, Stable isotopes in Sedimentary Geology: Society of Economic Paleontologists and Mineralogists, Short Course, 10: 3-1 - 3-100.

Veizer, J., Clayton, R. N., and Hinton, R. W., 1992, Geochemistry of Precambrian carbonates: IV. Early Paleoproterozoic (2.25 ± 0.25 Ga) seawater: Geochimica et Cosmochimica Acta, v. 56, p. 875-885.

Veizer, J., Plumb, K. A., Clayton, R. N., Hinton, R. W., and Grotzinger, J. P., 1992, Geochemistry of Precambrian carbonates: V. Late Paleoproterozoic seawater: Geochimica et Cosmochimica Acta, v. 56, p. 2487-2501.

Visser, J. N. J., 1971 - 1972, The Timeball Hill Formation at Pretoria - A prograding shore-line deposit: Annals of the Geological Survey, Pretoria (South Africa), v. 9, p. 115-118.

-------1981, The Mid-Precambrian tillite in the Griqualand West and Transvaal Basins, South Africa, *in* Hambrey, M. J., and Harland, W. B., editors, Earth's pre-Pleistocene glacial record: New York, Cambridge University Press, p. 180-184.

Walraven, F., 1997, Geochronology of the Rooiberg Group, Transvaal Supergroup, South Africa: Economic Geology Research Unit, University of the Witwatersrand, Information Circular, v. 316, 21 p.

Walraven, F., Armstrong, R. A., and Kruger, F. J., 1990, A chronostratigraphic framework for the north-central Kaapvaal craton, the Bushveld Complex and the Vredefort structure: Tectonophysics, v. 171, p. 23-48.

Williams, G. E., and Schmidt, P. W., 1997, Paleomagnetism of the Paleoproterozoic Gowganda and Lorrain formations, Ontario: low paleolatitude for Huronian glaciation: Earth and Planetary Science Letters, v. 153, p. 157-169.

Williams, H., Hoffman, P. F., Lewry, J. F., Monger, J. W. H., and Rivers, T., 1991, Anatomy of North America: thematic geologic portrayals of the continent: Tectonophysics, v. 187, p. 117-134.

Wood, J., 1979, No. 18 Regional Geology of the Cobalt Embayment, District of Sudbury, Nipissing, and Timiskaming: Summary of Fieldwork, Ontario Geological Survey, Miscellaneous paper 90, p. 79-81.

Young, G. M., 1973, Tillites and aluminous quartzites as possible time markers for middle Precambrian (Aphebian) rocks of North America, *in* Young, G. M., editor, Huronian Stratigraphy and Sedimentation: Geological Association of Canada, Special Paper, 12, p. 97-127.

Young, G. M., 1988, Proterozoic plate tectonics, glaciation and iron-formations: Sedimentary Geology, v. 58, p. 127-144.

CHAPTER 2

A PALEOPROTEROZOIC DROWNED CARBONATE PLATFORM ON THE SOUTHEASTERN MARGIN OF THE WYOMING CRATON: A RECORD OF THE KENORLAND BREAKUP

ABSTRACT. The Nash Fork Formation in the upper part of the early Paleoproterozoic Snowy Pass Supergroup, Medicine Bow Mountains of Wyoming was deposited on a mature passive margin along the southern flank of the Wyoming Craton and straddles the end of the ca. 2.2-2.1 Ga carbon isotope excursion. Two drowning events marked by black shales subdivide the carbonate platform into three parts. The lower Nash Fork Formation consists of outer shelf to peritidal deposits represented by massive and stromatolitic dolomites, heterolithic siliciclastics-carbonates, large silicified domal digitate stromatolites, nodular dolomites and stromatolitic dolomites. Molds after evaporite crystals are pervasive in the heterolithic siliciclastics-carbonates. Large silicified domal digitate stromatolites formed biostromes and bioherms following flooding events. The middle Nash Fork Formation comprises two intervals of black shale separated by inner shelf heterolithic siliciclastics-nodular carbonates. Black shales are organic- and pyrite-rich, contain turbidites and developed in response to drowning of the platform. Overlying massive dolomite of the upper Nash Fork Formation was deposited in an outer shelf setting and displays an upward-shallowing trend terminated by a prominent karstic surface in the middle of the unit. The Nash Fork Formation is open-marine with no evidence for restricted circulation on the carbonate platform. The two drowning events on the carbonate platform are likely related to dissection of the mature passive margin associated with the breakup of Kenorland. The younger drowning event is associated with the end of the carbon isotope excursion.

The main building elements of the lower and middle Nash Fork carbonate platform are dolomitic mudstones, stromatolites and dolosiltites. Macroscopic seafloor precipitates are lacking with the exception of tufa deposits and domes in the massive and stromatolitic dolomites and, possibly, digitate stromatolites within domal digitate stromatolites. The upper Nash Fork Formation comprises dolomitic mudstones, relatively rare stromatolites and inorganic

precipitates that are more common than in the underlying carbonates. Styles of carbonate deposition on this early Paleoproterozoic platform differ from those documented on late Archean carbonate platforms; there are fewer macroscopic seafloor precipitates and more dolomitic mudstones. This pattern is considered to be related to a rise of the atmospheric oxygen level that led to a decrease in bicarbonate saturation in the ocean.

INTRODUCTION

The early Paleoproterozoic (2.5-2.0 Ga) was marked by a series of major events including: 1) protracted rifting of a northern supercontinent that may have started at ca. 2.45 Ga and which led to the breakup of the Kenorland (Heaman, 1997); 2) global glaciations (Ojakangas, 1988) that are interpreted to have extended into low latitudes (Evans et al., 1997; Williams and Schmidt, 1997; Buchan et al., 1998; Schmidt and Williams, 1999; Mertanen, 2001); and 3) high relative burial rates of organic carbon that probably led to a rise in the level of atmospheric oxygen (Karhu and Holland, 1996). These events undoubtedly influenced carbonate deposition, which is an excellent record of environmental changes (Grotzinger and James, 2000).

Protracted rifting of northern continents led to the final breakup of the Late Archean supercontinent (*Kenorland*). The age of the breakup is constrained in Fennoscandia and on the eastern margin of the Hearne Province, Canada to 2.1-2.0 Ga (Kohonen, 1995; Aspler and Chiarenzelli, 1998). The same time is also marked by the Trans-Amazonian Orogeny in South America and West Africa (Ledru et al., 1994; Machado et al., 1996) and by a collisional event in Tanzania (Möller et al., 1995**)**. These events probably led to large-scale fluctuations in sea level that can be used for interbasinal correlations. Since the record of eustatic changes is least complicated by tectonic processes on mature passive margins, such margins are especially appropriate for studies of eustatic controls on relative sea-level changes.

Considerable attention has been paid in the last two decades to the evolution of carbonate production on Archean (e.g. Beukes, 1987; Simonson et al., 1993; Sumner, 1997), middle Paleoproterozoic (e.g. Cecile and Campbell, 1978; Grotzinger, 1986a, b; Sami and James, 1993, 1994, 1996; Sami et al., 2000; Pope and Grotzinger, 2000) and Mesoproterozoic (e.g. Kah and Knoll, 1996; Sherman et al., 2000) carbonate platforms. These studies have shown that

inorganic precipitation played an important role in carbonate production on Archean and, to a smaller extent, Paleoproterozoic platforms but was restricted to shallow-water, evaporitic settings during the Mesoproterozoic (Grotzinger and James, 2000). This trend has been explained by bicarbonate supersaturation in Archean and Paleoproterozoic oceans when carbonate precipitation within the water column was inhibited by high concentrations of iron and manganese (Sumner and Grotzinger, 2000). Few studies have been carried out on early Paleoproterozoic carbonate platforms on which Fe and Mn inhibition of carbonate precipitation was probably suppressed by a rise in the level of atmospheric oxygen. It might be expected that early Paleoproterozoic carbonate platforms would be marked by extensive carbonate mud deposition, a decrease in bicarbonate saturation in the ocean, and a decline in abundance of inorganic precipitates such as aragonite fans, micro stromatolites, isopachously encrusting layers of calcite and herringbone calcite, and marine tufas with branching dendritic morphologies (cf. Grotzinger and James, 2000). In addition, early Paleoproterozoic carbonate platforms should be marked by the appearance of sulfate evaporites as a result of either a rise in atmospheric oxygen with a consequent increase in the sulfate content of the ocean (Cameron, 1982; Hattori et al., 1983a, b; Walker and Brimblecombe, 1985), or a decrease in the bicarbonate oversaturation leading to the availability of Ca ions for sulfate deposition (Grotzinger and Kasting, 1993).

High relative burial rates of organic carbon between ca. 2.2-2.1 Ga were inferred to explain extremely high positive $\delta^{13}C$ values in carbonates of that age (Karhu and Holland, 1996). Recently, carbon isotope values above +5‰ V-PDB in Paleoproterozoic carbonates have been attributed to local ^{13}C-enrichment related to high stromatolite productivity or evaporation in restricted lacustrine basins superimposed on a global positive excursion (Melezhik et al., 1999; 2000). Clearly, a restricted vs. open-marine origin of early Paleoproterozoic carbonates with extremely high (up to +28‰ V-PDB) carbon isotope values has significant implications for the understanding of biogeochemical carbon cycling at that time, as well as its role in the rise of atmospheric oxygen level.

In this paper we report the results of a study of the early Paleoproterozoic Nash Fork Formation in Wyoming. This succession of carbonates is of relevance for the debates outlined above, because of its age and because the lower part of the Nash Fork Formation is characterized

by positive $\delta^{13}C$ values (Bekker et al., 2001a, in prep.). Thus, this paper has four goals: 1) to document several styles of early Paleoproterozoic carbonate production; 2) to investigate an open-marine versus closed-basin depositional setting for the Nash Fork Formation; 3) to compile a curve of relative sea-level changes for this carbonate platform; and 4) to add to the understanding of the early Paleoproterozoic tectonic history of the Wyoming Craton.

REGIONAL GEOLOGY AND STRATIGRAPHY

The Nash Fork Formation is a carbonate unit in the upper part of the Paleoproterozoic Snowy Pass Supergroup exposed on the southeastern margin of the Wyoming Craton in the Medicine Bow Mountains, Wyoming (Fig. 2.1). The Snowy Pass Supergroup was strongly deformed during the 1.74-1.78 Ga Medicine Bow Orogeny (Chamberlain, 1998) when island arcs approached from the south and overrode the passive margin of the Wyoming Craton to form a collisional zone known as the Cheyenne Belt Suture (Karlstrom and Houston, 1984). The passive margin exposed in the Medicine Bow Mountains is also developed in the Sierra Madre to the west and in the Hartville Uplift to the east **(**Fig. 2.1; Karlstrom and Houston, 1984, Bekker et al., 2001a). The eastern margin of the Wyoming Craton is bounded by the Trans-Hudson orogen (Sims, 1995).

The early Paleoproterozoic succession in the Medicine Bow Mountains experienced greenschist facies metamorphism during the collisional event when the rocks were deformed into broad open folds (Houston et al., 1981). U-Pb conventional ages of detrital zircon grains from the Magnolia Formation and the age of volcanic and plutonic rocks associated with arc-continent collision constrain the age of the supergroup to between 2.45 and 1.78 Ga (Fig. 2.2; Premo and Van Schmus, 1989). The Snowy Pass Supergroup unconformably overlies or is in fault contact with Late Archean basement and is subdivided by structural contacts (rotated thrust faults) into the Deep Lake Group and the lower and upper Libby Creek Group (Fig. 2.2; Houston et al., 1992). Houston et al. (1992) argued that only a small part of the succession and a minor stratigraphic gap are represented by the Reservoir Lake Fault, which is a structural contact between the Deep Lake Group and the lower Libby Creek Group. This interpretation is based on the presence of glacially influenced units in the upper part of the Deep Lake Group (Vagner Formation) and in the lower Libby Creek Group (Headquarters Formation), and correlation with

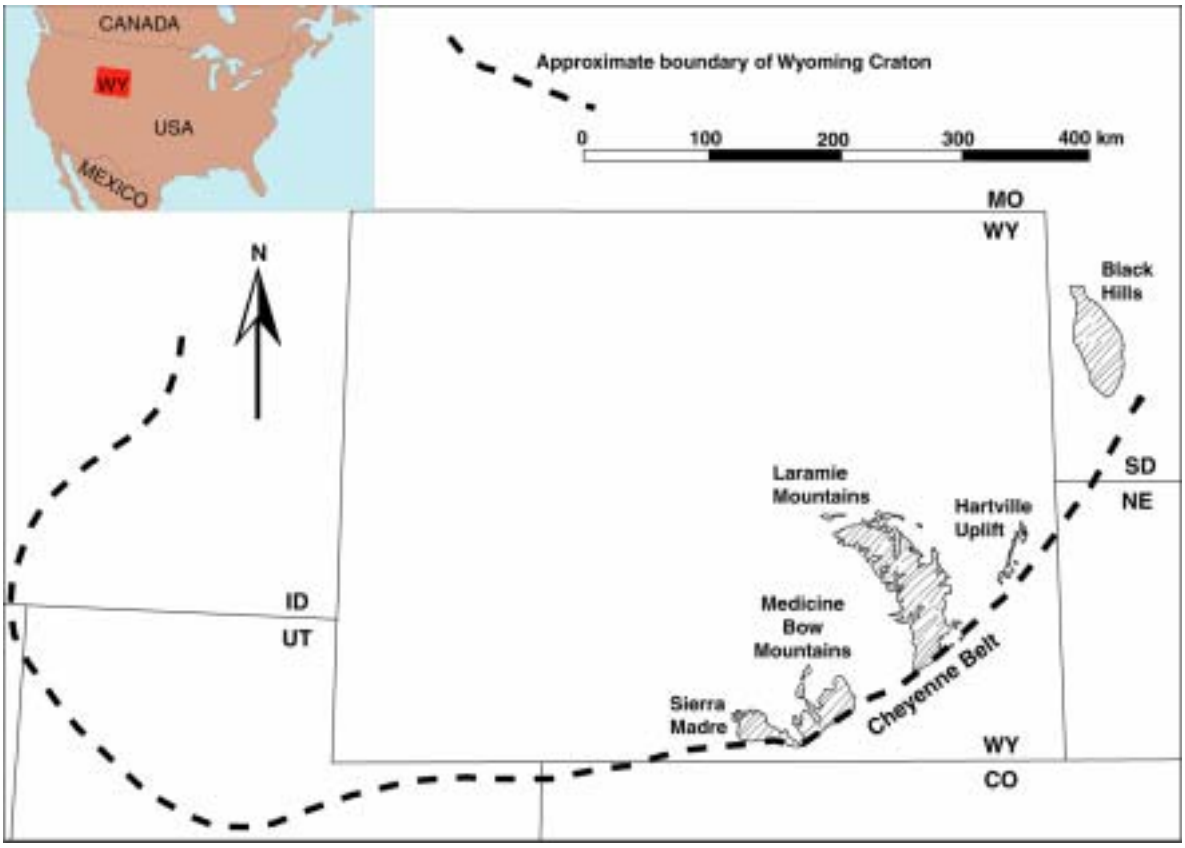

Fig. 2.1. Map of the Wyoming Craton flanked by exposures of Paleoproterozoic supracrustal rocks.

the Huronian Supergroup of Canada, where correlative diamictites are separated by a package of fluvial deposits (Long, 1976). In contrast, the Lewis Lake Fault that separates the lower from the upper Libby Creek Group may represent a major time break since the upper and lower parts are lithologically different and the upper part is allochtonous to parautochtonous with respect to the lower part (Houston et al., 1992).

The Deep Lake Group (Fig. 2.2) begins with fluvial deposits including pyritic and uraniferous quartz-pebble conglomerates (Magnolia Formation) and contains two glacial horizons (Campbell Lake and Vagner diamictites) sandwiched between quartzites, metapelites and a thin carbonate unit. Another diamictite, the Headquarters Formation, is present in the

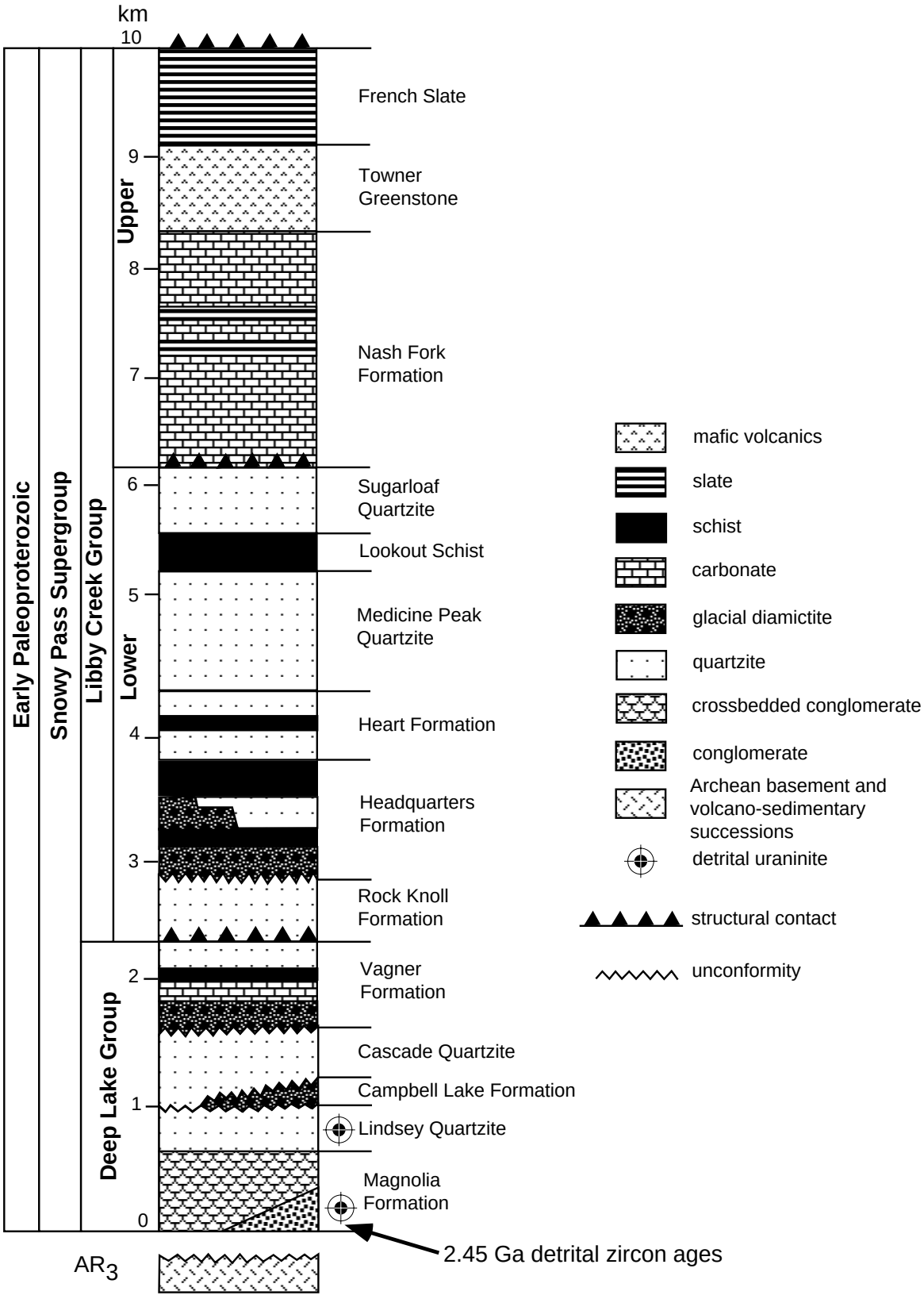

Fig. 2.2. Generalized stratigraphic column for the Snowy Pass Supergroup (after Houston et al., 1992).

lower Libby Creek Group in association with arenites and mudstones. The upper Libby Creek Group includes a thick carbonate succession (Nash Fork Formation), a subaqueous mafic volcanic unit (Towner Greenstone), and, at the top, slates and phyllites of the French Slate. C-isotope data for the Nash Fork Formation provide further constraints for the age of this unit. Carbonates in the lower part of the formation are highly enriched in ^{13}C, whereas those in the upper part have carbon isotope values close to 0‰ V-PDB indicating deposition after the end of the ca. 2.2-2.1 Ga carbon isotope excursion (Bekker et al., 2001a). The end of the Paleoproterozoic carbon isotope excursion in Fennoscandia and South Africa is presently constrained between 2113 ± 4 and 2062 ± 2 Ma (Karhu and Holland, 1996; Bekker et al., 2001b) and, based on chemostratigraphic data, a similar age is likely for the Nash Fork Formation.

The Deep Lake Group and the lower Libby Creek Group were deposited, respectively, in rift and passive margin settings, whereas the upper Libby Creek Group records either a transition from passive margin to foredeep sedimentation (Karlstrom et al., 1983) or continued deposition on a passive margin (Ball and Farmer, 1991; Crichton and Condie, 1993; Bekker et al., 2001a). The age of rifting is poorly constrained for the Snowy Pass Supergroup but, based on the correlation with the Huronian Supergroup in Canada (Houston et al., 1992) and the age of detrital zircons at the base of the succession, rifting possibly commenced at ~2.45 Ga. The entire succession was intruded by multiple generations of mafic sills and dikes that range in composition from tholeiitic to calc-alkaline. Tholeiitic gabbros and their felsic differentiates that intruded the Deep Lake Group prior to folding are likely related to a younger rifting event (Karlstrom et al., 1981) rather than that which formed the basin at ~2.45 Ga, but the stratigraphic expression of this event is poorly documented on the southern margin of the Wyoming Craton. This event was dated in the Sierra Madre and Laramie Range at 2092 ± 9 Ma and 2011 ± 1.2 Ma (Premo and Van Schmus, 1989; Snyder et al., 1995; Cox et al., 2000). Evolution to calc-alkaline composition of mafic sills and dikes was explained by a progressive change in tectonic environment from rift to open ocean to foredeep (Karlstrom et al., 1983). The age of the calc-alkaline dikes and sills is unknown.

NASH FORK FORMATION

The Nash Fork Formation is a ~2 km thick succession of mainly dolomite that contains thick intervals of graphitic and pyritic argillite and thin interbeds of quartzite, chert and sulfidic iron-formation (Karlstrom et al., 1983; Houston and Karlstrom, 1992). The Nash Fork Formation is in fault contact with the underlying Sugarloaf Quartzite along the Lewis Lake Fault (Fig. 2.2). Its upper contact is not exposed but the formation is structurally conformable with the overlying Towner Greenstone (Karlstrom et al., 1983).

Blackwelder (1926) divided the Nash Fork Formation into three units from the base to the top: the Nash marble series, Anderson phyllite, and Ranger marble. However, this stratigraphy was abandoned during regional mapping (Houston et al., 1968) due to variable degrees of exposure, structural complexity and the lack of apparent traceable marker beds. A range of paleoenvironments has been interpreted for the Nash Fork Formation including intertidal flats on a shallow-marine platform flanked by anoxygenic, restricted subtidal bays in which the graphitic and pyritic argillite developed (Karlstrom et al., 1983; Houston and Karlstrom, 1992).

A well-exposed area stretching for ~3 km along strike between Small Telephone Lake in the east and Libby Lake in the west was mapped during this study (Fig. 2.3). Twelve mappable units or members were identified, and these are characterized by distinctive facies or facies associations (Fig. 2.4). Similar facies associations were recognised outside the mapped area, but poor exposure did not permit detailed mapping. Sections were measured through the Nash Fork Formation in the map area where exposure was adequate. Facies associations typically are preserved in upward-shallowing increments of strata or parasequences (sensu Van Wagoner et al., 1988). The following section includes descriptions of the facies associations from the lower (shallow-water; L1-L8), middle (deepening; M1-M3) and upper (shallowing; U1) Nash Fork Formation (Fig. 2.4). A discussion of depositional environments and relative sealevel changes follows in the next section.

DESCRIPTIONS OF FACIES ASSOCIATIONS

Massive and stromatolitic dolomite facies association (L1 Member)

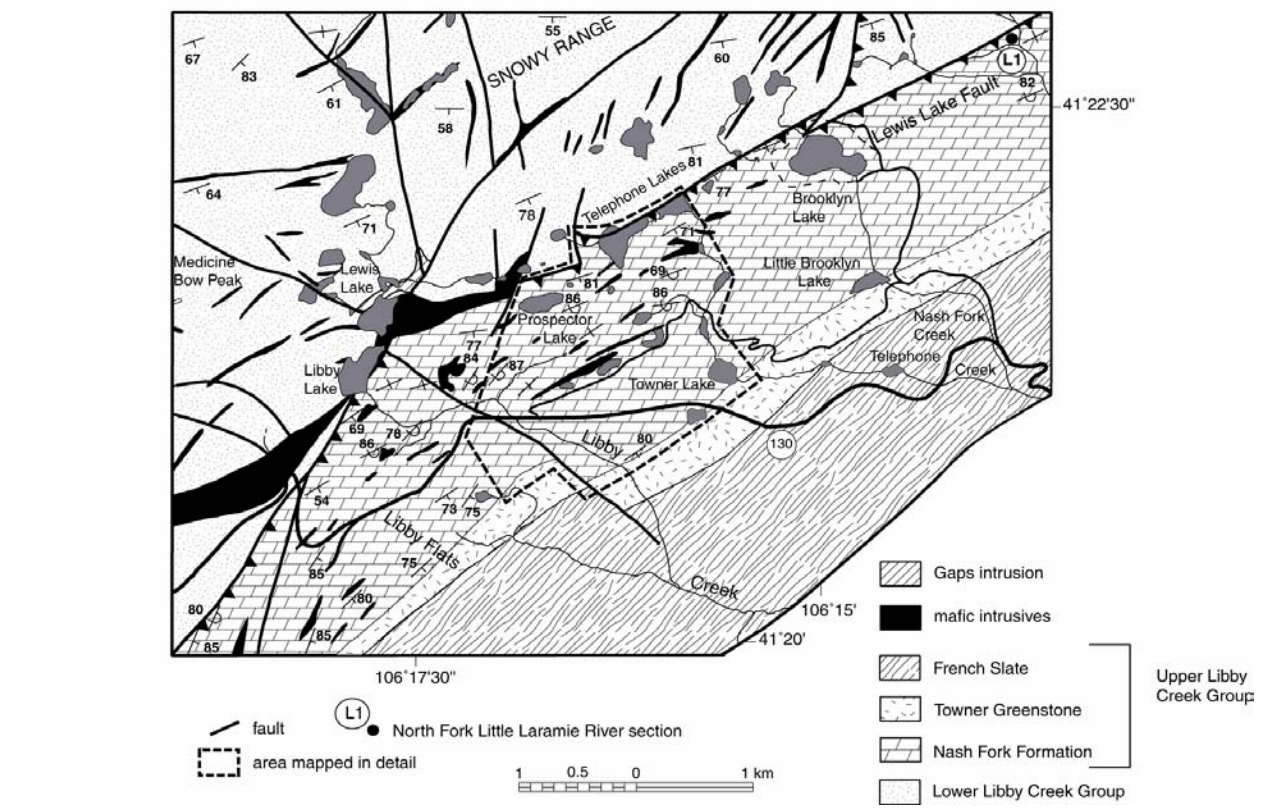

Fig. 2.3. Map of the Nash Fork Formation in the area between Brooklyn Lake and Libby Flats in the Medicine Bow Mountains (modified from Houston et al., 1992).

This facies association makes up the lowermost member of the Nash Fork Formation that is exposed only in the North Fork of the Little Laramie River two miles northeast of the area that was mapped in detail (Fig. 2.3). L1 has an apparent thickness of ~38 m and has a structural lower contact and a sharp upper contact. In its lower half, L1 is comprised of light-brown to gray, massive quartz-rich dolomite. The upper part of L1 contains small (up to 15–20 cm in diameter) domal stromatolites with radial structures that are visible on bedding and in vertical cross-sections. Also present are stratiform stromatolites similar to tufa deposits (cf. Hoffman, 1989).

Heterolithic facies association (L2 and L7 Members)

This facies association comprises the lowermost exposed member of the Nash Fork Formation in the mapped area and recurs higher up in the section (Fig. 2.4). The lower contact

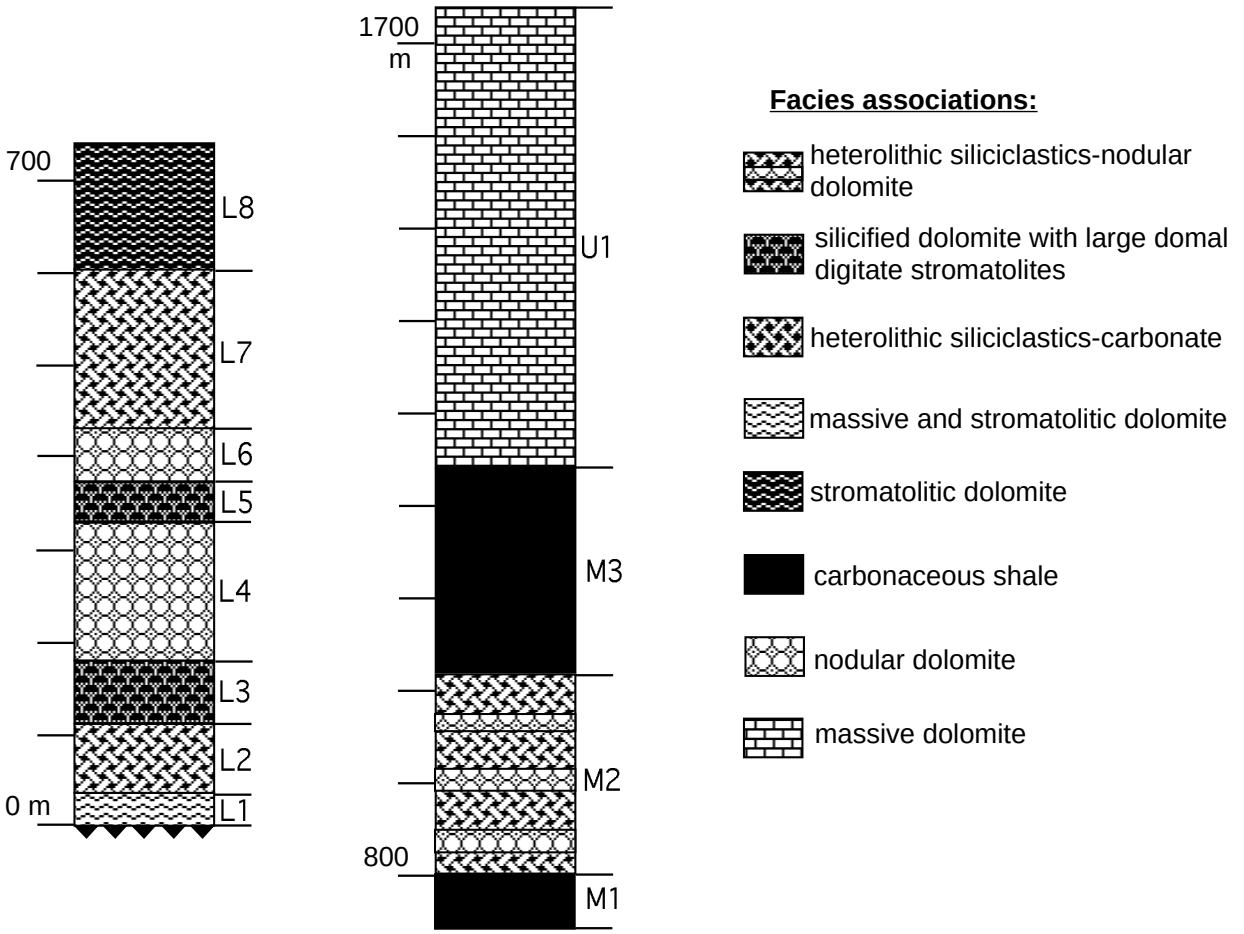

Fig. 2.4. Stratigraphic column of the Nash Fork Formation in the area mapped in detail. Members are shown with letters and numbers and facies associations with patterns.

of L2 is not exposed in the mapped area, where it is cut by the Lewis Lake Fault. However, outside the mapped area in the North Fork of the Little Laramie River, the observed lithologies within 10 meters of the contact indicate that the lower contact is sharp. The heterolithic facies comprising L2 consist of interlayered sandstone, siltstone, argillite and brown dolomite. Argillite and siltstone contain wavy bedding and thin laminations; the sandstone is structured by low-angle cross-bedding and wave ripples. Molds after gypsum and anhydrite are developed in argillite at several localities. The argillite contains rare microscopic cubic pseudomorphs of quartz after halite. Brown, iron-rich dolomite is developed as interlayers within dark-colored (chocolate) argillite. Small, oblate silicified domal stromatolites with digitate structures,

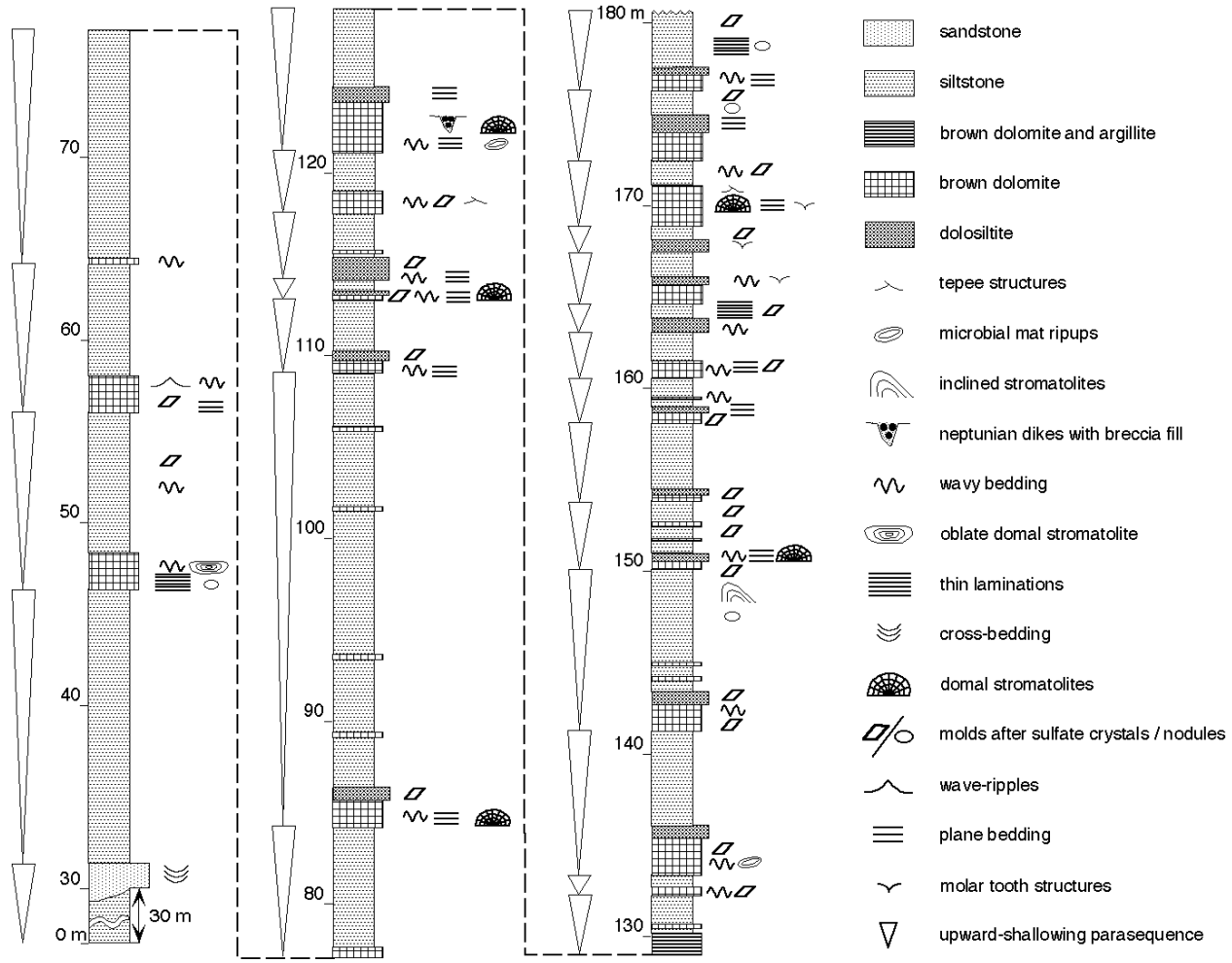

Fig. 2.5. Measured section of L7 member.

stratiform stromatolites, and planar, cross, lenticular and intricate wavy bedding are developed within the brown dolomite.

L7 is up to 180 m-thick and has a gradational lower and a sharp upper contact. It consists

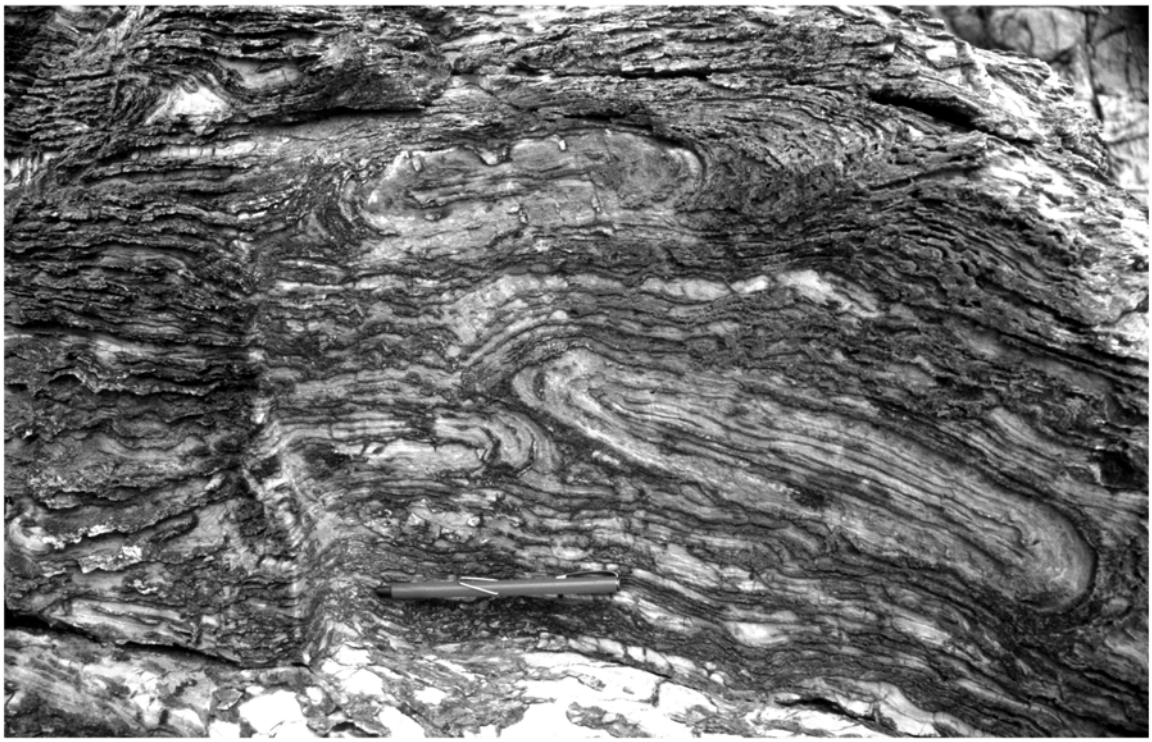

Fig. 2.6. Imbricated microbial mat ripups at the base of a parasequence in the L7 member. Pen is 10 cm long.

of stacked parasequences that range in thickness from 1.5 to 33 m (Fig. 2.5). Parasequences grade from brown dolomite at the base to silicified, iron-rich siltstone and argillite at the top. Lag deposits of angular dolomite clasts are present at the base of some parasequences. Pebbles are silicified and recrystallized, and occur in a calcisiltite matrix. Thicknesses of dolomitic intervals increase up-section whereas siliciclastic intervals become thinner. A prominent 2 m-thick lens of red, cross-bedded, mature quartzite is present 30 m above the base of L7. Dolomitic intervals are either massive or wavy and plane bedded and may contain small LLH stromatolites at the base and dolosiltites at the top. Rare imbricated microbial mat rip-ups are present at the base of LLH stromatolites (Fig. 2.6). Some dolomite layers contain molar-tooth structures, neptunian dikes, rare teepee structures, wave ripples, poorly preserved pseudomorphs after evaporites and desiccation cracks (Fig. 2.7). Siliciclastic intervals are dominated by argillites that contain pervasive isolated molds and layers of molds after gypsum crystals (Fig. 2.8) and

Fig. 2.7. Desiccation cracks in stromatolitic dolomite of the L7 member. Pencil for scale.

anhydrite nodules. Some of these molds have discoidal or swallow-tail shapes. Petrographic studies reveal that laminae are displaced in the growth direction of the crystals. Also present in the siliciclastic intervals are rare wavy bedding, fine laminations and thin beds and lenses of carbonate.

Silicified domal digitate stromatolite facies association (L3 and L5 Members)

This facies association is characterized by large, silicified stromatolitic domes up to 15-20 m in width and 5 m in height and repeated twice in the lower Nash Fork Formation (Fig. 2.4). Contacts of L3 were not observed, whereas the lower and upper contacts of L5 are gradational over 8 to 10 m. The thickness of L3 is variable and the best estimate is ~70 m, whereas L5 is ~45 m thick. L3 and L5 consist of brown, parted and ribbon dolomite (cf. James and Stevens, 1986; Coniglio and James, 1990) interlayered with domal digitate stromatolites in their lower half, and large stromatolitic domes with digitate stromatolites in their upper half. Brown

Fig. 2.8. Sulfate molds in the argillite of the L7 member. Pen 10 cm long.

dolomite contains layers of intraformational breccia. Domal stromatolites are up to 8 m in width and 5 m in relief. Knight and Keefer (1966) and Knight (1968) recognised that the domal stromatolites define large reefs. Digitate stromatolites (vertical pillars of Fenton and Fenton,1939) are aligned perpendicular to the laminae and are 2-5 cm in height and 2-3 cm in width (Fig. 2.9). Large oblate spheroids (up to 2.0 m in length and 0.5 m in width) are developed at the top of the L3 and at the base and top of the L5. Spheroids typically are enclosed in brown, planar laminated, ribbon dolomite. Some of the spheroids envelop argillitic and dolomitic blocks up to 20 cm in diameter. Walcott (referenced in Blackwelder, 1926) identified the domal stromatolites as belonging to the genus Collenia, but Fenton and Fenton (1939) later described them as a new species – *Hadrophycus immanis sp. nov.*

Nodular dolomite facies association (L4 and L6 Members)

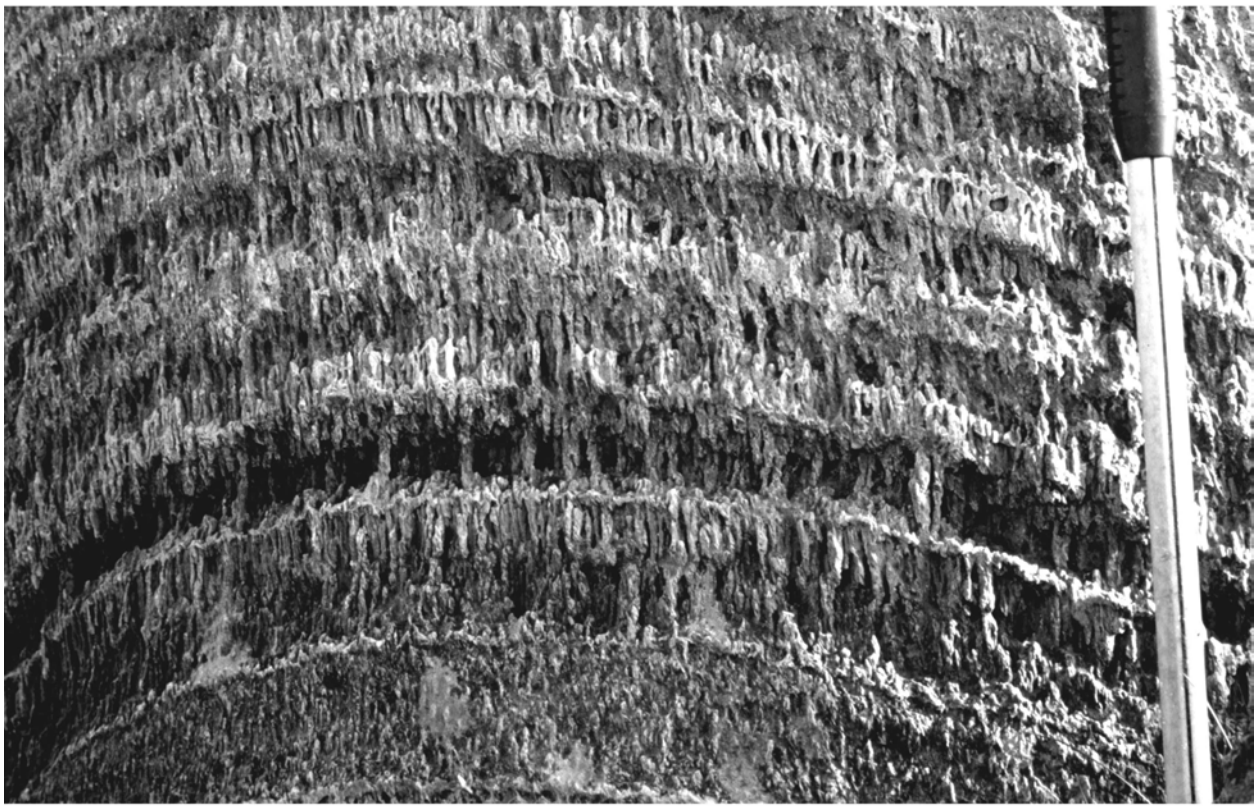

Fig. 2.9. Domal digitate stromatolites of the L3 member. Note that digitate forms are oriented perpendicular to the laminae. Hammer 70 cm long.

This facies association is characterized by massive, light-colored dolomitic mudstone with silicified nodules up to 10 cm in diameter (Fig. 2.10) and is repeated twice in the Lower Nash Fork Formation (Fig. 2.4). L4 is poorly exposed and has an estimated thickness of ~150 m. It contains rare small columnar and stratiform stromatolites and a more than 8 m-thick interval of blue argillite with pyrite crystals. Also present is an intraformational breccia lens up to 2 m thick.

Fig. 2.10. Silicified flattened nodules and layers of coalesced nodules in the L6 member. Hammer is 70 cm long.

L6 is better exposed than L4 and is up to 59 m thick. Lower and upper contacts are transitional over 6 to 10 m. Facies are stacked in parasequences between 2 to 25 m in thickness (Fig. 2.11).

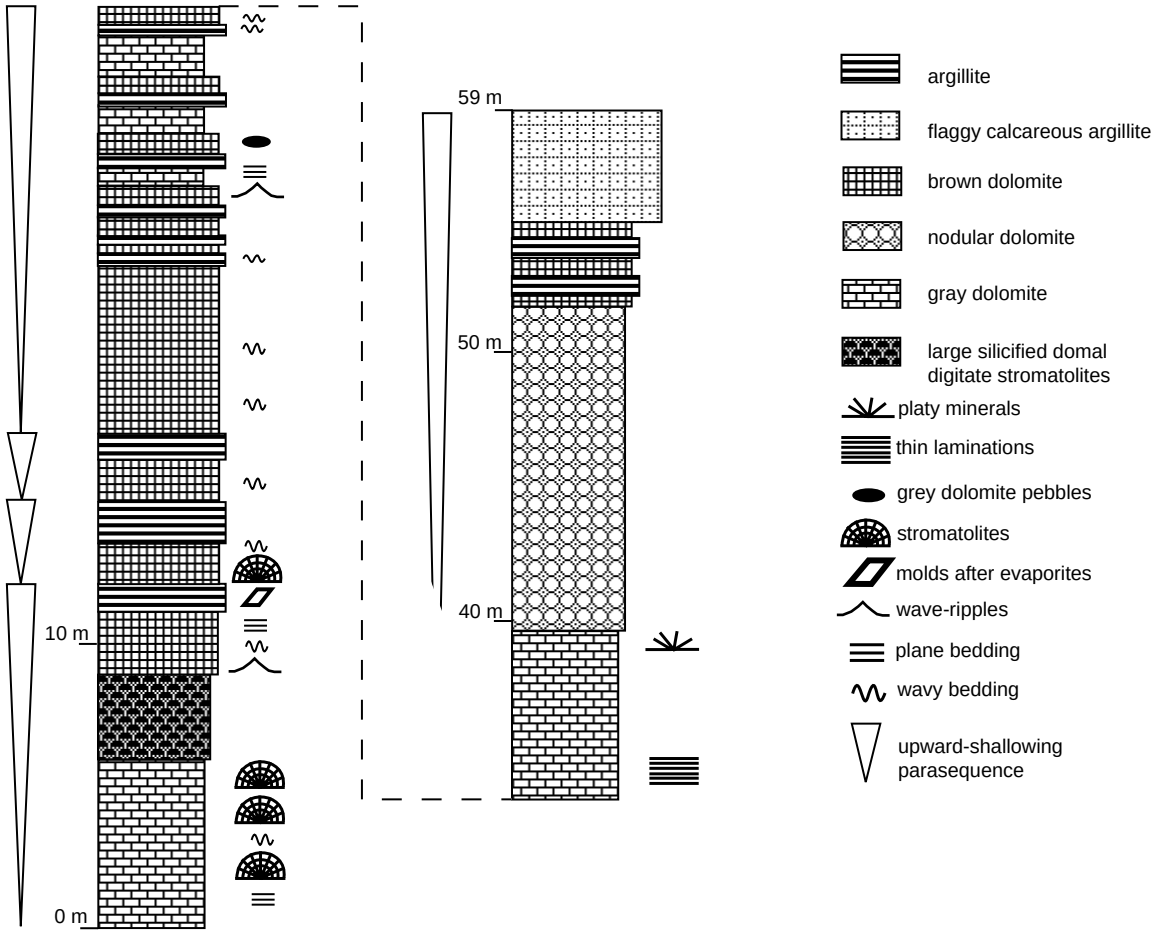

Fig. 2.11. Measured section of L6 member.

The lowermost parasequence consists of gray dolomite with wavy and plane bedding overlain by large, silicified, domal digitate stromatolites. Brown dolomite and dark argillite with molds after gypsum crystals define the top of the parasequence. The brown dolomite is massive and plane bedded and contains wave ripples near the base. Most parasequences in L6 consist of interlayered calcareous argillite and brown and gray dolomite. Gray dolomite is massive or plane and lenticular bedded and typically is overlain by brown dolomite that is massive or contains wavy, lenticular, and plane bedding, wave ripples, and, locally, small domal stromatolites at the base. Pebbles of gray dolomite occur rarely within brown dolomite beds. Calcareous argillite with horizontal laminations and wavy or lenticular bedding commonly defines the top of parasequences. The uppermost parasequence consists mostly of gray dolomite

that changes up-section from thinly laminated to massive to nodular (Fig. 2.11). Massive dolomite contains chert pseudomorphs after a platy mineral near the contact with the overlying nodular dolomite. Nodular dolomite is 11.5 m thick and contains silicified nodules that may coalesce to form lenses. The parasequence grades upwards into interlayered calcareous argillite and dolomite, and is capped by flaggy calcareous argillite.

Stromatolitic dolomite facies association (L8 Member)

L8 is well exposed, is up 140 m thick and has sharp upper and lower contacts. The member consists of stacked parasequences that range in thickness from 1.5 to 16 m (Fig. 2.12). Parasequences in the lower 90 m consist of massive and thinly laminated, dark gray dolomite, dolosiltite and black and green chert overlain by argillite with thin grainstone and brown dolomite layers. A 4 m – thick interval of cross-bedded, feldspathic sandstone caps one of the parasequences (Fig. 2.12). The dark-gray dolomite is organic-rich and has fenestrae and stromatactis structures filled with light-colored micrite (cf. Tucker and Wright, 1990). Dolosiltite layers are usually massive and structureless; chert nodules and mud rip-ups are present rarely. Argillites and argillaceous dolomites capping parasequences commonly contain evaporitic molds. Upwards within L8, argillites with evaporitic molds disappear and parasequences are capped by dolosiltite which, in turn, is replaced by large domal stromatolites at the top of L8. Silicified and recrystallized dolomite bands and sheets similar to molar-tooth structures (Fig. 2.13) occur within massive, dark-gray dolomite in the upper half of L8. Also present within this interval are stratiform stromatolites. Within two parasequences, microbial mat rip-ups form layers and lenses of elongated spheroids (Fig. 2.12). Spheroids are up to 5 cm wide and 20 cm long and in some cases show imbrication. Overlying columnar stromatolites have small synoptic relief (10-15 cm) and smooth laminae of equal thickness. Large silicified domal digitate stromatolites at the top of L8 are up to 2 m in height and are developed through a thickness of 10 m (Fig. 2.12). Some of the domal stromatolites contain silicified, digitate spheroids at their bases. The digitate structures are similar to *Djulmekella Sundica* from the upper part of the Jatulian Group close to the Jatulian/Ludikovian boundary in Russia (Pavel Medvedev, pers. com., 2001, stromatolite description in Makarikhin and Kononova, 1983).

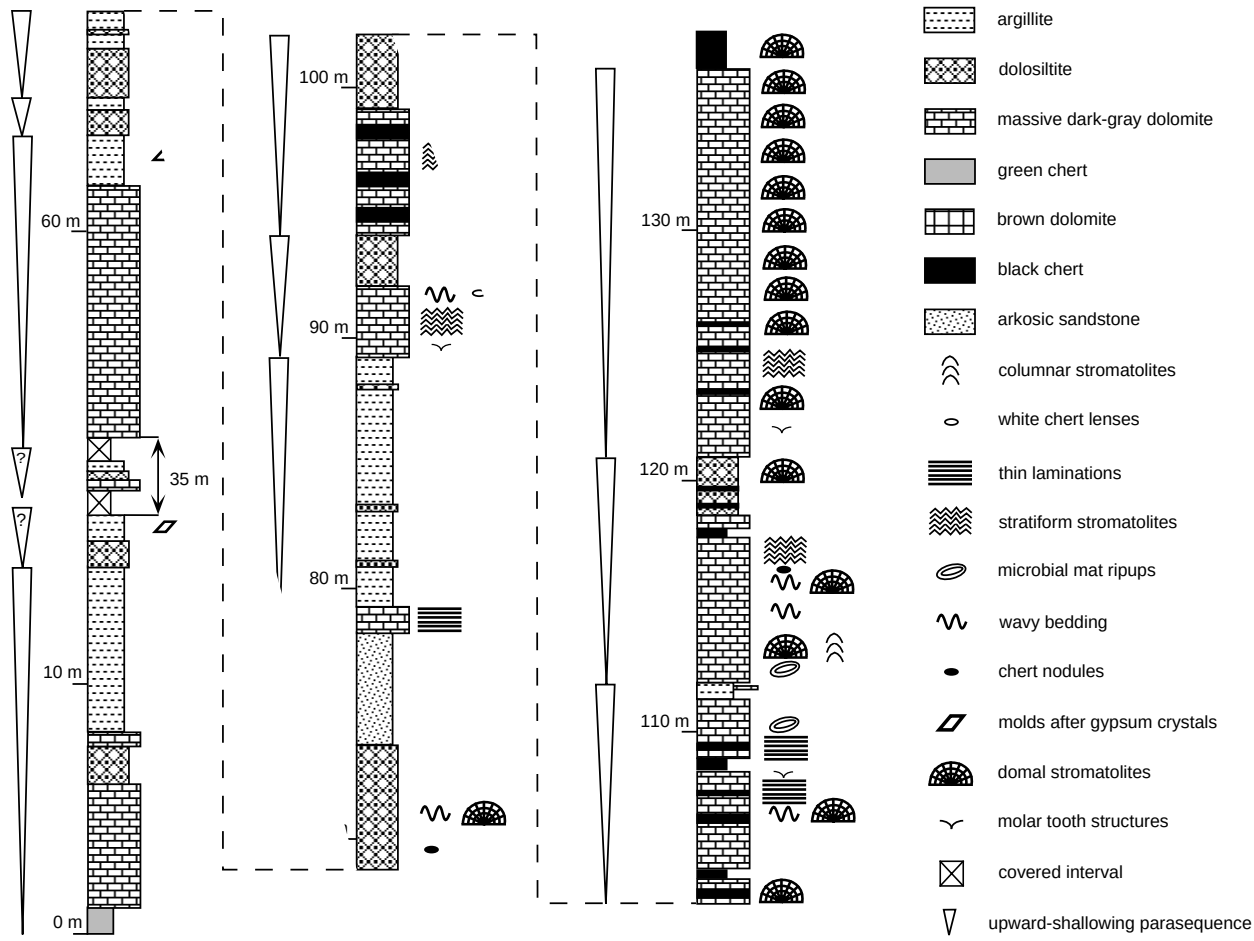

Fig. 2.12. Measured section of L8 member.

Black shale facies association (M1 and M3 members)

M1 and M3 crop out poorly and form valleys. M1 has thickness of 60 to 70 m. The base of M1 is in sharp contact with the 10 m-thick, large domal digital stromatolitic dolomite interval at the top of L8 (Fig. 2.4). A parasequence at the base of the M1 consists of black chert, brown ribbon dolomite, followed by a 20 m-thick interval of turbidites that are capped by brown plane-bedded dolomite. Black chert contains poorly developed digital stromatolites, whereas the brown ribbon dolomite is characterized by wavy, convoluted, and soft-sediment slump structures. Individual turbidite beds are made up of massive sandstone, planar-bedded siltstone, ripple-drift cross laminated siltstone with convolute laminations, and shale (Tabce Bouma beds). The remainder of M1 consists of black organic-rich shale with rare starved ripples and euhedral crystals of pyrite up to 1.5 cm in size, and thin beds of sandy brown dolomite with phyllite partings. M3 is

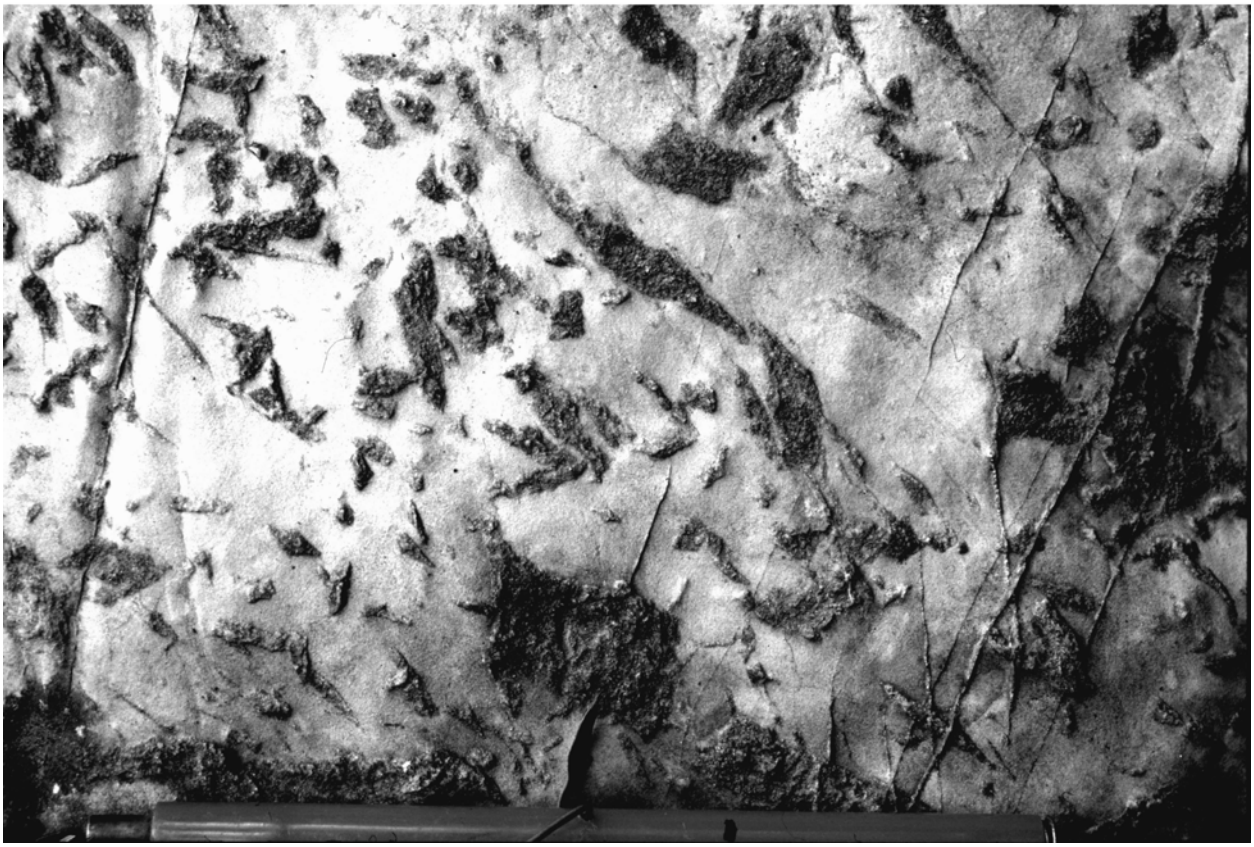

Fig. 2.13. Molar-tooth structures in the L8 member. Pen is 10 cm long.

260 m thick and comprises a single parasequence. The lower contact is not exposed, whereas the upper contact is gradational and is defined by the disappearance of siliciclastics and the first appearance of blue dolomite. Gray organic-rich phyllites with pyrite crystals form the lower part of M3 and are transitional upwards into laminated siltstone followed by wavy bedded sandstone containing thin beds of brown, plane-bedded dolomite (Fig. 2.14). Locally, a bed of hematitic ironstone several meter thick is interlayered with the organic-rich phyllites.

Heterolithic siliciclastics-nodular dolomite facies association (M2 member)

M2 is poorly exposed and is cut by mafic sills. Neither the upper nor the lower contact was observed. However, the upper contact is likely sharp since black shale of M3 occurs within 10 m of the contact. M2 has a thickness of ~215 m. Two partial sections through M2 were measured, one through the lower part and another through the upper part of the member (Fig. 2.15). Parasequences consist of gray or brown dolomite at the base and siltstone at the top. The

dolomite is massive, wavy or nodular, and locally is trough cross-bedded or plane bedded. Silicified, iron-rich siltstone at the top of parasequences is thinly laminated and wavy bedded and contains molds after anhydrite nodules and gypsum crystals (Fig. 2.15A). The uppermost parasequence in M2 shows an upward transition from massive to plane-bedded brown dolomite followed by domal stromatolites (Fig 15B). The domal stromatolites contain chert nodules and locally are overlain by large loaf-shaped spheroids. Poorly-preserved oncolites with diameters between 1 and 1.5 mm occur within red dolomite of M2 in the Libby Flats area and were ascribed by Knight (1968) to the genus *Osagia*.

Massive dolomite facies association (U1 Member)

The upper part of the Nash Fork Formation is poorly exposed, lacks traceable beds and thus was not subdivided during mapping. The lower contact with M3 is gradational as discussed above, but the contact with the overlying Towner Greenstone is not exposed. U1 has a thickness of ~495 m (Fig. 2.4) and is significantly different from the underlying members in that it lacks thick siliciclastic intervals and chert layers, as well as large silicified stromatolite domes with digitate structures. A prominent breccia up to 30 m in thickness divides U1 into two parts (Fig. 2.16).

The lower part of U1 (between 0 and 210 m) consists of parasequences that range in thickness from 50 to 80 m (Fig. 2.16). These parasequences contain massive blue dolomite overlain by thinly laminated, lenticular and wavy bedded blue dolomite and brown flaggy dolomite. The massive dolomite contains voids filled with isopachous cement and internal sediments (Fig. 2.17), intraformational breccias with clasts up to 5 cm in size and neptunian dikes. The thinly laminated dolomites are typically organic-rich and contain cherty fenestral fabrics. Both the massive and the thinly laminated dolomites contain layers with pseudomorphs after a tabular mineral with hexagonal cross-section and after a platy mineral. Some of these pseudomorphs have swallow-tail structures and likely formed after gypsum. Rare oncolites or oolites are present in the massive dolomite. Overlying brown dolomite contains an intraformational breccia that has fitted-fabrics with remaining open space filled with isopachous cement. Both the blue and brown dolomite in the parasequence between 130 and 210 m (Fig. 2.16) contain intraformational breccia beds. The upper 30 m of this parasequence consists of

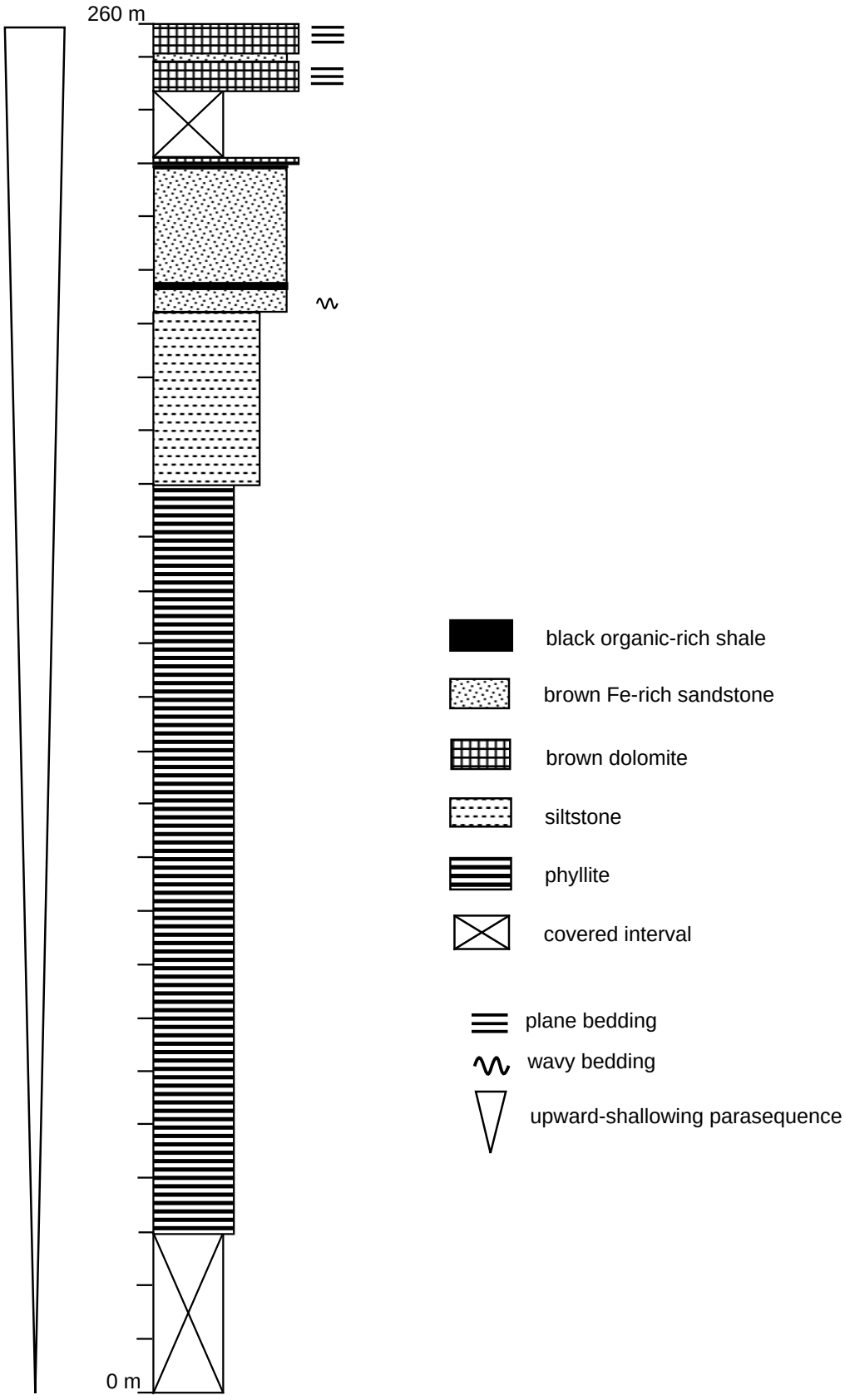

Fig. 2.14. Measured section of M3 member.

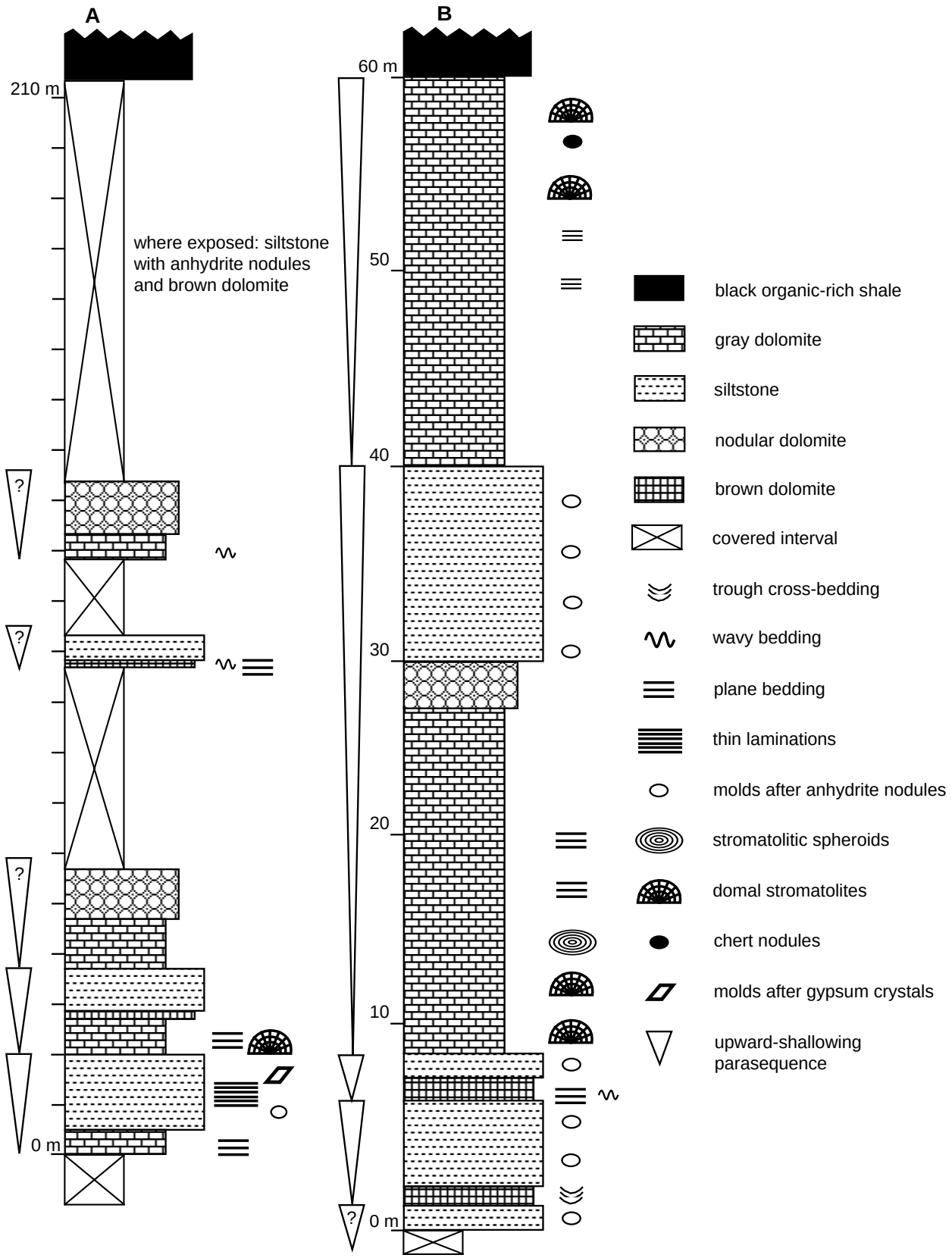

Fig. 2.15. Measured sections of M2. A - total thickness of the member including the poorly exposed upper part; B - well-exposed upper part of the member.

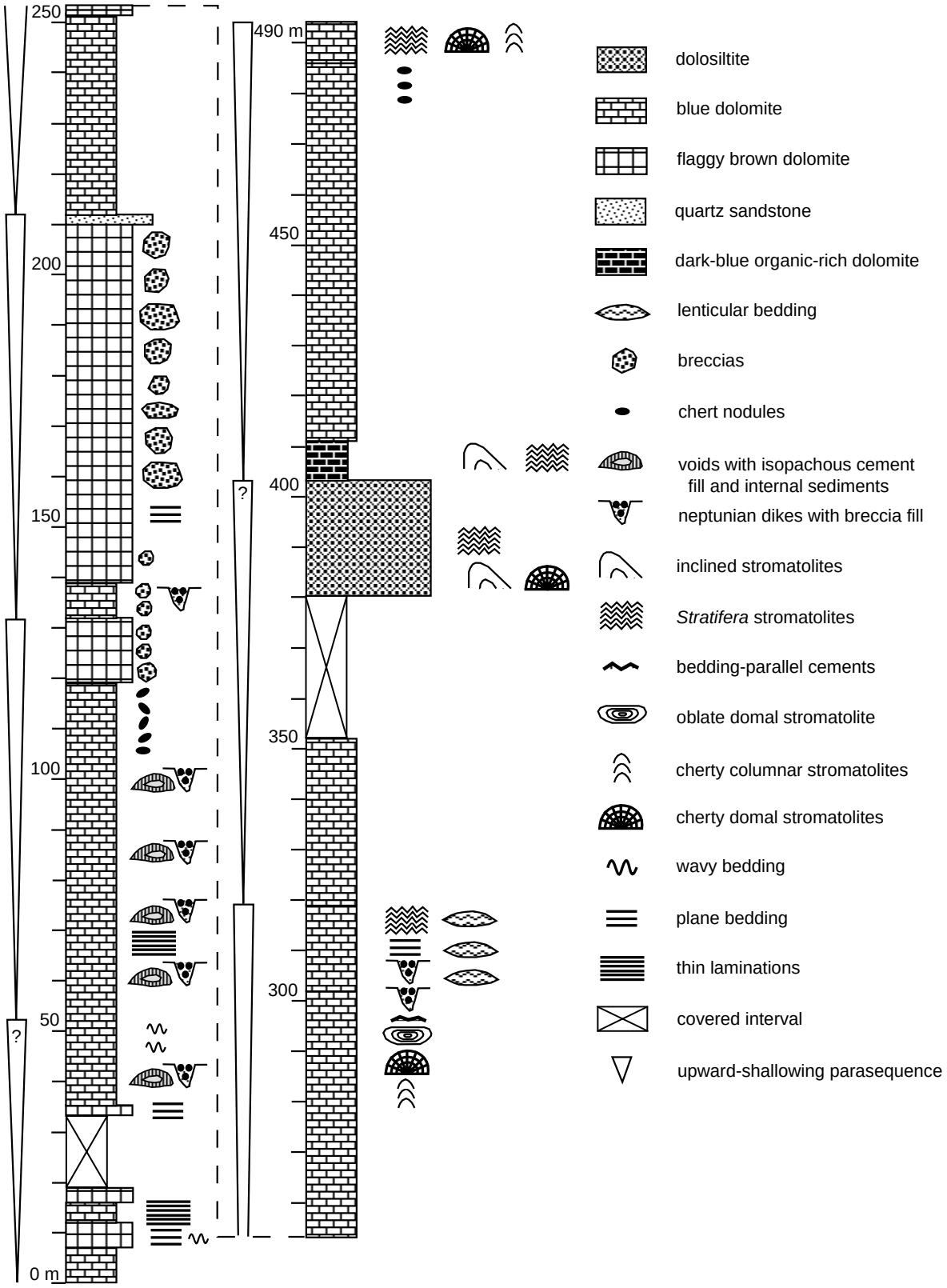

Fig. 2.16. Measured section of U1 member.

Fig. 2.17. Cements filling voids in the lower part of the U1 member. Note growth of crystals into the cavity from its margins. Pencil for scale.

Parasequences in the upper part of the U1 average 90 m in thickness and consist of massive blue dolomite at the base capped by stromatolitic dolomite or dolosiltite (Fig. 2.16). Massive dolomite is organic-rich and, locally, chert nodules merge to form lenses. Stromatolitic dolomites are locally silicified and include wavy stratiform, domal, oblate domal and columnar forms. Bedding-parallel cements, lenticular and plane bedding, and neptunian dikes are common in the stromatolitic caps. The dolosiltite consists of brown sand-sized carbonate grains in an organic-rich dolomite matrix and rarely displays normal grading. Dolomite at the top of U1 in the Towner Lake area (Fig. 2.3) contains voids filled with cements and internal sediments and rare small fans (<3 cm in diameter) with radial structures (Fig. 2.19). Cement is replaced by chert that preserves an isopachous texture. Internal sediments are predominantly red-colored

Fig. 2.18. Breccia cemented by laminated dolomite, U1 member. Pen is 10 cm long.

micrites but in some cases greenish micrites are also present. Reddish micrite also fills neptunian dikes in proximity to cemented cavities. Cavities follow the bedding and, in some cases, cross-cut bedding. The uppermost part of U1 contains a number of layers with intraformational breccia in a red dolomitic matrix.

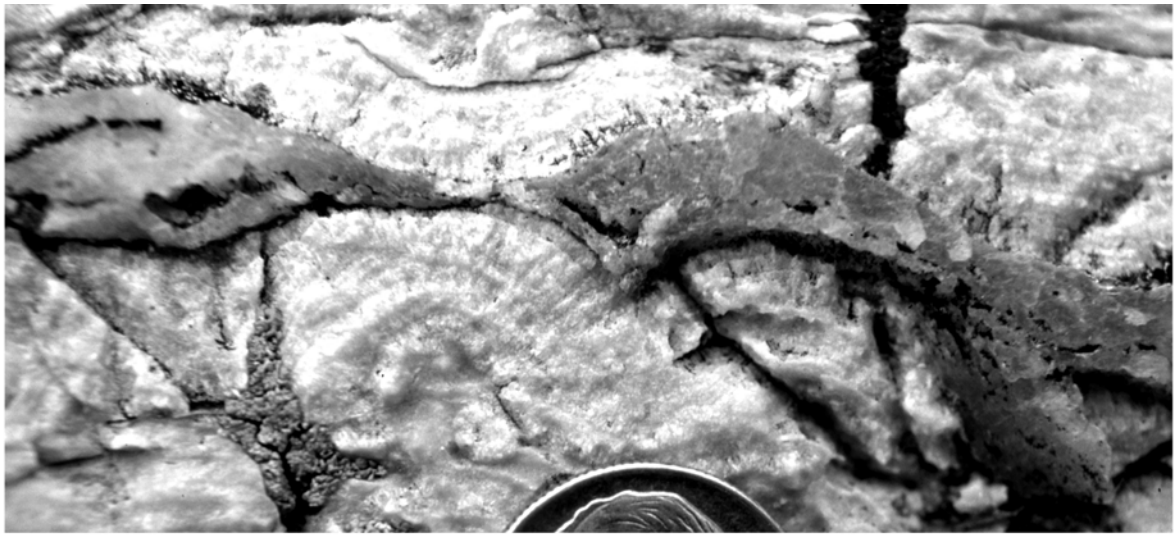

Fig. 2.19. Small domes with radial structures in the upper part of the U1 member. Coin is 1 cm in diameter.

INTERPRETATION OF DEPOSITIONAL ENVIRONMENTS

Based on characteristic stacking patterns of lithologies and sedimentary structures, six idealized parasequence types can be recognised in the Nash Fork Formation (Fig. 2.20, A–F). Parasequences A, B and D occur only in the lower part, C in the lower and middle parts, E in the upper part, and F in the middle part of the Nash Fork Formation. Interpretations of the parasequences in terms of depositional environment are presented below.

Upper intertidal–supratidal parasequences

This parasequence type contains massive, light-brown to gray, siliciclastic-rich dolomite with small domal stromatolites with radial structures at the base and tufa structures at the top

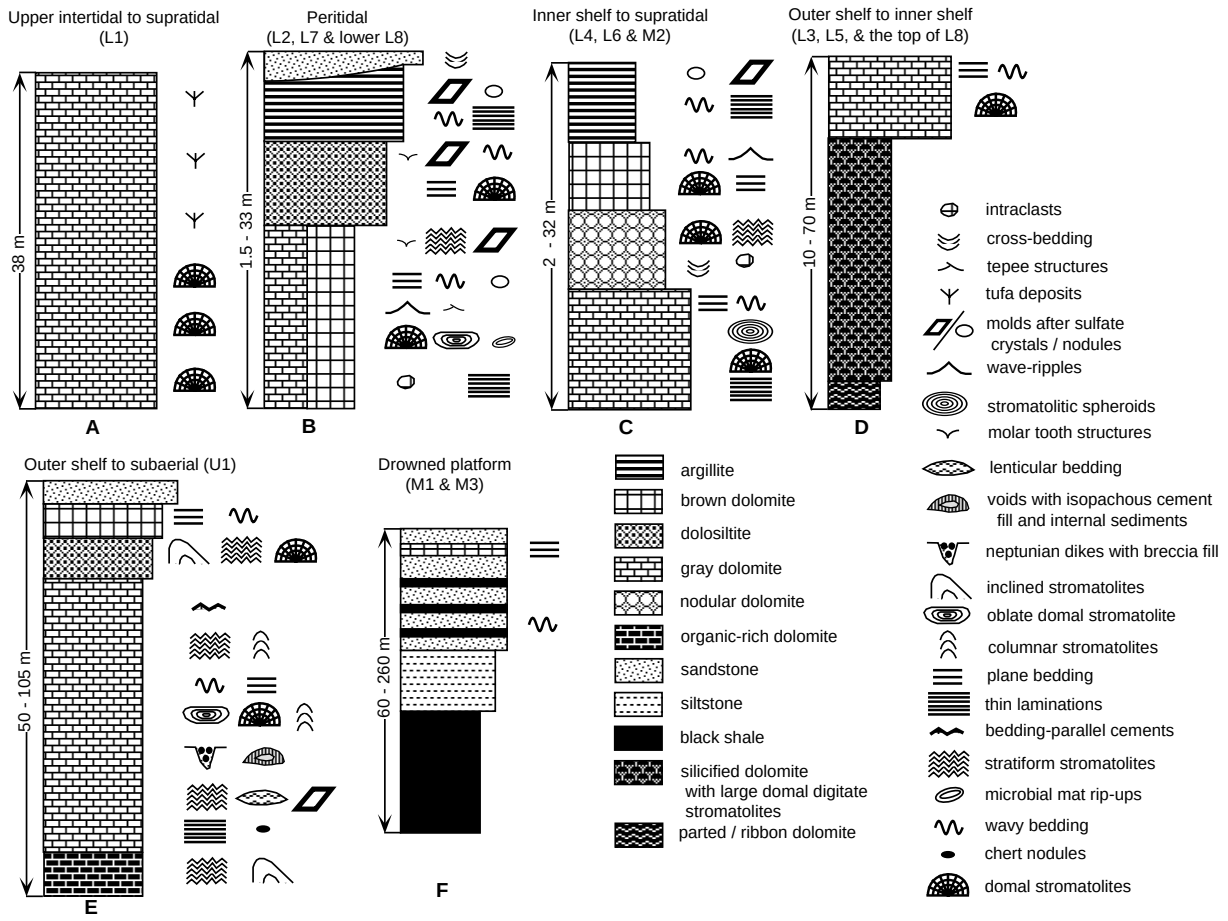

Fig. 2.20. Parasequence types in the Nash Fork Formation.

(Fig. 2.20 A). Small domal stromatolites with radial structures are similar to aragonite fans described by Sumner and Grotzinger (1996) from the Campbellrand-Malmani platformal carbonates. The small relief of the stromatolites suggests that they likely formed in an upper intertidal setting. Tufa structures (digitate stromatolites up to several centimeters in height) are common in Archean and Paleoproterozoic supratidal settings and have been interpreted as aragonite precipitates (Grotzinger, 1986b). In combination, these structures suggest a shallow-water, low-energy setting for this parasequence type. Lack of siliciclastics implies that the environment of deposition was separated from a terrigenous source.

Peritidal parasequences

This parasequence type comprises from the base to the top: brown or gray dolomite, dolosiltite, argillite and mature quartz sandstone (Fig. 2.20 B). The base of the parasequence is rarely defined by carbonate intraclast lags and more commonly by microbial mat rip-ups overgrown by stromatolites. Upwards within parasequences, stromatolites decrease in relief and traction-produced sedimentary structures including wavy and plane bedding, and wave ripples decrease in abundance. In contrast, swallow-tail and discoidal sulfate pseudomorphs increase in abundance upwards. Parasequences rarely are capped by cross-bedded quartz sandstones.

The above characteristics are comparable to low-energy, evaporitic parasequences of peritidal origin described by Pratt et al. (1992). Basal lags and microbial mat rip-ups developed in a relatively high-energy, ravinement zone during drowning of the underlying parasequence. Associated traction-produced structures support a shallow-subtidal setting for the brown and gray dolomite facies. Upward trends in sedimentary structures within parasequences described above, including the decrease in relief of stromatolites, are consistent with shoaling of the depositional environment into evaporitic mudflats (cf. Warren, 1999) to which siliciclastic sediment was provided by fluvial and possibly eolian processes. Discoidal-shaped molds are common after gypsum crystals that form displacively within sediments (Kendall, 1992).

Inner shelf to supratidal parasequences

From its base to the top this parasequence type consists of: massive gray dolomite, nodular dolomite and brown dolomite, with an argillite cap (Fig. 2.20 C). Bases of parasequences are marked by the appearance of massive gray dolomite with rare, thin laminations and large domal and oblate domal stromatolites. Stromatolites decrease in size and abundance upsection, whereas sulfate pseudomorphs are confined to the top of the parasequence. Traction-produced sedimentary structures, including trough and tabular cross bedding, plane and wavy bedding, and wave ripples, are most common in the middle of the parasequence. Nodular dolomites rarely pass along strike (over a distance of several meters) into, or are interlayered with, gray dolomite that contains stratiform and small domal stromatolites, trough and tabular cross-bedding and intraclast layers.

Stacking patterns of facies described above are comparable to low-energy, evaporitic parasequences of Pratt et al. (1992). The presence of domal stromatolites, lack of traction-produced sedimentary structures except near the top of the massive gray dolomite and rare thin laminations support an inner-shelf setting for the lower part of the parasequence. An upward increase in abundance of traction-produced sedimentary structures, coupled with the appearance of rare layers of intraclasts and a decrease in stromatolite size and abundance supports an intertidal setting for the nodular and brown dolomite facies. Ubiquitous sulfate pseudomorphs and thin laminations in argillites at the top of the parasequence reflect deposition on evaporitic, supratidal mudflats. The above interpretation of depositional environments is consistent with wave energy patterns on shallow shelves that show a general increase from deep to shallow waters followed by decrease into subaerial settings (Reading and Collinson, 1996).

Silicified nodules developed in massive, gray, organic-poor dolomite in the middle of the parasequence may have formed after anhydrite. Although the nodules lack a cauliflower outline, such structures may not be preserved if replacement occurs in a deep burial setting (Warren, 1999). The generally flattened shape and lack of compactional drapes around the silicified nodules favors deep burial replacement.

Outer shelf to inner shelf parasequences

This parasequence type comprises from the base to the top: parted and ribbon dolomite, silicified dolomite with large domal digitate stromatolites and massive gray dolomite (Fig. 2.20 D). Bases of parasequences are defined by parted/ribbon brown dolomite or, where absent, by silicified dolomite with large domal digitate stromatolites that make up most of the parasequence. Domal digitate stromatolites form tabular stromatolite buildups with large aerial extent. Relief of individual stromatolites is up to several meters and they are pervasively silicified. Masssive gray dolomite capping this parasequence is the same facies as that at the base of the inner shelf to supratidal parasequence (Fig. 20 C); it rarely contains domal stromatolites up to 1.5 m in height that are similar to those in the underlying facies except that they are not silicified.

The above characteristics are compatible with a prograding low-energy, outer to inner shelf transition (cf. Jones and Desrochers, 1992). Ribbon/parted dolomite facies are diagnostic of deposition below wave base (cf. James and Stevens, 1986; Coniglio and James, 1990). Lack of high-energy indicators such as oolites, traction-produced structures, and intraclasts in association with the large domal digitate stromatolites, as well as the tabular rather than elongated shape of the buildups, suggests that they formed below wave base and were located behind a reef that protected them from open-marine, high-energy waves (cf. Jones and Desrochers, 1992). Traction-produced structures in overlying gray dolomite support shoaling of the depositional environment to an inner shelf influenced by wave processes. Digitate stromatolites in the late Paleoproterozoic McArthur Basin of northern Australia similar to those present within this parasequence type were related to growth on a hard substrate in a low-energy lagoonal environment with low sediment flux, and abundant accommodation space (Sami et al., 2000). Reefs generally form during sea-level rise when increased accommodation and low sediment flux provide the most favorable conditions for reef growth (cf. Grotzinger, 1989, Grotzinger et al., 2000).

Outer shelf to subaerial parasequences

This parasequence contains from the base to the top: organic-rich dolomite, gray dolomite, dolosiltite, brown dolomite and mature quartz sandstone (Fig. 2.20 E). Organic-rich dolomite containing stratiform and inclined stromatolites is rare at the base of parasequences; most parasequences commence with thinly laminated, gray fenestral dolomite with neptunian dikes, rare oolites or oncolites and sulfate pseudomorphs. Traction-produced sedimentary structures including lenticular, wavy, and plane bedding are most abundant in the middle and upper parts of the parasequence. Stromatolites in the gray dolomite are rare and isolated but include stratiform, domal and columnar forms. The top of the parasequence is marked by brown dolomite with wavy and plane bedding or, in rare cases, by karstic breccia overlain by cross-bedded, quartz sandstone.

This parasequence type is interpreted to be a result of shoreline progradation over an outer shelf. The high organic carbon content of and presence of stromatolites in the basal dolomite suggests deposition in reducing environment below the oxic-anoxic boundary but

within the photic zone. Based on the presence of ubiquitous fine-scale laminations and fenestral structures, rare oolites or oncolites, normal grading, traction-produced structures and sulfate pseudomorphs, the overlying gray dolomite is ascribed to the peritidal zone of an open shelf (cf. Wright, 1990).

The characteristics of the stromatolites in the gray dolomite, and especially the isolated columnar forms, support a relatively deep, open-marine setting in which stromatolites accreted vertically to remain in the photic zone (cf. Grotzinger, 1989). The dominance of traction-produced sedimentary structures in the brown dolomite suggests deposition in the upper peritidal zone. Karst breccia at the top of the parasequence records dissolution related to a fall in relative sea level. The overlying quartz sandstone is interpreted as a fluvial deposit.

Drowned platform parasequences

This parasequence contains from the base to the top: black organic-rich shale with pyrite, siltstone, sandstone with shale and brown dolomite (Fig. 2.20 F). Where exposed, the base of the parasequence is marked by black chert with small digitate stromatolites. Organic-rich shale contains interbeds of brown ribbon dolomite with soft-sediment deformation structures, and turbidite beds. The remainder of the parasequence displays an upward-coarsening trend and sedimentary structures such as wavy and plane bedding appear towards the top of the parasequence.

This parasequence type records progradation following drowning of a carbonate shelf (cf. Wright and Burchette, 1996). Black chert at the base of the parasequence represents a condensed section (cf. Van Wagoner et al., 1987) that formed below wave base and below the oxic-anoxic boundary. The upward-coarsening trend and appearance of traction-produced structures upwards in the parasequence suggests shoaling. Turbidites and ribbon dolomite with soft-sediment deformation structures indicate slope instability. Associations of lithologies present in this parasequence are similar to Phanerozoic hemipelagic terrigenous clastics (cf. Coniglio and Dix, 1992).

RELATIVE SEA LEVEL CHANGES AND CARBONATE PLATFORM ARCHITECTURE

Stacking patterns of parasequences in the Nash Fork Formation permit construction of a relative sea level curve (Fig. 2.21). The lower two members of the Nash Fork Formation (L1 and L2) are dominated by parasequence types A and B and developed in peritidal settings during a relative lowstand of sea level. Overlying L3 consisting of parasequence type D records an increase in accommodation that favored the growth of large domal digitate stromatolites below wavebase. Parasequence type C dominates L4 and indicates a decrease in accommodation. The inner shelf to supratidal deposits of the L4 member have a high content of dolomitic mudstone suggesting that growth of domal digitate stromatolites was inhibited by a high flux of carbonate mud. Reappearance of domal digitate stromatolites in L5 indicates another increase in accommodation. Inner shelf to peritidal parasequence types B and C that make up L6 and L7 demarcate another shallowing of the basin that culminated in subaerial exposure and deposition of fluvial sandstone in the lower part of L7 (see Fig. 2.5). The upward decrease in abundance of siliciclastic and the increase in abundance of carbonate facies in parasequence type B that dominates L7 and the lower part of L8 (see Figs. 2.5 and 2.12), coupled with the transition into large domal digitate stromatolites in the upper half of L8, implies a progressive increase in accommodation following the earlier exposure. This deepening trend culminated in the deposition of organic-rich shales of M1 under relatively deep-water, anoxic conditions. The overlying transition into shelf to supratidal conditions recorded by parasequence type C of M2 reflects a subsequent decrease in accommodation and reestablishment of a carbonate platform. Another drowning event at the base of M3 was followed by upward shallowing through M3 into the lower part of U1 culminating in subearial exposure and formation of the prominent karstic breccia and overlying incised fluvial channel sandstone (Fig 2.16). Outer shelf to peritidal deposits of the remainder of U1 indicate an subsequent increase in accommodation prior to volcanic outpouring and termination of carbonate deposition.

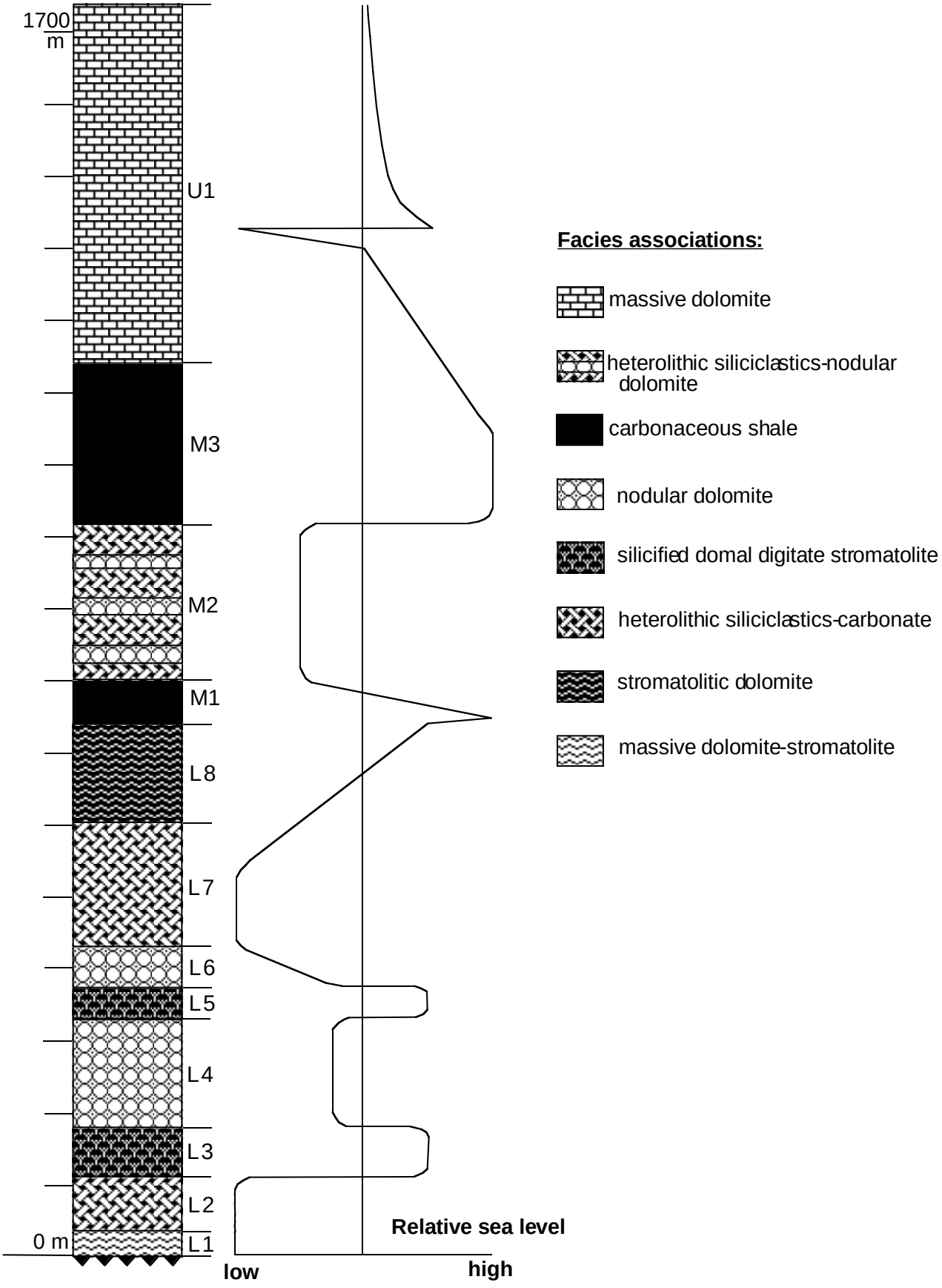

Fig. 2.21. Relative sealevel curve for the Nash Fork Formation.

The limited extent of the outcrop belt precludes a detailed reconstruction of the profile of the carbonate platform. However, facies associations in the lower Nash Fork Formation are most compatible with a low-energy, low-gradient protected platform. Protected shelves are characterized by wide lagoons that may contain tabular stromatolite mounds and may develop high salinity due to restricted circulation (Wright and Burchette, 1996). Several features of the lower Nash Fork Formation are compatible with this interpretation including: 1) lack of oolites or oncolites and rare intraformational breccias that indicate an overall low-energy depositional environment (cf. Sherman et al., 2000); 2) presence of sulfate pseudomorphs suggestive of hypersaline conditions (cf. Kendall, 1992); 3) low diversity but high abundance of stromatolites implying stable environmental conditions (cf. Gebelein, 1974; Serebryakov and Semikhatov, 1974; Swett and Knoll, 1985); and 4) lack of any preferred orientation to stromatolites perpendicular to paleostrike supporting a low-energy platform lacking appreciable currents. Microbial mat ripups and rare layers with intraclasts are likely related to periodic storm events. Parasequence types A and B are interpreted as interdeltaic, peritidal deposits that graded basinwards into lagoonal facies represented by parasequence type C facies (Fig. 2.22 A). Domal digitate stromatolites of parasequence type D likely represent reefal deposits but no evidence exists in the preserved record that these developed along the platform edge. Rather, reefal buildups probaly developed on the platform following drowning events. Associated digitate spheroids in ribbon dolomite likely represent stromatolite blocks dislodged from the reef. Reefal stromatolites and spheroids were silicified during early diagenesis by precipitation from silica oversaturated sea-water (cf. Maliva et al., 1989; Siever, 1977, 1992).

Two drowning events in the middle part of the Nash Fork modified the depositional profile of the platform. Drowning caused a shut-down of carbonate production and changed the depositional profile from a low-energy, low-gradient protected platform to an unprotected shelf with a higher gradient for the middle and upper Nash Fork Formation (Fig. 2.22 B). Black mudstones of the drowned platform (parasequence type F) overlie carbonate platform deposits and record high organic matter burial in anoxic waters of the drowned platform. A similar transition from shallow-water platformal carbonates to deep-water carbonaceous shales associated with drowning of the platform was recognized in the Carboniferous Lower Limestone Shale Group of South Wales and Western England (Burchette, 1987) and in Toarcian

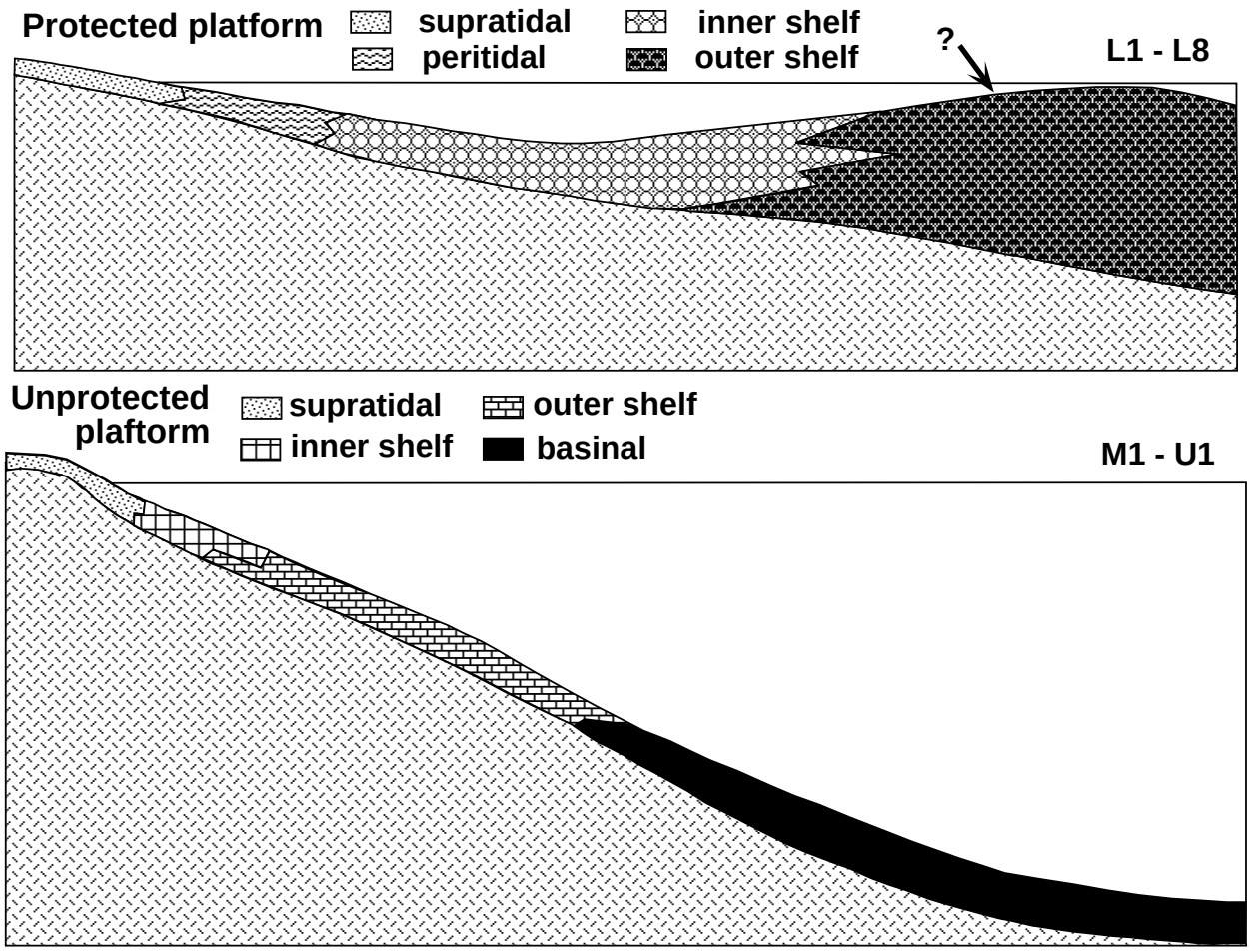

Fig. 2.22. Depositional Model for the Nash Fork Formation; (A) L1 - L8 members were deposited on a protected platform; (B) M1 - U1 members were deposited on an unprotected platform.

epicontinental successions of Western Europe (Riegraf, 1982; Jenkyns et al., 1985). Comparison with these younger examples suggests that the high organic matter content of the shales can be attributed to the incursion of nutrient-rich, deep-waters that stimulated high phytoplankton productivity. The presence in the upper Nash Fork Formation of ubiquitous thin laminations and silicified fenestrae supports a tidal- or storm-influence on development of the outer-shelf to subaerial deposits of the parasequence type E (cf. Wright, 1990). Rare oolites or oncolites and normal grading in dolosiltite also indicate an unprotected environment. Stromatolites, although diverse, are rare, isolated and small in the upper Nash Formation. Organic-rich dolomites and columnar stromatolites in the lower part of the outer shelf to subaerial deposits of the parasequence type E (Fig. 2.20) indicate an outer to mid-shelf setting with restricted circulation.

No evidence for restricted depositional environments in the form of such features as bedded evaporites are present in the Nash Fork Formation. Rather, the presence of facies indicative of tidal flat, lagoonal, inner and outer shelf, and drowned platform depositional environments suggests that the Nash Fork Formation developed entirely in open-marine settings on a mature passive margin along the southern edge of the Archean Wyoming Craton as proposed by Karlstrom et al. (1983).

CAUSE OF PLATFORM DROWNING

Possible causes of drowning of carbonate platforms include: tectonically enhanced subsidence, glacioeustatic sea level rise and decline in carbonate production (Schlager, 1981; Wright and Burchette, 1996). The two main building elements of the Nash Fork carbonate platform are stromatolites and dolomitic mudstones. Both of these elements persisted without noticeable change until the first drowning event mitigating against a decline in carbonate production. Paleoproterozoic glaciations are confined to the time interval 2.45-2.22 Ga (Young, 1991; but see for different view Salop, 1982 and Akhmedov et al., 1996) and are significantly older than the Nash Fork Formation. This leaves tectonically influenced subsidence as the likely cause of platform drowning.

The upper Libby Creek Group was interpreted to have been deposited in a foreland basin related to the 1.78-1.74 Ga Medicine Bow Orogeny based on the transition from the underlying shallow-water tidally influenced passive margin quartz sandstones to mafic submarine volcanics and deep-water shales (Karlstrom et al., 1983). This view was challenged on the basis of a provenance study of the upper Libby Creek Group that showed sediment derivation from the Wyoming Craton with no evidence for proximity to a Paleoproterozoic volcanic arc (Ball and Farmer, 1991; Crichton and Condie, 1993). Chemostratigraphic age constraints for the Nash Fork Formation suggest that the upper Libby Creek is significantly older than the 1.74-1.78 Ga old Medicine Bow Orogeny (Bekker et al., 2001a). Evidence for a 2.1-2.0 Ga old compressional event are lacking on northern continents although orogenic events of this age did affect southern continents (Ledru et al., 1994; Möller et al., 1995; Machado et al., 1996).

The Paleoproterozoic tectonic history of northern continents has been interpreted in terms of protracted rifting leading to the final breakup of the Kenorland supercontinent between 2.1 and 2.0 Ga (Williams et al., 1991; Kohonen, 1995; Aspler and Chiarenzelli, 1998). Geochronologic and tectonostratigraphic data suggest that the Wyoming, Superior and Hearne cratons were contiguous during the early Paleoproterozoic (Houston, 1993; Roscoe and Card, 1993; Aspler and Chiarenzelli, 1998). Mafic sills and dikes and their felsic differentiates on these cratons constrain the age of the breakup to 2.1-2.0 Ga (Fig. 2.23). Older, 2.2-2.1 Ga ages likely record protracted rifting before the breakup of the Kenorland (Aspler and Chiarenzelli, 1998). The metagranite of the Farmington Canyon Complex in the Wasatch Mountains, Utah on the western margin of the Wyoming Craton has been dated at 2023 ± 4 Ma (Hedge et al., 1983) and is likely related to this breakup event.

Geochronologic data suggest that the rifting and breakup of Kenorland at 2.1-2.0 Ga that led to the opening of the Manikewan ocean on the eastern margin of the Wyoming Craton (Stauffer, 1984) affected the mature, thermally subsiding, passive margin on which the Nash Fork carbonate platform was developing. Lithostratigraphic and chemostratigraphic data indicate that the passive margin extended at least to the Sierra Madre and the Hartville Uplift (Fig. 2.1; Karlstrom et al., 1983; Bekker et al., 2001a). This platform was likely dissected and reactivated by the breakup on the eastern margin of the Wyoming Craton in a similar way that the upper Triassic carbonate platform of the Southern Alps was affected by the opening of the Ligurian-Piedmont ocean (Carulli et al., 1998). Additional support for the extensional regime on the Nash Fork carbonate platform is provided by ubiquitous neptunian dikes in the upper part of the platform. Neptunian dikes are generally related to recurrent extensional activity (Lehner, 1991; Cozzi, 2000).

STYLES OF CARBONATE DEPOSITION

The lower and middle Nash Fork Formation consist of the following building elements: dolomitic mudstones, stromatolites, dolosiltites and rare macroscopic seafloor precipitates at the sediment-water interface. The main deposit was dolomitic mudstone that now makes up gray and nodular dolomite. Mudstone was likely precipitated directly from seawater in a similar

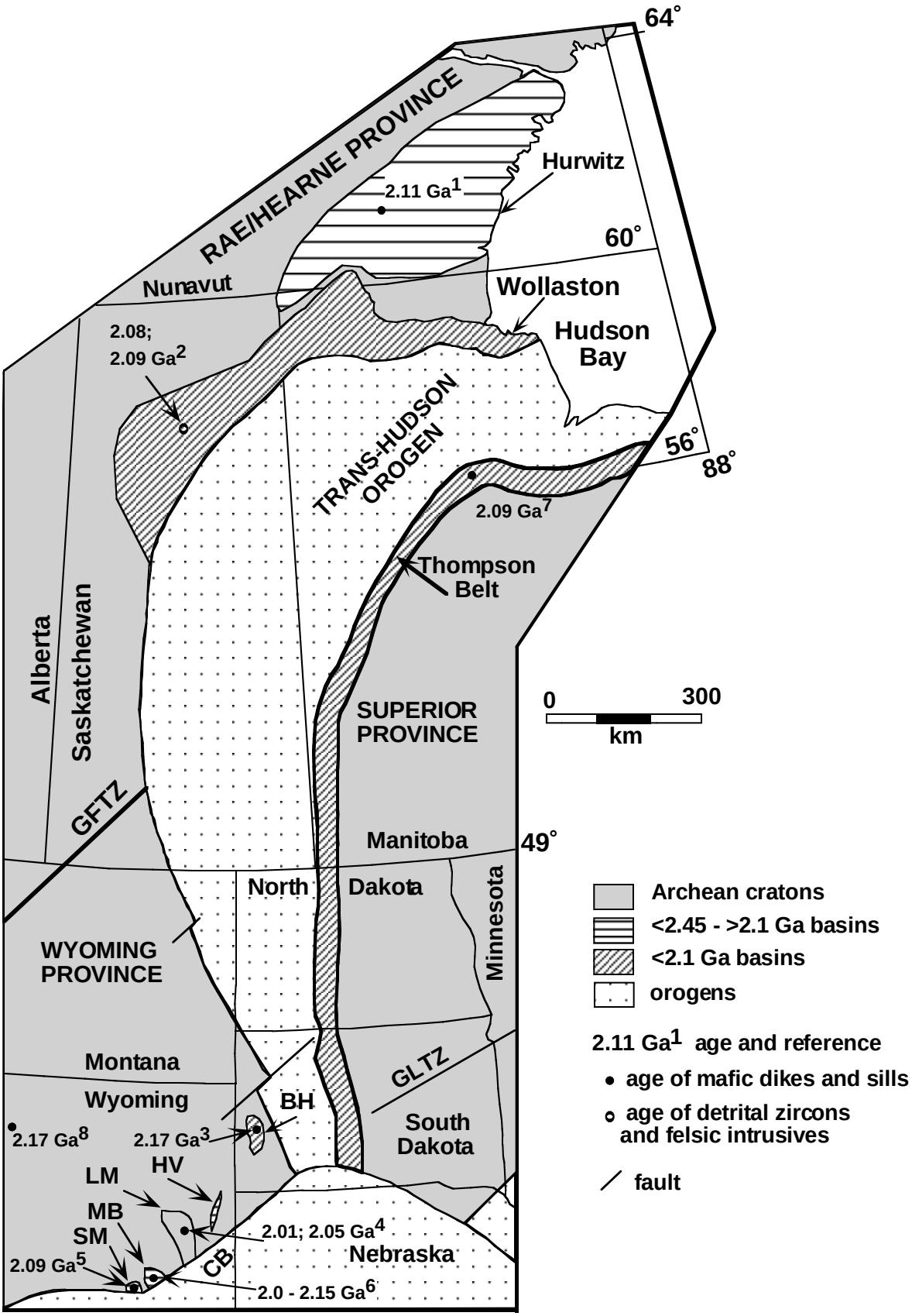

Fig. 2.23. Map showing the Archean Wyoming, Superior and Hearne provinces, early Paleoproterozoic basins and ages of 2.2-2.0 Ga mafic dikes and sills and their felsic differentiates. Ages are based on U-Pb dating of zircon and baddelyite crystals unless otherwise

stated. 1. 2111 ± 0.6 Ma Hurwitz gabbro sills (Heaman and LeCheminant, 1993); 2. 2086 + 52/-8 Ma granite and 2076 ± 3 Ma detrital zircon grains, Wollaston Basin (Annesley et al., 1992; Delaney, 1995); 3. 2170 ± 120 Ma Blue Draw Metagabbro, Black Hills, SD (Redden et al., 1990); 4. 2011 ± 1.2 Ma Kennedy diabase dikes and 2051 ± 9 Ma Boy Scout Camp granodiorite (Cox et al., 2000); 5. 2092 ± 9 Ma metagabbro, Sierra Madre (Premo and Van Schmus, 1989); 6. 2.1–2.15 Ga Gap quartz diorite, Medicine Bow Mountains (Rb-Sr age, Houston et al., 1992, p. 48); 7. 2091 ± 2 Ma Cauchon Lake dikes (Halls and Heaman, 2000); 8. 2170 ± 8 Ma quartz diorite dikes, southern Wind River Mountains, WY (Harlan et al., 2000; Harlan et al., submitted.).

fashion to whitings in the Bahamas (cf. Robbins and Blackwelder, 1992, Robbins et al., 1997). Dolomitic mudstones are common on Mesoproterozoic and younger carbonate platforms (e.g.Sherman et al., 2000) but are rare in older Archean and Paleoproterozoic successions where cements and stromatolites were the dominant building blocks (Grotzinger, 1989; Sumner and Grotzinger, 2000; Sherman et al., 2000). Macroscopic seafloor precipitates formed at the sediment-water interface are rare in the lower and middle parts of the Nash Fork Formation. Tufa structures and small domes with radial structures in the L1 member were possibly formed by inorganic precipitation from supersaturated shallow waters in the upper intertidal to supratidal setting. Vertical pillars in domal digitate stromatolites of L3, L5 and the top of L8 members (Fenton and Fenton, 1939; Hofmann and Davidson, 1998) are similar to micro stromatolites generally interpreted as crystallization features (Grotzinger and Read, 1983; Grotzinger, 1989, 1990; for different view see Raaben, 1998). Other indications of macroscopic seafloor precipitation are lacking in this more than 1 km thick carbonate succession. This is somewhat surprising because these inorganic structures are ubiquitous on Archean and Middle Paleoproterozoic carbonate platforms (Sumner and Grotzinger, 2000; Grotzinger and Read, 1983; Sami and James, 1996). Our observations and a literature review of other carbonate platforms formed during the ca. 2.2-2.1 Ga carbon isotope excursion suggest that these structures are lacking on platforms of this age. In this respect it is significant that carbonate deposition on this platform occurred shortly after the rise in atmospheric oxygen. Since Fe^{2+} and Mn^{2+} were likely major inhibitors of carbonate precipitation during the Archean (cf. Sumner and Grotzinger,

1996, 2000), the rise in atmospheric oxygen level resulted in a decrease in the Fe and Mn content of the ocean and allowed carbonate precipitation within the ocean water column saturated with respect to bicarbonate. We propose that the atmospheric oxygen level rise in the early Paleoproterozoic was accompanied by prolific micrite precipitation on carbonate platforms.

The upper Nash Fork Formation consists of dolomitic mudstone, relatively rare and isolated, although diverse stromatolites, dolosiltite and more common inorganic precipitates. Inorganic precipitates are represented by bedding-parallel cements, voids filled with isopachous cements and rare small fans with radial structures. Reappearance of these structures after the end of the carbon isotope excursion suggests that the oxygen content of the atmosphere and ocean may have decreased after the end of the carbon isotope excursion. This change in the redox state was likely related to environmental changes at the end of the carbon isotope excursion and is consistent with ubiquitous inorganic precipitates, lack of evidence for sulfate evaporites, reappearance of BIFs, and highly positive sulfur isotope values of sedimentary sulfides in Middle Paleoproterozoic successions (Simonson and Hassler, 1996; Canfield, 1998; Pope and Grotzinger, 2000). These data support a decrease in the oxygen content of the Proterozoic ocean shortly after the end of the carbon isotope excursion.

CONCLUSIONS

1. The Paleoproterozoic Nash Fork Formation was deposited on an open-marine, passive margin along the southern flank of the Archean Wyoming Craton. Facies analysis reveals that the formation developed in tidal-flat, lagoonal, inner- and outer-shelf, and drowned platform settings.

2. Style of carbonate deposition was strongly influenced by a dramatic rise in the levels of atmospheric oxygen during the early Paleoproterozoic. Inorganic precipitates at the water-sediment interface are rare in the lower part of the formation whereas pseudomorphs after sulfate evaporites are ubiquitous. This observation is consistent with a decrease in the Fe and Mn content and an increase in sulfate content in the ocean related to the rise in the level of atmospheric oxygen.

3. The presence of ubiquitous inorganic precipitates and the rarity of sulfate pseudomorphs in the upper Nash Fork Formation that developed after the end of the Paleoproterozoic carbon isotope excursion suggest that the redox state of the oceans decreased in concert with the change in biogeochemical cycling of carbon.

4. The lower Nash Fork platform experienced low amplitude, relative sea level changes whereas two major drowning events are recorded in the middle Nash Fork Formation. Drowning resulted in a change of the platform profile from a low-energy, low-gradient protected setting to an unprotected shelf with a higher gradient.

5. Drowning is attributed to dissection and reactivation of the thermally subsiding platform in response to tectonically driven subsidence associated with rifting and breakup on the eastern flank of the Wyoming Craton. This rifting event is related to the final breakup of the Kenorland supercontinent at 2.1-2.0 Ga.

REFERENCES

Akhmedov, A.M., Travin, L.V., Tikhomirova, M., 1996. Glacial and evaporate epochs in the early Proterozoic and interregional correlation. Regional Geology and Metallogeny 5, 84-97, in Russian.

Annesley, I.R., Madore, C., Krogh, T.E., 1992. U-Pb geochronology of some granitoids from the Peter Lake Domain: A summary. Summary of Investigations 1992. Saskatchewan Geological Survey, Sask. Energy Mines Misc. Rep. 92-4, 168-171.

Aspler, L. B., Chiarenzelli, J. R., 1998, Two Neoarchean supercontinents? Evidence from the Paleoproterozoic, Sediment. Geol. 120, 75-104.

Ball, T. T., Farmer, G. L., 1991. Identification of 2.0 to 2.4 Ga Nd model age crustal material in the Cheyenne belt, northeastern Wyoming: implications for Proterozoic accretionary tectonics at the southern margin of the Wyoming craton. Geology 19, 360-363.

Bekker, A., Karhu, J. A., Kaufman, A. J., 2001a, Tectonic implications of a chemostratigraphic study of Early Paleoproterozoic carbonates from the southeastern margin of the Wyoming Craton, Geol. Soc. Am., Abstracts with Programs 33 (5), p. A-44.

Bekker, A., Kaufman, A.J., Karhu, J.A., Beukes, N.J., Swart, Q.D., Coetzee, L.L., Eriksson, K.A., 2001b. Chemostratigraphy of the Paleoproterozoic Duitschland Formation, South Africa: Implications for coupled climate change and carbon cycling. Am. J. Sci. 301, 261-285.

Beukes, N. J., 1987. Facies relations, depositional environments and diagenesis in a major early Proterozoic stromatolitic carbonate platform to basinal sequence, Campbellrand Subgroup, Transvaal Supergroup, Southern Africa. Sediment. Geol. 54, 1–46.

Blackwelder, E., 1926. Precambrian geology of the Medicine Bow Mountains. Geol. Soc. Am. Bull. 37, 617-658.

Buchan, K. L., Mortensen, J. K., Card, K. D., Percival, J. A., 1998. Paleomagnetism and U-Pb geochronology of diabase dyke swarms of Minto block, Superior Province, Quebec, Canada. Can. J. Earth Sci. 35, 1054-1069.

Burchette, T.P., 1987. Carbonate-barrier shorelines during the basal Carboniferous transgression: the Lower Limestone Shale Group, South Wales and western England. In: Miller, J., Adams, A.E., Wright, V.P. (Eds.), European Dinantian Environments. Wiley, Chichester, pp. 239-263.

Burchette, T.P., Wright, V.P., 1992. Carbonate ramp depositional systems. Sediment. Geol. 79, 3-57.

Cameron, E. M., 1982. Sulphate and sulphate reduction in early Precambrian oceans. Nature 296, 145-148.

Canfield, D.E., 1998. A new model for Proterozoic ocean chemistry. Nature 396, 450-453.

Carulli, G.B., Cozzi, A., Longo Salvador, G., Ponton, M., Podda, F., 1998. Evidence of synsedimentary tectonic activity during the Norian-Lias (Carnian Prealps, Northern Italy). Mem. Soc. Geol. It. 53, 403-415.

Cecile, M. P., and Campbell, F. H. A., 1978, Regressive stromatolite reefs and associated facies, middle Goulburn Group (lower Proterozoic), in Kilohigok Basin, N.W.T.: an example of environmental control of stromatolite form. Can. Soc. Pet. Geol. Bull. 26, 237–267.

Chamberlain, K. R., 1998. Medicine Bow orogeny: Timing of deformation and model of crustal structure produced during continent-arc collision ca. 1.78 Ga, southeastern Wyoming. Rocky Mountain Geol. 33, 259-277.

Coniglio, M., Dix, G.R., 1992. Carbonate slopes. In: Walker, R.G., James, J.P. (Eds.), Facies models: response to sea level changes. Geological Association of Canada, pp. 349-373.

Coniglio, M. and James, N.P., 1990. Origin of fine-grained siliciclastic and carbonate sediments in early Paleozoic slope sequence: Cow Head Group of western Newfoundland. Sedimentology 37, 215-230.

Cox, D. M., Frost, C. D., Chamberlain, K. R., 2000. 2.01-Ga Kennedy dike swarm, southeastern Wyoming: Record of a rifted margin along the southern Wyoming province. Rocky Mountain Geol. 35, 7–30.

Cozzi, A., 2000. Synsedimentary tensional features in Upper Triassic shallow-water platform carbonates of the Carnian Prealps (northern Italy) and their importance as palaeostress indicators. Basin Res. 12, 133-146.

Crichton, J. G., Condie, K. C., 1993. Trace elements as source indicators in cratonic sediments: A case study from the Paleoproterozoic Libby Creek Group, Southeastern Wyoming. J. Geol. 101, 319-332.

Delaney, G.D., 1995. Some perspectives on the stratigraphy and metallogeny of the eastern margin of the Wollaston Domain. In: Hajnal, Z., Lewry, J. (Eds.), Lithoprobe Trans-Hudson Orogen Transect, Report of Fifth Transect Meeting, Report No. 48. University of Saskatchewan, Regina, SK, pp. 87-101.

Evans, D. A., Beukes, N. J., Kirschvink, J. L., 1997. Low-latitude glaciation in the Paleoproterozoic era. Nature 386, 262-266.

Fenton, C.L., Fenton, M.A., 1939. Precambrian and Paleozoic algae. GSA Bull. 50, 89-126.

Gebelein, C.D., 1974. Biologic control of stromatolite microstructure: implications for Precambrian time stratigraphy. Am. J. Sci. 274, 575-598.

Grotzinger, J.P., 1990. Geochemical model for Proterozoic stromatolite decline. Am. J. Sci. 290-A, 80 - 103.

Grotzinger, J.P., 1989. Facies and evolution of Precambrian carbonate depositional systems: Emergence of the modern platform archetype. In: Crevello, P.D., Wilson, J.L., Sarg, J.F., Read, J.F. (Eds.), Controls on Carbonate platform and Basin Development. SEPM Spec. Publ. 44, pp. 79 - 106.

Grotzinger, J. P., 1986a. Evolution of early Proterozoic passive margin carbonate platform: Rocknest Formation, Wopmay Orogen, N.W.T., Canada. J. Sed. Petr. 56, 831–847.

Grotzinger, J.P., 1986b. Cyclicity and paleoenvironmental dynamics, Rocknest platform, northwest Canada. Geol. Soc. Am. Bull. 97, 1208-1231.

Grotzinger, J. P., James, N. P., 2000, Precambrian carbonates: evolution of understanding, In: Grotzinger, J. P., James, N. P., (Eds.), Carbonate sedimentation and diagenesis in the evolving Precambrian world. SEPM Spec. Publ. 67, p. 3–20.

Grotzinger, J. P., Kasting, J. F., 1993. New constraints on Precambrian ocean composition. J. Geol. 101, 235-243.

Grotzinger, J.P., Read, J.F., 1983. Evidence for primary aragonite precipitation, lower Proterozoic (1.9 Ga) dolomite, Wopmay orogen, northwest Canada. Geology 11, 710-713.

Grotzinger, J.P., Watters, W.A., Knoll, A.H., 2000. Calcified metazoans in thrombolite-stromatolite reefs of the terminal Proterozoic Nama Group, Namibia. Paleobiology 26, 334-359.

Halls, H.C., Heaman, L.M., 2000. The paleomagnetic significance of new U-Pb age data from the Molson dyke swarm, Cauchon Lake area, Manitoba. Can. J. Earth Sci. 37, 957-966.

Harlan, S.S., Geissman, J.W., Premo, W.R., Paleomagnetism and geochronology of an Early Proterozoic quartz diorite in the Southern Wind River Mountains, Wyoming. Tectonophys., submit.

Harlan, S.S., Geissman, J.W., Premo, W.R., 2000. Preliminary geochronologic and paleomagnetic results from an Early Proterozoic dike in the Southern Wind River Mountains, Wyoming. Geol. Soc. Am., Abstracts with Programs, 32(7), pp. A-453.

Hattori, K., Krouse, H. R., Campbell, F. A., 1983a. The start of sulfur oxidation in continental environments: about 2.2 x 10^9 years ago. Science 221, 549–551.

Hattori, K., Campbell, F. A., Krouse, H. R., 1983b. Sulphur isotope abundances in Aphebian clastic rocks: implications for the coeval atmosphere. Nature 302. 323–326.

Heaman, L. M., 1997. Global mafic magmatism at 2.45 Ga: Remnants of an ancient large igneous province? Geology 25, 299-302.

Heaman, L.M., LeCheminant, A.N., 1993. Paragenesis and U-Pb systematics of baddeleyite (ZrO_2). Chem. Geol. 110, 95-126.

Hedge, C.E., Stacey, J.S., Bryant, B., 1983. Geochronology of the Farmington Canyon Complex, Wastch Mountains, Utah, Geol. Soc. Am. Mem. 157, pp. 37-44.

Hoffman, P.F., 1989. Pethei Reef Complex (1.9 Ga), Great Slave Lake N.W.T. In: Geldsetzer, H.J., James, N.P., Tebbutt, G.E. (Eds.), Reefs: Canada and adjacent areas. Can. Soc. Pet. Geol. Mem. 13, pp. 38-48.

Hofmann, H.J., Davidson, A., 1998. Paleoproterozoic stromatolites, Hurwitz Group, Quartzite Lake area, Northwest Territories, Canada. Can. J. Earth Sci. 35, 280-289.

Houston, R. S., 1993. Late Archean and Paleoproterozoic geology of southeastern Wyoming. In: Snoke, A. W., Steidtmann, J. R., Roberts, S. M., (Eds.), Geology of Wyoming. Geol. Surv. Wyoming Mem. 5, 78-116.

Houston, R. S., Karlstrom, K. E., 1992. Geological map of Precambrian metasedimentary rocks of the Medicine Bow Mountains, Albany and Carbon Counties, Wyoming. U. S. Geol. Surv. Misc. Inv. Ser. Map I-2280.

Houston, R. S., Karlstrom, K. E., Graff, P. J., Flurkey, A. J., 1992. New stratigraphic subdivisions and redefinition of subdivisions of Late Archean and Paleoproterozoic metasedimentary and metavolcanic rocks of the Sierra Madre and Medicine Bow Mountains, southern Wyoming. U. S. Geol. Surv. Prof. Pap. 1520, 50p.

Houston, R. S., Lanthier, L. R., Karlstrom, K. E., Sylvester, G. G., 1981. Paleoproterozoic diamictite of southern Wyoming. In: Hambrey, M. J., Harland, W. B., (Eds.), Earth's Pre-Pleistocene Glacial Record. Cambridge University Press, New York, pp. 795-799.

Houston, R. S., and others, 1968. A regional study of rocks of Precambrian age in the part of the Medicine Bow Mountains lying in southeastern Wyoming, with a chapter on the relationship between Precambrian and Laramide structure. Wyoming Geol. Surv. Mem. 1.

James, N.P. and Stevens, R.K., 1986. Stratigraphy and correlation of the Cambro-Ordovician Cow Head Group, western Newfoundland. Geol. Surv. Can. Bull. 366.

Jenkyns, H.C., Sarti, M., Masetti, D., Howarth, M.K., 1985. Ammonites and stratigraphy of Lower Jurassic black shales and pelagic limestones from the Belluno Trough, Southern Alps, Italy. Ecl. Geol. Helv. 78, 299-311.

Jones, B., Desrochers, A., 1992. Shallow platform carbonates. In: Walker, R.G., James, N.P. (Eds.), Facies models: response to sea level changes. Geological Association of Canada, pp. 277-301.

Kah, L. C., Knoll, A. H., 1996. Microbenthic distribution of Proterozoic tidal flats: environmental and taphonomic considerations. Geology 24, 79–82.

Kohonen, J., 1995, From continental rifting to collisional crustal shortening – Paleoproterozoic Kaleva metasediments of the Höytiäinen area in North Karelia, Finland, Geol. Surv. Finland, Bull. 380, 79p.

Karhu, J. A., Holland, H. D., 1996, Carbon isotopes and the rise of atmospheric oxygen: Geology 24, 867-870.

Karlstron, K. E., Houston, R. S., 1984. The Cheyenne Belt: Analysis of a Proterozoic suture in Southern Wyoming. Precambrian Res. 25, 415–446.

Karlstrom, K. E, Flurkey, A. J., Houston, R. S., 1983. Stratigraphy and depositional setting of the Proterozoic Snowy Pass Supergroup, southeastern Wyoming: Record of a Paleoproterozoic Atlantic-type cratonic margin. Geol. Soc. Am. Bull. 94, 1257-1274.

Kendall, A.C., 1992. Evaporites. In: Walker, R.G., James, J.P. (Eds.), Facies models: response to sea level changes. Geological Association of Canada, pp. 375-409.

Knight, S.H., 1968. Precambrian stromatolites, bioherms and reefs in the lower part of the Nash Formation. Contr. Geol. 7, 73-116.

Knight, S.H., Keefer, D.K., 1966. Preliminary report on the Precambrian stromatolites in the Nash Formation, Medicine Bow Mountains, Wyoming. Contr. Geol. 5, 1-11.

Ledru, P., Johan, V., Milési, J. P., and Tegyey, M., 1994, Markers of the last stages of the Paleoproterozoic collision: evidence for a 2 Ga continent involving circum-South Atlantic provinces. Precambrian Res. 69, 169-191.

Lehner, B.L., 1991. Neptunian dykes along a drowned carbonate platform margin: an indication for recurrent extensional tectonic activity? Terra Nova 3, 593-602.

Long, D. G. F., 1976. The stratigraphy and sedimentology of the Huronian (Lower Aphebian) Mississagi and Serpent formations. Unpubl. PhD thesis, University of Western Ontario, London, ON.

Machado, N., Schrank, A., Noce, C. M., Gauthier, G., 1996. Ages of detrital zircon from Archean-Paleoproterozoic sequences: implications for greenstone belt setting and evolution of a Transamazonian foreland basin in Quadrilátero Ferrífero, southeast Brazil. Earth Planet. Sci. Lett. 141, 259–276.

Makarikhin, V.V. and Kononova, G.M., 1983. Phylotites of the Lower Proterozoic of Karelia. Nauka, Leningrad, 180 pp., in Russian.

Maliva, R.G., Knoll, A.H., Siever, R., 1989. Secular change in chert distribution: A reflection of evolving biological precipitation in the silica cycle. Palaios 4, 519-532.

Melezhik, V. A., Fallick, A. E., Medvedev, P. V., Makarikhin, V. V., 2000. Palaeoproterozoic magnesite-stromatolite-dolostone-'red bed' association, Russian Karelia: paleoenvironmental constraints on the 2.0 Ga-positive carbon isotope shift, Norsk Geologisk Tidsskrift 80, 163-186.

Melezhik, V. A., Fallick, A. E., Medvedev, P. V., Makarikhin, V. V., 1999. Extreme $^{13}C_{carb}$ enrichment in ca. 2.0 Ga magnesite-stromatolite-dolomite-'red beds' association in a global context: a case for the world-wide signal enhanced by a local environment. Earth-Sci. Rev. 48, 71–120.

Mertanen, S., 2001, Palaeomagnetic evidences for the evolution of the Earth during Early Paleoproterozoic, European Union of Geosciences, Abstract Suppl. No. 1, v. 13, p. 190.

Möller, A., Appel, P., Mezger, K., Schenk, V., 1995, Evidence for a 2 Ga subduction zone: eclogites in the Usagaran belt of Tanzania, Geology 23, 1067–1070.

Ojakangas, R.W., 1988. Glaciation: an uncommon "mega-event" as a key to intracontinental and intercontinental correlation of Paleoproterozoic basin fills, North American and Baltic cratons. In: Kleinspehn, K.L., Paola, C. (Eds.), New perspectives in basin analysis. Springer-Verlag, pp. 431-444.

Pope, M. C., Grotzinger, J. P., 2000. Controls on fabric development and morphology of tufas and stromatolites, uppermost Pethei Group (1.8 Ga), Great Slave Lake, Northwest Canada. In: Grotzinger, J. P., James, N. P., (Eds.), Carbonate sedimentation and diagenesis in the evolving Precambrian world. SEPM Spec. Publ. 67, pp. 103-121.

Pratt, B.R., James, N.P., Cowan, C.A., 1992. Peritidal carbonates. In: Walker, R.G., James, N.P. (Eds.), Facies models: response to sea level changes. Geological Association of Canada, pp. 303-322.

Premo, W. R., Van Schmus, W. R., 1989. Zircon geochronology of Precambrian rocks in southeastern Wyoming and northern Colorado. In: Grambling, J. A., Tewksbury, B. J., (Eds.), Proterozoic Geology of the Southern Rocky Mountains. Geol. Soc. Am. Spec. Pap. 235, pp. 13-32.

Raaben, M.E., 1998. Microstromatolites and their origin. Lithology and Mineral Resources 33(2), 133-141.

Reading, H.G., Collinson, J.D., 1996. Clastic coasts. In: H.G. Reading (Ed.), Sedimentary environments: processes, facies and stratigraphy. Blackwell Science, pp. 154-231.

Redden, J.A., Peterman, Z.E., Zartman, R.E., DeWitt, E., 1990. U-Th-Pb geochronology and preliminary interpretation of Precambrian tectonic events in the Black Hills, South Dakota. In: Lewry, J.F., Stauffer, M.R. (Eds.), The Early Proterozoic Trans-Hudson Orogen of North America. Geological Association of Canada, Spec. Pap. 37, pp. 229-251.

Riegraf, W., 1982. The Bituminous Lower Toarcian at the Truc de Balduc near Mende (Département de la Lozére, S-France). In: Einsele, G., Seilacher, A. (Eds.), Cyclic and event stratification. Springer-Verlag, pp. 506 - 511.

Robbins, L.L., Tao, Y., Evans, C.A., 1997. Temporal and spatial distribution of whitings on Great Bahama Bank and a new lime mud budget. Geology 25, 947-950.

Robbins, L.L., Blackwelder, P.L., 1992. Biochemical and ultrastructural evidence for the origin of whitings: A biologically induced calcium carbonate precipitation mechanism. Geology 20, 464-468.

Roscoe, S.M., Card, K.D., 1993. The reappearance of the Huronian in Wyoming: rifting and drifting of ancient continents. Can. J. Earth Sci. 30, 2475-2480.

Salop, L.I., 1982. Geologic development of the Earth in Precambrian. Nedra, Leningrad, 343p, in Russian.

Sami, T. T., James, N. P., 1996. Synsedimentary cements as Paleoproterozoic platform building blocks, Pethei Group, northwest Canada. J. Sed. Res. 66, 209–222.

Sami, T. T., James, N. P., 1994. Peritidal carbonate platform growth and cyclicity in an early Proterozoic foreland basin, upper Pethei Group, northwest Canada. J. Sed. Res. B64, 111–131.

Sami, T. T., James, N. P., 1993. Evolution of an early Proterozoic foreland basin carbonate platform, lower Pathei Group, Great Slave Lake, northwest Canada. Sedimentology 40, 403–430.

Sami, T. T., James, N. P., Kyser, T. K., Southgate, P. N., Jackson, M. J., Page, R. W., 2000. Evolution of Late Paleoproterozoic ramp systems, Lower McNamara Group,

Northeastern Australia. In: Grotzinger, J. P., James, N. P., (Eds.), Carbonate sedimentation and diagenesis in the evolving Precambrian world, SEPM Spec. Publ. 67, pp. 243–274.

Schlager, W., 1981. The paradox of drowned reefs and carbonate platforms. Geol. Soc. Am. Bull. 92, 197-211.

Schmidt, P. W., Williams, G. E., 1999, Paleomagnetism of the Paleoproterozoic hematitic breccia and paleosol at Ville-Marie, Québec: further evidence for the low paleolatitude of Huronian glaciation: Earth Planet. Sci. Lett. 172, 273–285.

Serebryakov, S.N., Semikhatov, M.A., 1974. Riphean and recent stromatolites: a comparison. Am. J. Sci. 274, 556-574.

Sherman, A.G., James, N.P., Narbonne, G.M., 2000. Sedimentology of a Late Mesoproterozoic Muddy Carbonate Ramp, Northern Baffin Island, Arctic Canada. In: Grotzinger, J.P., James, N.P. (Eds.), Carbonate sedimentation and diagenesis in the evolving Precambrian world. SEPM Spec. Publ. 67, pp. 275-294.

Siever, R., 1992. The silica cycle in the Precambrian. Geochim. Cosmochim. Acta 56, 3265-3272.

Siever, R., 1977. Early Precamrbian weathering and sedimentation: an impressionistic view. In: Ponnamperuma, C. (Ed.), Chemical evolution of the Early Precambrian. Academic Press, pp. 13-23.

Simonson, B.M., Hassler, S.W., 1996. Was the deposition of large Precambrian Iron Formations linked to major marine transgressions? J. Geol. 104, 665-676.

Simonson, B. M., Schubel, K. A., Hassler, S. W., 1993, Carbonate sedimentology of the early Precambrian Hamersley Group of Western Australia, Precambrian Research 60, 287–335.

Sims, P. K., 1995. Archean and Early Proterozoic tectonic framework of north-central United States and adjacent Canada. U.S. Geol. Surv. Bull. 1904-T, 12p.

Snyder, G. L., Siems, D. F., Grossman, J. N., Ludwig, K. R., Nealey, L. D., 1995, Geological map, petrochemistry, and geochronology of the Precambrian rocks of the Fletcher Park – Johnson Mountain area, Albany and Platte counties, Wyoming, with a section on the Fletcher Park shear zone by Frost, B. R., Chamberlain, K. R., Snyder. G. L. U.S. Geol. Surv. Misc. Inv. Ser. I-2235, scale 1:24,000, 2 sheets.

Stauffer, M.R., 1984. Manikewan: An Early Proterozoic ocean in Central Canada, its igneous history and orogenic closure. Precambrian Res. 25, 257-281.

Sumner, D. Y., Grotzinger, J. P., 2000. Late Archean aragonite precipitation: petrography, facies associations, and environmental significance. In: Grotzinger, J. P., James, N. P., (Eds.), Carbonate sedimentation and diagenesis in the evolving Precambrian world, SEPM Spec. Publ. 67, pp. 123-144.

Sumner, D. Y., 1997, Carbonate precipitation and oxygen stratification in Late Archean seawater as deduced from facies and stratigraphy of the Gamohaan and Frisco formations, Transvaal Supergroup, South Africa, Am. J. Sci. 297, 455–487.

Sumner, D.Y., Grotzinger, J.P., 1996. Were the kinetics of calcium carbonate precipitation related to oxygen concentration? Geology 24, 119-122.

Swett, K., Knoll, A.H., 1985. Stromatolitic bioherms and microphytolites from the Late Proterozoic Draken Conglomerate Formation, Spitsbergen. Precambrian Res. 28, 327-347.

Tucker, M.E., Wright, V.P., 1990. Carbonate sedimentology. Blackwell Scientific Publications.

Van Wagoner, J. C., Posamentier, H. W., Mitchum, R. M., Vail, P. R., Sarg, J. F., Loutit, T. S., Hardenbol, J., 1988. An overview of the fundamentals of sequence stratigraphy and key definitions. In: Wilgus, C. K., Hastings, B. S., Kendall, C. G. S. C., Posamentier, H. W., Ross, C. A., Van Wagoner, J. C., (Eds.), Sea-level changes: An intergrated approach. SEPM Spec. Publ. 42, pp. 39–45.

Van Wagoner, J.C., Mitchum, R.M.J., Posamentier, H.W., Vail, P.R., 1987. Seismic stratigraphy interpretation using sequence stratigraphy. Part II: Key definitions of sequence stratigraphy. In: Bally, A.W. (Ed.), Atlas of seismic stratigraphy. AAPG Studies in Geol. 27, Tulsa, OK, pp. 11-14.

Walker, J. C. G., Brimblecombe, P., 1985. Iron and sulfur in the pre-biologic ocean. Precambrian Res. 28, 205–222.

Warren, J., 1999. Evaporites: their evolution and economics. Blackwell Science, 438p.

Williams, G. E., Schmidt, P. W., 1997, Paleomagnetism of the Paleoproterozoic Gowganda and Lorrain formations, Ontario: low paleolatitude for Huronian glaciation: Earth Planet. Sci. Lett., 153, 157-169.

Williams, H., Hoffman, P.F., Lewry, J.F., Monger, J.W.H., Rivers, T., 1991. Anatomy of North America: thematic geologic portrayals of the continent. Tectonophys. 187, 117-134.

Wright, V.P., 1990. Peritidal carbonates. In: Tucker, M.E., Wright, V.P. (Eds.), Carbonate Sedimentology. Blackwell Scientific Publications, pp. 137-164.

Wright, V.P., Burchette, T.P., 1996. Shallow-water carbonate environments. In: H.G. Reading (Ed.), Sedimentary Environments: Processes, facies and stratigraphy. Blackwell Science, pp. 325-394.

Young, G.M., 1991. The geologic record of glaciation: relevance to the climatic history of Earth. Geosci. Can. 18(3), 100-108.

CHAPTER 3

CHEMOSTRATIGRAPHY OF THE EARLY PALEOPROTEROZOIC SNOWY PASS SUPERGROUP, WYOMING CRATON: A RECORD OF SECULAR CARBON ISOTOPE CHANGES

ABSTRACT. The ~10 km thick early Paleoproterozoic Snowy Pass Supergroup in the Medicine Bow Mountains was deposited on the present-day southern flank of the Wyoming Craton; it contains three discrete levels of glacial diamictite. Carbonate strata are preserved directly above the middle diamictite (Vagner Formation) and well above the upper diamictite in the Nash Fork Formation. Vagner Formation carbonates record a narrow range of negative $\delta^{13}C$ values (-1.5 to -3.8‰, V-PDB), typical of post-glacial cap carbonates in the Neoproterozoic. Trace element concentrations and well-preserved sedimentary structures support a primary origin for these negative carbon isotope values. Notably, Vagner carbonates are isotopically indistingishable from those of the Espanola Formation (Veizer et al., 1992) which overlie the middle of three glacial horizons in the Paleoproterozoic Huronian Supergroup, ON. The intimate association of these isotopically distinct carbonates and glacial strata suggest that chemical precipitation resulted as a response to high alkalinity fluxes into shallow seawater during post-glacial transgression.

Carbonates at the base of the Nash Fork Formation record $\delta^{13}C$ values up to +28‰, whereas overlying members have $\delta^{13}C$ values between +6 and +8‰. Carbonates from the upper part of the Nash Fork Formation above black carbonaceous shale have carbon isotope values ranging between 0 and +2.5‰. The transition from high carbon isotope values to those near 0‰ in the Nash Fork Formation is similar to that observed at the end of the ca. 2.2-2.1 Ga carbon isotope excursion in Fennoscandia at the Jatulian/Ludikovian boundary. This chemostratigraphic trend and the appearance of specific lithologies (BIFs, Mn-rich carbonates, carbonaceous shales and phosphorites) at the end of the carbon isotope excursion worldwide are explained by ocean overturn associated with the final breakup of the Kenorland supercontinent.

INTRODUCTION

Research over the last two decades has revealed that the carbon and strontium isotope composition of the Paleoproterozoic ocean experienced high amplitude changes (e.g. Schidlowski et al., 1975, 1976; Veizer and Compston, 1976; Veizer et al., 1992, 1992a; Karhu, 1993; Mirota and Veizer, 1994; Karhu and Holland, 1996; Melezhik and Fallick, 1996; Bekker et al., 2001). Chemostratigraphic studies of middle Paleoproterozoic carbonates from Fennoscandia and elsewhere were used to define a positive carbon isotope excursion with an age between ca. 2.2-2.1 Ga (Karhu, 1993; Karhu and Holland, 1996). Secular carbon and strontium isotope variations in seawater between 2.45 and 2.22 Ga are, however, still poorly defined especially during the Paleoproterozoic glacial epoch (2.45-2.22 Ga) since carbonates of this age are rare, thin, little studied, and in general highly deformed. The sedimentary record of the glacial epoch in North America contains evidence for three discrete ice ages and intervening times of warm climate (Young, 1991). Veizer et al. (1992) studied post-glacial carbonates of the Espanola Formation in the Huronian Supergroup, ON and interpreted their negative $\delta^{13}C$ values as reflecting a lacustrine environment of deposition. In contrast, Bekker et al. (2001) studied carbonates from the Duitschland Formation, which is sandwiched between two glacials in the Pretoria Group, South Africa; and these authors concluded that negative carbon isotope values in carbonates from the lower part of this unit above glacial diamictite reflect a seawater signiture. Understanding of detailed secular carbon isotope variations in the early Paleoproterozoic ocean is important for evaluating the relationship between biogeochemical cycling of carbon and climatic change (Kaufman, 1997). Comparison and correlation of these trends worldwide should aid in our understanding of the severity and duration of the glaciations (cf. Hoffman et al., 1998).

Worldwide, the end of the Paleoproterozoic glacial epoch was followed by deposition of mature, Al-rich quartzites suggesting a climate change to greenhouse conditions favoring strong chemical weathering (Young, 1973; Karlstrom et al., 1983; Marmo, 1992; Schreiber and Eriksson, 1992; Gutzmer and Beukes, 1996; Ojakangas, 1997). The ca. 2.2-2.1 Ga carbon isotope excursion (Karhu and Holland, 1996) also succeeds the glacial epoch but the temporal or stratigraphic relationship between the beginning of the carbon isotope excursion and deposition of mature quartzites is poorly constrained. The carbon isotope excursion is thought to have

lasted more than 100 Ma and was likely accompanied by an increase in atmospheric oxygen (Karhu and Holland, 1996).

The end of the carbon isotope excursion on the Fennoscandian Shield (between 2062 ± 2 Ma and 2113 ± 4 Ma) was accompanied by voluminous mafic volcanism which has been related to supercontinent breakup (Karhu, 1993). Deposition of BIFs, phosphorites, Mn-rich carbonates, organic-rich shales with high organic carbon contents and with some carbon isotope values of organic matter as low as -40 - -45‰ coincides in age with the end of the carbon isotope excursion on the Fennoscandian Shield (Karhu, 1993; Melezhik et al., 1999). Melezhik et al. (1997) also noticed a temporal relationship between the end of the carbon isotope excursion and the decline in stromatolite abundance and diversity on the Fennoscandian Shield. Fennoscandian chemostratigraphic data records the end of the carbon isotope excursion, but lacks high resolution due to the absence of continuous outcrops and a prominent unconformity (Melezhik et al., 1999). The detailed record of secular carbon isotope variations and accompanying lithological and geochemical changes at the end of the carbon isotope excursion from a separate basin would be important in order to separate global vs. local, basin-scale trends and to understand underlying causes of these changes.

In this paper, data from carbonate units in the early Paleoproterozoic Snowy Pass Supergroup, Wyoming are presented to provide an independent record and fill gaps in our knowledge of early Paleoproterozoic secular carbon isotope variations during the glacial epoch and at the end of the ca. 2.2-2.1 Ga carbon isotope excursion. This paper has four objectives: 1) to provide new data on the secular carbon isotope variations during the glacial epoch and on their relationship to climate changes; 2) to provide a high-resolution record of secular carbon isotope and lithological changes at the end of the carbon isotope excursion; 3) to test earlier proposed lithostratigraphic correlations and constrain the age of the studied units based on chemostratigraphic data; and 4) to present a model for the end of the ca. 2.2-2.1 Ga carbon isotope excursion.

REGIONAL GEOLOGY AND STRATIGRAPHY

The Wyoming Craton is a triangular block of Archean crust surrounded by exposed and buried Paleoproterozoic mobile belts. Paleoproterozoic sedimentary and subordinate volcanic rocks are well exposed on the southeastern margin of the Wyoming craton in the Sierra Madre and Medicine Bow Mountains, Wyoming as well as in the Black Hills, South Dakota (Fig. 3.1). These rocks were strongly deformed during the 1.78-1.74 Ga Medicine Bow Orogeny when the southern passive margin of the Wyoming Craton collided along the Cheyenne Belt Suture with island arcs approaching from the south (Karlstrom and Houston, 1984; Chamberlain, 1998). The Cheyenne Belt is well-exposed in the Sierra Madre and Medicine Bow Mountains and is traceable to the east through the Laramie Mountains and Racheau Hills, but further to the east it disappears under Phanerozoic cover and can only be inferred from geophysical data (Sims, 1995). The projection of the Cheyenne Belt and, therefore, the early Proterozoic passive margin runs south of the Hartville Uplift (Fig. 3.1). The eastern margin of the Wyoming Craton is bounded by Trans-Hudson orogen and is poorly exposed in the Black Hills, South Dakota (Redden et al., 1990; Sims, 1995).

Volcano-sedimentary rocks in the Medicine Bow Mountains form the Snowy Pass Supergroup. The degree of metamorphism in the Medicine Bow Mountains is greenschist facies, biotite grade, and units are generally preserved in broad open folds (Houston et al., 1981). The age of the succession is constrained by U-Pb conventional dating of detrital zircons from the base of the succession (Magnolia Formation) in the Sierra Madre range, and the age of the arc-continent collision in the Cheyenne Belt to between 2451 ± 9 Ma and 1.78-1.74 Ga (Karlstrom and Houston, 1984; Premo and Van Schmus, 1989; Chamberlain, 1998). The Snowy Pass Supergroup unconformably overlies or is in fault contact with the Late Archean basement. The supergroup is subdivided by structural contacts (rotated thrust faults) into the Deep Lake Group and the lower and upper parts of the Libby Creek Group (Houston et al., 1992; see Fig. 3.2). Based on the presence of glaciogenic sediments in both the Deep Lake Group and Lower Libby Creek Group, Houston et al. (1992) inferred that only a small portion of the succession and a limited amount of time is missing along the Reservoir Lake fault; however the Lewis Lake fault that separates the lower and upper parts of the Libby Creek Group might represent a major time break (Fig. 3.2).

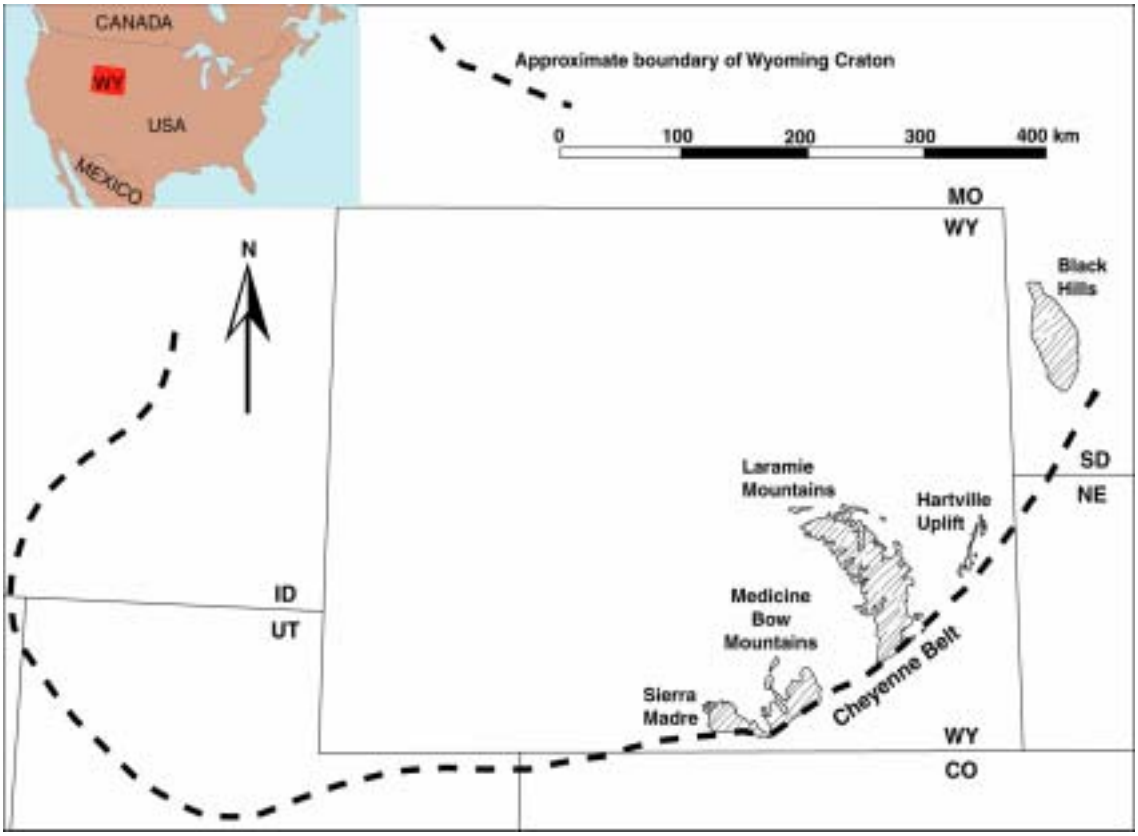

Fig. 3.1. Location of Early Paleoproterozoic sedimentary successions on the southeastern margin of the Wyoming Craton.

The Deep Lake Group and the lower part of the Libby Creek Group record rift and passive margin settings, whereas the upper part of the Libby Creek Group is considered to reflect a transition from a passive margin to a foredeep (Karlstrom et al., 1983), or dissection of mature passive margin (Bekker and Eriksson, submitted). The whole succession was intruded by mafic sills and dikes that range in composition from tholeiitic to calc-alkaline. Tholeiitic gabbros that intrude pre-folded Deep Lake Group and are likely related to rifting (Karlstrom et al., 1981) were dated in the Sierra Madre and Laramie Mountains at 2.09-2.01 Ga (U-Pb zircon and baddeleyite, Premo and Van Schmus, 1989; Snyder et al., 1995; Cox et al., 2000). Evolution in composition of dikes and sills to calc-alkaline magmatism was explained by a progressive change in the tectonic environment from rift to passive margin to foredeep (Karlstrom et al., 1983). Pegmatitic metagabbro that intrudes the Cascade Quartzite of the Snowy Pass Group in the Sierra Madre was dated at 2,092 ± 9 Ma (U-Pb zircon, Premo and Van Schmus, 1989). The latter provides a minimum age for the Deep Lake Group in the Medicine Bow Mountains.

The Snowy Pass Supergroup (Fig. 3.2) commences with fluvial rift deposits including pyritic and uraniferous, quartz-pebble conglomerates (Magnolia Formation) and contains three glacial horizons (Campbell Lake, Vagner and Headquarters diamictites) sandwiched between quartzites, metapelites, and a thin carbonate unit that overlies the middle glacial horizon. A transition from rift to open marine conditions of sedimentation is considered to have occurred at the level of the Vagner Formation (Karlstrom et al., 1983). The youngest glacial horizon is overlain by thick, mature, Al-rich and hematite-bearing quartzites (Medicine Peak Quartzite). The upper part of the Libby Creek Group includes a thick carbonate succession (Nash Fork Formation), subaqueous mafic volcanic unit (Towner Greenstone), and, at the top, slates and phyllites of the French Slate.

METHODS

Whole-rock (marked by asterisk in Table 3.1) as well as microdrilled powders were prepared from samples collected from measured sections and isolated outcrops. Major and trace element concentrations on whole-rock samples were determined through dissolution of ~10 mg of carbonate in 5 ml of 0.5 M acetic acid, and subsequent analysis by ICP-AES at the Geological Survey of Finland (Table 3.1). Uncertainties in the analytical data based on the measurement of multiple standard materials by this method are 5% for major elements and better than 10% for trace elements. Microdrilled powders of ~20 to 40 mg were dissolved in 5 ml of 2% nitric acid and analyzed for Mn and Sr contents on a Buck Scientific 200-A AAS at Virginia Tech. Uncertainties based on the measurement of multiple standard materials by this method are better than 5% for Sr and 10% for Mn. Samples that had low yields indicating carbonate contents below 50% were not analyzed for major and trace elements.

Carbon dioxide was extracted at the Geological Survey of Finland from whole-rock powders by closed tube reaction with anhydrous phosphoric acid ($\rho > 1.89$ g/cc) at a temperature of 25^{o}C for limestone and 100^{o}C for dolomite and isolated by cryogenic distillation for mass spectrometric analysis on a Finnigan MAT 251. The fractionation factors used for mineral correction of oxygen isotopes in calcite prepared at 25^{o}C and dolomite at 100^{o}C were 1.01025 and 1.00913, respectively. A second generation of carbonate samples (without asterisk in Table

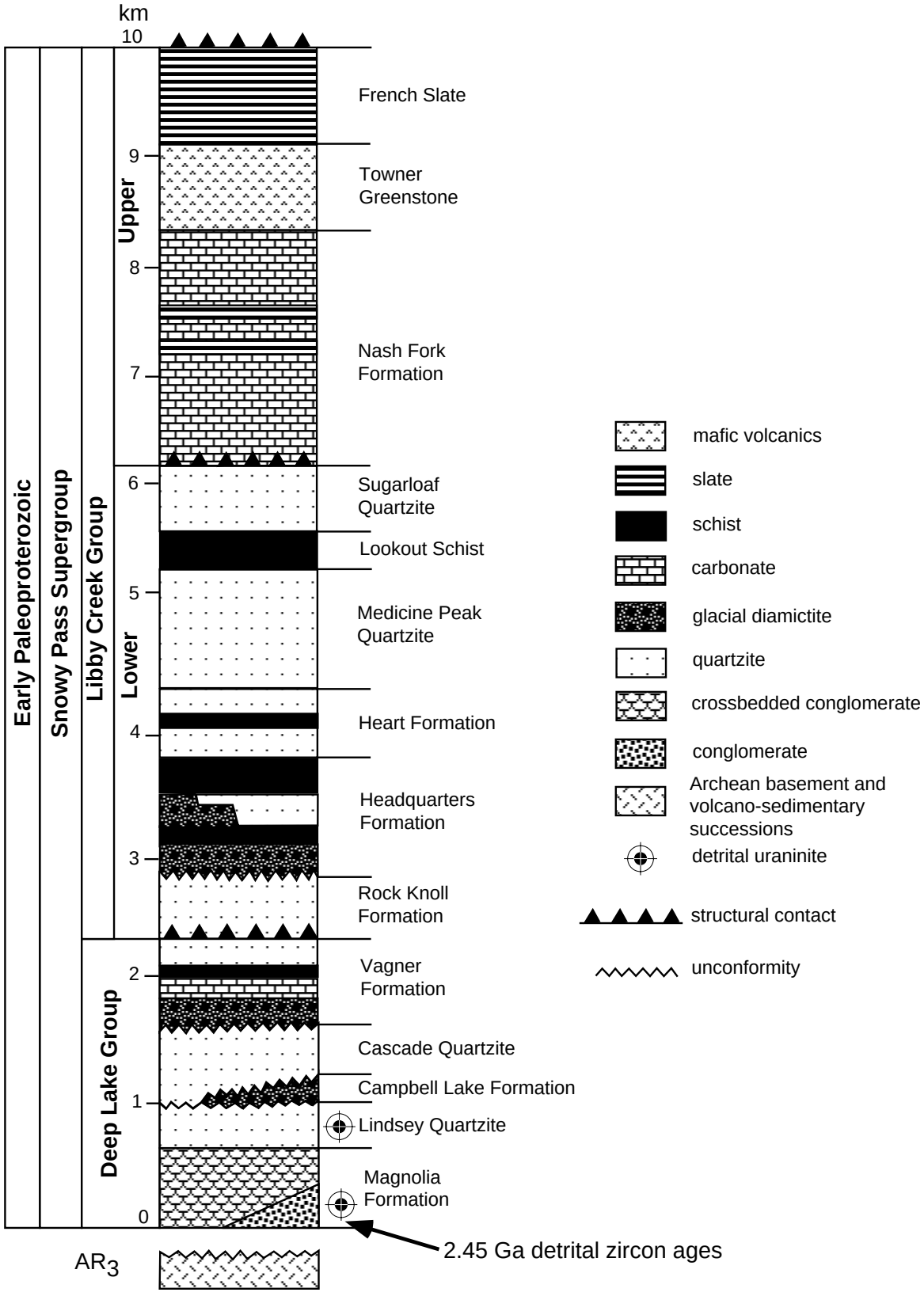

Fig. 3.2. Stratigraphic column of the Snowy Pass Supergroup, Medicine Bow Mountains, WY (after Houston et al., 1992).

Table 3.1. Carbon, oxygen, and strontium isotope values and trace and major element concentrations of studied carbonates.

Sample #	Mineral / Lithology	$\delta^{13}C$, PDB	$\delta^{18}O$, PDB	TOC, mgC/g sample	$\delta^{13}C_{TOC}$, PDB	$\Delta\delta$	Ca (%)	Mg (%)	Fe (ppm)	Mn (ppm)	Sr (ppm)	Mn/Sr	$^{87}Sr/^{86}Sr$
Vagner Formation													
BE-C-95-1*	calcite	-2.3	-19.8				42.76	0.03	504	1055	128	8.3	
BE-C-95-2*	calcite	-2.5	-19.4	0.05	-17.7	15.3							
BE-C-95-3*	calcite	-2	-20.9				42.77	<0.01	92	496	117	4.2	
BE-C-95-4*	calcite	-2.5	-18.2	0.05	-11.0	8.5	42.21	<0.01	94	443	187	2.4	0.7080747
BE-C-95-7*	calcite	-1.9	-18.8	0.11	-13.1	11.2	38.9	0.57	6306	1461	181	8.1	
BE-C-95-8*	calcite	-1.5	-19.9	0.09	-19.6	18.1							
BE-C-95-9*	calcite	-2.6	-16.4										
BE-C-95-10a*	calcite	-2.3	-17.4	0.1	-12.6	10.3	42.31	<0.01	288	393	217	1.8	0.7152574
BE-C-95-10b*	calcite	-2.2	-19.6	0.08	-14.8	12.6	42.29	0.02	390	520	187	2.8	
BE-C-95-11*	calcite	-1.9	-19.4				42.17	0.1	2228	831	217	3.8	
BE-C-95-12*	calcite	-1.7	-18.9				42.79	0.09	1829	630	187	3.4	
BE-C-95-20*	calcite	-1.7	-19.0	0.08	-18.8	17.1							
BE-C-95-21*	calcite	-2.2	-17.7	0.07	-14.1	11.9							
BE-C-95-24*	calcite	-2.2	-16.7	0.3	-19.1	16.9	41.89	0.03	748	529	145	3.7	
BW99.1	calcite	-2.3	-15.3							295	59	5.0	
BW99.2	calcite	-2.1	-15.7							352	61	5.8	
BW99.3	calcite	-2.4	-16.1							453	59	7.7	
BW99.4	calcite	-2.0	-15.4							523	48	10.9	
BW99.5	calcite	-2.6	-16.7							527	59	8.9	
BW99.6	calcite	-2.1	-15.9							513	95	5.4	
BW99.7	calcite	-2.0	-14.5							571	125	4.6	
BW99.8	calcite	-2.0	-16.8							568	161	3.5	
BW99.9	calcite	-1.9	-15.8							468	73	6.4	
BW99.10	calcite	-2.1	-17.9							408	52	7.8	
BW99.11	calcite	-1.9	-18.3							480	62	7.8	
5	calcite	-2.9	-18.6							343	21	16.3	
6	calcite	-3.6	-18.1							548	42	13.0	
8	calcite	-3.8	-17.2							566	36	15.7	
Nash Fork Formation													
Lower part													
Massive dolomite – stromatolite (L1) member													
97-78-5	Dolomite	26.6	-8.9							1916	6	306.3	
97-78-1	Dolomite	13.7	-10.9							1561	tr.	-	
2000-4	Dolomite	13.3	-12.5							1227	58	21.2	
2000-4/1	Dolomite	13.2	-11.0							1349	30	44.6	
2000-4/2	Dolomite	24.0	-9.4							2157	92	23.4	
2000-4/3	Dolomite	25.7	-10.1							1369	57	24.0	

2000-4/4	Dolomite	26.5	-11.4							1314	43	30.6	
2000-4/5	Dolomite	26.0	-11.5							1816	54	33.9	
2000-4/6	Dolomite	26.7	-11.1							1245	64	19.6	
2000-4/7	Dolomite	28.2	-10.3							1036	52	20	
2000-4/8	Dolomite	26.0	-11.8							1276	72	17.7	
2000-4/9	Dolomite	26.4	-10.9							1438	36	40.0	
Heterolithic siliciclastics-carbonate (L2) member													
97-3-1	dolomite	6.1	-17.5							3040	190	16.0	
97-3-2	dolomite	9.0	-16.5	0.1						3921	96	40.7	
97-3-3	shale			0.2									
97-3-4	dolomite	7.3	-7.8							1715	65	26.3	
97-3-5	shale			0.04	-13.4								
97-3-6	dolomite	5.1	-12.8							2279	7	316.7	
97-13-1	dolomite	8.5	-13.7							2665	138	19.3	
97-13-2	dolomite	8.6	-14.4							3384	178	19.0	
97-13-3	dolomite	8.5	-15.0							1927	158	12.2	
97-13-4	dolomite	9.0	-14.0							2511	110	22.9	
97-13-5	dolomite	9.9	-15.4							937	tr.	-	
97-13-6	dolomite	8.2	-16.2	0.1	-20.6	28.4				1334	tr.	-	
97-13-7	dolomite	8.6	-14.7							928	tr.	-	
118-1	dolomite	4.8	-11.8							5059	110	46.0	
97-78-2	dolomite	8.8	-14.1							1908	224	8.5	
97-78-3	dolomite	6.1	-15.8							563	tr.	-	
97-78-4	dolomite	8.9	-14.7							2320	236	9.8	
BE-C-95-17*	dolomite	4.8	-17.2				23.13	12.56	18867	4252	206	20.7	
BE-C-95-18*	dolomite	6.8	-15.9				21.94	12.69	3284	1122	140	8.0	
WY-96-35*	dolomite	7.0	-14.3				23.09	11.88	36883	2848	265	10.8	
WY-96-36	dolomite	7.7	-12.4							704	107	6.6	
WY-96-37	dolomite	7.1	-12.0							1249	77	16.1	
WY-96-24	dolomite	7.2	-13.7							959	112	8.6	
WY-96-25*	dolomite	7.4	-12.8				23.05	12.46	22942	2371	196	12.1	
97-116A	dolomite	7.0	-9.2							322	15	20.8	
97-9-1	dolomite	8.0	-11.6							1188	64	18.4	
97-9-2	dolomite	7.1	-10.6							849	5	161.9	
2000-20	dolomite	8.6	-16.7							1769	194	9.1	
Silicified dolomite with large domal digitate stromatolites (L3) member													
97-20-1	dolomite	6.6	-10.3							958	20	46.9	
2000-18	dolomite	7.3	-10.5							449	135	3.3	
Nodular dolomite (L4) member													
97-56-2	dolomite	7.0	-10.8							367	140	2.6	
WY-96-23*	dolomite	6.9	-11.1				22.72	13.21	7197	1074	104	10.4	
WY-96-26	dolomite	8.3	-9.8							167	121	1.4	
WY-96-27*	dolomite	8.2	-8.8				22.82	13.59	4541	623	249	2.5	0.7049467
2000-16	dolomite	8.2	-15.5							1327	51	26.1	
2000-17	dolomite	7.1	-11.7							872	113	7.7	

97-56-1	argillite			0.1							
2000-19	dolomite	8.0	-11.9						107	190	0.6
Silicified dolomite with large domal digitate stromatolites (L5) member											
WY-96-33*	dolomite	6.4	-10.6			22.63	12.97	9005	1173	95	12.4
Nodular dolomite (L6) member											
WY-96-22	dolomite	7.5	-10.7						240	97	2.5
WY-96-38	dolomite	7.5	-10.6						330	20	16.8
WY-96-39	dolomite	7.5	-9.6						582	192	3.0
97-65-1	dolomite	6.3	-9.5						438	54	8.1
2000-10/1	dolomite	7.3	-9.7						440	190	2.3
2000-11/1	dolomite	8.2	-8.1						185	148	1.3
2000-12/1	dolomite	7.2	-9.7						456	32	14.2
2000-13/1	dolomite	6.3	-10.5						1345	77	17.4
2000-14	dolomite	6.6	-9.8						750	134	5.6
2000-15	dolomite	7.1	-9.7						434	156	2.8
Heterolithic siliciclastics-carbonate (L7) member											
WY-96-20*	dolomite	8.1	-8.6			23.19	13.85	1884	382	72	5.3
WY-96-32*	dolomite	6.4	-11.9			22.95	13.75	5876	826	112	7.4
BE-C-95-19*	dolomite	8.2	-10.1			21.81	12.66	3389	391	234	1.7
WY-96-21	dolomite	7.5	-12.4						520	131	4.0
97-66-1	dolomite	6.2	-13.1						416	114	3.6
97-66-2	dolomite	6.9	-11.6						952	186	5.1
Stromatolitic dolomite (L8) member											
97-23-1	dolomite	6.7	-9.0						643	20	32.9
97-23-2	dolomite	5.5	-7.6						1391	63	22.2
97-41-1	dolomite	5.9	-8.6						712	38	19.0
WY-96-13*	dolomite	5.6	-12.2			21.77	12.46	19988	1566	161	9.7
WY-96-14	dolomite	6.5	-12.5						251	159	1.6
WY-96-15*	dolomite	6.0	-11.1			22.38	12.88	10890	710	172	4.1
WY-96-16	dolomite	4.7	-12.0						382	98	3.9
WY-96-17	dolomite	4.5	-10.5						384	176	2.2
WY-96-19	dolomite	5.4	-11.8						885	88	10.0
WY-96-31	dolomite	6.2	-11.7						583	161	3.6
97-5-1	dolomite	6.2	-9.2						407	101	4.0
97-7-1	dolomite	6.1	-9.4						678	153	4.4
97-7-2	dolomite	5.6	-8.7						512	100	5.1
97-7-3	dolomite	5.6	-7.8						726	63	11.5
97-7-4	shale			1.3	-16.2						
97-8-1	dolomite	6.1	-7.7						281	239	1.2
97-8-2str	dolomite	5.7	-9.9						155	107	1.5
97-8-2l	dolomite	7.0	-6.6						151	80	1.9
97-8-2d	dolomite	6.4	-8.5						545	117	4.6
Lower part, undivided											
WY-96-1*	dolomite	7.1	-10.3			22.72	13.19	8686	1610	121	13.3
WY-96-1a	dolomite	3.9	-13.3						338	133	2.5

WY-96-2/1*	dolomite	5.2	-14.1			21.70	12.54	9378	2110	177	11.9	
WY-96-2/2*	dolomite	5.0	-14.4			22.39	12.38	10000	2223	185	12	
97-11-1	dolomite	8.1	-7.4						204	tr.	-	
97-12-1	dolomite	7.2	-6.8						610	tr.	-	
Lower carbonaceous shale (M1) member												
97-6-1	shale			6.2	-17.4							
97-39-1	shale			26.8	-21.9							
97-40-1	shale			27.3	-30.8							
97-42-1	shale			98.3	-23.0							
97-43-2	dolomite	5.5	-9.8						758	tr.	-	
97-64-1	shale			4.3	-6.9							
97-67-1	shale			3.0	-9.8							
Heterolithic siliciclastics-nodular dolomite (M2) member												
97-74-1	dolomite	7.6	-7.1						650	206	3.1	
97-37-1	dolomite	7.7	-10.1						298	165	1.8	
97-46-2	dolomite	6.3	-12.7						2180	145	15.0	
WY-96-40*	dolomite	7.9	-9.8			23.1	13.56	3727	358	234	1.5	
WY-96-43	dolomite	7.0	-8.8						1106	60	18.4	
WY-96-8	dolomite	6.6	-9.1						82	221	0.4	
97-63-1	dolomite	5.8	-11.1						1013	70	14.5	
2000-8	dolomite	6.2	-12.3						518	162	3.2	
2000-9/1	dolomite	7.4	-10.6						84	16	5.2	
2000-9/2	dolomite	7.6	-9.7						158	130	1.2	
2000-10	dolomite	7.0	-14.9						393	150	2.6	
2000-11	dolomite	7.2	-8.9						429	172	2.5	
2000-12	dolomite	7.1	-10.1						240	135	1.8	
2000-13	dolomite	5.5	-12.2						1159	145	8.0	
WY-96-10*	dolomite	3.1	-14.5			22.42	13.14	11159	590	293	2	0.7142474
Upper carbonaceous shale (M3) member												
WY-96-9	shale			4.6								
97-73-1	shale			3.5	-15.8							
97-15-1	shale			9.4	-19.2							
97-46-1	shale			4.1	-15.7							
97-46-3	shale			12.0	-22.2							
97-51-1	schist			0.01	-13.6							
97-54-1	shale			121.8	-17.7							
97-54-2	dolomite	2.0	-7.8						396	51	7.8	
97-54-3a	dolomite	2.4	-7.8						79	tr.	-	
97-54-3b	dolomite	2.4	-7.6						235	1	308	
97-60-1	shale			5.9	-28.2							
97-63a-1	shale			203.6	-22.3							
97-105-1	shale			2.4	-21.9							
Massive dolomite (U1) member												
Lower part												
WY-96-11*	dolomite	2.5	-8.9			22.91	13.69	1167	192	54	3.6	

WY-96-28*	dolomite	2.2	-9.0				23.14	13.89	1445	230	54	4.3
WY-96-45	dolomite	2.4	-8.2							78	15	5.2
97-29-1	dolomite	2.5	-7.0							168	10	16.6
97-29-2	dolomite	2.5	-7.2							68	tr.	-
97-52-1	dolomite	2.4	-4.5							342	tr.	-
97-45-1	dolomite	1.9	-8.9							496	29	17.1
97-45-2	dolomite	2.4	-7.6							105	1	143.8
97-120-1	dolomite	1.9	-10.3							403	7	54.4
WY-96-29*	dolomite	0.7	-13.1				22.6	13.39	7514	695	132	5.3
WY-96-41*	dolomite	2.4	-9.2				23.09	13.76	2711	552	42	13.2
97-30-1	dolomite	2.5	-8.6							402	tr.	-
WY-96-44*	dolomite	1.5	-7.9				23.17	13.05	2495	199	55	3.6
97-34-1	dolomite	1.1	-18.4							364	3	121.7
2000-1A	dolomite	0.1	-10.3							321	72	4.5
2000-1B	dolomite	-0.2	-11.8									
Upper part												
WY-96-12-1	dolomite	2.5	-9.6							389	17	22.3
WY-96-12-2	dolomite	1.0	-5.8							376	17	21.6
97-31-1	dolomite	1.1	-6.3							514	13	40.0
2000-3	dolomite	1.5	-5.8							84	47	1.8
WY-96-3*	dolomite	1.3	-9.0				22.33	13.34	3277	425	32	13.4
WY-96-4	dolomite	1.6	-6.6							116	35	3.3
97-2-1	dolomite	0.2	-11.7							373	159	2.4
97-2-2	dolomite	0.8	-9.8							364	30	12.3
97-2-3	dolomite	0.6	-6.4							172	21	8.2
97-2-4	dolomite	0.6	-7.6							268	73	3.7
97-14-1	dolomite	0.3	-6.0							392	17	22.8
97-14-2	dolomite	1.1	-5.5							256	45	5.7
BE-C-95-5*	dolomite	0.2	-7.4	0.1	-19.6	19.8	22.87	13.36	1564	253	83	3.1
97-32-1	dolomite	0.5	-8.2							1773	1	2317
97-33-4	dolomite	0.1	-10.1							613	12	49.8
2000-6	dolomite	1.2	-9.2							207	46	4.5
WY-96-5*	dolomite	1.9	-8.7				22.69	13.58	2454	159	34	4.7
WY-96-6*	dolomite	1.4	-7.4				23.06	13.39	7811	404	69	5.9
2000.2.2	argillite			0.1								

3.1) were micro-drilled and the powders reacted with anhydrous phosphoric acid at 90°C in a Micromass Multiprep carbonate device. The resulting carbon dioxide was measured with a Micromass IsoPrime mass spectrometer at the University of Maryland, College Park. The fractionation factors used for mineral correction of oxygen isotopes in calcite and dolomite prepared at 90°C were 1.00798 and 1.00895, respectively. For both techniques, the external precision based on multiple standard measurements of NBS-19 was better than 0.1‰ vs. PDB for carbon and 0.1‰ vs. PDB.

Total organic carbon (TOC) was isolated from the carbonate samples by repeated acidification and centrifugation with concentrated HCl followed by washing until the sample reached neutral pH (Kaufman and Knoll, 1995). Dried samples in Vycor tubes were then mixed with CuO as an oxidant, evacuated, sealed and combusted at 850°C for 12h. The volume of CO_2 quantified during cryogenic distillation was used to calculate organic carbon concentrations in the samples. Carbon isotope abundance in extracted and purified CO_2 was measured with a VG PRISM mass spectrometer at Mountain Mass Spectrometry. To test for the uncertainty of abundance and isotopic composition measurements on TOC, we run in previous study (Bekker et al., 2001) replicate (n = 4) analysis of organic-rich and organic-poor powders. For analyses of the organic-rich sample, uncertainties were ± 0.26 mgC/g for abundance (5.57 mgC/g average) and ± 0.03‰ for carbon-isotopic composition (-34.47‰ average); for the organic-poor sample uncertainties were ± 0.06 mgC/g (0.18 mgC/g average) and ± 1.3‰ (-24.1‰ average) for abundances and carbon isotopic compositions, respectively.

Samples chosen for Sr isotopic analysis were treated repeatedly with 0.4 M ammonium acetate (3 times; pH = 8.2) prior to dissolution with 0.5 M acetic acid in order to remove diagenetic components (Gorokhov and others, 1995; Montañez and others, 1996). Strontium was eluted from solution by ion exchange chromatography using ElChrom Sr spec resin and weak 0.05 M nitric acid, and measured on a VG Sector 54 multi-collector thermal ionization mass spectrometer at the University of Maryland. Repeated analysis of NBS-987 over a period of three months gave a value of 0.710248 +/- 0.000005.

VAGNER FORMATION

Description

The Vagner Formation at the top of the Deep Lake Group overlies the Cascade Quartzite and is up to 800 m thick (Karlstrom et al., 1983; see Fig. 3.2). A three-fold subdivision is recognised: (1) a basal diamictite up to 300 m thick; (2) a middle marble unit with variable thickness from 5 to 60 m; and (3) an upper quartz-rich phyllite and fine-grained quartzite unit (Karlstrom, 1977; Karlstrom and Houston, 1979).

An unconformity at the base of the Vagner Formation is inferred from the variable thickness of the underlying Cascade Quartzite, the presence of channels along the contact, and pebbles of Cascade Quartzite in the basal Vagner Formation (Karlstrom, 1977; Bekker, 1998). The diamictite includes angular to subangular clasts in a greenish and sometimes reddish (due to hematite staining) coarse-grained subarkosic matrix. Warping and piercing of laminations in varved phyllite by dropstones, and faint stratification in some conglomerate layers characterize the diamictite (Sylvester, 1973; Houston et al., 1981). The contact with the overlying carbonate unit was not observed in the field but is believed to be conformable.

The marble unit consists of rhythmically interlayered (1 to 5 cm-thick) massive, fine-grained carbonate and coarse-grained siliciclastic carbonate. Contacts between lithologies are transitional. Siliciclastic carbonate is brown whereas pure carbonate has a gray-blue or brown color. Petrographic studies indicate that siliciclastic carbonates contain common quartz, perthite, and plagioclase. These carbonates are recrystallized into a coarse to very coarse calcite mosaic. Soft-sediment deformation structures (convoluted bedding), fine-laminations, normal grading, hummocky cross-stratification, lensoidal bedding, and flat-pebble conglomerate are restricted to the upper part of this unit. The marble unit to the west of the Reservoir Lake includes basal rhythmites of sandstone-siltstone-carbonate. Phyllite with lonestones of granite-granodiorite from 1 to 5 cm in diameter are interlayered with carbonate to the east of the Reservoir Lake. The only relatively complete exposed section of carbonates is in the Rock Creek area in close proximity to a mafic sill. This section has finely laminated carbonates with stratiform stromatolites and small oolites at the base that grade into massive and siliciclastic-rich carbonates upsection with flat-pebble conglomerates at the top (shallowing-upward trend).

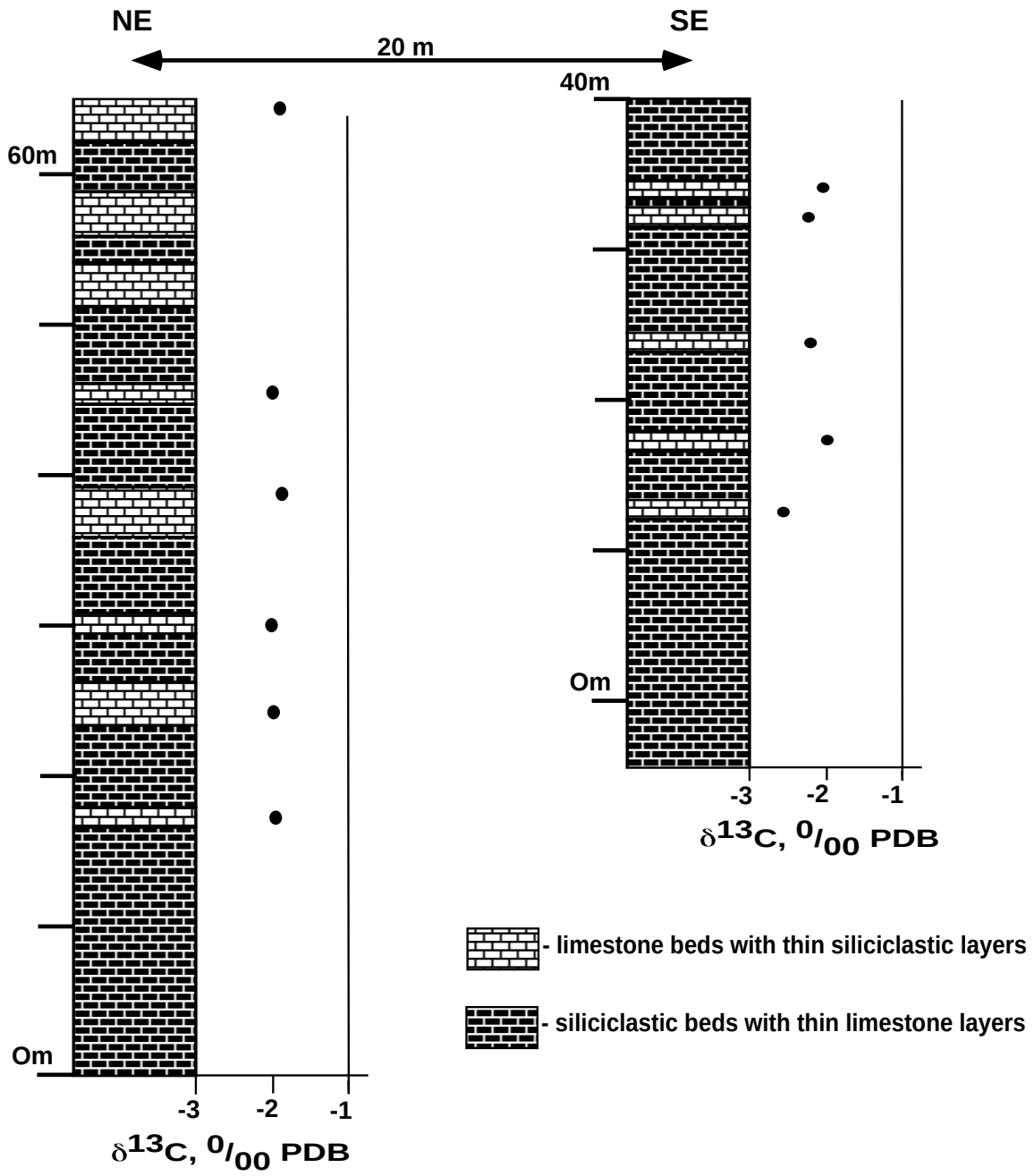

Fig. 3.3. $\delta^{13}C_{carb}$ variations in the marble unit of the Vagner Formation, Snowy Pass Supergroup, Medicine Bow Mountains, WY. Two closely-spaced partial sections (samples of BW-series in Table 3.1) were sampled near the small lake to the north of the Dipper Lake (NE1/4, Sec. 11, T. 16N., R. 80W., Medicine Bow Peak Quadrangle; 41°22'23"N, 106°20'39"W).

Due to poor exposure and high degree of deformation, only partial sections of the marble unit were measured and samples with measured stratigraphic positions were collected from these sections (Fig. 3.3). Additional samples were collected across the whole area of outcrop of the marble unit from siliciclastic-poor carbonates to test the variability of stable isotope compositions over the outcrop area. Most samples from the Rock Creek section were rejected based on a study of polished thick sections that showed abundant metamorphic minerals.

Quartzites in the overlying phyllite-quartzite unit contain climbing ripples, plane and wavy bedding, and rare cross-beds and ripples. Carbonate clasts in this unit are rarely present. Warping or piercing of layers beneath clasts was not observed. Phyllite is strongly deformed and contains pyrite.

Geochemical data and diagenesis

All studied samples from the marble unit of the Vagner Formation are low-Mg calcites (Table 3.1). They have variable contents of Mn (295-1461 ppm), Sr (21-217 ppm) and Mn/Sr ratios (1.8-16) suggesting that all samples were affected to various degrees by post-depositional alteration processes. Iron content co-varies with Mn content. Oxygen isotope values are low and range between -20.9 and -14.5‰ (V-PDB). It is most likely that calcites remained open to hot, circulating fluids long after their deposition. Notably, oxygen isotope values of correlative post-glacial carbonates from the Espanola Formation in the Huronian Supergroup, ON, Canada (Veizer et al., 1992) show similar depletion in oxygen isotope values, although these were affected only by lower greenschist facies of metamorphism. Carbon isotope values vary between –1.5 and –3.8‰ V-PDB, also comparable with those found in the Espanola Formation (Veizer et al., 1992; Bekker et al., 1999). Measured samples have low contents of total organic carbon (0.05 to 0.3 mgC/g sample) that is highly ^{13}C-enriched (ranging between -19.6 and -11.0‰ vs. V-PDB), and small fractionation ($\Delta\delta$) between carbonate and organic carbon (8.5-18.1‰). Lack of correlation between TOC content and $\delta^{13}C_{org}$ (Fig. 3.4 a) might be related to analytical resolution rather than primary composition of organic carbon. Small fractionation between carbonate and organic carbon likely records carbon exchange at greenschist facies of metamorphism. Lack of correlation between $\delta^{13}C$ and Mn, Sr and $\delta^{18}O$ (Fig. 3.4 b, c, d) suggest that carbon isotope systematics of carbonate carbon were not significantly affected by post-

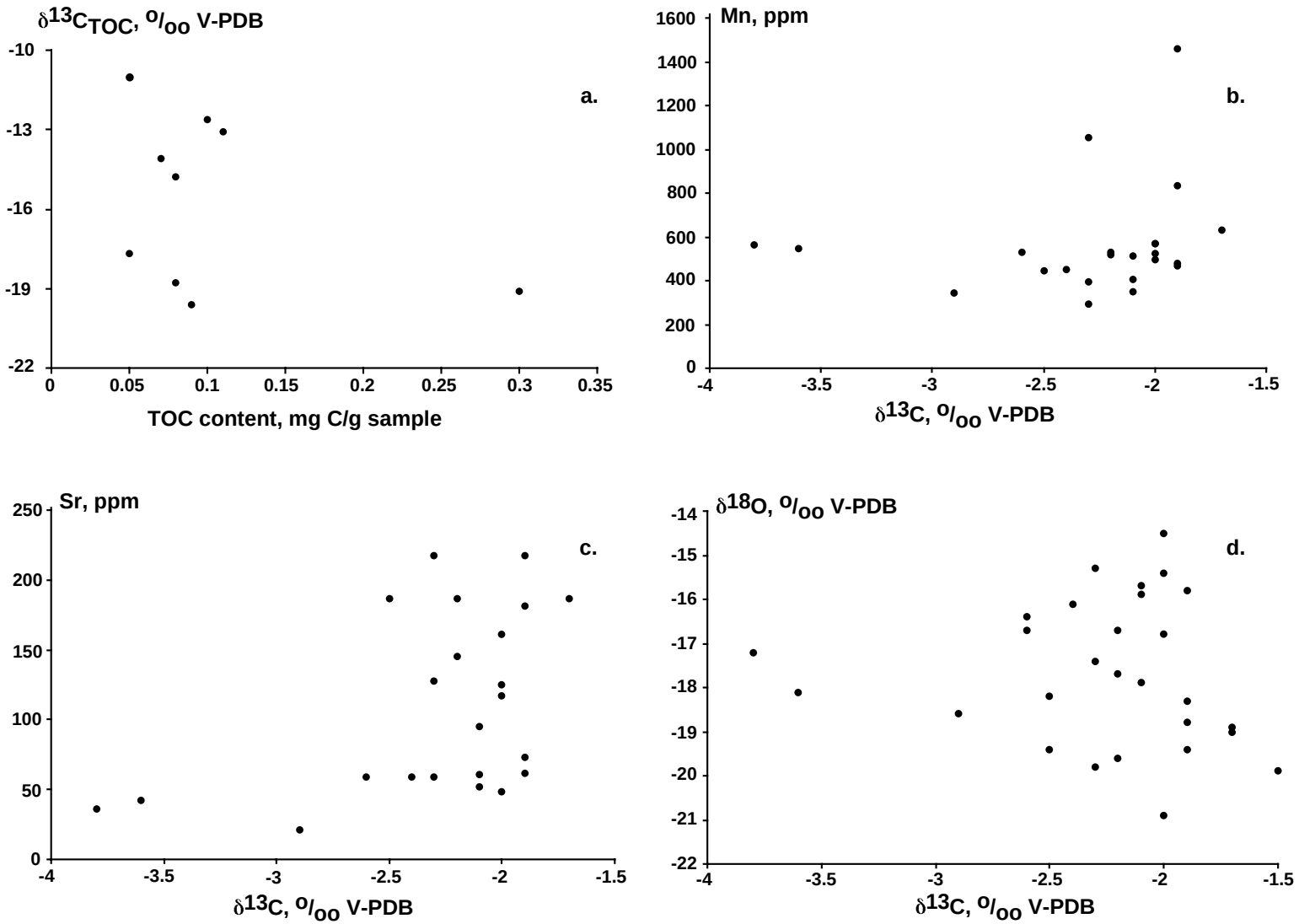

Fig. 3.4. Scatter diagrams for the Vagner Formation. a – $\delta^{13}C_{TOC}$, ‰ V-PDB vs. TOC content, mg C/g sample; b – Mn, ppm vs. $\delta^{13}C$, ‰ V-PDB; c – Sr ppm vs. $\delta^{13}C$, ‰ V-PDB; d - $\delta^{18}O$, ‰ V-PDB vs. $\delta^{13}C$, ‰ V-PDB; e – Mn/Sr vs. $\delta^{13}C$, ‰ V-PDB; f – Mn, ppm vs. $\delta^{18}O$, ‰ V-PDB; g – Sr, ppm vs. $\delta^{18}O$, ‰ V-PDB; h – Mn/Sr vs. $\delta^{18}O$, ‰ V-PDB.

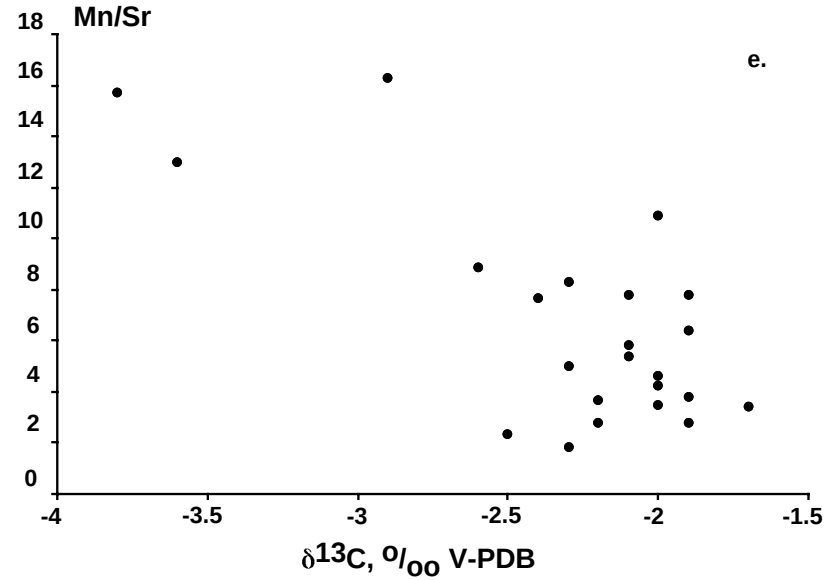
Mn/Sr
e.
18
16
14
12
10
8
6
4
2
0
-4
-3.5
-3
-2.5
-2
-1.5
δ13C, o/oo V-PDB

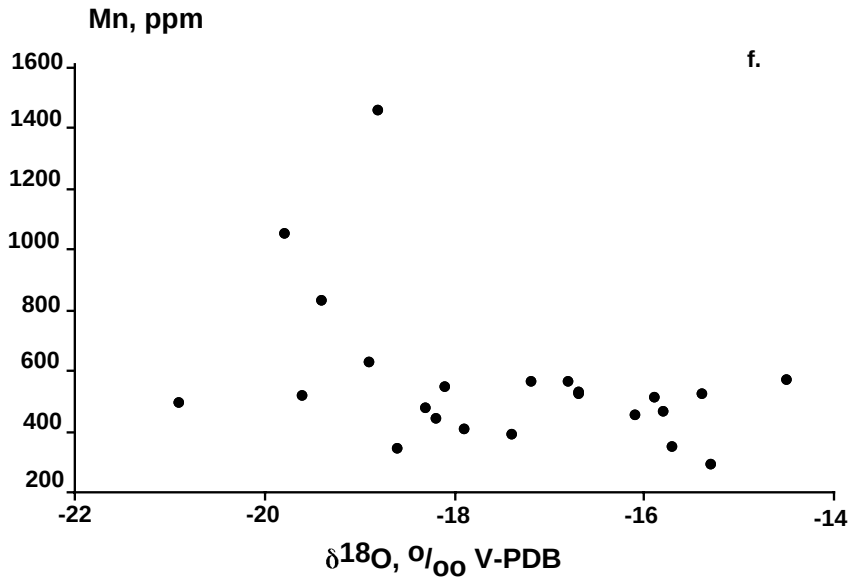
Mn, ppm
f.
1600
1400
1200
1000
800
600
400
200
-22
-20
-18
-16
-14
δ18O, o/oo V-PDB

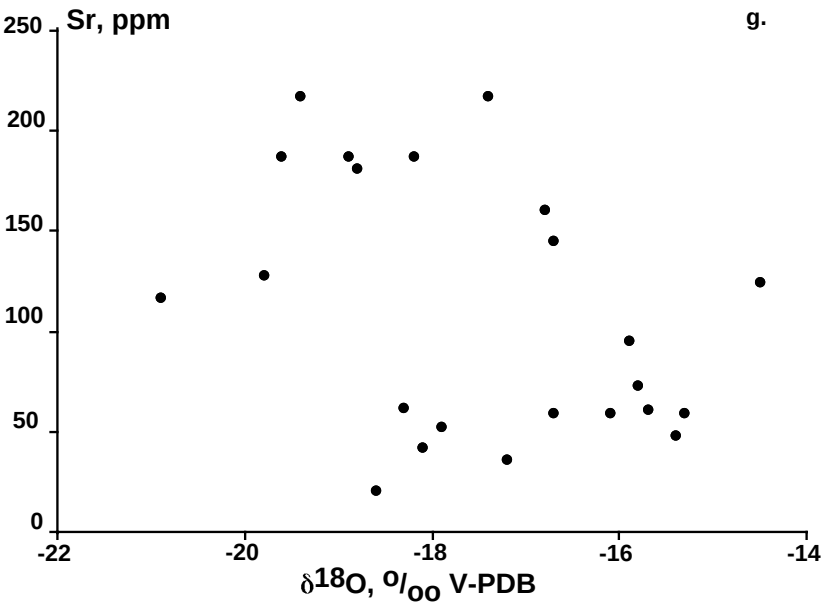
Sr, ppm
g.
250
200
150
100
50
0
-22
-20
-18
-16
-14
δ18O, o/oo V-PDB

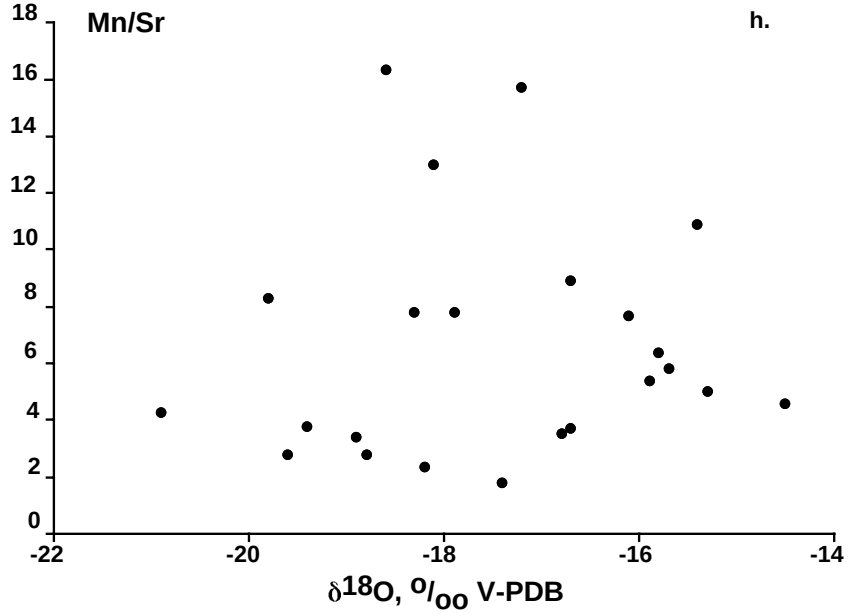
Mn/Sr
h.
18
16
14
12
10
8
6
4
2
0
-22
-20
-18
-16
-14
δ18O, o/oo V-PDB

depositional alteration. Weak correlation (R^2 = 0.5183) is however shown between $\delta^{13}C$ and Mn/Sr (Fig. 3.4 e) suggesting a moderate degree of alteration. Weak correlation also exists between $\delta^{18}O$ and Mn, Sr and Mn/Sr (Fig. 3.4 f, g, h) suggesting that oxygen isotope values were stronger affected by alteration than carbon isotope values.

Carbon isotope values of samples collected from measured sections do not show a stratigraphic trend (Fig. 3.3). In combination with regional coverage provided by the rest of samples and excluding samples from the most altered section (Rock Creek section) with the lowermost $\delta^{13}C$ values, primary carbon isotope values of the Vagner carbonates vary between –1.5 - -2.6‰.

Two samples with Mn/Sr ratios below 3 were analyzed for Sr isotope ratios. The lowest value (0.708075; sample BE-C-95-4) might be too high to reflect the composition of the Paleoproterozoic ocean since Sr isotope values of Late Archean and younger Paleoproterozoic carbonates are significantly lower (Veizer et al., 1990, 1992a, b; Master et al., 1990; Mirota and Veizer, 1994; Gorokhov et al., 1998; Bekker et al., 2001). However, it should be noted that this value is much lower than the lowest value from the correlative Espanola Formation, Huronian Supergroup, ON, Canada (0.71128; Veizer et al., 1992) and combined they could imply a significant continental flux at the time of deposition of the Vagner and Espanola formations.

CAP CARBONATE ORIGIN FOR LIMESTONE OF THE VAGNER FORMATION

The Vagner Formation has been interpreted as the deposit of a retreating dry-based glacier with the diamictite deposited in the floating shelf-ice and iceberg zone, the middle (marble) unit in the iceberg zone from carbonate brines caused by freezing of marine water onto the base of a glacier (the model of Carey and Ahmad, 1961), and the upper (phyllite) unit deposited seaward of the glacier (Sylvester, 1973; Houston et al., 1981). The Carey and Ahmad (1961) model for carbonate precipitation in a glacial environment has not been confirmed by studies in modern glaciomarine environments (Fairchild, 1993). The basal diamictite was interpreted as a glaciomarine deposit, based on the presence of dropstones in laminated phyllite, faint stratification in some conglomerate layers and major element analyses of fine-grained

matrix from the diamictite (Sylvester, 1973; Houston et al., 1981). The large strike length of the marble unit in the Medicine Bow Mountains (about 30 km) and the presence of calcareous beds in the correlative Bottle Creek Formation, Sierra Madre (Houston et al. 1992) suggest an open-marine depositional setting for the marble unit. Fine rhythmic laminations and lack of indicators for high energy conditions suggest a subtidal and, likely, deep-water environment of deposition for the most of the marble unit. Associated graded beds may represent the deposits of offshore-directed storm-surge currents. Hummocky cross-stratification and flat-pebble conglomerates developed near the top of the marble unit indicate shoaling of the depositional environment to near storm wave base.

Several lines of evidence suggest that the marble unit in the Vagner Formation is a cap carbonate similar to those found immediately above Neoproterozoic glacial deposits worldwide (e.g. Kennedy, 1996; Kaufman et al., 1997; Hoffman et al., 1998). This thin (5-60 m thick) carbonate unit represents the only interval of carbonate deposition in the more than 6-km thick lower part of the Snowy Pass Supergroup. The marble unit occurs directly above a thick diamictite that contains evidence for glacial deposition such as dropstones in rhythmites. The carbonates have negative $\delta^{13}C$ and reduced $\Delta\delta$ values similar to Neoproterozoic cap carbonates (e.g. Kaufman and Knoll, 1995; Kaufman et al., 1997, in prep.). The marble unit developed following transgression. Even though it has variable thickness, the marble unit is laterally persistent in that it is exposed over most of the Medicine Bow Mountains. Based on lack of traction-produced sedimentary structures except towards the top, the marble unit is inferred to have been deposited below wave base as an inorganically precipitated micrite; this interpretation is further supported by the lack of stromatolites. Based on the absence of carbonates in older units of the Snowy Pass Supergroup, a detrital or mechanically redeposited origin in the sense of Fairchild (1983) is not a viable option for carbonates of the Vagner Formation.

Fine-scale laminations and graded event beds are similar to those in Neoproterozoic cap carbonates (Lithofacies I and II in Kennedy, 1996), but many features common to Neoproterozoic cap carbonates are lacking. These include tepee-like slump (?) structures, marine cement laminae, cement-filled sheet cracks, stromatolites, and cement fans (cf. Kennedy, 1996). Some of these structures could have been destroyed by recrystallization during

deformation and metamorphism, but others (e.g. stromatolites) were likely not developed. Carbon isotope values of carbonates from the Vagner Formation and the correlative Espanola Formation of the Huronian Supergroup (Veizer et 1992; Bekker et al., 1999) show a much smaller range of variation than Neoproterozoic cap carbonates. This might be partially related to a shallower depth of deposition compared with the Neoproterozoic cap carbonates for which more depleted isotope values are found in deeper-water facies (cf. Kennedy, 1996; Kaufman et al., 1997; Myrow and Kaufman, 1999). An absence of barite crystals or pseudomorphs as occur in Neoproterozoic cap carbonates might be explained by a low atmospheric oxygen content in the Paleoproterozoic and, therefore, a low sufate content in the ocean (Canfield and Raiswell, 1999).

The following depositional model is proposed for the Vagner cap carbonate. High siliciclastic influx and a high energy environment precluded carbonate precipitation during deposition of the Lower Snowy Pass Supergroup. A sea-level rise resulting from glacial melting temporally shut down siliciclastic influx to the deep-water environment and promoted carbonate precipitation. One necessary prerequisite for carbonate deposition is a high pH due to high carbonate alkalinity. High alkalinity in the Neoproterozoic post-glacial ocean has been related to either ocean overturn at the end of glaciations (e.g. Kaufman et al., 1991; Grotzinger and Knoll, 1995, Hoffman et al., 1998) or high rates of continental weathering (e.g. Myrow and Kaufman, 1999; Hoffman and Schrag, 2000). High continental alkalinity flux into the ocean is supported by high chemical indices of alteration (CIA) of mature siliciclastic sediments between diamictites in the Huronian and Snowy Pass supergroups (Sylvester, 1973, Houston et al., 1981, Nesbitt and Young, 1982, Bekker, 1998). High CIA values indicate that the source areas of these sediments experienced high rates of weathering and could have supplied carbonate alkalinity to the ocean.

The model that relies on ocean overturn and mixing at the end of a glacial event requires a high temperature gradient between the equator and the poles to drive ocean circulation. The Paleoproterozoic glacial epoch was marked by oscillations between greenhouse and icehouse conditions. Low temperature gradients between the equator and the poles and, consequently, stratified anoxic oceans will have existed during both conditions. In contrast, during the

transition from one condition to the other, high temperature gradients will have existed between the equator and the poles resulting in an increase in ocean circulation and ocean overturn.

NASH FORK FORMATION

Description

The Nash Fork Formation is the lower unit in the upper Libby Creek Group and has thickness of 1.7 km. The lower contact is structural along the Lewis Lake Fault and the upper contact is not exposed but is considered to be comformable with the Towner Greenstone (Fig. 3.2). The results of detailed sedimentologic studies of the Nash Fork Formation are presented in Bekker and Eriksson (submit.) and only short summary will be given here. The Nash Fork Formation is separated by two black shale members interpreted as drowning events into the lower, middle and upper divisions. The whole formation is further subdivided into twelve members based on detailed mapping in an area between the Small Telephone Lake and Prospector Lake about 2.2 km along strike (Fig. 3.5). The lower division consists of interlayered massive and stromatolitic dolomite, heterolithic siliciclastics–carbonate, silicified domal digitate stromatolite, and nodular dolomite facies associations (Fig. 3.6). L1 member consists of massive and stromatolitic dolomite facies and contains tufa structures and small domal stromatolites with radial structures (Fig. 3.7) suggesting deposition in an upper intertidal to supratidal setting. Heterolithic siliciclastics–carbonate facies associations make up L2, L7, and lower L8 members (Fig. 3.6) and represents peritidal deposits. This facies association contains upward-shallowing parasequences of gray or brown dolomite, dolosiltite and argillite, rarely capped by sandstone. Ubiquitous sulfate molds in argillites and dolomites suggest an arid environment of deposition. Nodular dolomite facies associations consist of parasequences including from the base to the top: gray dolomite, dolomite with silicified nodules, brown dolomite and argillite which are interpreted as inner-shelf to supratidal deposits. Domal digitate stromatolite facies associations consist predominantly of silicified domal digitate stromatolites with thin parted and ribbon dolomite facies at the base and gray dolomite at the top. This facies association developed during flooding of the carbonate platform.

The middle Nash Fork Formation consists of three members and includes carbonaceous shale and heterolithic siliciclastics–nodular dolomite facies associations. Carbonaceous shale

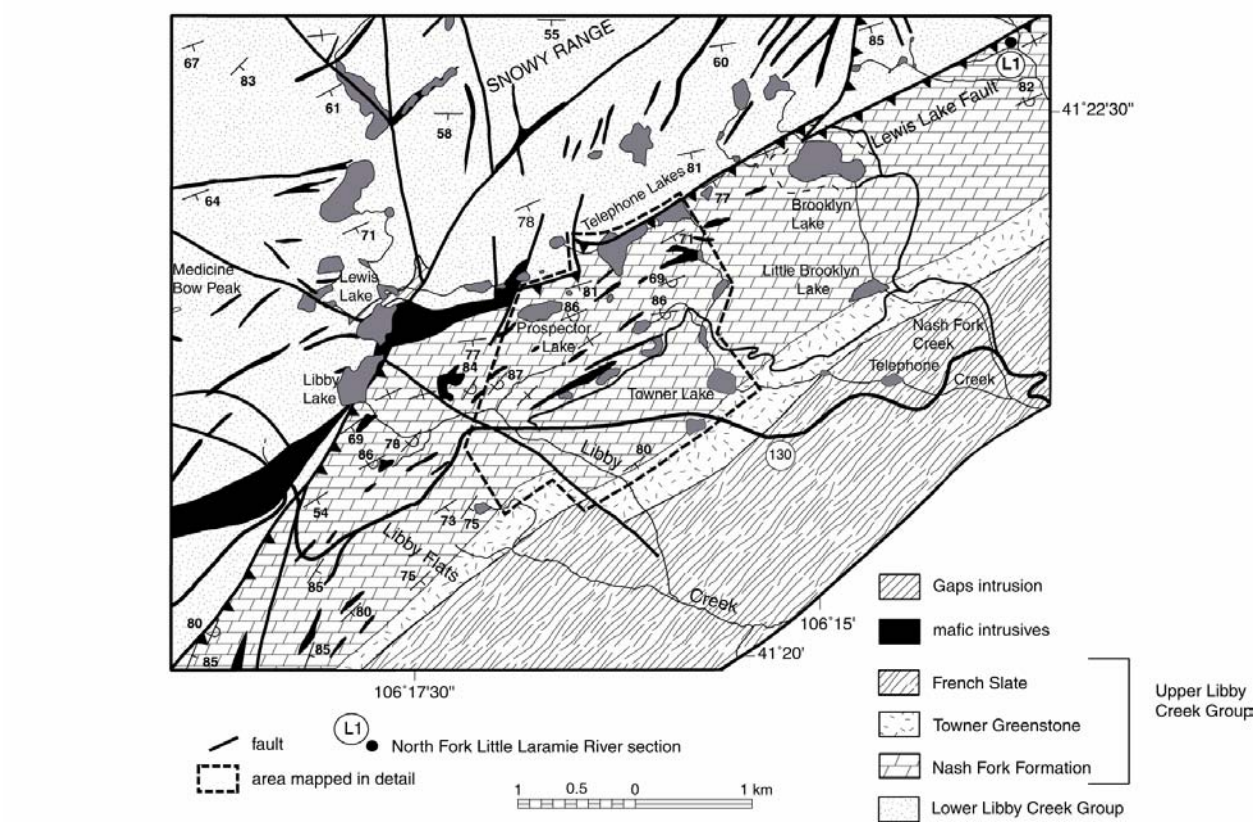

Fig. 3.5. Detailed map of the Nash Fork Formation in the area between the Small Telephone Lake and Libby Creek in Medicine Bow Peak Quadrangle.

facies associations developed in response to platform drowning and consist of upward-coarsening parasequences of black organic-rich shale with pyrite, siltstone and sandstone with thin beds of brown dolomite and black shale. Heterolithic siliciclastics–nodular dolomite facies associations consist of upward-shallowing parasequences of gray dolomite, dolomite with silicified nodules, brown dolomite and siltstone with sulfate molds that record inner-shelf to supratidal depositional conditions. The upper Nash Fork Formation includes massive dolomite facies association and contains a prominent karstic surface overlain by fluvial quartzite dividing this member into two parts. This facies association consists of upward-shallowing parasequences of organic-rich dolomite, gray dolomite, dolosiltite and brown dolomite and reflects deposition in outer shelf to subaerial environments.

No evidence for restricted depositional environments in the form of such features as bedded evaporites are present in the Nash Fork Formation. Rather, the presence of facies indicative of tidal flat, lagoonal, inner and outer shelf and drowned platform depositional

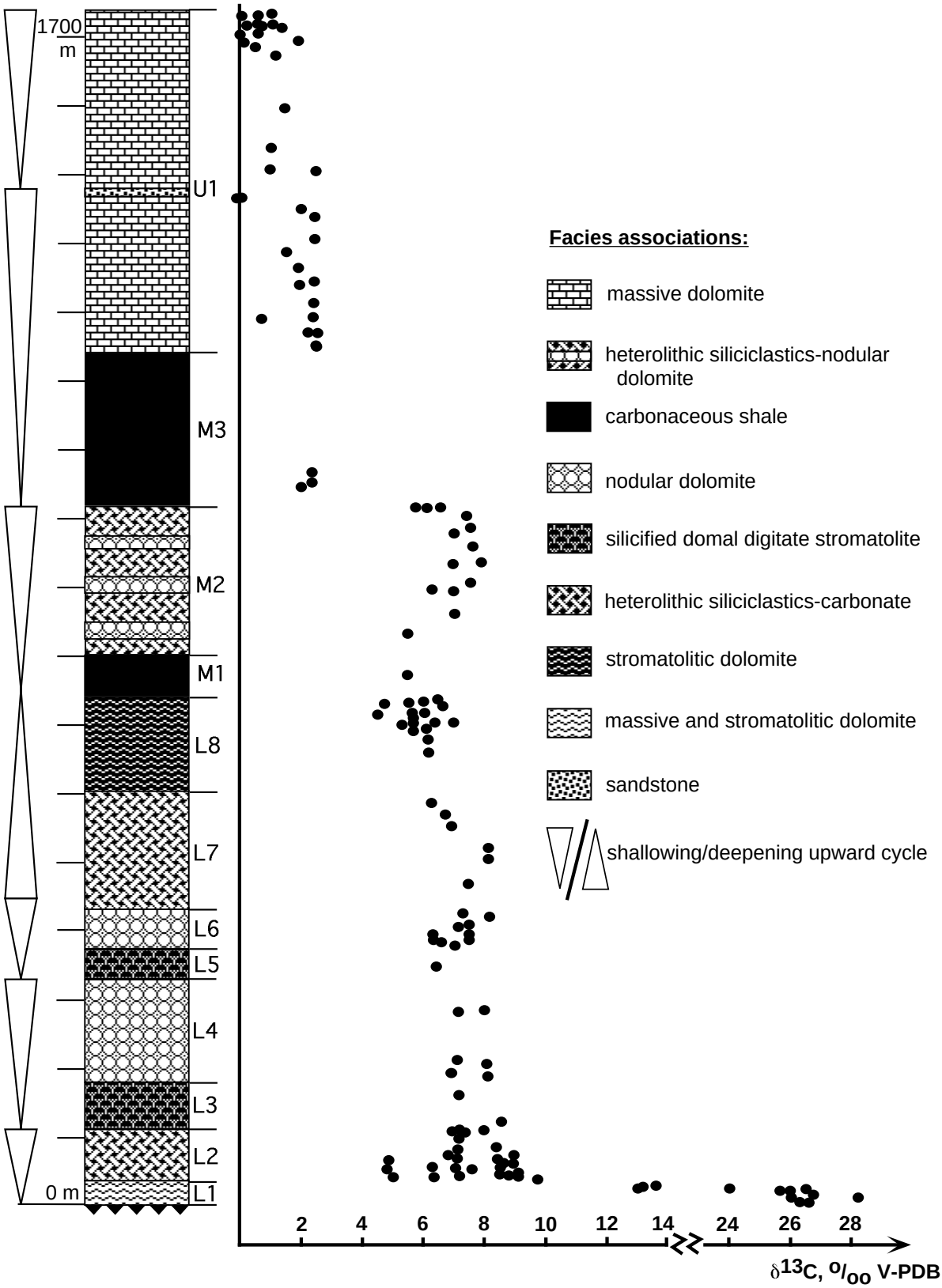

Fig. 3.6. Stratigraphic column, inferred cycles, and variations of $\delta^{13}C_{carb}$ values in the Nash Fork Formation.

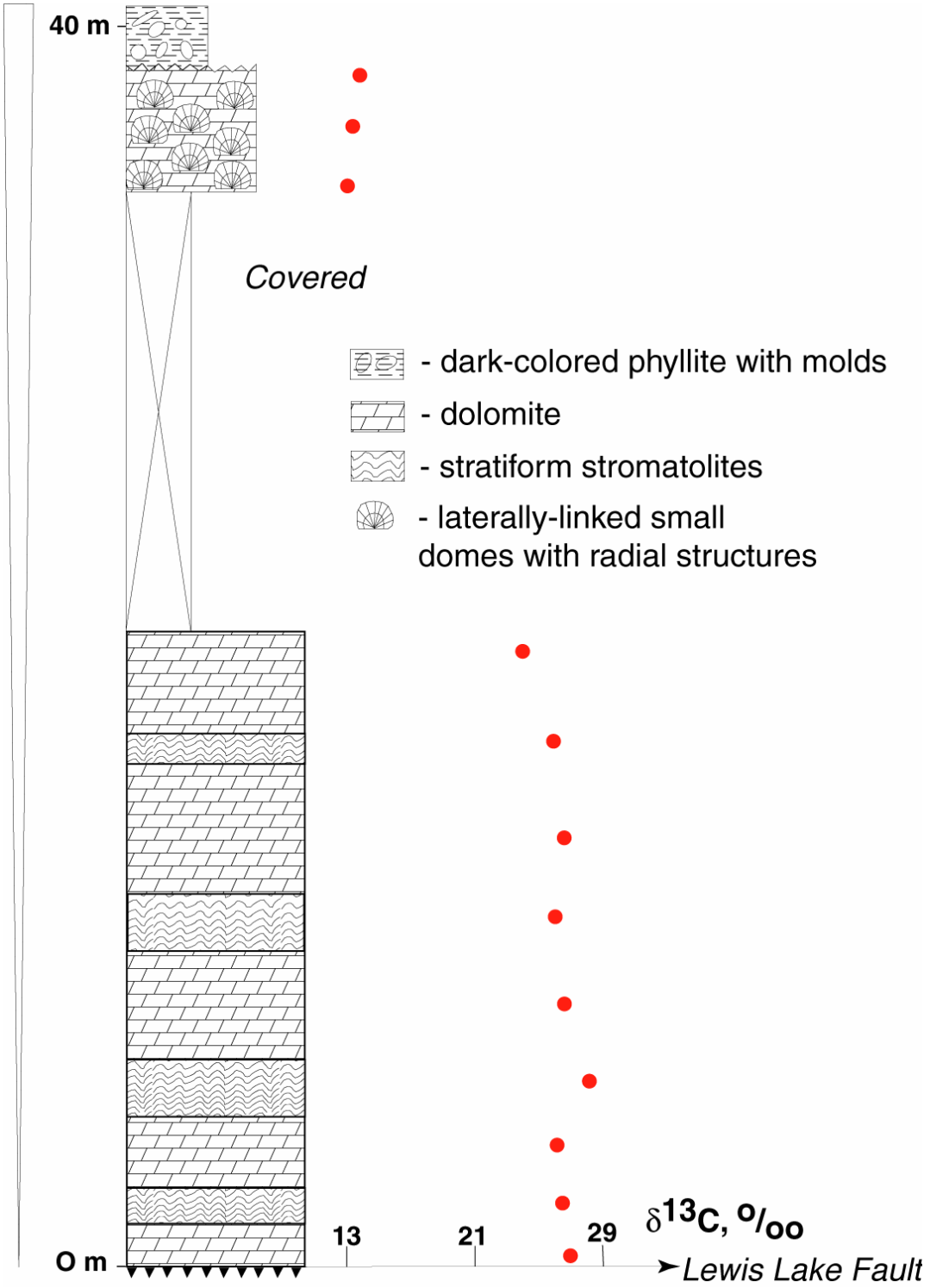

Fig. 3.7. Stratigraphic column and variations of $\delta^{13}C$ values in section of the basal dolomite member in the North Fork of the Little Laramie River.

environments (Bekker and Eriksson, submit.) suggests that the Nash Fork Formation developed entirely in open marine settings on a mature passive margin along the southern edge of the Archean Wyoming Craton (Karlstrom et al., 1983). Facies associations in the lower Nash Fork Formation are most compatible with a low-energy, low-gradient protected platform. Two drowning events in the middle part of the Nash Fork modified the depositional profile of the platform. Drowning caused a shut-down of carbonate production and changed the depositional profile from a low-energy, low-gradient protected platform to an unprotected shelf with a higher gradient for the middle and upper Nash Fork Formation.

Samples for this study were collected in the area mapped in detail (Fig. 3.5). Wherever possible, detailed sections of members were measured and samples were collected within this framework. However, for some members, poor outcrop did not permit section measuring and collected samples were tied to a generalized stratigraphic section (Fig. 3.6) by their position with respect to the top or the bottom of these members. In addition, samples were collected in several places within the mapped area to test variability within members. In sum, all samples are confidently assigned to members.

Geochemical data and diagenesis

All studied carbonate samples are dolomites (Table 3.1). The dolomites have highly variable Mn (68-5059 ppm), Fe (1167-36883 ppm) and Sr (tr.-293 ppm) contents, and Mn/Sr (0.4-2317) ratios suggesting variable post-depositional alteration. Oxygen isotope values are also variable ranging between -18.4 and -4.6‰ V-PDB, but most values are above -14‰ V-PDB and higher than oxygen isotope values of Vagner marbles. This is likely related to higher dolomite stability in respect to limestone coupled with synsedimentary to early diagenetic dolomitization. The most enriched oxygen values are consistent with those found in well-preserved Paleoproterozoic and Mesoproterozoic successions worldwide (cf. Burdett et al., 1990; Veizer et al., 1992, 1992a; Melezhik et al., 1997a; Kah, 2000; Frank and Lyons, 2000; Bekker et al., 2001; and our unpubl. data). The average oxygen isotope values for the upper Nash Fork formation are higher than for the lower part of the formation that has more diverse lithologies and likely experienced more diverse diagenetic conditions. Dolomites have low TOC content (ca. 0.1 mgC/g sample) and decreased fractionation between organic and carbonate carbon (19.8-

28.6‰) likely related to metamorphic reequilibration in greenschist facies. Shales have higher organic carbon content between 0.01 and 203.6 mgC/g sample (most samples higher than 3 mgC/g sample) and $\delta^{13}C_{org}$ values ranging between –6.9 and –30.8‰. The upper end of this range is likely related to metamorphic alteration and the least altered samples with high organic carbon content carry values below -20‰. Carbonate carbon isotope data also show significant yet stratigraphically distinctive variations. The L1 member has extremely high carbon isotope values (between +24 and +28.2‰ V-PDB) within the lower 20 m followed by decrease to +13‰ V-PDB values at top of the member (Fig. 3.7). For the remainder of the lower and middle Nash Fork Formation (L2 to L8 and M1-M2 members), carbon isotope values are in +6 - +8‰ V-PDB envelope (Fig. 3.6). The trend changes in the M3 member and overlying carbonates have $\delta^{13}C$ values of 0 - +2.5‰.

Cross-plots between geochemical parameters can demonstrate to what degree post-depositional processes altered primary geochemical signatures. There is no correlation between $\delta^{13}C$ and $\delta^{18}O$, Mn, Sr, and Mn/Sr (Table 3.1, Fig. 3.8 a–d) suggesting that carbon isotope values were not strongly affected by postdepositional processes. Correlation between $\delta^{18}O$ and Mn, Sr or Mn/Sr is also lacking (Fig. 3.8 e-g). There is, however, weak co-variance between a decrease in oxygen isotope values and an increase in Mn content in carbonates of the L1-M2 members (Fig. 3.8e) suggesting that their oxygen isotope values were stronger altered than those of carbonates from the upper Nash Fork Formation.

Two samples with low Mn/Sr values were analyzed for Sr isotope ratios. Sample WY-96-27 from the lower part of the Nash Fork Formation has a $^{87}Sr/^{86}Sr$ isotope ratio of 0.704947 that is comparable although slightly higher than the lowest Sr isotope values (~0.7035) measured from likely correlative successions in Fennoscandia and Zimbabwe (Master et al., 1990; Gorokhov et al., 1998). A sample from the middle part of the Nash Fork Formation has a very high $^{87}Sr/^{86}Sr$ isotope ratio (0.714247) suggesting that this value is not primary. The high Fe content and low oxygen and carbon isotope values of this sample support significant alteration.

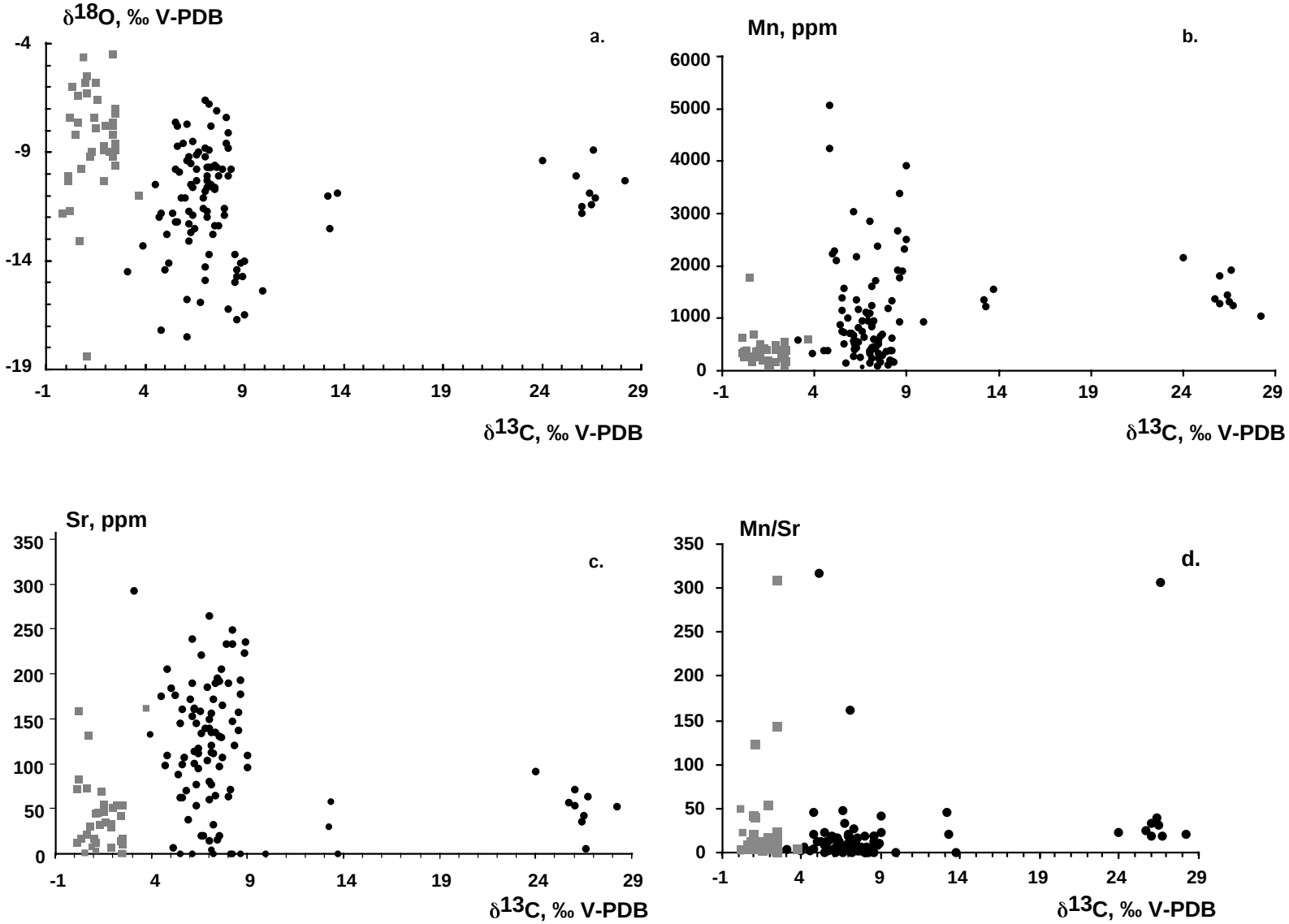

Fig. 3.8. Scatter diagrams for the Nash Fork Formation. a - $\delta^{18}O$, ‰ V-PDB vs. $\delta^{13}C$, ‰ V-PDB; b – Mn, ppm vs. $\delta^{13}C$, ‰ V-PDB; c - Sr, ppm vs. $\delta^{13}C$, ‰ V-PDB; d – Mn/Sr vs. $\delta^{13}C$, ‰ V-PDB; e – Mn, ppm vs. $\delta^{18}O$, ‰ V-PDB; f – Sr, ppm vs. $\delta^{18}O$, ‰ V-PDB; g – Mn/Sr vs. $\delta^{18}O$, ‰ V-PDB.

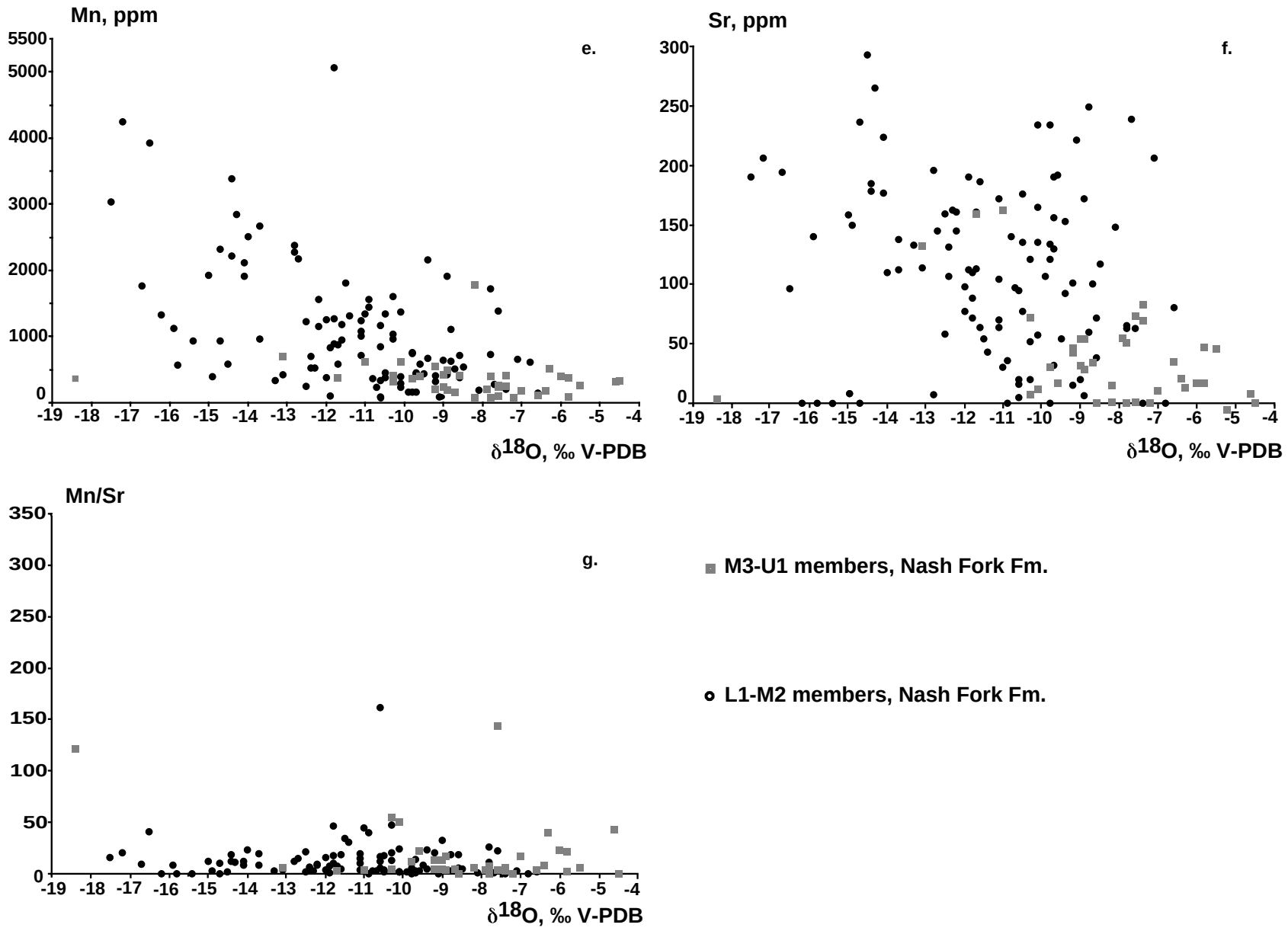
Mn, ppm
e.
5500
5000
4000
3000
2000
1000
0
-19 -18 -17 -16 -15 -14 -13 -12 -11 -10 -9 -8 -7 -6 -5 -4
δ18O, ‰ V-PDB
Sr, ppm
f.
300
250
200
150
100
50
0
-19 -18 -17 -16 -15 -14 -13 -12 -11 -10 -9 -8 -7 -6 -5 -4
δ18O, ‰ V-PDB
Mn/Sr
g.
350
300
250
200
150
100
50
0
-19 -18 -17 -16 -15 -14 -13 -12 -11 -10 -9 -8 -7 -6 -5 -4
δ18O, ‰ V-PDB
M3-U1 members, Nash Fork Fm.
L1-M2 members, Nash Fork Fm.

CHEMOSTRATIGRAPHIC CONSTRAINTS ON AGE OF NASH FORK FORMATION

The age of the Nash Fork Formation is geochronologically poorly constrained (see Regional Geology and Stratigraphy section). However, chemostratigraphic data along with lithostratigraphy can provide better constraints on the age of the Nash Fork Formation. The L1 member has carbon isotope values up to +28‰ which are anomalously high for carbonates precipitated in equilibrium with the ocean, whereas values above +10‰ and as high as +18‰ are common in Paleoproterozoic carbonate successions worldwide (Baker and Fallick, 1989a, b; Master et al., 1993; Karhu, 1993; Melezhik et al., 1997a; Bekker et al., 2001a; Table 3.2). These carbonate successions cluster around 2.15 Ga in age but likewise have poor age constraints. Marine carbonates of the Seward and Pistolet subgroups of the Kaniapiskau Supergroup, New Quebec Orogen are also highly enriched in ^{13}C reaching a $\delta^{13}C$ value +15.4‰ (Melezhik et al., 1997a), while the extreme enrichment to values around +28‰ has not been observed elsewhere. The age of these units is well constrained between 2169 ± 2 Ma and 2142 $^{+4}/_{-2}$ Ma (Rohon et al., 1993). Carbonate units with carbon isotope values of the same magnitude as that found in the L2–M2 members of the Nash Fork Formation (between +6 and +8‰) occur in Fennoscandia where they are constrained in age to ca. 2.2-2.1 Ga (Karhu and Holland, 1996). The M3 member records a change in carbon isotope trend from high carbon isotope values to values near 0‰. This isotopic shift was accompanied by deposition of black organic-rich shales (upper carbonaceous shale member with TOC content up to 203.6 mgC/g sample). Similar change in carbon isotope values of carbonates accompanied by deposition of black organic-rich shales occur in Fennoscandia (Jatulian/Ludikovian boundary; Karhu, 1993; Melezhik et al., 1999), Gabon (Francevillian Series; Weber et al., 1983; Gauthier-Lafaye and Weber, 1989) and Quebec (Lower Albanel Formation; Mirota and Veizer, 1994; Bekker et al., 1997). The end of the carbon isotope excursion in the Fennoscandia is constrained between 2062 ± 2 Ma and 2113 ± 4 Ma (Karhu, 1993). Age constraints for the Francevillian Series, Gabon (Bros et al., 1992) agree with the Fennoscandian age constraints for the end of the carbon isotope excursion. In addition, the end of the carbon isotope excursion in the upper Pretoria Group, South Africa preceded intrusion of the Bushveld complex and associated Rooiberg Felsites dated at 2061 ± 2 Ma (Walraven, 1997; Bekker et al., 2001). A minimum age for the Nash Fork Formation is constrained by younger mafic volcanism that has been dated elsewhere on the Wyoming Craton to approximately 2.0-1.97 Ga (Redden et al., 1990; Cox et al., 2000). Combined, these age

Table 3.2. Paleoproterozoic succession containing carbonates with $\delta^{13}C_{carb}$ values > +8‰.

Name of unit	Location	Age constraints	$\delta^{13}C_{max}$ values	Reference
Dunphy, Uvé and Alder fms.	Labrador Trough, Canada	2169–2142 Ma	15.4 ‰	Melezhik et al., 1997a
Juderina Fm.	Nabberu Province, Australia	ca. 2173 Ma	9.4‰	El Tabakh et al., 1999; our unpubl. data
Aravalli Supergroup	India	1900–2200 Ma	11.1‰	Sreenivas et al., 2001; our unpubl. data
Unnamed marble unit	Lofoten-Vesterålen, Norway	Early PR_1	12.1‰	Baker & Fallick, 1989a
Loch Maree Gr.	Scotland	Early PR_1	12.9‰	Baker & Fallick, 1989b
Nash Fork Fm.	Wyoming, USA	Early PR_1	28.2‰	Bekker et al., 2001b
Slaughterhouse Fm.	Wyoming, USA	Early PR_1	16.6‰	Bekker et al., 2001b
Lomagundi & Deweras grs.	Zimbabwe	Early PR_1 (>~2.0 Ga)	16.3‰	Bekker et al., 2001a
Mako Supergroup	Eastern Senegal	ca. 2.15 Ga	~10‰	Master et al., unpubl.
Silverton & Lucknow fms.	South Africa	Early PR_1 (>2061 Ma)	11.3‰	Master et al., 1993; Buick et al., 1998; Swart, 1999; Bekker et al., 2001
Peribonca Fm.	Otish Basin, Quebec, Canada	Early PR_1	10.3‰	Our unpubl. data
Kona Dolomite	MI, USA	Early PR_1	9.5‰	Our unpubl. data
Carbonate unit from the Hurwitz Group	Quartzite Lake, Nunavut, Canada	Early PR_1 (>2.11 Ga)	9.1‰	Our unpubl. data
Paso Severino Fm.	San Jose Belt, Uruquay	2145–2074 Ma	11.6‰	Our unpubl. data
Jatulian carbonates	Finland; Karelia and Kola Peninsula, Russia	>2116-<2113 Ma	12.9‰	Karhu, 1993; Melezhik & Fallick, 1996; Melezhik et al., 1999
Yakovlevskaya Suite	Voronezh Massif, Russia	Early PR_1	11.7‰	Akhmedov et al., 1996

constraints suggest that the Nash Fork Formation was deposited between ~2.17 and 1.97 Ga.

IMPLICATIONS FOR INTRABASINAL CORRELATION

The Deep Lake and lower Libby Creek groups are considered correlative with the Huronian Supergroup, Ontario, Canada based on the presence in both successions of characteristic lithologies: ca. 2.48-2.45 Ga old pyritic and uraniferous quartz pebble conglomerates followed by three glacial horizons, a carbonate unit above the middle of three diamictites and thick mature Al-rich hematite-bearing quartzites (Houston et al., 1992; Roscoe and Card, 1993; Table 3.3). However, Sims (1995) suggested that the Early Paleoproterozoic successions in Wyoming and Lake Superior area are homotaxial and are not necessary time correlative due to deposition in similar tectonic environments but on margins of separate cratons. Chemostratigraphic data for the Vagner carbonates presented in this paper are similar to isotopic data for carbonates of the Espanola Formation (Veizer, et al., 1992; Bekker et al., 1999) that has a similar stratigraphic position with respect to the North American three glacial horizons. These data provide independent support for lithostratigraphic correlation between these units.

Houston et al. (1992) correlated the Nash Fork Formation with the Gordon Lake and Bar River formations of the upper Huronian Supergroup and the Randville Dolomite of the Marquette Range Supergroup, Michigan. This correlation is equivocal since, as was discussed above, the characteristic carbon isotope trend in the Nash Fork Formation supports an age designation close to 2.1 Ga whereas the whole Huronian Supergroup is cut by Nippissing sills with an age 2.219.4 ± 3.5 Ma (U-Pb zircon, Corfu and Andrews, 1986). Correlation with the Randville Dolomite, Marquette Range Supergroup is also unlikely because the Randville Dolomite is considered to be correlative with the Gordon Lake Formation of the Huronian Supergroup, ON based on its conformable stratigraphic position above a glacial diamictite and a mature quartzite unit (Young, 1983).

IMPLICATIONS FOR THE END OF THE CARBON ISOTOPE EXCURSION

The present study supports earlier suggestions, based on Fennoscandian data, that the end of the carbon isotope excursion closely accompanied breakup of the Kenorland supercontinent at ca. 2.1 Ga (Karhu, 1993). In addition, and in common with the Fennoscandian record (Karhu, 1993, Melezhik et al., 1999), the end of the carbon isotope excursion was accompanied by

Table 3.3. Correlation between the Snowy Pass, Huronian and Marquette Range supergroups (after Houston et al., 1992 with additional chemostratigraphic constraints from this study).

	Snowy Pass Supergroup, Medicine Bow Mountains, WY	Huronian Supergroup, ON	Marquette Range Supergroup, MI
Fine-grained siliciclastics with BIFs	French Slate		Vulcan Iron Formation
ca. 2.0–1.95 Ga mafic volcanism	Towner Greenstone		Hemlock Formation
Carbonates with $\delta^{13}C$ values close to 0‰	Upper part of the Nash Fork Formation		
Black organic-rich shales	Middle part of the Nash Fork Formation		
Carbonates with $\delta^{13}C$ values <+10‰ (ca. 2.14–2.1 Ga)	Lower part of the Nash Fork Formation except the basal dolomite member		
Carbonates with $\delta^{13}C$ values >+10‰ (ca. 2.17–2.14 Ga)	Basal member of the Nash Fork Formation		
Carbonates with $\delta^{13}C$ values >+4 and <+10‰ (older than ca. 2.17 Ga)		Gordon Lake Formation	
Carbonates with $\delta^{13}C$ values <+4‰ (older than ca. 2.22 Ga)			Randville Dolomite
Mature Al-rich hematite bearing q-tes	Medicine Peak Quartzite	Lorrain Formation	Sturgeon Quartzite
Third glacial horizon	Headquarters Formation	Gowganda Formation	Fern Creek Formation
Carbonate above the second glacial horizon	Vagner Formation	Espanola Formation	
Second glacial horizon	Vagner Formation	Bruce Formation	
First glacial horizon	Campbell Lake Formation	Ramsay Lake Formation	
Pyrite and uraninite-rich mature quartzites	Lindsey Quartzite and Magnolia Formation	Matinenda Formation	

deposition of organic-rich shales and thin, discontinuous BIF in the M3 member of the Nash Fork Formation. On a global scale, successions straddling the end of the carbon isotope excursion contain organic-rich shales, BIFs and also are marked by Mn-rich carbonates and phosphorites (Table 3.4). Furthermore, $\delta^{13}C$ values of reduced carbon in the Francevillian and

Table 3.4. Paleoenvironmental indicators within early Paleoproterozoic successions with ages of ca. 2.1 Ga based on geochronologic and chemostratigraphic constraints.

Name of the succession and basin	BIF	Mn-rich carbonates	Organic-rich shales	Most depleted $\delta^{13}C_{org}$ values	Phosphorites	Mafic volcanics	Reference to age and $\delta^{13}C_{carb}$ values >+4‰
Nash Fork Formation, WY, USA	Thin discontinuous BIF (Bekker and Eriksson, submit.)		Black organic-rich shales (Bekker and Eriksson, submit.)			Overlain by Towner Greenstone	This study
Lower Albanel Formation, Mistassini Basin, Quebec, Canada			Mirota and Veizer (1994)	-39.0‰ (Bekker et al., unpubl.)			Mirota and Veizer (1994); Bekker et al., unpubl.
Jatulian/Ludikovian groups, Fennoscandian Shield	Laajoki and Saikkonen (1977); Paakkola (1971)	Paakkola (1971); Golubev et al. (1984)	Shungites (Karhu, 1993; Melezhik et al., 1999)	-44.4‰ (Karhu, 1993; Melezhik et al., 1999)	Äikäs (1980); Gehör (1994); Bekasova and Dudkin (1982); Golubev et al. (1984); Melezhik and Predovsky (1984)	Karhu (1993), Melezhik et al. (1999), Hanski et al. (2001)	Karhu (1993), Melezhik and Fallick (1996)
Hapschan Group, Anabar Shield, Russia		Rhodonite and spessartine (Ponomarenko, 1973)	Ponomarenko (1973)		Apatite (Ponomarenko, 1973)	Ponomarenko (1973); Rozen et al. (1990)	Rozen et al. (1990, 1994)
Fyodorov Suite, Aldan Supergroup, Aldan Shield, Russia	Salop (1982), Pavlov et al. (1987)	Mn-rich silicates (Kulish, 1970)	Kulish (1970)		Apatite (Salop, 1982; Guliy, 1995a, b)	Rundqvist and Mitrofanov (1993)	Sidorenko et al. (1977); Guliy (1995a, b)
Slyudyanka Crystalline Compex, Eastern Siberia, Russia		Rhodonite, bustamite and spessartine (Reznitsky et al., 1976)	Yudin and Arsenev (1970)		Apatite (Yudin and Arsenev, 1970)	Yudin and Arsenev (1970); Kotov et al. (2000)	Borshchevsky et al. (1982); Reznitsky et al. (1998); Kotov et al. (2000)
Upper Yakovlevskaya and Timskaya suites, Oskolskaya Series (=Vorontzovskaya Series), KMA, Russia	Hematite- and martite-rich slates (Nikitina and Schipansky, 1987)	Mn-rich sulfides in carbonates and slates (Lazur et al., 1981)	Sozinov and Kazantsev (1978); Zhmur and Stepanov (1987)	-44.2‰ (Sozinov et al., 1988; Lobzova and Esikov, 1981)	Phosphatic slates and quartzites (Sozinov and Kazantsev, 1978; Nikitina and Shchipansky, 1987)	Sozinov and Kazantsev (1978)	Shchipansky and Bogdanova (1996); Akhmedov et al. (1996)
West limb of the Central Periazov Syncline, Ukraine	Boiko et al. (1989)	Rhodonite (Kanygin et al., 1969)	Kanygin et al. (1969); Boiko et al. (1989)	-35.3‰ (Sidorenko et al., 1972)	Apatite (Kanygin et al., 1969)		Boiko et al. (1989); Zagnitko and Lugovaya (1985, 1989); Shchipansky and Bogdanova (1996)
Gdantzevskaya Suite,	Boiko et al. (1989)		Prilutzky et al.	-34.9‰			Boiko et al. (1989);

Krivorozhskaya Series, Krivoy Rog, Ukraine			(1992)	(Sidorenko et al., 1972)			Zagnitko and Lugovaya (1985); Prilutzky et al. (1992)
Hoshchevat-Zavalsky Suite, Bugskaya Series, Ukraine	Boiko et al. (1989)	Rhodochrosite (Shnyukov and Orlovsky, 1980; Varentsov and Rakhmanov, 1980)	Zagnitko and Lugovaya (1986); Boiko et al. (1989)	-35.8‰ (Zagnitko and Lugovaya, 1986)	Apatite (Zagnitko and Lugovaya, 1989)	Boiko et al. (1989); Zagnitko and Lugovaya (1985)	Boiko et al. (1989); Zagnitko and Lugovaya (1985, 1989)
Rodionovskaya Suite, Ingulo-Inguletzkaya Series, Ukraine			Graphitic schists (Boiko et al., 1989)		Apatite in quartzites (Yur'ev, 1968)		Zagnitko and Lugovaya (1985, 1989); Boiko et al. (1989)
Francevillian Series, Gabon	Leclerc and Weber (1980)	Rhodochrosite (Leclerc and Weber, 1980; Hein et al., 1989; Hein and Bolton, 1993)	Gauthier-Lafaye and Weber (1989)	-46.2‰ (Weber et al., 1983)	High phosphate content of iron formation (Leclerc and Weber, 1980)	Weber (1973)	Gauthier-Lafaye and Weber (1989), Bros et al. (1992)
Birimian Supergroup, West Africa (Nsuta, Ghana; Tambao Birkina Faso; Mokta and Ziemougoula, Côte d'Ivoire)		Rhodochrosite (Dzigbodi-Adjimah and Sogbor, 1993; Weber, 1997; Mücke et al., 1999)	Mücke et al. (1999)			Mücke et al. (1999)	Master et al. (1993); Davis et al. (1994); Hirdes and Davis (1998)
Lukoshi Complex, Zaire		Mn-rich carbonates (Doyen, 1973, 1974)	Doyen (1973, 1974)			Doyen (1973, 1974)	André (1993); Feybesse et al. (1998)
Upper Lomagundi / Piriwiri Group, Zimbabwe	Oxide- and silicate-facies iron formations (Master, 1991)	Mn-oxides (Master, 1991)	Black graphitic slates (Master, 1991)		Phosphate-bearing shale (Master, 1991)	Overlain by andesitic volcanics (Master, 1991)	Schidlowski et al. (1976); Master (1991); Schidlowski and Todt (1998); Bekker et al. (2001)
Horseshoe basin, Nabberu Province, Western Australia	Iron-rich shale (Krapez and Martin, 1999)	Mn-oxides and carbonates (Krapez and Martin, 1999)	Krapez and Martin (1999)			Krapez and Martin (1999)	Russell (1992); Woodhead and Hergt (1997); Krapez and Martin (1999); Bekker et al., unpubl.
Aravalli Group, India	Nayak (1980)	Mn-oxides (Nayak, 1980; Roy, 1980)	Carbonaceous phyllites (Banerjee, 1971)		Stromatolitic phosphorites (Banerjee, 1971)		Maheshwari et al. (1999); Sreenivas et al. (2001); Banerjee, 1986)

Fennoscandian organic-rich shales show a consistent negative shift up section to -46 and -45‰, respectively (Weber et al., 1983; Karhu, 1993; Melezhik et al., 1999). These organic-rich shales have low S/C ratios that are considered to reflect a non-marine origin or Fe limitation (Karhu, 1993; Melezhik et al., 1999). The end of the carbon isotope excursion was also accompanied by voluminous mafic volcanism on the Fennoscandian Shield and elsewhere including the Wyoming Craton (Karhu, 1993; Melezhik et al., 1999; Hanski et al., 2001; see Table 3.4). Melezhik et al. (1997) argued for a decline in stromatolite abundance and diversity on the Fennoscandian Shield at the end of the carbon isotope excursion and a similar decline was inferred from Indian and Chinese data (Semikhatov and Raaben, 1994). A short-term decline in stromatolite abundance after the carbon isotope excursion was also observed in the U1 member of the Nash Fork Formation (Bekker and Eriksson, submit.) and in the Lower Albanel Formation, Quebec, Canada (Bekker, pers. obs.). Although the significance of the change in stromatolite abundance and diversity is equivocal (see Semikhatov and Raaben, 1996; Semikhatov et al., 1999; Awramik and Sprinkle, 1999), clearly conditions for stromatolite growth at the end of the carbon isotope excursion were unfavorable on several cratons at least for a short period of time.

The unusual lithologies and paleoenvironmental conditions, and their consistent position at a chemostratigraphically distinctive level in globally correlative successions, argues for major paleooceanographic changes at the end of the Paleoproterozoic carbon isotope excursion, similar to those at the Precambrian-Cambrian boundary (e.g. Cook, 1992, Donnelly et al., 1990; Hein et al., 1999). Mn-rich carbonates, phosphorites and BIFs common in Late Neoproterozoic to Early Cambrian successions were attributed to ocean overturn either at the end of glaciations (Klein and Beukes, 1993; Bühn and Stanistreet, 1997) or at the Precambrian/Cambrian boundary following supercontinent breakup (Donnelly et al., 1990; Hein et al., 1999). Oceanic overturns were preceded by ocean anoxic events (OAE) when burial rates of organic carbon were high as inferred from highly positive carbon isotope values of carbonates (e.g. Knoll et al., 1986). Reasons for these OAE's remain conjectural with two models proposed. Knoll et al. (1996) argue for a decrease in the rate of ocean circulation and dissolved oxygen in the ocean as a result of the low-latitude position of landmasses coupled with a greenhouse climate. Des Marais

(1994) and Hoffman et al. (1998), in contrast, relate high burial rates of organic carbon to an increase in the length of continental margins as the Rodinia supercontinent was breaking apart.

A similar model is suggested here for the end of the Paleoproterozoic carbon isotope excursion at ca. 2.1 Ga. Highly positive carbon isotope values (Table 3.2 and 3.4; Karhu and Holland, 1996) in ca. 2.2-2.1 Ga-old carbonates and evidence for the accompanying rise in atmospheric oxygen levels (Holland, 1994; Karhu and Holland, 1996; Beukes et al., 1999; Bekker et al., 2001) suggest high burial rates of organic matter in the deep ocean. Consequently, the ocean was likely stratified with the deep ocean waters being anoxic. In this respect, the lower carbonaceous shale member of the Nash Fork Formation (M1) positioned within the ^{13}C-enriched carbonate interval is informative since it provides the first unequivocal evidence that deposition of shallow-water, ^{13}C-enriched carbonates was accompanied by high burial rates of organic carbon in deeper waters. In addition, extensive deposits of phosphorites, Mn-rich carbonates and BIFs at the end of the carbon isotope excursion suggests limited mixing between the deep and shallow parts of the ocean during the Paleoproterozoic carbon isotope excursion (cf. Klein and Beukes, 1993). Whereas Mn and Fe were provided to the deep ocean by hydrothermal activity at MOR's, phosphorus was likely released from organic matter and ferric oxyhydroxides (Van Cappellen and Ingall, 1994; Ingall and Jahnke, 1994). BIF's deposited after the Paleoproterozoic OAE are thin, lean and incomparable in size to those preserved in older (e.g. ca. 2.45 Ga in age) or younger (1.9-1.8 Ga old) successions (Isley, 1995; Simonson and Hassler, 1996; Isley and Abbott, 1999; Table 3.4). This observation implies that Fe flux into the deep ocean was higher than H_2S production (cf. Canfield, 1998) during the carbon isotope excursion that could be related to a low sulfate content of the ocean (Canfield and Raiswell, 1999); low rates of sulfate delivery to the deep ocean due to slow circulation; incomplete inhabitation of the deep ocean by sulfate-reducers or high Fe hydrothermal flux (Glasby, 1997). In contrast to BIF's, manganese deposits post-dating the carbon isotope excursion are large. A likely explanation is that iron was deposited in the deeper ocean as pyrite as a result of sulfate reduction thereby separating Fe from Mn. Sulfate reduction also led to the buildup of deep-ocean carbonate alkalinity enriched in ^{12}C (Canfield and Raiswell, 1991; Knoll et al., 1996, Grotzinger and Knoll, 1995).

The temporal relationship between the end of the carbon isotope excursion and Kenorland breakup suggests that ocean circulation could have been invigorated by changes in paleogeography related to the opening of new seaways and continent movement to high latitudes and/or an increase in atmospheric and oceanic temperatures due to a buildup in atmopsheric CO_2 related to abundant mafic volcanism. Driven by one or both of these factors, ocean mixing brought deep-ocean waters charged with carbonate alkalinity and nutrients (P, Fe, and Mn) to shallow waters. Mixing with deep-ocean waters enriched in ^{12}C shifted the carbon isotope composition of shallow waters to near 0‰ values as shown by carbonates from the upper Nash Fork Formation (Fig. 3.6). Negative carbon isotope values (ranging between –20 and 0‰) in carbonates associated with organic-rich shales on the Fennoscandian Shield and Voronezh Massif, Russia are likely related in part to diagenetic and metamorphic processes (Zhmur and Stepanova, 1987; Sozinov et al., 1988; Karhu, 1993, Melezhik et al., 1999), but some might record upwelling of deep waters depleted in ^{13}C. High nutrient flux to shallow waters likely enhanced productivity locally. This increase in productivity might explain the apparent stromatolite decline since abundant planktonic forms in shallow-waters would decrease water transparency confining stromatolites to very shallow areas within basins (cf. Hallock and Schlager, 1986). The upper Nash Fork Formation chemostratigraphic record suggests that the carbon isotope composition of the ocean was relatively stable near 0‰ after the end of the carbon isotope excursion despite ocean overturn and the effects of localized areas with high productivity. Iron and manganese were deposited as oxides once they entered oxygenated shallow waters and Mn oxides were diagenetically transformed to Mn-carbonates as evidenced by limited stable isotope studies on these Mn-rich carbonates (Hein et al., 1989; Yeh et al., 1995a, b; Hein and Bolton, 1993).

The upward trend towards more negative carbon isotope values in organic carbon observed in Francevillian and Fennoscandian basins (Weber et al., 1983; Karhu, 1993, Melezhik et al., 1999) could be explained by the release of methane clathrates during ocean overturn (cf. Kennedy et al., 2001). However, we note that this trend persists over large thicknesses (~800 m in Karelia, Russia; see Melezhik et al., 1999) and it seems unlikely that release of methane clathrates or its effect on ocean composition would be significant over such thick stratigraphic intervals. An increasingly important role of secondary productivity by methylotrophic bacteria

living on methane produced during early diagenesis in organic-rich sediments is our preferred explanation for this trend (cf. Hayes, 1983, 1994). Low S/C ratios found in organic-rich shales in several Fennoscandian basins (Karhu, 1993; Melezhik et al., 1999) could be explained by dilution and reduction of dissolved sulfate in shallow waters after mixing with deep waters that had low sulfate and H_2S contents and were charged with reducing compounds.

The above discussion has several important implications for our understanding of the carbon cycle. Contrary to the widely held view (Des Marais, 1994; Hoffman et al., 1998), supercontinent breakup did not enhance organic carbon burial. On the contrary, breakup of Kenorland succeeded the Paleoproterozoic positive carbon isotope excursion. Similarly, the Early Paleoproterozoic record does not support arguments that high rates of organic matter burial due to high productivity and nutrient flux into semi-restricted basins leads to either a local or global carbon isotope excursion. Somewhat puzzling to our understanding of carbon cycling and climatic changes, the ca. 2.2-2.1 Ga positive carbon isotope excursion did not end with a glaciation, contrary to the proposed cause and effect relationship in the Neoproterozoic (Kaufman et al, 1997; Hoffman et al., 1998). The early Paleoproterozoic record does not support any relationship between a ca. 2.1-2.0 Ga mantle plume (Puchtel et al., 1998; Hanski et al., 2001), deposition of organic-rich shales, and the carbon isotope excursion. Mantle plume activity, expressed in the form of mafic volcanism, and deposition of organic-rich shales followed the carbon isotope excursion rather than being synchronous with it. Finally, deposition of sedimentary mineral deposits in the Early Paleoproterozoic was likely confined to narrow time intervals and related to global tectonic, climatic and paleoceanographic changes. This observation has significant potential for mineral exploration in successions of this age.

CONCLUSIONS

1. Carbonates of the Vagner Formation were deposited during a post-glacial transgression and have negative carbon isotope values ranging between –1.5 and –3.8‰ V-PDB. These carbon isotope values, combined with the stratigraphic position above the glacial unit in the otherwise siliciclastic succession devoid of carbonates and indications for decreased fractionation between carbonate and organic carbon, allow an analogy to be drawn with the Neoproterozoic cap carbonates. By analogy, deposition of the Vagner Formation carbonates

was likely related to high carbonate alkalinity flux into the shallow waters at the end of the Paleoproterozoic glaciation.

2. The Vagner Formation is correlative with the Espanola Formation, Huronian Supergroup, ON based on similar carbon isotope systematics as well as stratigraphic position above the middle of three glacials. Combined data from these units argue for coupling of biogeochemical cycling of carbon and climatic changes during the Paleoproterozoic glacial epoch.

3. The Nash Fork Formation was deposited after the Paleoproterozoic glacial epoch. The lower member of the Nash Fork Formation has extremely high $\delta^{13}C$ values up to +28‰ followed by $\delta^{13}C$ values ranging between +6 and +8‰ in the overlying members of the lower and middle parts of the Nash Fork Formation. Carbonates in the upper Nash Fork Formation above the carbonaceous shale have $\delta^{13}C$ values ranging between 0 and +2.5‰. This carbon isotope trend is similar to that observed in the Jatulian and Ludikovian groups in Fennoscandia where it was geochronologically constrained between 2.11 and 2.06 Ga (Karhu, 1993). Organic-rich shales also straddle the change from high to near 0‰ $\delta^{13}C$ values in the Fennoscandian successions. Based on the similar chemo- and lithostratigraphy of these successions, Fennoscandian age constraints for the end of the carbon isotope excursion can be inferred for the depositional age of the Nash Fork Formation. These new age constraints conflict with the earlier proposed lithostratigraphic correlation of this unit with the Gordon Lake Formation, Huronian Supergroup, ON and Randville Dolomite, Marquette Range Supergroup, MI (Houston et al., 1992). These age constraints also imply that the Upper Libby Creek Group including the Nash Fork Formation was deposited on a passive margin rather than in a foreland basin as was inferred earlier (Karlstrom et al., 1983) since it is significantly older than 1.78-1.74 Ga old volcanic arc that overrode the southern flank of the Wyoming Craton.

4. In addition to correlation between the Nash Fork Formation and Jatulian/Ludikovain groups of the Fennoscandian Shield, correlation can be drawn with the Lower Albanel Formation, Mistassini Basin, Quebec and Francevillian Series, Gabon based on similar chemo- and lithostratigraphy. These and other correlative successions worldwide straddling the end of

the ca. 2.2-2.1 Ga carbon isotope excursion contain BIFs, Mn-rich carbonates, organic-rich shales with very low $\delta^{13}C_{org}$ values, phosphorites and voluminous mafic volcanics.

5. The stratified anoxic ocean that existed during the ca. 2.2-2.1 Ga carbon isotope excursion was overturned as new seaways opened and/or atmospheric and ocean temperatures rose as a result of voluminous volcanism during the Kenorland breakup. Deep waters enriched in P, Mn, Fe and carbonate alkalinity with highly ^{13}C-depleted carbon isotope values were delivered to the shallow part of the ocean and mixed with oxygenated waters. Mixing of deep and shallow waters led to precipitation of Fe and Mn oxides and phosphorites at the redoxocline. High nutrient flux stimulated productivity and led to increased organic carbon burial in localized areas.

REFERENCES

Äikäs, O., 1980. Uraniferous phosphorite and apatite-bearing gneisses in the Proterozoic of Finland, Proc. Intl. Uranium Symp. on the Pine Creek Geosyncline, pp. 675-681.

Akhmedov, A.M., Travin, L.V., Tikhomirova, M., 1996. Glacial and evaporate epochs in the early Proterozoic and interregional correlation. Regional geology and metallogeny (5), 84-97.

André, L., 1993. Age Rb-Sr Proterozoique inferieur du magmatisme continental du Groupe de la Lulua (Kasai, Zaire): Ses implications geodynamiques. Annales de la Société géologique de Belgique 116(1), 1-12.

Awramik, S.M., Sprinkle, J., 1999. Proterozoic stromatolites: the first marine evolutionary biota. Historical Biol. 13, 241-253.

Baker, A.J., Fallick, A.E., 1989a. Heavy carbon in two-billion-year-old marbles from Lofoten-Vesterålen, Norway: implications for the Precambrian carbon cycle. Geochim. Cosmochim. Acta 53, 1111-1115.

Baker, A.J., Fallick, A.E., 1989b. Evidence from the Lewisian limestone for isotopically heavy carbon in two-thousand-million-year-old sea water. Nature 337, 352-354.

Banerjee, D.M., 1971. Precambrian stromatolitic phosphorites of Udaipur, Rajasthan, India. Geol. Soc. Am. Bull. 82, 2319-2330.

Banerjee, D.M., Schidlowski, M., Arneth, J.D., 1986. Genesis of Upper Proterozoic-Cambrian phosphorite deposits of India: isotopic inferences from carbonate fluorapatite, carbonate and organic carbon. Precambrian Res. 33, 239-253.

Bekasova, N.B., Dudkin, O.B., 1982. Composition and nature of concretionary phosphorites from the Early Precambrian of Pechenga (Kola Peninsula). Lithology and Mineral Resources, 625-630.

Bekker, A., 1998. Chemostratigraphy and climatostratigraphy of the Paleoproterozoic Snowy Pass Supergroup, Wyoming and its application for correlation with other sequences in North America. M.S. Thesis, University of Minnesota, Duluth, 104 pp.

Bekker, A., Eriksson, K.A., submit. Paleoproterozoic drowned carbonate platform on the southeastern margin of the Wyoming Craton: a record of the Kenorland breakup. Precambrian Res.

Bekker, A., Eriksson, K.A., Kaufman, A.J., Karhu, J.A., Beukes, N.J., 1999. Paleoproterozoic record of biogeochemical events and ice ages, GSA Annual Meeting, Abst. with Programs, v. 31, No. 7, A-487.

Bekker, A., Karhu, J.A., Eriksson, K.A., 1997. Paleoenvironmental changes at the end of the Paleoproterozoic carbon isotope excursion (~2.06 Ga), GSA Annual Meeting, Abst. with Programs v. 29, n. 6, p. 467.

Bekker, A., Kaufman, A.J., Karhu, J.A., Beukes, N.J., Swart, Q.D., Coetzee, L.L., Eriksson, K.A., 2001. Chemostratigraphy of the Paleoproterozoic Duitschland Formation, South Africa: Implications for coupled climate change and carbon cycling. Am. J. Sci. 301, 261-285.

Bekker, A., Master, S., Karhu, J.A., Verhagen, B.T., 2001a. Chemostratigraphy of the Paleoproterozoic Magondi Supergroup, Zimbabwe, 11th Ann. V. M. Goldschmidt Conference, Abst. 3772. LPI Contr.1088, Lunar and Planetary Institute, Houston (CD-ROM).

Bekker, A., Karhu, J.A., Kaufman, A.J., 2001b. Tectonic implications of a chemostratigraphic study of Early Paleoproterozoic carbonates from the southeastern margin of the Wyoming Craton, Meeting of the Rocky Mountain section of GSA. GSA, pp. A-44.

Beukes, N.J., Gutzmer, J., Dorland, H., 1999. Paleoproterozoic laterites, supergene iron and manganese ores and atmospheric oxygen, Geol. Soc. Aust. Abstr., pp. 20-23.

Boiko, V.L., Dobrokhotov, M.N., Esipchuk, K.E., Semenenko, N.P., Shcherbak, N.P., 1989. Lower Precambrian stratigraphy of the Ukraine Shield. In: Sokolov, B.S. (Ed.), Stratigraphy of the USSR. Lower Precambrian. Nedra, Moscow, pp. 194-257.

Borshchevsky, Y.A., Borisova, S.L., Yudin, N.I., Medvedovskaya, N.I., Stepanova, T.I., Krasotov, Y.M., Popova, N.K., Voronina, Y.V., Belkov, E.I., 1982. Isotope characteristics of apatite-calcite associations of Slyudyanka Series, peri-Baykal, Abstracts 9th All-Union symposium on stable isotopes in geochemistry, Moscow, pp. 421-423.

Bros, R., Stille, P., Gauthier-Lafaye, F., Weber, F., Clauer, N., 1992. Sm-Nd isotopic dating of Proterozoic clay material: An example from the Francevillian sedimentary series, Gabon. Earth Plan. Sci. Lett. 113, 207-218.

Bühn, B., Stanistreet, I.G., 1997. Insight into enigma of Neoproterozoic manganese and iron formations from the perspective of supercontinent breakup and assembly. In: Nicholson, K., Hein, J.R., Bühn, B., Dasgupta, S. (Eds.), Manganese mineralization: Geochemistry and Mineralogy of Terrestrial and marine deposits. Geol. Soc. Spec. Publ. 119, London, pp. 81-90.

Buick, I.S., Uken, R., Gibson, R.L., Wallmach, T., 1998. High-$\delta^{13}C$ Paleoproterozoic carbonates from the Transvaal Supergroup, South Africa. Geology 26, 875-878.

Burdett, J.W., Grotzinger, J.P., Arthur, M.A., 1990. Did major changes in the stable-isotope composition of Proterozoic seawater occur? Geology 18, 227-230.

Canfield, D.E., 1998. A new model for Proterozoic ocean chemistry. Nature 396, 450-453.

Canfield, D.E., Raiswell, R., 1991. Carbonate precipitation and dissolution: its relevance to fossil preservation. In: Allison, P.A., Briggs, D.E.G. (Eds.), Taphonomy: Releasing the Data Locked in the Fossil Record. Plenum Press, London, pp. 411-453.

Canfield, D.E., Raiswell, R., 1999. The evolution of the secular cycle. Am. J. Sci. 299, 697-723.

Carey, S.W., Ahmad, N., 1961. Glacial marine sedimentation. In: Raasch, G.O. (Ed.), Geology of the Arctic v. 2. Toronto University Press, Toronto, pp. 865-894.

Chamberlain, K.R., 1998. Medicine Bow orogeny: Timing of deformation and model of crustal structure produced during continent-arc collision, ca. 1.78 Ga, southern Wyoming. Rocky Mnt. Geol. 33, 259-277.

Cook, P., 1992. Phosphogenesis around the Proterozoic-Phanerozoic transition. J. Geol. Soc., London 149, 615-620.

Corfu, F., Andrews, A., 1986. A U-Pb age for mineralized Nipissing diabase, Gowganda, Ontario. Can. J. Earth Sci. 23, 107-112.

Cox, D.M., Frost, C.D., Chamberlain, K.R., 2000. 2.01-Ga Kennedy dike swarm, southeastern Wyoming: Record of a rifted margin along the southern Wyoming province. Rocky Mount. Geol. 35(1), 7-30.

Davis, D.W., Hirdes, W., Schaltegger, U., Nunoo, E.A., 1994. U-Pb age constraints on deposition and provenance of Birimian and gold-bearing Tarkwaian sediments in Ghana, West Africa. Precambrian Res. 67, 89-107.

Des Marais, D.J., 1994. Tectonic control of the crustal organic carbon reservoir during the Precambrian. Chem. Geol. 114, 303-314.

Donnelly, T.H., Shergold, J.H., Southgate, P.N., Barnes, C.J., 1990. Events leading to global phosphogenesis around the Proterozoic/Cambrian boundary. In: Notholt, A.J.G., Jarvis, I. (Eds.), Phosphorite Research and Development. Geol. Soc. Spec. Publ. 52, pp. 273-287.

Doyen, L., 1973. The Manganese Ore Deposit of Kisenge-Kamata (Western Katanga). Mineralogical and Sedimentological Aspects of the Primary Ore. In: Amstutz, G.C., Bernard, A.J. (Eds.), VIII. Internat. Sedimentological Congress. Ores in Sediments. Springer-Verlag, Heidelberg, pp. 93-100.

Doyen, L., 1974. The manganese ore deposit of Kisenge-Kamata-Kapolo (Western Katanga-Shaba-Zaire). Geochemical composition of the primary carbonate ore., 4th IAGOD Symposium: Problems of ore deposition, Varna, Bulgaria, v.3, pp. 122-128.

Dzigbodi-Adjimah, K., Sogbor, S.F., 1993. The minerology and genetic significance of the manganese carbonate ore at Nsuta, Ghana. In: Tsidzi, K.E.N. (Ed.), Proceedings of the National Seminar on Current Developments in the Minerals Industry of Ghana. University of Science and Technology, Kumasi, Ghana and Institute of Mining and Mineral Engineering (IMME), Kumasi, Ghana, pp. 25-32.

El Tabakh, M., Grey, K., Pirajno, F., Schreiber, B.C., 1999. Pseudomorphs after evaporitic minerals interbedded with 2.2 Ga strmatolites of the Yerriba basin, Western Australia: Origin and significance. Geology 27, 871-874.

Fairchild, I.J., 1983. Effects of glacial transport and neomorphism on Precambrian dolomites crystal sizes. Nature 304, 714-716.

Fairchild, I.J., 1993. Balmy shores and icy wastes: the paradox of carbonates associated with glacial deposits in Neoproterozoic times. Sed. Rev. 1, 1-16.

Feybesse, J.L., Johan, V., Triboulet, C., Guerrot, C., Mayaga-Mikolo, F., Bouchot, V., Eco N'dong, J., 1998. The West Central African belt: a model of 2.5-2.0 Ga accretion and two-phase orogenic evolution. Precambrian Res. 87, 161-216.

Frank, T.D., Lyons, T.W., 2000. The intergrity of $\delta^{18}O$ records in Precambrian carbonates; A Mesoproterozoic case study. In: Grotzinger, J.P., James, N.P. (Eds.), Carbonate sedimentation and diagenesis in the evolving Precambrian world. SEPM Spec. Publ. 67, pp. 315-326.

Gauthier-Lafaye, F., Weber, F., 1989. The Francevillian (Lower Proterozoic) uranium ore deposits of Gabon. Econ. Geol. 84, 2267-2285.

Gehör, S., 1994. REE distribution in the phosphorite bands within the Paleoproterozoic Tuomivaara and Pahtavaara iron-formations, central and nothern Finland. In: Nironen, M., Kähkönen, Y. (Eds.), Geochemistry of Proterozoic supracrustal rocks in Finland. Geol. Survey Finland Spec. Pap. 19, Espoo, pp. 71-84.

Glasby, G.P., 1997. Fractionation of manganese from iron in Archaean and Proterozoic sedimentary ores. In: Hein, J.R., Bühn, B., Dasgupta, S. (Eds.), Manganese Mineralization: Geochemistry and Mineralogy of Terrestrial and Marine Deposits. Geol. Soc. Spec. Pub., pp. 29-42.

Golubev, A.I., Akhmedov, A.M., Galdobina, L.P., 1984. Geochemistry of the Lower Proterozoic black shale complexes from the Karelia-Kola region. Nauka, Leningrad, 192 pp.

Gorokhov, I.M., Kuznetsov, A.B., Melezhik, V.A., Konstantinova, G.V., Melnikov, N.N., 1998. Sr Isotopic Composition in the Upper Jatulian (Early Proterozoic) Dolomites of the Tulomozero Formation, Southeastern Karelia. Doklady Akademii Nauk 360(4), 533-536.

Gorokhov, I.M., Semikhatov, M.A., Baskakov, A.V., Kutyavin, E.P., Melnikov, N.N., Sochava, A.V., Turchenko, T.L., 1995. Sr isotopic composition in Riphean, Vendian, and Lower Cambrian carbonates from Siberia. Str. Geol. Cor. 3, 1-28.

Grotzinger, J.P., Knoll, A.H., 1995. Anomalous Carbonate Precipitates: Is the Precambrian the Key to the Permian? Palaios 10, 578-596.

Guliy, V.N., 1995. Main features of composition and origin of apatite deposits in metamorphic rocks of the Aldan Shield, Siberia, Russian Federation. Trans. Instn. Min. Metall. (Sect. B: Appl. earth sci.) 104, B171-B178.

Guliy, V.N., 1995. Metasedimentary apatite deposits of the Birikeen area, Aldan Shield. Lithology and Mineral Resources 30(6), 545-555.

Gutzmer, J., Beukes, N.J., 1996. Karst-hosted fresh-water Paleoproterozoic manganese deposits, Postmasburg, South Africa. Econ. Geol. 91, 1435-1454.

Hallock, P., Schlager, W., 1986. Nutrient excess and the demise of coral reefs and carbonate platforms. Palaios 1, 389-398.

Hanski, E., Huhma, H., Rastas, P., Kamenetsky, V.S., 2001. The Paleoproterozoic komatiite-picrite association of Finnish Lapland. J. Petr. 42(5), 855-876.

Hayes, J.M., 1983. Geochemical evidence bearing on the origin of aerobiosis, a speculative interpretation. In: Schopf, J.W. (Ed.), The Earth's Earliest Biosphere: Its Origin and Evolution. Princeton University Press, Princeton, NJ, pp. 93-134.

Hayes, J.M., 1994. Global methanotrophy at the Archean-Proerozoic transition. In: Bengston, S. (Ed.), Proc. Nobel Symp. 84, Early Life on Earth. Columbia University Press, New York, pp. 220-236.

Hein, J.R., Bolton, B.R., 1993. Composition and origin of the Moanda manganese deposit, Gabon, 16th Intern. Coll. on African Geol. Extended Abstracts. Geological Survey and Mines Department of Swaziland, Ezulwini, Swaziland, pp. 150-152.

Hein, J.R., Bolton, B.R., Nziengui, P., McKirdy, D., Frakes, L., 1989. Chemical, isotopic and lithologic associations within the Moanda manganese deposit, Gabon, 28th Intern. Geol. Congr. Abstracts, Washington, D.C., pp. 2-46.

Hein, J.R., Fan, D., Ye, J., Liu, T., Yeh, H.-W., 1999. Composition and origin of Early Cambrian Tiantaishan phosphorite-Mn carbonate ores, Shaanxi Province, China. Ore Geol. Rev. 15, 95-134.

Hirdes, W., Davis, D.W., 1998. First U-Pb zircon age of extrusive volcanism in the Birimian Supergroup of Ghana/West Africa. J. Afr. Earth Sci. 27(2), 291-294.

Hoffman, P.F., Kaufman, A.J., Halverson, G.P., Schrag, D.P., 1998. A Neoproterozoic Snowball Earth. Science 281, 1342-1346.

Hoffman, P.F., Schrag, D.P., 2000. Snowball Earth. Scientific American 282(1), 68-75.

Holland, H.D., 1994. Early Proterozoic atmospheric change. In: Bengston, S. (Ed.). Early Life on Earth, Nobel Symp. 84. Columbia University Press, New York, pp. 237-244.

Houston, R.S., Karlstrom, K.E., Graff, P.J., Flurkey, A.J., 1992. New stratigraphic subdivisions and redefinition of subdivisions of Late Archean and Paleoproterozoic metasedimentary and metavolcanic rocks of the Sierra Madre and Medicine Bow Mountains, southern Wyoming. U. S. Geological Survey Prof. Pap. 1520, 50 pp.

Houston, R.S., Lanthier, L.R., Karlstrom, K.E., Sylvester, G., 1981. Paleoproterozoic diamictite of southern Wyoming. In: Hambrey, M.J., Harland, W.B. (Eds.), Earth's Pre-Pleistocene Glacial Record. Cambridge Univercity Press, New York, pp. 795-799.

Ingall, E.D., Jahnke, R., 1994. Evidence for enhanced phosphorus regeneration from marine sediments overlain by oxygen depleted waters. Geochim. Cosmochim. Acta 58(11), 2571-2575.

Isley, A.E., 1995. Hydrothermal plumes and the delivery of iron to banded iron formation. J. Geol. 103, 169-185.

Isley, A.E., Abbott, D.H., 1999. Plume-related mafic volcanism and the deposition of banded iron formation. J. Geophys. Res. 104(B7), 15,461-15,477.

Kah, L.C., 2000. Depositional $\delta^{18}O$ signatures in Proterozoic dolostones: constraints on seawater chemistry and early diagenesis. In: Grotzinger, J.P., James, N.P. (Eds.), Carbonate sedimentation and diagenesis in the evolving Precambrian world. SEPM Spec. Publ. 67, pp. 345-360.

Kanygin, L.I., Kirikilitsa, S.I., Krivonos, V.P., Levenshteyn, M.L., Polunovsky, R.M., Porokhnenko, A.F., Kharagezov, M.K., 1969. On finding perspectives of metamorphogenic deposits of manganese and phosphate in Precambrian carbonate units of peri-Azov. Geol. Jour. 29(4), 146-147.

Karhu, J.A., 1993. Paleoproterozoic evolution of the carbon isotope ratios of sedimentary carbonates in the Fennoscandian Shield. Geol. Surv. Finland Bull. 371, Espoo, 87 pp.

Karhu, J.A., Holland, H.D., 1996. Carbon isotopes and the rise of atmospheric oxygen. Geology 24(10), 867-870.

Karlstrom, K.E., 1977. Geology of the Proterozoic Deep Lake Group, central Medicine Bow Mountains, Wyoming. M.S. Thesis, University of Wyoming, Laramie, 116 pp.

Karlstrom, K.E., Flurkey, A.J., Houston, R.S., 1983. Stratigraphy and depositional setting of the Proterozoic Snowy Pass Supergroup, southeastern Wyoming: Record of a Paleoproterozoic Atlantic-type cratonic margin. Geol. Soc. Am. Bull. 94, 1257-1274.

Karlstrom, K.E., Houston, R.S., 1979. Stratigraphy of the Phantom Lake Metamorphic Suite and Deep Lake Group and a review of the Precambrian tectonic history of the Medicine Bow Mountains. Contr. to Geol. 17(2), 111-133.

Karlstrom, K.E., Houston, R.S., 1984. The Cheyenne belt: Analysis of a Proterozoic suture in southern Wyoming. Precambrian Res. 25, 415-446.

Karlstrom, K.E., Houston, R.S., Flurkey, A.J., Coolidge, C.M., Kratochvil, A.L., Sever, C.K., 1981. A summary of the geology and uranium potential of Precambrian conglomerates in southeastern Wyoming. U.S. Dept. Energy GJBX-139- 81, Grand Junction, Colorado, 537 pp.

Kaufman, A.J., 1997. An ice age in the tropics. Nature 386, 227-228.

Kaufman, A.J., Hayes, J.M., Knoll, A.H., Germs, G.J.B., 1991. Isotope compositions of carbonates and organic carbon from upper Proterozoic successions in Namibia: Stratigraphic variation and the effects of diagenesis and metamorphism. Precambrian Res. 49, 301-327.

Kaufman, A.J., Knoll, A.H., 1995. Neoproterozoic variations in the C-isotopic composition of seawater: stratigraphic and biogeochemical implications. Precambrian Res. 73, 27-49.

Kaufman, A.J., Knoll, A.H., Narbonne, G.M., 1997. Isotopes, ice ages, and terminal Proterozoic Earth history. Nat. Ac. Sci. Proc. 94, 6600-6605.

Kennedy, M.J., 1996. Stratigraphy, sedimentology, and isotopic geochemistry of Australian Neoproterozoic postglacial cap dolostones: deglaciation $\delta^{13}C$ excursions, and carbonate precipitation. J. Sed. Res. 66(6), 1050-1064.

Kennedy, M.J., Christie-Blick, N., Sohl, L., 2001. Are Proterozoic cap carbonates and isotopic excursions a record of gas hydrate destabilization following Earth's coldest intervals? Geology 29(5), 443-446.

Klein, C., Beukes, N.J., 1993. Sedimentology and geochemistry of the glaciogenic Late Proterozoic Rapitan iron formation in Canada. Econ. Geol. 88, 542-565.

Knoll, A.H., Bambach, R.E., Canfield, D.E., Grotzinger, J.P., 1996. Comparative Earth history and Late Permian mass extinction. Science 273, 452-457.

Knoll, A.H., Hayes, J.M., Kaufman, A.J., Swett, K., Lambert, I.B., 1986. Secular variations in carbon isotope ratios from Upper Proterozoic successions of Svalbard and East Greenland. Nature 321, 832-838.

Kotov, A.B., Salnikova, E.B., Reznitskii, L.Z., Natman, A., Kovach, V.P., Zagornaya, N.Y., Belyaevskii, N.A., 2000. Age and sources of deeply-metamorphosed supracrustal deposits of the Slyudyanka crystalline complex (Southern peri-Baykal). In: Negrutza, T.F., Negrutza, V.Z. (Eds.), General issues of Precambrian subdivision. Materials of 3d All-Union conference. Geological Institute of the Kola Science Centre, Apatity, pp. 124-125.

Krapez, B., Martin, D.M., 1999. Sequence stratigraphy of the Paleoproterozoic Nabberu Province of Western Australia. Aust. J. Earth Sci. 46, 89-103.

Kulish, E.A., 1970. Behaviour of oxygen in the Archean Aldanian atmosphere. Doklady Akademii Nauk SSSR 191(4), 921-923.

Laajoki, K., Saikkonen, R., 1977. On the geology and geochemistry of the Precambrian iron formations in Väyrylänkylä, South Puolanka area, Finland. Geol. Survey Finland, Bull. 292, 1-137.

Lazur, Y.M., Kazantsev, V.A., Ermilov, V.V., 1981. Manganiferous sulfide mineralization in Proterozoic carbonaceous deposits of KMA district. Doklady Akademii Nauk SSSR 256(3), 677-680, in Russian.

Leclerc, J., Weber, F., 1980. Geology and genesis of the Moanda manganese deposits, Republic of Gabon. In: Varentsov, I.M., Grasselly, G. (Eds.), Geology and geochemistry of manganese, Stuttgart, pp. 89-109.

Lobzova, R.V., Esikov, A.D., 1981. On carbon sources for the origin of graphite deposits in light of isotopic data, Materials of the All-Union conference on carbon geochemistry. Nauka, Moscow, pp. 63-64.

Maheshwari, A., Sial, A.N., Chittora, V.K., 1999. high-$\delta^{13}C$ Paleoproterozoic carbonates from the Aravalli Supergroup, Western India. Int. Geol. Rev. 41, 949-954.

Marmo, J.S., 1992. The lower Proterozoic Hokkalampi paleosol in North Karelia, eastern Finland. In: Schidlowski, M., Golubic, S., Kimberly, M.M., Trudinger, P.A. (Eds.), Early Organic Evolution: Implications for Mineral and Energy Resources. Springer, Berlin, Heidelberg, pp. 41-66.

Master, S., Verhagen, B.T., Bassot, J.P., Beukes, N.J., Lemoine, S., 1993. Stable isotopic signatures of Paleoproterozoic carbonate rocks from Guinea, Sinegal, South Africa and Zimbabwe: constrains on the timing of the ca .2 Ga "Lomagundi" $\delta^{13}C$ excursion, Symposium: Early Proterozoic geochemical and structural constraints – metallogeny: Publication Occasionnelle 1993/23, p. 38-41, Dacar, Sénégal.

Master, S., Verhagen, B.T., Duane, M.J., 1990. Isotopic signatures of continental and marine carbonates from the Magondi Belt, Zimbabwe: Implications for the global carbon cycle at 2,0 Ga, 23rd Earth Sci. Cong. Geol. Soc. S.Af. Abstr., Cape Town, pp. 346-348.

Melezhik, V.A., Fallick, A.E., 1996. A widespread positive $\delta^{13}C_{carb}$ anomaly at around 2.33-2.06 Ga on the Fennoscandian Shield: a paradox? Terra Nova 8, 141-157.

Melezhik, V.A., Fallick, A.E., Clark, T., 1997a. Two billion year old isotopically heavy carbon: evidence from the Labrador Trough, Canada. Can. J. Earth Sci. 34(3), 271-285.

Melezhik, V.A., Fallick, A.E., Filippov, M.M., Larsen, O., 1999. Karelian shungite - an indication of 2.0-Ga-old metamorphosed oil-shale and generation of petroleum: geology, lithology and geochemistry. Earth-Sci. Rev. 47, 1-40.

Melezhik, V.A., Fallick, A.E., Makarikhin, V.V., Lyubtsov, V.V., 1997. Links between Paleoproterozoic palaeogeography and rise and decline of stromatolites: Fennoscandian Shield. Precambrian Res. 82, 311-348.

Melezhik, V.A., Predovsky, A.A., 1982. Geochemistry of the Early Proterozoic lithogenesis (using the north-east of the Baltic Shield as an example). Nauka, Leningrad, 208 pp.

Mirota, M.D., Veizer, J., 1994. Geochemistry of Precambrian Carbonates: IV. Aphebian Albanel Formations, Quebec, Canada. Geochim. Cosmochim. Acta 58, 1735-1745.

Montañez, I.P., Banner, J.L., Osleger, D.A., Borg, L.E., Bosserman, P.J., 1996. Integral Sr isotope variations and sea-level history of Middle to Upper Cambrian platform carbonates: Implications for the evolution of Cambrian seawater $^{87}Sr/^{86}Sr$. Geology 24(10), 917-920.

Mücke, A., Dzigbodi-Adjimah, K., Annor, A., 1999. Minerology, petrology, geochemistry and genesis of the Paleoproterozoic Birimian manganese-formation of Nsuta/Ghana. Min. Dep. 34, 297-311.

Myrow, P.M., Kaufman, A.J., 1999. A newly discovered cap carbonate above Varanger-age glacial deposits in Newfoundland, Canada. J. Sed. Res. 69(3), 784-793.

Nesbitt, H.W., Young, G.M., 1982. Early Proterozoic climates and plate motions inferred from major element chemistry of lutites. Nature 299, 715-717.

Nikitina, A.P., Shchipanskiy, A.A., 1987. Phosphorus resources in the early Proterozoic deposits of Belgorod district, KMA. Izvestiya Akademii Nauk SSSR, Seriya Geologicheskaya (2), 113-124.

Ojakangas, R.W., 1997. Correlative sequence within the Marquette Range Supergroup (Michigan) and the Huronian Supergroup (Ontario); Glaciogenics, paleosols, and orthoquartzites (Abs), 43rd Inst. Lake Superior Geol., pp. 47-48.

Paakola, J., 1971. The volcanic complex and associated manganiferous iron formation of the Porkonen-Pahtavaara area in Finnish Lapland. Bull. Com. Geol. Finl. N. 247, 82 pp.

Pavlov, V.A., Cherdakov, V.I., Komarov, P.V., 1987. Mineralogic-geochemical pecularities of rocks and ores in iron-bearing deposits of the southern Aldan. Geology of ore deposits 5, 75-83.

Ponomarenko, A.I., 1973. Rhodonite-spessartine rocks of the Anabar massif. Doklady Akademii Nauk SSSR 212(6), 1426-1429.

Premo, W.R., Van Schmus, W.R., 1989. Zircon geocronology of Precambrian rocks in southeastern Wyoming and nothern Colorado. In: Grambling, J.A., Tewksbury, B.J. (Eds.), Proterozoic Geology of the Southern Rocky Mountains. Geol. Soc. Am. Spec. Pap. 235, pp. 1-12.

Prilutzky, R.E., Suslova, S.N., Nalivkina, Y.B., 1992. Reconstruction of environmental conditions of early Proterozoic carbonate deposits of the Ukrainian and Baltic Shields based on isotopic studies. Lithology and Mineral Deposits 5, 76-88.

Puchtel, I.S., Arndt, N.T., Hofmann, A.W., Haase, K.M., Kröner, A., Kulikov, V.S., Kilikova, V.V., Garbe-Schönberg, C.-D., Nemchin, A.A., 1998. Petrology of mafic lavas within the Onega plateau , central Karelia: evidence for 2.0 Ga plume-related continental crustal growth in the Baltic Schield. Contr. Mineral. Petrol. 130, 134-153.

Redden, J.A., Peterman, Z.E., Zartman, R.E., DeWitt, E., 1990. U-Th-Pb geochronology and preliminary interpretation of Precambrian tectonic events in the Black Hills, South Dakota. In: Lewry, J.F., Stauffer, M.R. (Eds.), The Early Proterozoic Trans-Hudson Orogen of North America. Geol. Ass. Canada, Spec. Pap. 37, pp. 229-251.

Reznitsky, L.Z., Fefelov, N.N., Vasil'ev, E.P., Zarudneva, N.V., Nekrasova, E.A., 1998. Isotopic composition of lead from metaphosphorites and problem of the Slyudyanka Group age, the Southern Baykal-Western Khamar Daban Region. Lithology and Mineral Resources 33(5), 432-441.

Reznitsky, L.Z., Vasil'ev, E.P., Vishnyakov, V.N., 1976. First finding of gondites in the Precambrian of the southern peri-Baikal. Doklady Akademii Nauk SSSR 229(5), 1195-1197.

Rohon, M.-L., Vialette, Y., Clark, T., Roger, G., Ohnenstetter, D., Vidal, P., 1993. Aphebian mafic-ultramafic magmatism in the Labrador Trough (New Quebec): its age and the nature of its mafic source. Can. J. Earth Sci. 30, 1582-1593.

Roscoe, S.M., Card, K.D., 1993. The reappearance of the Huronian in Wyoming: rifting and drifting of ancient continents. Can. J. Earth Sci. 30, 2475-2480.

Roy, S., 1980. Manganese ore deposits of India. In: Varentsov, I.M., Grasselly, G. (Eds.), Geology and geochemistry of manganese, Stuttgart, pp. 237-264.

Rozen, O.M., Condie, K.C., Natapov, L.M., Nozhkin, A.D., 1994. Archean and Early Proterozoic evolution of the Siberian Craton: A preliminary assessment. In: Condie, K.C. (Ed.), Archean crustal evolution. Elsevier, Amsterdam, pp. 411-459.

Rozen, O.M., Zlobin, V.L., Syngaevskiy, E.D., 1990. Metamorphic carbonate rocks of granulite complex of the Anabar Shield: pecularities of primary composition and sedimentation. Lithology and Mineral Deposits (6), 72-81.

Rundqvist, D.V., Mitrofanov, F.P., 1993. Precambrian geology of the USSR. Developments in Precambrian Geology, 9. Elsevier, Amsterdam, 528 pp.

Russell, J.R., 1992. Investigation of the potential of Pb/Pb radiometric dating for the direct age determination of carbonates. D. Phil. (unpublished) Thesis, University of Oxford, Oxford, England.

Salop, L.I., 1982. Geologic development of the Earth in Precambrian. Nedra, Leningrad, 343 pp.

Schidlowski, M., Eichmann, R., Junge, C.E., 1975. Precambrian Sedimentary Carbonates: Carbon and oxygen isotope geochemistry and implications for the terrestrial oxygen budget. Precambrian Res. 2, 1-69.

Schidlowski, M., Eichmann, R., Junge, C.E., 1976. Carbon isotope geochemistry of the Precambrian Lomagundi carbonate province, Rhodesia. Geochim.Cosmochim.Acta 40, 449-455.

Schidlowski, M., Todt, W., 1998. The Proterozoic Lomagundi carbonate province as paragon of a ^{13}C-enriched carbonate facies: geology, radiometric age and geochemical significance, Chinese Sci. Bull., Abst. ICOG-9, Beijing, v.43, p. 114.

Schipansky, A.A., Bogdanova, S.V., 1996. The Sarmatian crustal segment: Precambrian correlation between the Voronezh Massif and the Ukrainian Shield across the Dniepr-Donets Aulacogen. Tectonophysics 268, 109-125.

Schreiber, U.M., Eriksson, P.G., 1992. An early Paleoproterozoic braid-delta system in the Pretoria Group, Transvaal Sequense, South Africa. J. Afr. Earth Sci. 15, 111-125.

Semikhatov, M.A., Raaben, M.E., 1994. Dynamics of the gloabl diversity of Proterozoic stromatolites. Article I: Northern Eurasia, China, and India. Stratigraphy and Geological Correlation 2, 492-513.

Semikhatov, M.A., Raaben, M.E., 1996. Dynamics of the global diversity of Proterozoic stromatolites. Article 2: Africa, Australia, North America, and general synthesis. Stratigraphy and Geological Correlation 4(1), 24-50.

Semikhatov, M.A., Raaben, M.E., Sergeev, V.N., Veis, A.F., Artemova, O.V., 1999. Biotic Events and Positive δC_{carb} Anomaly at 2.3-2.06 Ga. Stratigraphy and Geological Correlation 7(5), 413-436.

Shnyukov, E.F., Orlovsky, G.N., 1980. Manganese ores of the Ukrainian SSR. In: Varentsov, I.M., Grasselly, G. (Eds.), Geology and geochemistry of manganese, Stuttgart, pp. 393-402.

Sidorenko, A.V., Borshchevsky, Y.A., 1977. General tendencies in evolution of carbonate isotopic composition in the Precambrian and Phanerozoic. Doklady Akademii Nauk SSSR 234(4), 892-895.

Sidorenko, A.V., Borshchevsky, Y.A., Sidorenko, S.A., Ustinov, V.A., Popova, N.K., 1972. Isotopic composition of carbon from Precambrian metamorphic rocks. Doklady Akademii Nauk SSSR 206(2), 463-466.

Simonson, B.M., Hassler, S.W., 1996. Was the deposition of large Precambrian Iron Formations linked to major marine transgressions? J. Geol. 104, 665-676.

Sims, P.K., 1995. Archean and Early Proterozoic tectonic framework of north-central United States and adjacent Canada. US Geol. Surv. Bull, 1904-T, 12 pp.

Snyder, G.L., Siems, D.F., Grossman, J.N., Ludwig, K.R., Nealey, L.D., 1995. Geology, petrochemistry, and geochronology of the Precambrian rocks of the Fletcher Park-Johnson Mountain area, Albany and Platte counties, Wyoming *with a section on* the Fletcher Park shear zone by Frost, B.R., Chamberlain, K.R., and Snyder, G.L. US Geol. Surv. Misc. Inv. Ser. Map I-2233, scale 1:24,000, 3 sheets.

Sozinov, N.A., Chistyakova, N.N., Kazantsev, V.A., 1988. Metallogenic black shales of the Kursk Magnetic Anomaly. Nauka, Moscow, 149 pp.

Sozinov, N.A., Kazantsev, V.A., 1978. Phosphorite content of Proterozoic deposits in the Kursk Magnetic Anomaly (KMA) region. Lithology and Mineral Resources, 125-128.

Sreenivas, B., Das Sharma, S., Kumar, B., Patil, D.J., Roy, A.B., Srinivasan, R., 2001. Positive $\delta^{13}C$ excursion in carbonate and organic fractions from the Paleoproterozoic Aravalli Supergroup, Northwestern India. Precambrian Res. 106, 277-290.

Swart, Q.D., 1999. Carbonate rocks of the Paleoproterozoic Pretoria and Postmasburg Groups, Transvaal Supergroup. M.S. Thesis, Rand Africaans University, Johannesburg, South Africa, 126 pp.

Sylvester, G.H., 1973. Depositional environments of diamictites in the Headquarters Formation, Medicine Bow Mountains, southeastern Wyoming. M.S. Thesis, University of Wyoming, Laramie, 84 pp.

Van Cappellen, P., Ingall, E.D., 1994. Benthic phosphorus regeneration, net primary production, and ocean anoxia: A model of the coupled marine biogeochemical cycles of carbon and phosphorus. Paleoceanography 9(5), 677-692.

Varentsov, I.M., Rakhmanov, V.P., 1980. Manganese deposits of the USSR (A review). In: Varentsov, I.M., Grasselly, G. (Eds.), Geology and geochemistry of manganese, Stuttgart, pp. 319-391.

Veizer, J., Clayton, R.N., Hinton, R.W., 1992a. Geochemistry of Precambrian Carbonates: IV. Early Paleoproterozoic (2.25 ± 0.25 Ga) seawater. Geochim. Cosmochim. Acta 56, 875-885.

Veizer, J., Clayton, R.N., Hinton, R.W., Von Burn, V., Mason, T.R., Buck, S.G., Hoefs, J., 1990. Geochemistry of Precambrian carbonates: 3-shelf seas and non-marine environments of the Archean. Geochim. Cosmochim. Acta 54, 2717-2729.

Veizer, J., Compston, W., 1976. $^{87}Sr/^{86}Sr$ in Precambrian carbonates as an index of crustal evolution. Geochim. Cosmochim. Acta 40, 905-914.

Veizer, J., Plumb, K.A., Clayton, R.N., Hinton, R.W., Grotzinger, J.P., 1992a. Geochemistry of Precambrian Carbonates: V. Late Paleoproterozoic Seawater. Geochim. Cosmochim. Acta 56, 2487-2501.

Walraven, F., 1997. Geochronology of the Rooiberg Group, Transvaal Supergroup, South Africa. Econ. Geol. Res. Unit, University of the Witwatersrand, Inf. Circ. 316, Johannesburg, South Africa, 21 pp.

Weber, F., 1972. The origin and post-sedimentary evolution of Precambrian manganese deposits of Moanda in the Republic of Gabon, Geology and genesis of Precambrian iron and manganese formations of the world. Naukova Dumka, Kiev, pp. 320-332.

Weber, F., Schidlowski, M., Arneth, J.D., Gauthier-Lafaye, F., 1983. Carbon isotope geochemistry of the lower Proterozoic Francevillian series of Gabon (Africa). (Abst.). Terra Cognita 3, 220.

Woodhead, J.D., Hergt, J.M., 1997. Application of the 'double spike' technique to Pb-isotope geochronology. Chem. Geol. 138, 311-321.

Yeh, H.-W., Hein, J.R., Bolton, B.R., 1995a. Origin of the Nsuta manganese carbonate proto-ore, Ghana: Carbon- and oxygen-isotope evidence. J. Geol. Soc. China 38(4), 397-409.

Yeh, H.-W., Hein, J.R., Gutzmer, J., Beukes, N.J., Tan, L.-P., 1995b. Carbon isotopes and origin of rhodochrosite. J. Geol. Soc. China 38(4), 411-422.

Young, G.M., 1973. Tillites and aluminous quartzites as possible time markers for middle Precambrian (Aphebian) rocks of North America. In: Young, G.M. (Ed.), Huronian Stratigraphy and Sedimentation. Geol. Assn. Can. Spec. Pap.12, pp. 97-127.

Young, G.M., 1983. Tectono-sedimentary history of Early Proterozoic rocks of the northern Great Lakes region. In: Medaris, L.G., Jr. (Ed.), Early Proterozoic Geology of the Great Lake Region. Geol. Soc. Am. Mem. 160, pp. 15-32.

Young, G.M., 1991. The geologic record of glaciation: relevance to the climatic history of Earth. Geoscience Canada 18(3), 100 - 108.

Yudin, N.I., Arsenev, A.A., 1970. Phosphate content in old units in the southern part of Eastern Siberia. Nauka, Moscow, 123 pp.

Yur'ev, L.D., 1968. Phosphate perspectives of old deposits of the Ukrainian Shield. Razvedka i okhrana nedr 11, 7-9.

Yur'ev, L.D., 1969. Apatite ore deposit of the northern Krivoy Rog. Soviet Geol., 138-143.

Zagnitko, V.N., Lugovaya, I.P., 1985. Application of oxygen and carbon isotopes to some geologic problems in the Precambrian of the Ukranian Shield. Geochemistry and ore formation 13, 45-52.

Zagnitko, V.N., Lugovaya, I.P., 1986. Isotopic composition of graphite in rocks of the Ukrainian Shield. Minerologic Journal 8(1), 44-56.

Zagnitko, V.N., Lugovaya, I.P., 1989. Isotope geochemistry of carbonate and banded iron formation rocks from Ukraine Shield. Nauk. dumka, Kiev, 316 pp.

Zhmur, S.I., Stepanova, N.A., 1987. Conditions of carbonaceous rock accumulation in the Oskol'sk Series of the Lower Proterozoic in the Kursk Magnetic Anomaly (KMA) and their analogues in the Phanerozoic. Lithology and Mineral Resources 22(6), 606-615.

GHAPTER 4

CHEMOSTRATIGRAPHY OF EARLY PALEOPROTEROZOIC CARBONATE UNITS OF THE HARTVILLE UPLIFT AND SIERRA MADRE, WY AND BLACK HILLS, SD: IMPLICATIONS FOR CORRELATION AND TECTONIC SETTING

ABSTRACT. The Archean Wyoming Craton is flanked on the south and east by isolated outcrop belts of early Paleoproterozoic supracrustal successions whose correlation is complicated by lack of geochronologic constraints and continuous outcrop. However, carbonate units in these successions have the potential for correlation based on carbon isotope stratigraphy. Carbonate rocks from the lower and middle Nash Fork Formation of the Snowy Pass Supergroup in the Medicine Bow Mountains are characterized by highly positive carbon isotope values; remarkably $\delta^{13}C$ values as high as +28‰ are recognized at the base of the unit. In contrast, the upper Nash Fork Formation preserves carbon isotope values around 0‰ (V-PDB). Correlative carbonates from the Slaughterhouse Formation in the Sierra Madre, WY and from the Whalen Group in the Rawhide Creek area in the Hartville Uplift, WY have highly positive carbon isotope values. In contrast, carbonates from other exposures of the Whalen Group in the Hartville Uplift and all carbonate units in the Black Hills, SD have carbon isotope values close to 0‰ (V-PDB).

Combined with existing geochronologic and stratigraphic constraints, these data suggest that the Slaughterhouse Formation and the succession exposed in the Rawhide Creek area of the Hartville Uplift are correlative with the lower and middle parts of the Nash Fork Formation and were deposited during the ca. 2.2-2.1 Ga carbon isotope excursion. The Estes and Roberts Draw formations in the Black Hills and carbonates from other exposures in the Hartville Uplift post-date the positive carbon isotope excursion and are most likely correlative with the upper Nash Fork Formation. The passive margin, on which the carbonates with highly positive carbon isotope values were deposited, extended around the southern flank of the Wyoming Craton through the Sierra Madre, Medicine Bow Mountains and Hartville Uplift. The presence of carbonates with carbon isotope values close to 0‰ (V-PDB) in the upper Nash Fork Formation and the Whalen Group indicates that the passive margin persisted on the southern margin of the Wyoming craton beyond

the carbon isotope excursion. Rifting in the Black Hills, related to the final breakup of the Kenorland, likely succeeded the carbon isotope excursion, since the Estes and Roberts Draw formations, deposited during rifting and ocean opening on the eastern flank of the Wyoming Craton, post-date the carbon isotope excursion.

INTRODUCTION

Correlation of Precambrian sedimentary successions lacking biostratigraphic control is hindered by poor age constraints. It is possible to overcome this limitation by means of event stratigraphy based on marker beds that represent stratigraphic expressions of global events. This approach may be particularly useful for early Paleoproterozoic sedimentary successions since the 2.5-2.0 Ga exosphere was affected by a number of distinctive tectonic, climatic and biogeochemical perturbations that are recorded in the sedimentary transcript. These events, in ascending order, are: 1) a 2.48-2.45 Ga superplume event expressed in rock record by large igneous provinces with mafic volcanic and plutonic rocks, initiation of rifting and deposition of BIFs (Amelin et al., 1995; Heaman, 1997; Barley et al., 1997; Kump et al., 2000), 2) an extended glacial epoch (ca. 2.45-2.3 Ga; Young, 1991) accompanied by carbon isotope excursions (Bekker et al., 1999; 2001), 3) a period of enhanced weathering (Young, 1973; Marmo, 1992), 4) a major carbon isotope excursion between ca. 2.2–2.1 Ga not associated with a known glaciation (Karhu and Holland, 1996), 5) a great oxidation event (Karhu and Holland, 1996), and 6) final breakup of the Kenorland supercontinent at 2.1-2.0 Ga (Aspler and Chiarenzelli, 1998). Initial breakup of the Kenorland supercontinent was promoted by the superplume event. Associated sedimentary rift successions contain detrital uraninite and pyrite (Kirkham and Roscoe, 1993). Atmospheric pO_2 may have changed episodically during the glacial epoch in response to fluctuations in the oexogenic carbon cycle (Bekker et al., 2001). Termination of some glaciations was accompanied by a change from a stagnant glacial ocean to a well-mixed, post-glacial ocean resulting in the deposition of Mn- and Fe-rich sediments in open marine setting in South Africa and Botswana (Steyn et al., 1986; Beukes et al., 1999; Kirschvink et al., 2000). The glacial epoch was followed worldwide by deposition of mature, Al-rich quartzites suggesting a change to greenhouse conditions and enhanced chemical weathering (Young, 1973; Nesbitt and Young, 1982; Bekker et al., 2001). Overlying carbonate successions deposited during the ca. 2.2-2.1 Ga carbon isotope excursion contain pseudomorphs of sulfate minerals (Akhmedov, 1990; Bekker, 1998; El Tabakh et al., 2000; Bekker and Eriksson,

submitted) suggesting warm and arid climate. The end of the ca. 2.2-2.1 Ga carbon isotope excursion was accompanied by supercontinent breakup and voluminous mafic volcanism (Karhu, 1993). Contemporaneous ocean overturn led to deposition of large Mn- and Fe-rich deposits, phosphorites, and organic carbon-rich deposits worldwide (Bekker et al., submit.).

The Snowy Pass Supergroup in the Medicine Bow Mountains is the thickest and the most extensive early Paleoproterozoic succession of the Wyoming Craton (Fig. 4.1). Deposition of the supergroup on the southern flank of the Wyoming Craton followed the initial breakup of Kenorland at ca. 2.45 Ga. The supergroup contains, in ascending order, siliciclastic rift succession with detrital uraninite deposits near the base followed by three stratigraphically discrete diamictite horizons and passive margin succession containing mature Al-rich quartzites, thick carbonate succession, mafic volcanics and schist (Fig. 4.2; Houston et al., 1992). Bekker et al. (submitted) studied carbon isotope systematics of the carbonate unit (Vagner Formation) sandwiched between the middle and upper diamictites and the thick carbonate formation (Nash Fork Formation) in the upper part of the supergroup. Carbonates of the Vagner Formation, positioned above the second diamictite of glacial origin, have negative carbon isotope values and are interpreted as a cap carbonate. The Nash Fork Formation is subdivided into three parts by two carbonaceous shale members representing drowning events. Carbonates in the lower and middle Nash Fork Formation have highly positive carbon isotope values whereas those from the upper part of the formation have carbon isotope values close to 0‰ (Fig. 4.3). This trend in carbon isotope values along with stratigraphic position above three discrete glacial diamictites and Al-rich mature quartzite suggests deposition at the end of the Paleoproterozoic carbon isotope excursion constrained on the Fennoscandian Shield between 2.11 and 2.06 Ga (Karhu, 1993). Correlation with other early Paleoproterozoic supracrustal successions preserved along the southern flank of the Wyoming Craton is lacking with the exception of lithostratigraphic correlation with the Snowy Pass Group in the Sierra Madre (Houston et al., 1992). Other supracrustal successions on the flanks of the Wyoming Craton are poorly exposed and those that are exposed have poor geochronologic constraints.

This article presents new chemostratigraphic data from supracrustal successions in the Sierra Madre and Hartville Uplift, Wyoming and Black Hills, South Dakota (Fig. 4.1). The proposed correlation between these successions is based on the chemostratigraphic data as well as available

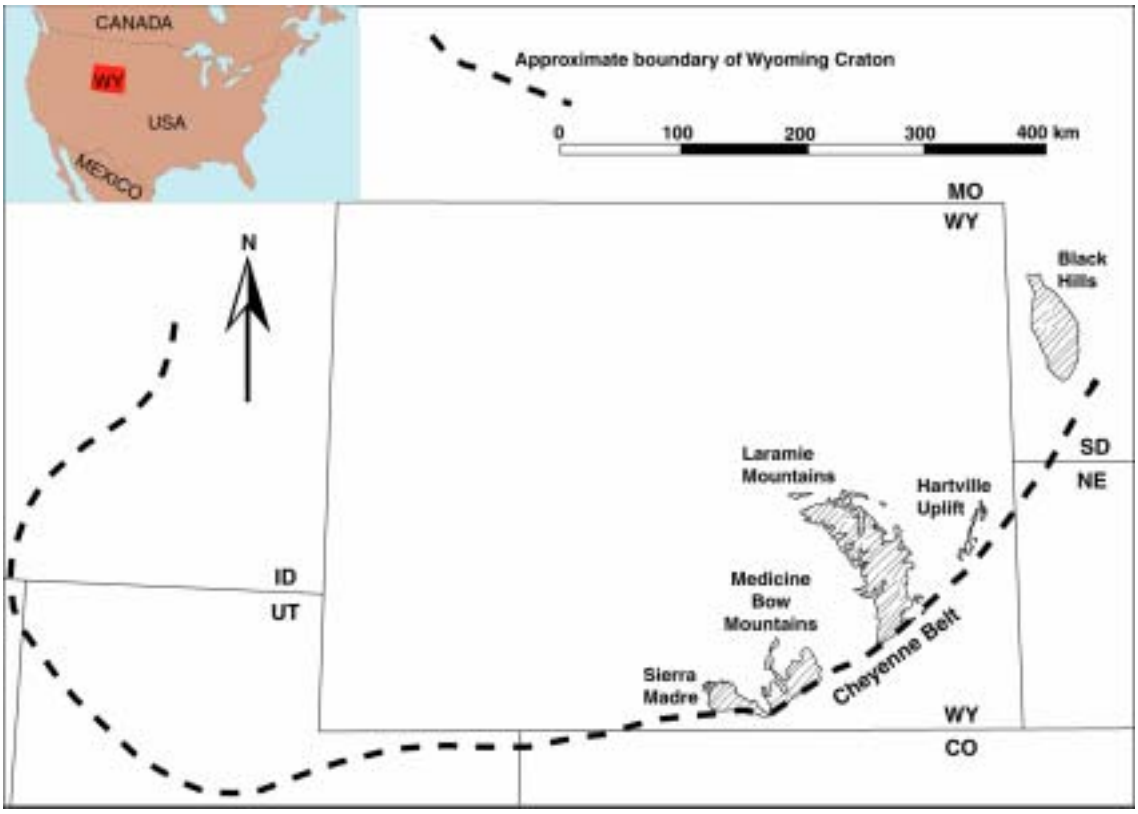

Fig. 4.1. Location of early Paleoproterozoic sedimentary successions on the southern and eastern margins of the Wyoming Craton.

geochronologic and stratigraphic data. In combination, these data permit a better understanding of the ages of the areally separated outcrop belts as well as the tectonic evolution of the Wyoming Craton in the early Paleoproterozoic.

REGIONAL GEOLOGY AND STRATIGRAPHY

The Wyoming Craton is a triangular block of Archean crust surrounded by locally exposed Paleoproterozoic mobile belts. Paleoproterozoic sedimentary and subordinate volcanic rocks are well exposed on the southeastern margin of the Wyoming craton in the Sierra Madre and Medicine Bow Mountains, Wyoming as well as in the Black Hills, South Dakota (Fig. 4.1). These rocks were strongly deformed during the 1.78-1.74 Ga Medicine Bow Orogeny when the southern passive margin of the Wyoming Craton collided along the Cheyenne Belt Suture with island arcs approaching from the south (Karlstrom and Houston, 1984; Chamberlain, 1998). The Cheyenne Belt

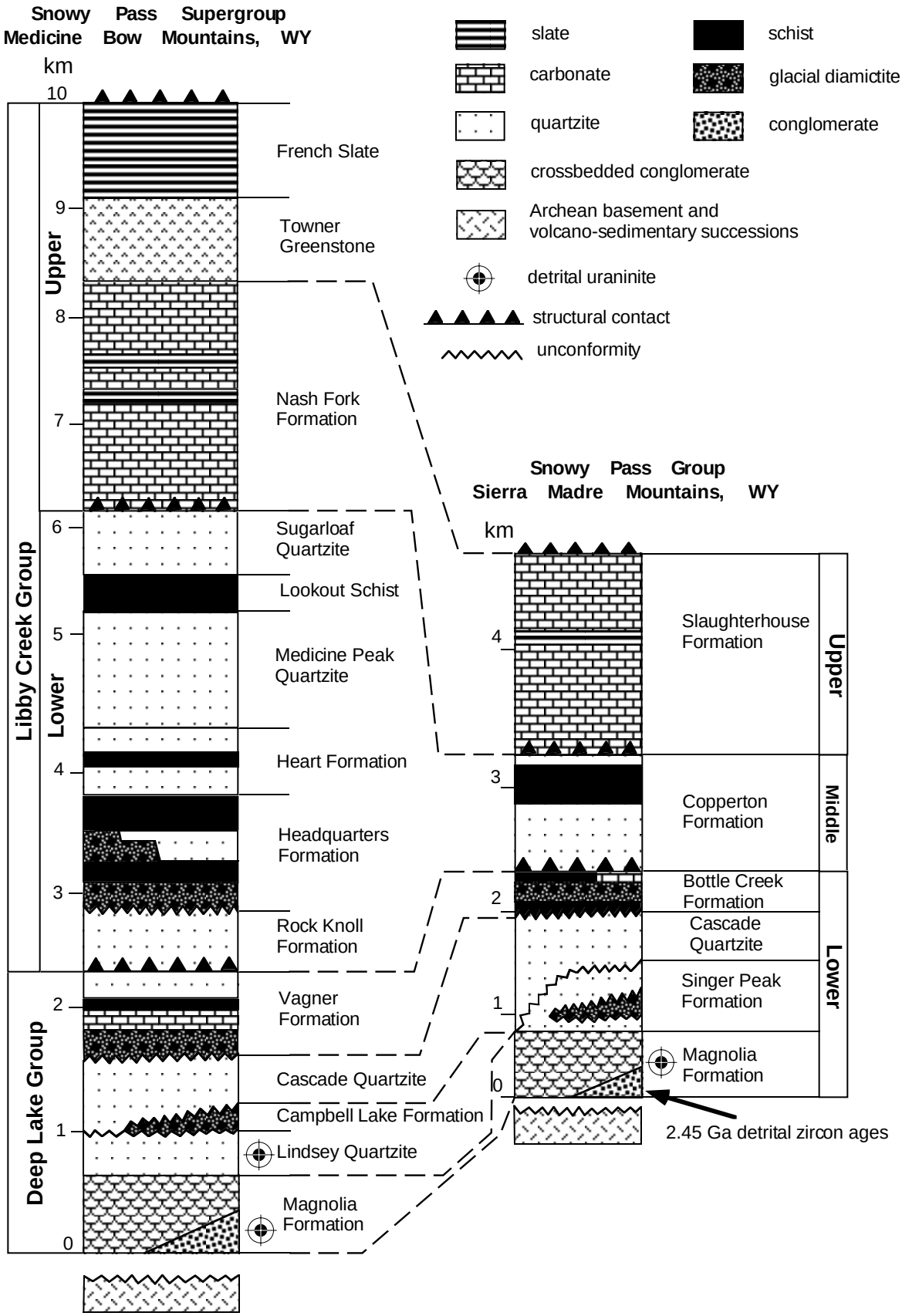

Fig. 4.2. Correlation between the Snowy Pass Supergroup, Medicine Bow Mountains, WY and the Snowy Pass Group, Sierra Madre (after Houston et al., 1992). Arrow with age shows stratigraphic position and the age of detrital zircon grains studied by Premo and Van Schmus (1989).

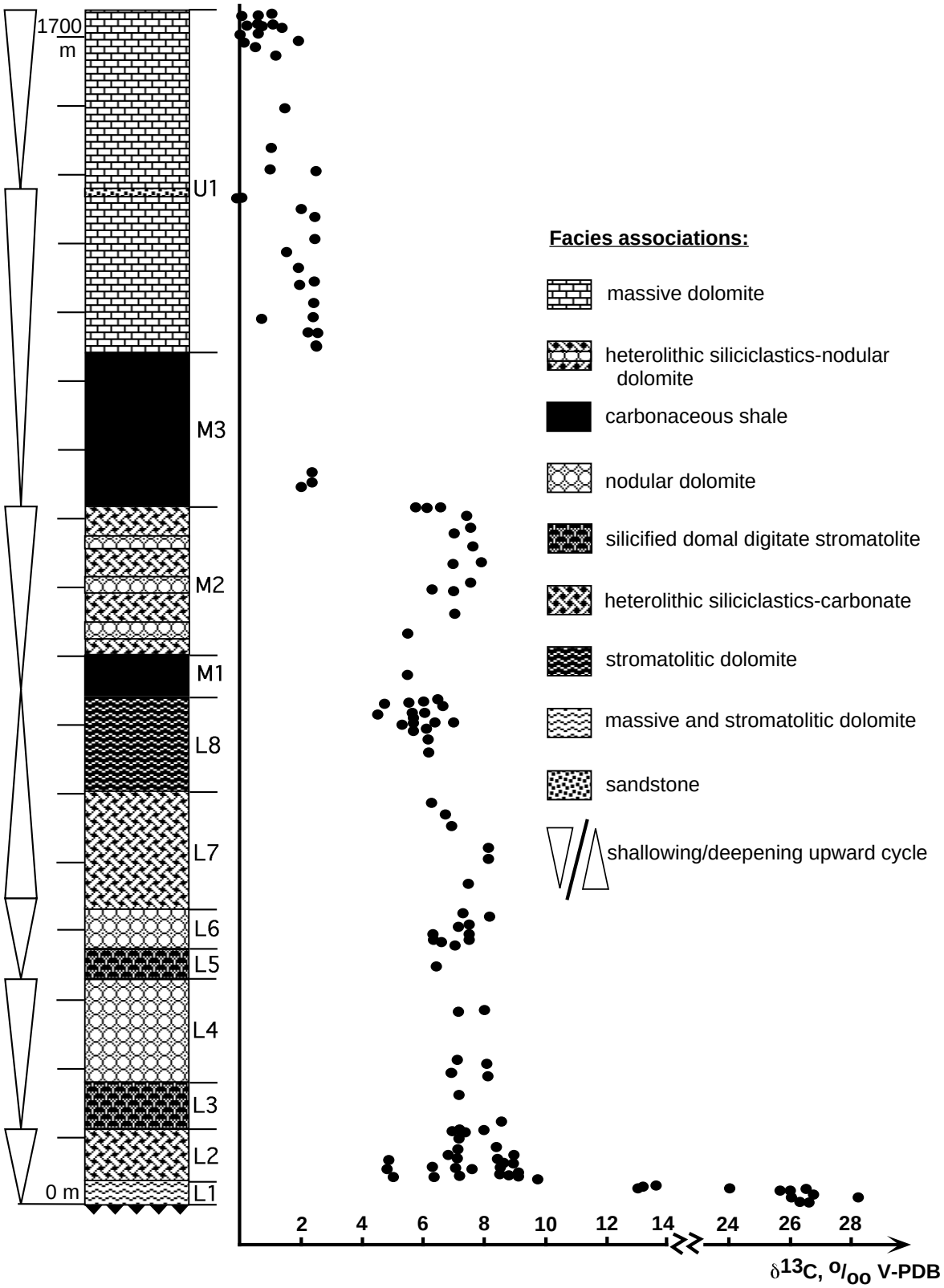

Fig. 4.3. Stratigraphic column, inferred cycles, and variations in $\delta^{13}C$ values for the Nash Fork Formation.

is well-exposed in the Sierra Madre and Medicine Bow Mountains and is traceable to the east through the Laramie Mountains and Racheau Hills; further to the east it disappears under Phanerozoic cover where it can only be inferred from geophysical data (Sims, 1995). The projection of the Cheyenne Belt and, therefore, the early Proterozoic passive margin passes south of the Hartville Uplift (Fig. 4.1). The eastern margin of the Wyoming Craton poorly exposed in the Black Hills, South Dakota is bounded by the Trans-Hudson orogen (Redden et al., 1990; Sims, 1995).

The Paleoproterozoic succession in the Sierra Madre (Fig. 4.1) is strongly deformed and dismembered by a late cataclastic event (Houston, 1993), but based primarily on lithostratigraphic similarities is considered to be correlative with the Snowy Pass Supergroup in the Medicine Bow Mountains (Houston et al., 1992; Fig. 4.2). The succession in the Sierra Madre is named the Snowy Pass Group (Houston et al., 1992) since it is structurally more complex and is less understood than the correlative supergroup. The correlative horizons in these successions include the lower siliciclastic rift sequences with basal conglomerates containing detrital uraninite and pyrite, glacial diamictites, Al-rich mature quartzites and thick carbonate units. The ca. 2.45 Ga age for the initiation of the early Paleoproterozoic deposition on the southern flank of the Wyoming Craton is inferred from: 1) the minimum age of detrital zircon grains in the Magnolia Formation of the Sierra Madre (2.451 ± 9 Ma, Premo and Van Schmus, 1989); 2) the correlation with the Huronian Supergroup (Houston et al., 1992) for which a rifting is well constrained to ca. 2.45 Ga (Krogh et al., 1984, 1996; Smith and Heaman, 1999), and 3) the age of the Baggot Rocks Granite in the western Medicine Bow Mountains (2429 ± 4 Ma, Premo and Van Schmus, 1989) that includes mafic dikes of the same age. Houston et al. (1992) considered the Slaughterhouse Formation carbonate rocks and carbonaceous phyllite in the Sierra Madre to be the deep-water time-equivalent of the Nash Fork Formation in the Snowy Pass Supergroup (Fig. 4.2).

Paleoproterozoic rocks exposed in the Black Hills, South Dakota (Fig. 4.1) were deposited on the eastern flank of the Wyoming Craton and contain two rift successions overlain by back-arc and foredeep deposits (Redden et al., 1990). The older rift succession is only exposed in the Nemo area

in the northeastern part of the Black Hills, whereas younger rift, back-arc and foredeep deposits outcrop in several areas in the Black Hills (Fig. 4.4). Early Paleoproterozoic glaciogenic diamictites are lacking in the Black Hills possibly due to removal along the unconformity separating the two rift successions. Both rift successions are younger than the Archean Little Elk Granite that has an U-Pb zircon age of 2549 ± 11 Ma and older than the overlying Ellison Formation that contains metatuffs dated at 1974.4 ± 8 Ma (U-Pb zircon, Redden et al., 1990). The older rift succession was intruded by and in-folded with the Blue Draw Metagabbro (2170 ± 120 Ma U-Pb zircon; Redden et al., 1990) prior to deposition of the younger rift succession.

A volcano-sedimentary supracrustal succession named the Whalen Group is also present in the Hartville Uplift (Fig. 4.1). The Whalen Group includes a thick carbonate succession and Lake Superior-type BIF's. The age of the Whalen Group is controversial. Sims (1995) suggested a Paleoproterozoic age based on rarity of Archean platformal carbonates and Lake Superior-type BIF's on northern hemisphere continents. Hofmann and Snyder (1985) described four types of stromatolites from the Whalen Group, two of which (*Hadrophycus* and *Gruneria*) are only known from Paleoproterozoic successions. *Hadrophycus* was originally described from the Paleoproterozoic Nash Fork Formation, Snowy Pass Supergroup, WY (Fenton and Fenton, 1939). Sims and Day (1999) proposed an Archean age for the Whalen Group based on intrusive contacts with the 2.65 Ga old Flattop Butte Granite. However, these intrusive relationships between supracrustal rocks and granites were observed only to the east from the Hartville Fault, a major N-S striking structural boundary in the Hartville Uplift, whereas the thicker carbonate intervals are confined to the lower metamorphic-grade western domain.

METHODS

Whole-rock (marked by asterisk in Table 4.1) as well as microdrilled powders were prepared from samples collected from measured sections and isolated outcrops. Major and trace element concentrations on whole-rock powders were determined through dissolution of ~10 mg of carbonate in 5 ml of 0.5 M acetic acid and subsequent analysis by ICP-AES at the Geological Survey of Finland (Table 4.1). Uncertainties in the analytical data based on the measurement of multiple standard materials by this method are 5% for major elements and better than 10% for trace elements. Microdrilled powders of ~20 to 40 mg were dissolved in 5 ml of 2% nitric acid and analyzed for Mn

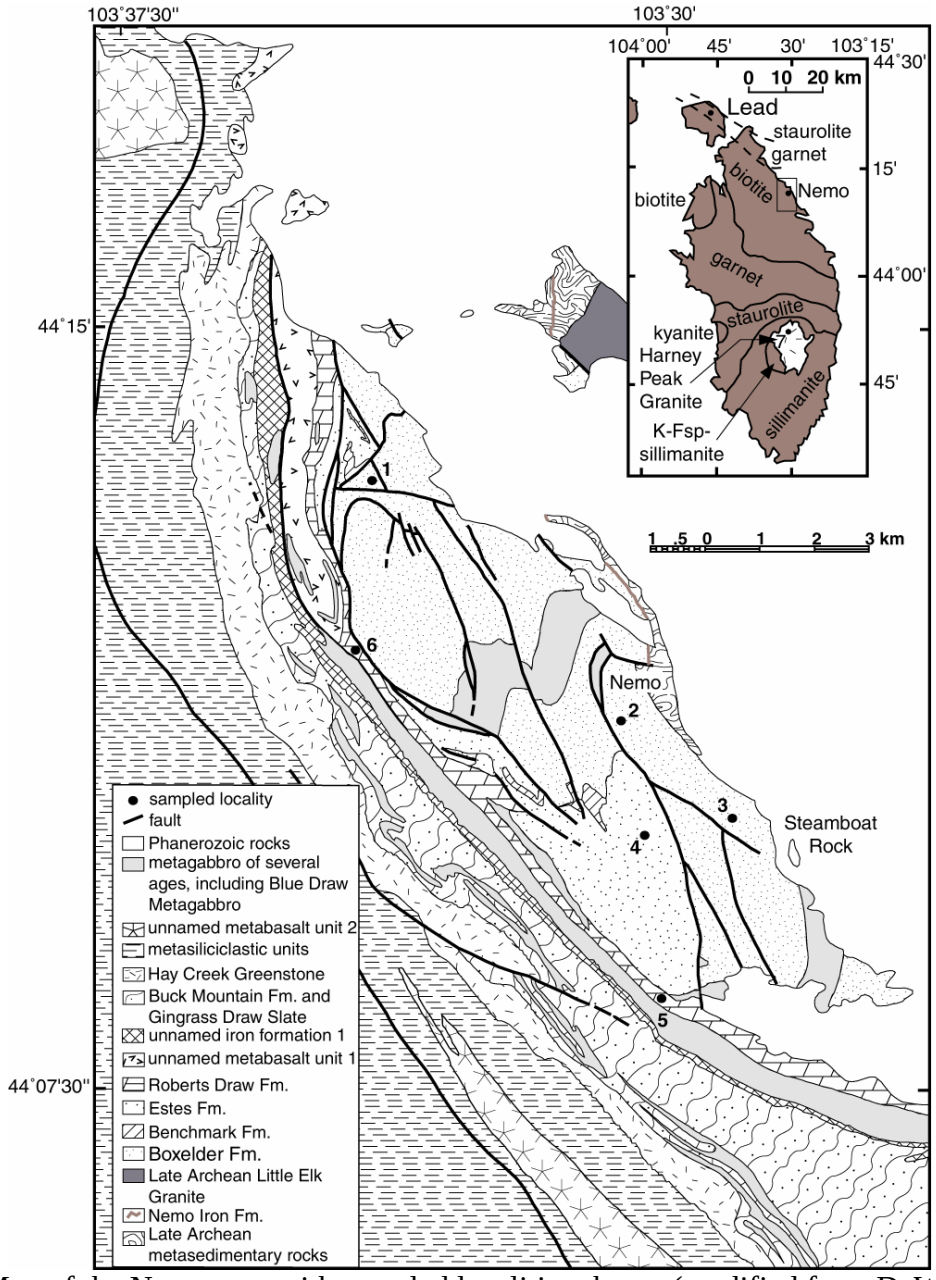

Fig. 4.4. Map of the Nemo area with sampled localities shown (modified from DeWitt et al., 1986, 1989). Inset (modified from Redden et al., 1990 and Dahl et al., 1999) shows Harney Peak Granite and metamorphic grades in the Black Hills. Sampled localities: Boxelder Formation -- 1 - Benchmark location; 2 - locality near Nemo cemetery; 3 - unnamed locality ~0.9 mi northwest from the Steamboat Rock; Estes Formation -- 4 - Estes Creek; Roberts Draw Formation -- 5 - Forest Service Rd. 201; 6 - South Boxelder Creek. Carbonates from roof pendants in the Harney Peak Granite were sampled in Loc. 7 (shown on inset).

and Sr contents on a Buck Scientific 200-A AAS at Virginia Tech. Uncertainties based on the measurement of multiple standard materials by this method are better than 5% for Sr and 10% for Mn. Samples that had low yields indicating carbonate contents below 50% were not analyzed for major and trace elements.

Carbon dioxide was extracted at the Geological Survey of Finland from whole-rock powders by closed tube reaction with anhydrous phosphoric acid ($\rho > 1.89$ g/cc) at a temperature of 25°C for limestone and 100°C for dolomite and isolated by cryogenic distillation for mass spectrometric analysis on a Finnigan MAT 251. The fractionation factors used for mineral correction of oxygen isotopes in calcite prepared at 25°C and dolomite at 100°C were 1.01025 and 1.00913, respectively. A second generation of carbonate samples (without asterisk in Table 4.1) was micro-drilled and the powders reacted with anhydrous phosphoric acid at 90°C in a Micromass Multiprep carbonate device. The resulting carbon dioxide was measured with a Micromass Isoprime mass spectrometer at the University of Maryland, College Park. The fractionation factors used for mineral correction of oxygen isotopes in calcite and dolomite prepared at 90°C were 1.00798 and 1.00895, respectively. For both techniques, the external precision based on multiple standard measurements of NBS-19 was better than 0.1‰ vs. V-PDB for carbon and 0.1‰ vs. V-PDB on a Finnigan MAT 251.

Total organic carbon (TOC) was isolated from the shale sample by repeated acidification and centrifugation with concentrated HCl followed by washing until the sample reached neutral pH (Kaufman and Knoll, 1995). Dried sample was then mixed with CuO as an oxidant, evacuated, sealed and combusted at 850°C for 12h in Vycor tubing. The volume of CO_2 quantified during cryogenic distillation was used to calculate organic carbon concentrations. Carbon isotope abundance in extracted and purified CO_2 was measured with a VG PRISM mass spectrometer at Mountain Mass Spectrometry. To test for the uncertainty of abundance and isotopic composition measurements on TOC, organic-rich and organic-poor standard powders were chosen for replicate ($n = 4$) analysis. For analyses of the organic-rich standard, uncertainties were ± 0.26 mgC/g for abundance (5.57 mgC/g average) and ± 0.03‰ for carbon-isotopic composition (-34.47‰ average); for the organic-poor standard uncertainties were ± 0.06 mgC/g (0.18 mgC/g average) and ± 1.3‰ (-24.1‰ average) for abundances and carbon-isotopic compositions, respectively.

Table 4.1. Carbon and oxygen isotope values and trace and major element concentrations of studied carbonates.

Sample #	Mineral / Lithology	$\delta^{13}C$, PDB	$\delta^{18}O$, PDB	TOC, mgC/g sample	$\delta^{13}C_{TOC}$, PDB	Ca (%)	Mg (%)	Fe (ppm)	Mn (ppm)	Sr (ppm)	Mn/ Sr
Slaughterhouse Formation, Sierra Madre											
97-SL-1*	dolomite	8.0	-10.4						228	32	7.1
97-SL-1/2*	dolomite	6.6	-11.6						280	33	8.5
97-SL-3*	dolomite	5.9	-14.6						780	77	10.2
97-SL-4*	dolomite	7.8	-12.7						1101	65	17.0
97-SL-5	phyllite			19.3	-22.6						
97-SL-6*	dolomite	8.7	-10.8						430	43	9.9
97-SL-7*	dolomite	7.3	-11.1						324	39	8.3
97-SL-8*	dolomite	16.6	-10.3						1469	153	9.6
97-SL-9*	dolomite	15.2	-4.2						1842	15	119
Whalen Group, Hartville Uplift											
Locality 1											
2HV-26	Dolomite	1.0	-8.4						46	17	2.7
2HV-27	Dolomite	0.9	-9.9						55	21	2.6
2HV-28	Dolomite	0.9	-10.0						51	17	3.0
Locality 2											
HV-2-1*	Dolomite	1.1	-6.5			21.38	13.02	988	62	50	1.2
HV-2-4*	Dolomite	1.4	-7.3			22.39	13.31	6381	462	32	14.3
Locality 3											
HV-96-1	Dolomite	0.8	-6.2						98	tr.	-
HV-96-2	Dolomite	-0.3	-5.2						97	25	3.8
HV-96-3	Dolomite	1.0	-6.2						84	9	9.6
Locality 4											
2HV-29	Dolomite	0.9	-5.9						35	56	0.6
Locality 5											
HV-4-2*	Dolomite	1.1	-8.4			22.06	12.96	1201	70	38	1.9
Locality 6											
HV-5-1	Dolomite	0.7	-7.3						499	35	14.4
Locality 7											
HV-9-1*	Mixture	1.3	-9.0			26.61	11.04	2138	234	38	6.1
HV-9-1*	Dolomite	2.1	-7.0								
2HV-24	Dolomite	1.2	-6.8						59	53	1.1
2HV-25	Dolomite	3.2	-6.6						169	53	3.2
Locality 8											
HV-13-1	Dolomite	6.3	-6.9						955	21	46.0
2HV-14	Dolomite	2.8	-16.0						2755	83	33.0
2HV16	Dolomite	7.3	-14.2						1762	95	18.6
2HV-17	Dolomite	5.9	-13.0						961	41	23.3
2HV-18	Dolomite	5.6	-10.5						602	57	10.6
2HV-19	Dolomite	8.2	-9.0						125	125	1.0
2HV21	Dolomite	4.5	-14.7						730	78	9.4
2HV-22	Dolomite	5.4	-9.8						612	68	9.1
2HV-23	Dolomite	8.0	-9.2						374	122	3.1
2HV-24-1	Dolomite	4.8	-10.6						1478	51	29.2
Locality 9											
2HV-1	Dolomite	0.1	-12.1						1068	71	15.1
2HV-2	Dolomite	5.2	-14.0						956	87	11.0
2HV-3	Dolomite	6.9	-12.6						481	89	5.4
2HV-4	Dolomite	5.6	-12.4						734	72	10.3
2HV-5	Dolomite	6.2	-10.5						386	108	3.6
Locality 10											

2HV-6	Dolomite	2.0	-13.6				2301	36	64.1
2HV-8	Dolomite	3.7	-14.7				3286	118	27.8
Locality 11									
2HV-9	Dolomite	0.5	-8.7				330	31	10.7
2HV-9-1	Dolomite	0.3	-7.7				363	47	7.8
2HV-10	Dolomite	-0.3	-8.9				38	115	0.3
2HV-11	Dolomite	0.4	-11.0				84	48	1.8
2HV-12	Dolomite	0.5	-7.5				216	60	3.6
Locality 12									
2HV-20	Dolomite	7.9	-10.8				311	136	2.3
Black Hills, SD									
Boxelder Formation									
B99.1	Dolomite	1.0	-11.7				3236	tr.	-
B99.2	Dolomite	0.7	-10.6				2866	tr.	-
B99.3	Dolomite	0.7	-21.8				3863	tr.	-
B99.3	Dolomite	0.8	-11.8						
B99.4	Dolomite	1.0	-12.1				4698	tr.	-
B99.5	Dolomite	0.5	-13.1				3391	tr.	-
B99.6	Dolomite	1.1	-12.8				3368	tr.	-
B99.7l	Dolomite	-0.7	-19.8				5040	tr.	-
B99.7d	Dolomite	-1.4	-13.0				5961	tr.	-
B99.8	Dolomite	-0.1	-14.4				9401	tr.	-
SD-96-6*	Dolomite	-1.1	-17.6						
SD-96-6*	Mixture	-1.3	-17.7	27.4	8.7	27430	10919	214	50.9
SD-96-6*	Calcite	-1.8	-17.1						
SD-96-9*	Dolomite	-0.7	-16.3	23.0	12.8	10297	7121	45	157
SD-96-13	Dolomite	-1.1	-14.2				6939	29	236
Estes Creek Formation									
SD99.2.1	Dolomite	1.3	-15.0				6776	5	1339
SD99.2.1	Dolomite	1.4	-14.5						
SD99.2.2	Dolomite	2.2	-17.8				537	tr.	-
SD99.2.2	Dolomite	2.3	-14.9						
SD99.2.3	Dolomite	2.1	-13.7				1382	17	82.1
SD99.2.4	Dolomite	2.1	-15.3				909	7	125.4
SD99.2.5	Dolomite	2.0	-14.2				1891	tr.	-
SD99.2.6	Dolomite	2.3	-15.2				1009	tr.	-
SD99.2.7	Dolomite	2.4	-12.7				729	6	127.2
SD99.2.8	Dolomite	2.2	-15.7				12118	tr.	-
SD99.2.9	Dolomite	2.5	-15.4				515	tr.	-
SD99.2.10	Dolomite	2.4	-7.2				638	tr.	-
Roberts Draw Formation									
B99.10	Dolomite	-0.4	-14.6				597	25	24.4
B99.11d	Dolomite	1.3	-10.7				394	tr.	-
B99.11l	Dolomite	1.6	-9.1				444	2	201.3
B99.12	Dolomite	1.2	-11.7				814	tr.	-
B99.13	Dolomite	1.9	-8.3				828	tr.	-
B99.14	Calcite	-0.2	-9.8				694	tr.	-
B99.14	Calcite	-0.2	-9.0						
B99.15	Calcite	-1.1	-10.1				2720	tr.	-
B99.16	Calcite	0.0	-11.0				871	tr.	-
SD-96-4*	Dolomite	-3.5	-15.6	22.87	12.8	13083	1075	106	10.1
SD-96-1*	Dolomite	1.1	-17.3	21.8	12.4	8961	2626	149	17.6
Marble from roof complex (country rock), Harney Peak Granite area, Black Hills, SD									
HP-1	Dolomite	2.1	-9.1				282	45	6.3
HP-2	Dolomite	2.2	-7.0				103	57	1.8
HP-3	Dolomite	2.3	-6.4				161	28	5.8

SLAUGHTERHOUSE FORMATION, SIERRA MADRE

Description

The Slaugherhouse Formation is the uppermost unit of the Snowy Pass Group in the Sierra Madre and has structural contacts with the underlying units in the type area north of the Rambler Guard station (Fig. 4.5). The Snowy Pass Group experienced amphibolite facies metamorphism (Divis, 1976). The Slaugherhouse Formation is highly dismembered by thrusts and no complete section is exposed. The lower part of the formation in the type section consists of yellow, red, buff, blue, and green massive dolomites that contain layers of quartzite and dark-green phyllite (Houston et al., 1992). Stromatolites are not present and the dolomites are generally fine-grained and massive with rare cross bedding. Dolomites are overlain by black graphitic phyllites, and the upper part of the section consists of fine-grained, chloritic calc-schist (Houston et al., 1992). The dolomitic member is about 400 m thick in the type section and the overlying phyllite and schist are about 100 m thick (Houston et al., 1992). Samples were collected from several outcrops in the type area (sec. 26, T. 14N, R. 86W; Fig. 4.5): 97-SL-1 to 5 in loc. 2, 97-SL-6 and 7 in loc. 3 and 97-SL-8 and 9 in loc. 4.

Geochemical data and diagenesis

Eight dolomite samples and one organic-rich phyllite were analyzed in this study (Table 4.1). The dolomites have highly variable Mn contents (228-1842 ppm), low Sr contents (15-153 ppm), and high Mn/Sr ratios (7.1-120). Oxygen isotope values display a narrow range between –10.3 and –14.6‰ (V-PDB) except for sample 97-SL-9 with a value of –4.2‰. Carbon isotope values range remarkably between +5.9 and +16.6‰ V-PDB. Two samples of cross bedded pink/red dolomite from the lower Slaughterhouse Formation near a fault contact (97-SL-8 and 9) have very high carbon isotope values (+16.6 and +15.2‰ respectively) and the highest Mn contents and oxygen isotope values. Organic-rich phyllite (SL-97-5) overlying the dolomite member has a relatively high TOC content (19.3 mgC/g sample) and $\delta^{13}C_{org}$ value –22.6‰. Assuming that dolomite samples 97-SL-4 and 97-SL-3 collected from the same outcrop immediately below the phyllite are broadly contemporaneous with phyllite, fractionation between carbonate and organic carbon is estimated to be near to 30‰; and within the range generally attributed to primary productivity (Hayes et al., 1999).

Cross-plots of $\delta^{18}O$ or Mn vs. $\delta^{13}C$ show weak correlation but correlation between $\delta^{13}C$ and Sr or Mn/Sr is lacking (Fig. 4.6). Whereas correlation between carbon and oxygen values is shown

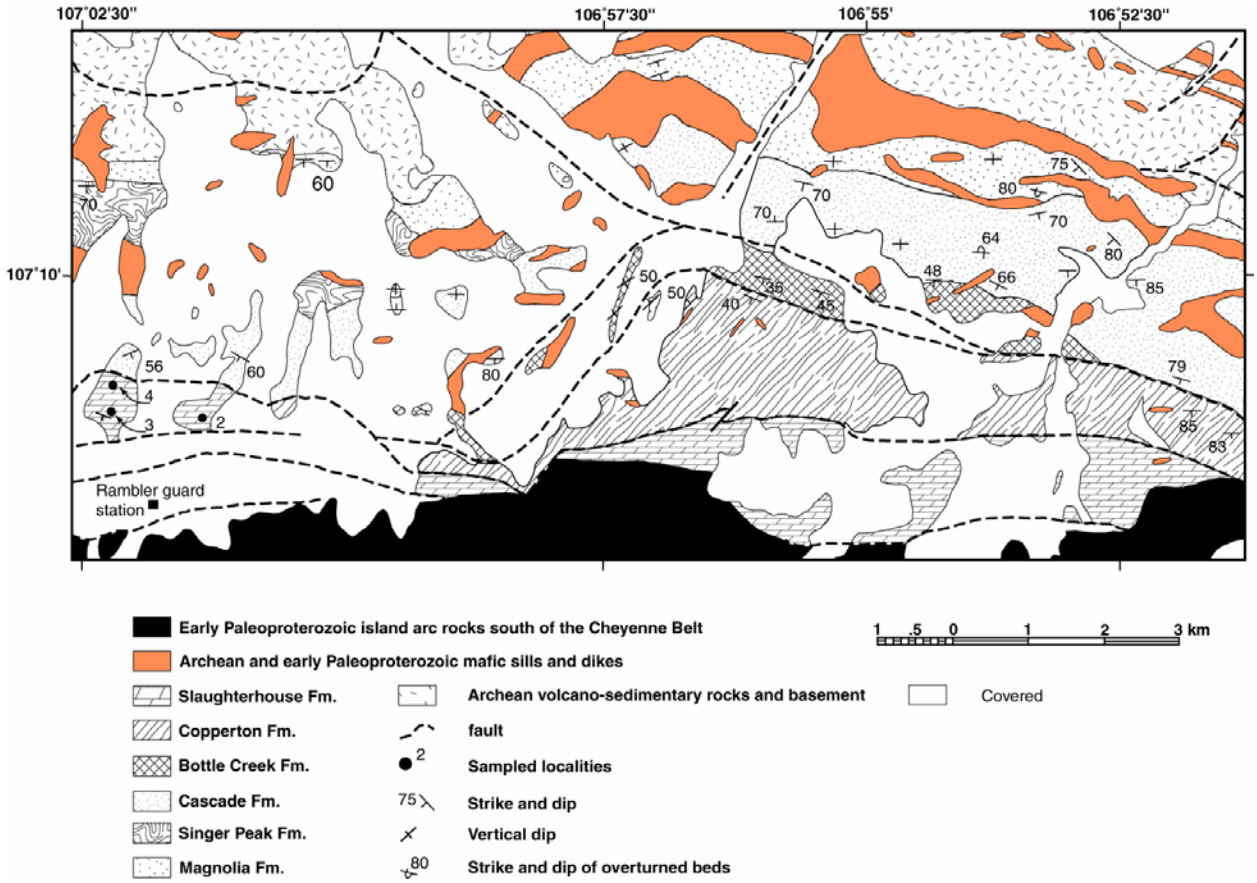

Fig. 4.5. Map of the type area of the Slaughterhouse Formation with sampled localities shown (modified from Houston and Graff, 1995).

by all points, correlation between $\delta^{13}C$ and Mn is strongly influenced by the two samples with high carbon isotope values and high Mn contents. If these samples that are from different stratigraphic level to the other samples are deleted, correlation become insignificant. Correlation between $\delta^{18}O$ and Mn is weak and does not follow an alteration trend. However, if the two samples with high oxygen isotope values are deleted, the correlation become more significant (R^2=0.52) and follows an alteration trend. There is no correlation between $\delta^{18}O$ and Sr or Mn/Sr.

In summary, although the Slaughterhouse Formation experienced a higher degree of deformation and metamorphism than the Nash Fork Formation, samples show relatively good degrees of preservation. This observation suggests that dolomites may preserve primary isotopic signals even at high metamorphic grade if dolomitization occurred early and carbonates were pure in

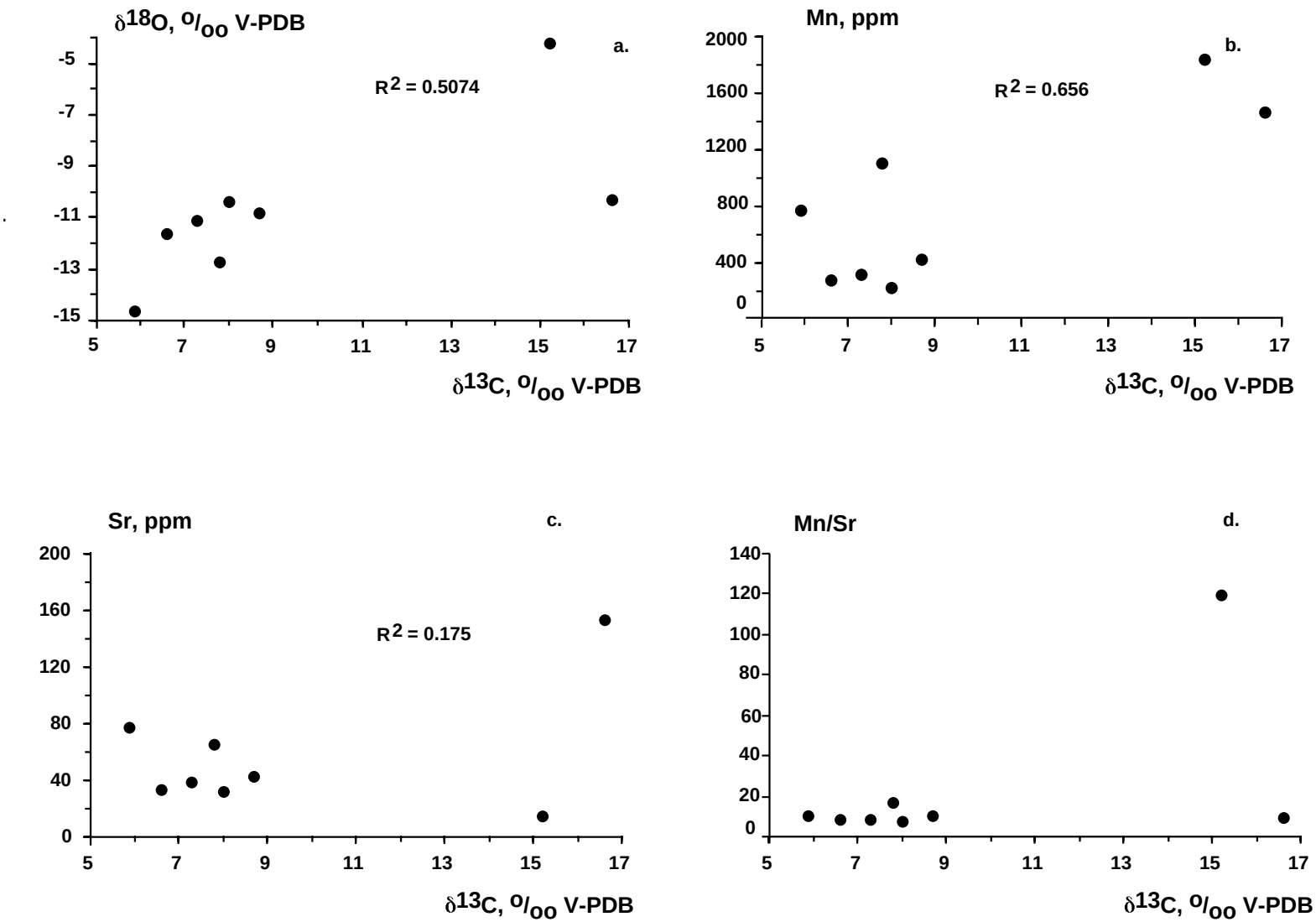

Fig. 4.6. Scatter diagrams for the Slaughterhouse Formation. a - $\delta^{18}O$, ‰ V-PDB vs. $\delta^{13}C$, ‰ V-PDB; b - Mn, ppm vs. $\delta^{13}C$, ‰ V-PDB; c - Sr, ppm vs. $\delta^{13}C$, ‰ V-PDB; d - Mn/Sr vs. $\delta^{13}C$, ‰ V-PDB; e - Mn, ppm vs. $\delta^{18}O$, ‰ V-PDB; f – Sr, ppm. vs. $\delta^{18}O$, ‰ V-PDB; g – Mn/Sr vs. $\delta^{18}O$, ‰ V-PDB.

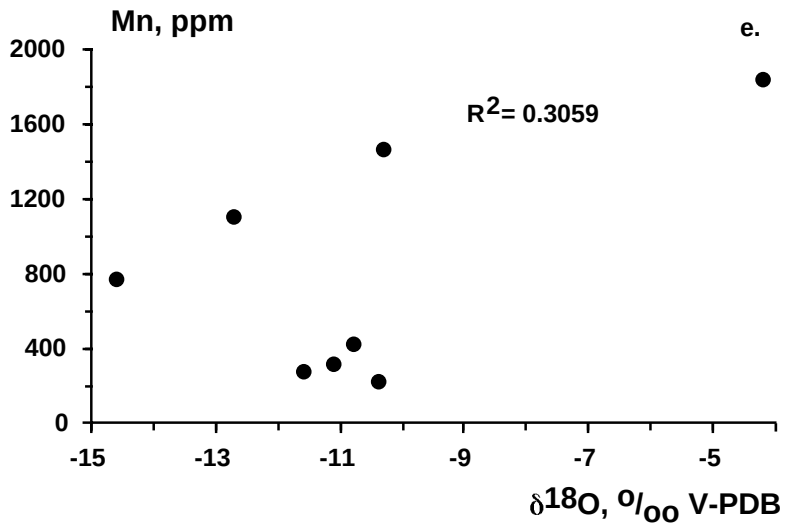
Mn, ppm
e.
R^2= 0.3059
2000
1600
1200
800
400
0
-15
-13
-11
-9
-7
-5
$\delta^{18}O$, $^{o}/_{oo}$ V-PDB

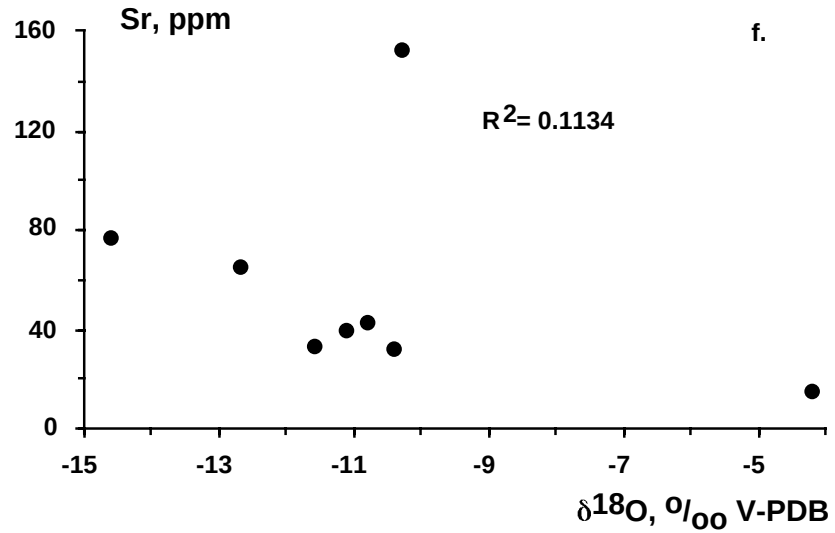
Sr, ppm
f.
R^2= 0.1134
160
120
80
40
0
-15
-13
-11
-9
-7
-5
$\delta^{18}O$, $^{o}/_{oo}$ V-PDB

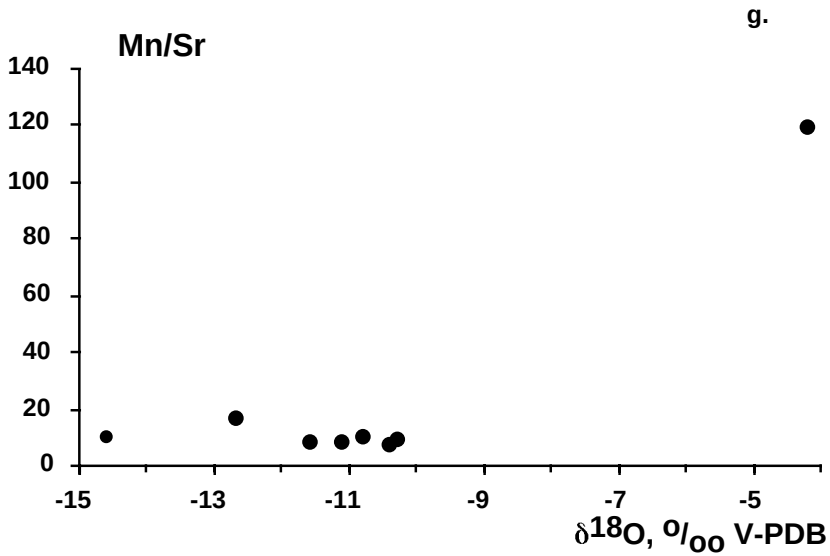
g.
Mn/Sr
140
120
100
80
60
40
20
0
-15
-13
-11
-9
-7
-5
$\delta^{18}O$, $^{o}/_{oo}$ V-PDB

composition. Carbon and oxygen isotope values of the Slaughterhouse dolomites are similar to those found in the L1-M2 members of the Nash Fork Formation. The two dolomite samples from the lower part of the Slaughterhouse Formation (97-SL-8 and 9) are comparable to those from the L1 member of the Nash Fork Formation with respect to their extremely high carbon isotope values. High oxygen isotope values and Mn contents similar to those in these two samples have been be attributed to extreme degrees of evaporation (Kah, 2000). However, evidence for evaporite environments in the Slaughterhouse Formation is lacking. Since a similar but much better constrained carbon isotope trend is also found in the Nash Fork Formation, we infer that the carbon isotope values may reflect the composition of the global ocean rather than of a local environment. Correlation with high Mn contents is enigmatic. However, we note that samples were collected close to the thrust and could have been more strongly affected by circulating fluids than other samples.

BLACK HILLS, SOUTH DAKOTA

Description

All studied units with the exception of carbonates with sillimanite-grade of metamorphism from the Harney Peak Granite area experienced biotite-grade metamorphism (inset in Fig. 4.4; Redden et al., 1990). The oldest unit of the Early Paleoproterozoic succession in the Black Hills area -- the Boxelder Creek Formation -- outcrops near Nemo (see Fig. 4.4) and belongs to the older rift sequence. Its contact with the underlying Nemo Iron Formation is not exposed but is inferred to be unconformable based on the presence of BIF clasts in conglomerates of the Boxelder Creek Formation (Redden, 1980) whereas the contact with the overlying Benchmark Iron Formation is conformable. The Boxelder Creek Formation consists of a basal interval of conglomerate and quartzite, containing lenses of pyriferous and uraniferous conglomerate and quartzite, and overlying quartzite succession that is over 3.3 km thick (Redden et al., 1990). Two ~30 m-thick siliceous dolomite intervals in the lower part of the quartzite succession are separated by thin blue-gray phyllite (Redden, 1981). Samples from dolomite lenses and layers (SD-series) were collected at the Benchmark location (Loc. 1 in Fig. 4.4) and near the Nemo cemetery (Loc. 2 in Fig. 4.4). In addition, the lower and upper carbonate intervals were sampled (B99-series) at an unnamed locality (Loc. 3 in Fig. 4.4) further southeast along strike (~0.9 mi northwest from the Steamboat Rock).

B99 samples were collected in stratigraphic order through the lower dolomite interval with sampling interval of several meters.

The Estes Formation which represents the younger rift succession, which unconformably overlies the Benchmark Iron Formation and Boxelder Formation, and consists of conglomerate overlain by quartzite (Redden, 1981). Siliceous fine to medium grained dolomite and phyllite occur in the middle part of the formation. Carbonate samples were collected at the intersection of Estes Creek Road and Estes Creek (SD-series; Loc. 4 in Fig. 4.4). Herringbone calcite structures (cf. Sumner and Grotzinger, 1996) were observed in one sample.

The Roberts Draw Formation, conformably overlying the Estes Formation, is 20-100 m thick and consists of dolomite gradationally overlain by limestone with interbedded dolomite and capped by graphitic, gray phyllite (Redden, 1981). Small (~5 cm height) domal stromatolites were observed in one outcrop. Samples were collected on Forest Service Road 201 (SD-96-4; Loc. 5 in Fig. 4.4) and along South Boxelder Creek (B99-series; Loc. 6 in Fig. 4.4). B99 samples were collected in stratigraphic order from the exposed lower part upsection with sampling interval of several meters. Rocks considered equivalent in age to the Roberts Draw Formation outcrop near Bear Mountain in the Medicine Mountain area and in large roof pendants associated with the Harney Peak Granite south of Harney Peak (DeWitt et al., 1986, p. 13). Pure carbonates were sampled (HP-series; Loc. 7 in inset in Fig. 4.4) from roof pendants in the Harney Peak Granite.

Geochemical data and diagenesis

Most studied samples are dolomites with the exception of several calcite samples from the Roberts Draw Formation. The degree of alteration as well as the geochemical signatures varies between units and the following descriptions are given separately for each unit.

Dolomites of the Boxelder Formation have high Mn contents (2866-10919 ppm), variable but generally very low Sr contents (trace amounts to 214 ppm), and very high Mn/Sr ratios (>50). Fe content is high in two samples (10297 and 27430 ppm). $\delta^{18}O$ values range between –10.6 and –21.8‰ and most samples are significantly depleted in ^{18}O. $\delta^{13}C$ values range between –1.8 and 1.1‰. Samples B99.1 – 6 collected from the lower dolomite interval have consistent $\delta^{13}C$ values

between 0.5 and 1.1‰, whereas samples collected from the upper dolomite interval (B99.7 and 8) have negative $\delta^{13}C$ values between –1.4 and -0.1‰. Because of poor outcrop, it is uncertain whether the SD-series samples belong to the lower or upper dolomite interval but since both carbon and oxygen isotope values are significantly depleted relative to the B99 series samples, the SD-series samples were likely stronger altered and did not preserve primary signatures. Correlation between $\delta^{18}O$ and Mn is lacking. However, weak to very weak correlation exists between $\delta^{18}O$ and $\delta^{13}C$, or $\delta^{13}C$ and Mn (Fig. 4.7).

Dolomites of the Estes Formation have high Mn contents (515-12118 ppm) and Mn/Sr ratios (>17), and low Sr contents (trace amounts to 149 ppm). One analyzed sample has a high Fe content (8961 ppm). Oxygen isotope values are low with the exception of one sample and range between –17.8 and –7.2‰. Carbon isotope values range between 1.1 and 2.5‰. Correlation between $\delta^{18}O$ and $\delta^{13}C$, $\delta^{13}C$ and Mn, and $\delta^{18}O$ and Mn is lacking (Fig. 4.7).

Calcites and dolomites of the Roberts Draw Formation have variable but generally intermediate Mn contents (394-2720 ppm), low Sr contents (trace amounts to 106 ppm), and high Mn/Sr ratios (>10). One analyzed sample has a high Fe content (13083 ppm). Oxygen isotope values range between –15.6 and –8.3‰ and are generally higher than those for carbonates of the Boxelder and Estes formations. Carbon isotope values with the exception of one sample range between –0.4 and 1.9‰. Sample SD-96-4 has very low carbon and oxygen isotope values and a high Fe and Mn content indicating a higher degree of alteration than for other samples of the Roberts Draw Formation. Correlation between $\delta^{18}O$ and $\delta^{13}C$ values is weak and there is no correlation between $\delta^{13}C$ and Mn, or $\delta^{18}O$ and Mn (Fig. 4.7).

The three dolomite samples from the roof complex of the Harney Peak Granite have relatively low Mn (103-282 ppm) and Sr (28-57 ppm) contents and Mn/Sr ratios ranging between 1.8 and 6.3. Oxygen isotope values range between –6.4 and –9.1‰ which is higher than those in carbonates of the correlative Roberts Draw Formation. $\delta^{13}C$ values are between 2.1 and 2.3‰ which are also slightly higher than the highest $\delta^{13}C$ value (1.9‰) in the Roberts Draw Formation dataset.

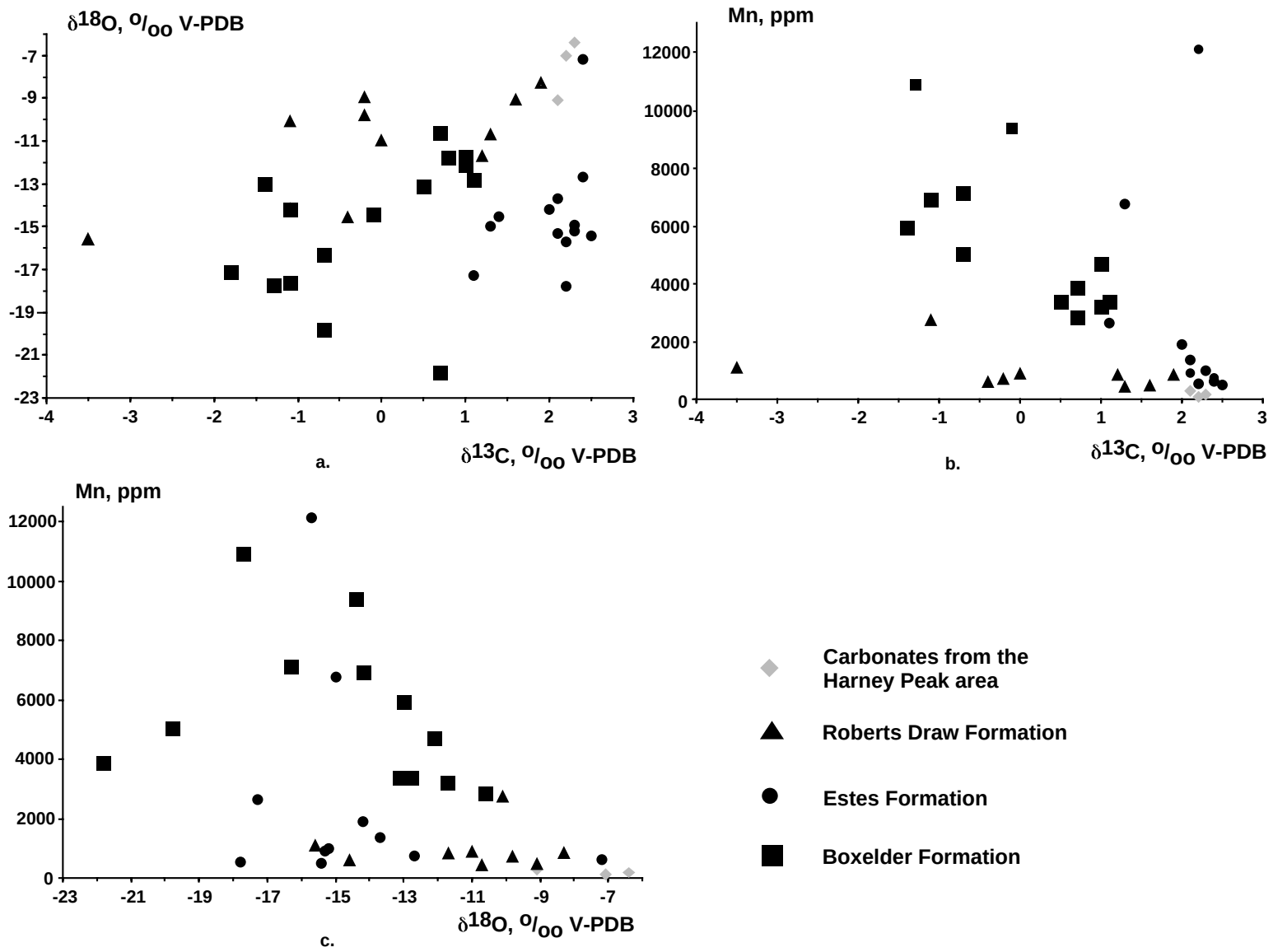

Fig. 4.7. Scatter diagrams for carbonates from the Black Hills, SD. a - $\delta^{18}O$, ‰ V-PDB vs. $\delta^{13}C$, ‰ V-PDB; b - Mn, ppm vs. $\delta^{13}C$, ‰ V-PDB; c - Mn, ppm vs. $\delta^{18}O$, ‰ V-PDB.

Since the samples from the Nemo area in the Black Hills experienced only biotite-grade metamorphism (Redden et al., 1990), depletion in ^{18}O and, in some samples, in ^{13}C is likely related to the occurrence of the carbonates as thin layers and lenses within thick siliciclastic succession, as well as their impure composition. Higher oxygen and carbon isotope values in carbonates of the Roberts Draw Formation are likely related to the greater thickness and the relatively pure composition of carbonates in this unit. Carbon isotope values of carbonates from the Black Hills area are close to 0‰ and resemble values in carbonates from the upper Nash Fork Formation.

WHALEN GROUP

Description

The Whalen Group is formally subdivided into four formations (from the oldest to the youngest): (1) Mother Featherlegs Metabasalt; (2) Silver Springs Formation (subgraywacke and ferruginous, graphitic and pyritic schist containing layers and lenses of Lake Superior type BIF), (3) Wildcat Hills Formation (dolomite), and (4) Muskrat Canyon Metabasalt (Sims et al., 1997; Sims and Day, 1999). This stratigraphy was constructed on the basis of lithological correlation between the eastern and western domains of different metamorphic grade, structural complexity, and likely depositional histories in an attempt to produce one stratigraphic scheme for the two juxtaposed domains (Fig. 4.8). Our study suggests that carbonates from the Hartville Uplift do not belong to a single stratigraphic unit since they differ in their depositional environment, degree of metamorphism, and isotopic signatures (see the following section). Structural complications, as well as limited outcrop, did not allow for the stratigraphic relationships between these distinctive carbonate units to be established in the field. The following discussion is focussed on three measured sections from the western domain and augmented by observations in both the western and eastern domains.

Several sections (Loc. 8, 9 and 11 in Fig. 4.9) were measured and sampled in the western domain near the mouth of the Rawhide Creek where the Whalen Group is in structural contact with the Archean Rawhide granite. The most complete section in this area (Loc. 8 in Fig. 4.9) is cut by a fault with unknown, but likely minor, displacement. The lower part of this section extending up to the fault consists of an upward-deepening cycle of red ferruginous quartzites, argillites with thin

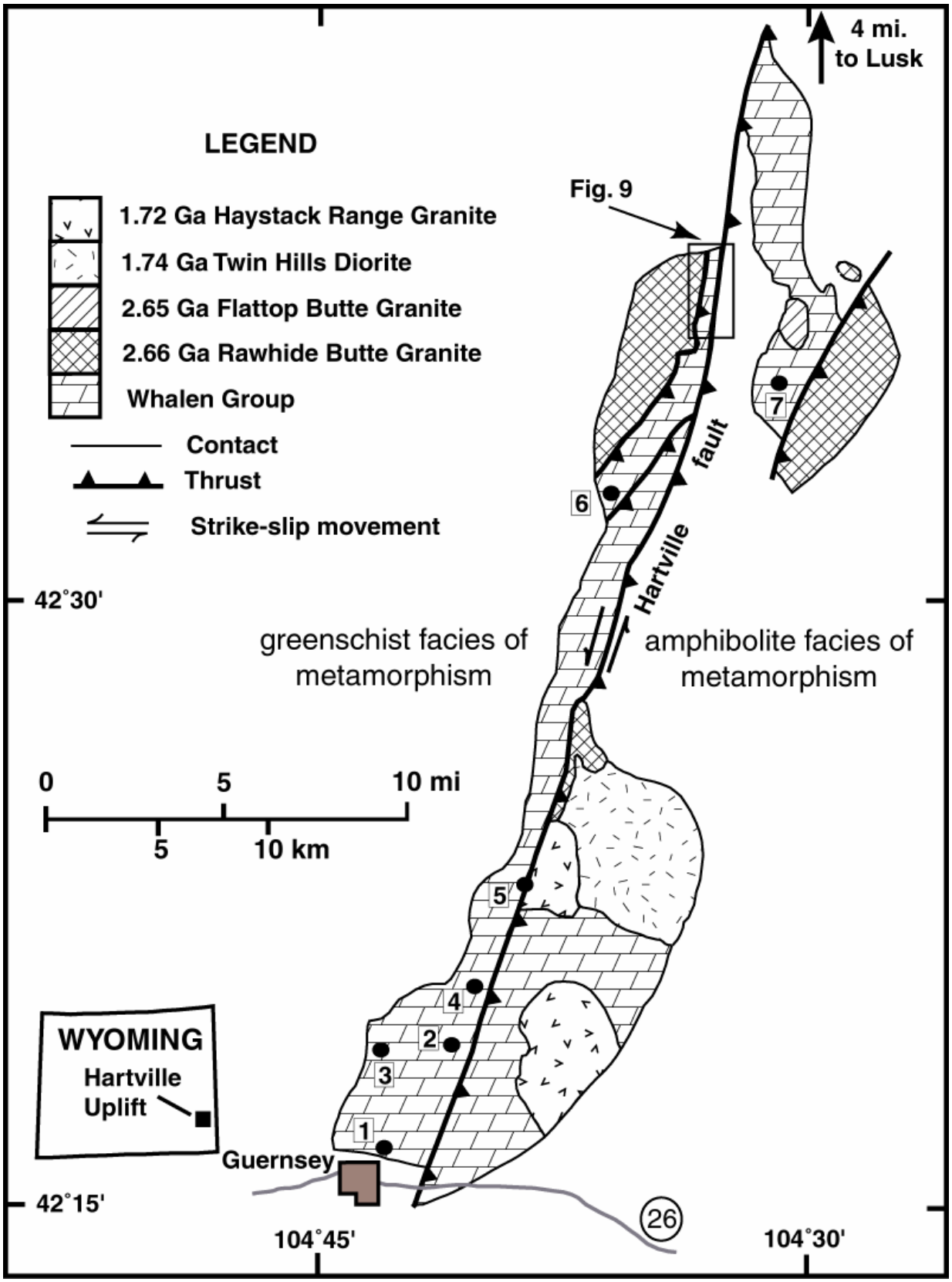

Fig. 4.8. Map of the Hartville Uplift, WY (modified from Sims and Day, 1999).

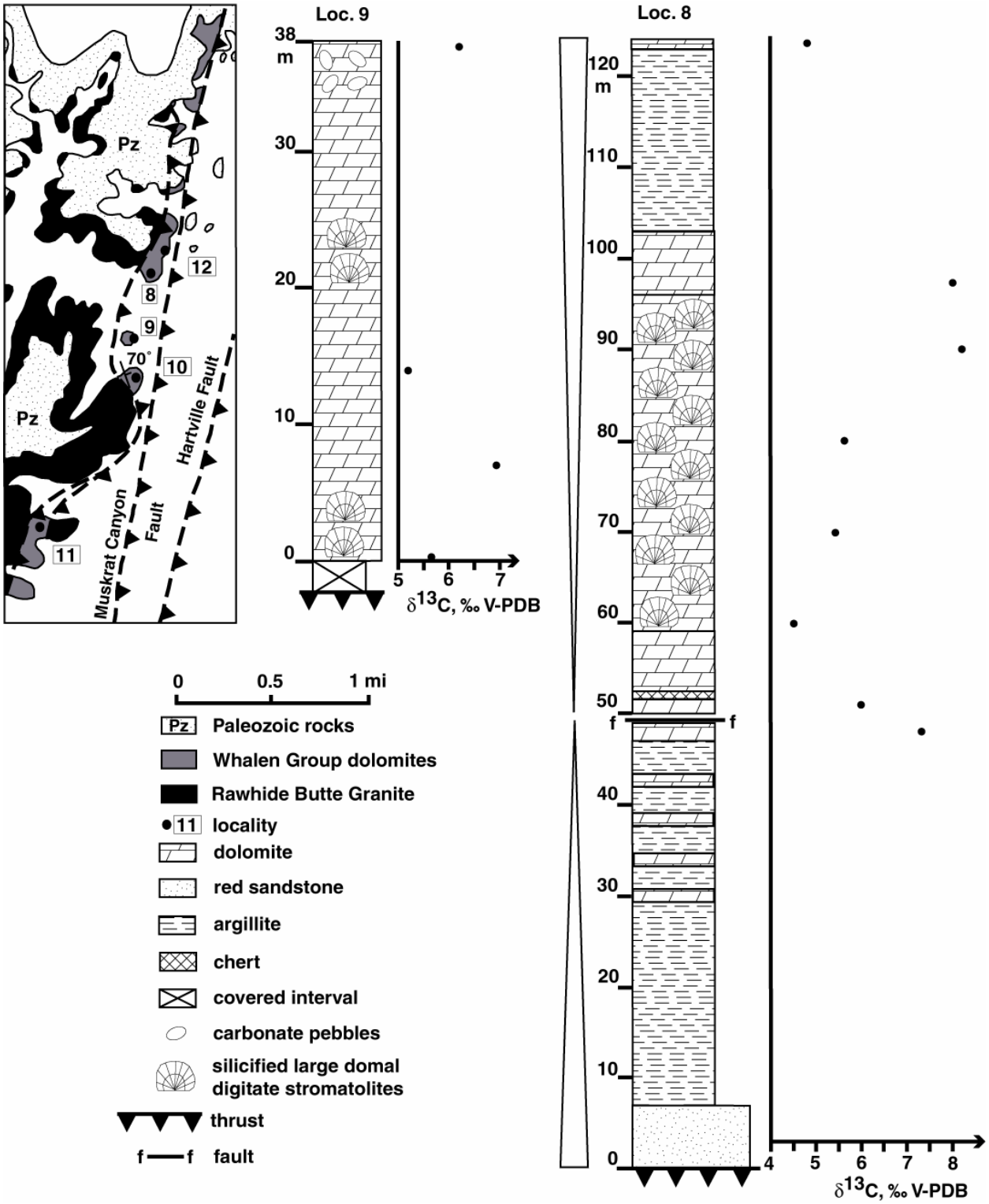

Fig. 4.9. Detailed map of the Rawhide Creek area (from Sims and Day, 1999, and Day et al., 1999) and measured sections in Loc. 8 and 9 with plotted $\delta^{13}C$ values.

layers of brown dolomite and brown dolomite. Across the fault, gray massive dolomite with chert beds underlies an upward-shallowing cycle that includes from the base to the top: ribbon dolomite, pink-gray dolomite with silicified domal digitate stromatolites forming a reef up to 30 m thick, pink dolomite and dark calc-schist. The section immediately to the south of the Rawhide Creek mouth (Loc. 9 in Fig. 4.9) contains two levels with silicified domal digitate stromatolites making up smaller stromatolite reefs than in the first section. Hofmann and Snyder (1985) described *Hadrophycus immanis* stromatolites from these reefs. A third section, further south of the Rawhide Creek mouth in a separate thrust sheet, consists of gray massive dolomite with three horizons of large domal stromatolites without digitate structures (Loc. 11 in Fig. 4.9). Domal stromatolites have diameters up to 10 m and are only partially silicified.

Gray and pink massive dolomite was sampled on the northern limb of the Graves Ranch anticline and on its southern limb in the Sparks Canyon (Loc. 2 and 3 in Fig. 4.8). Stratiform and small-scale columnar stratiform stromatolites occur in this area (Hofmann and Snyder, 1985). In addition, dolomites were sampled at several other locations in the western domain (Fig. 4.8), including the Guernsey Quarry (Loc. 1 in Fig. 4.8) where they have higher grade and contain tremolite 'turkey tail' structures and chert layers and nodules, but lack stromatolites**.** The base of the carbonate succession in this area lies above amphibolite. In the eastern domain, recrystallized dolomite was sampled in the Copperbelt-Omaha mine area (Loc. 7 in Fig. 4.8). Poorly preserved stratiform stromatolites up to 1 m in size rarely occur in this area.

Geochemical data and diagenesis

All studied samples are dolomites (Table 4.1). Samples have low Sr contents (trace amount to 136 ppm), highly variable Mn contents (35-3286 ppm) and variable but generally high Mn/Sr ratios (0.3-64.1). Fe contents measured in four samples are also high (988-6381 ppm). These data suggest that the carbonates were subjected to various degrees of post-depositional alteration. Oxygen isotope values range between –5.2 and –16.0‰ and show, on average, greater ^{18}O enrichment than dolomites of the Nash Fork Formation. Carbon isotope values of carbonates are bimodal. Carbonates from the Rawhide Creek area show ^{13}C-enrichment up to +8.2‰ whereas carbonates from all other localities have $\delta^{13}C$ values between –0.3 and +3.2‰.

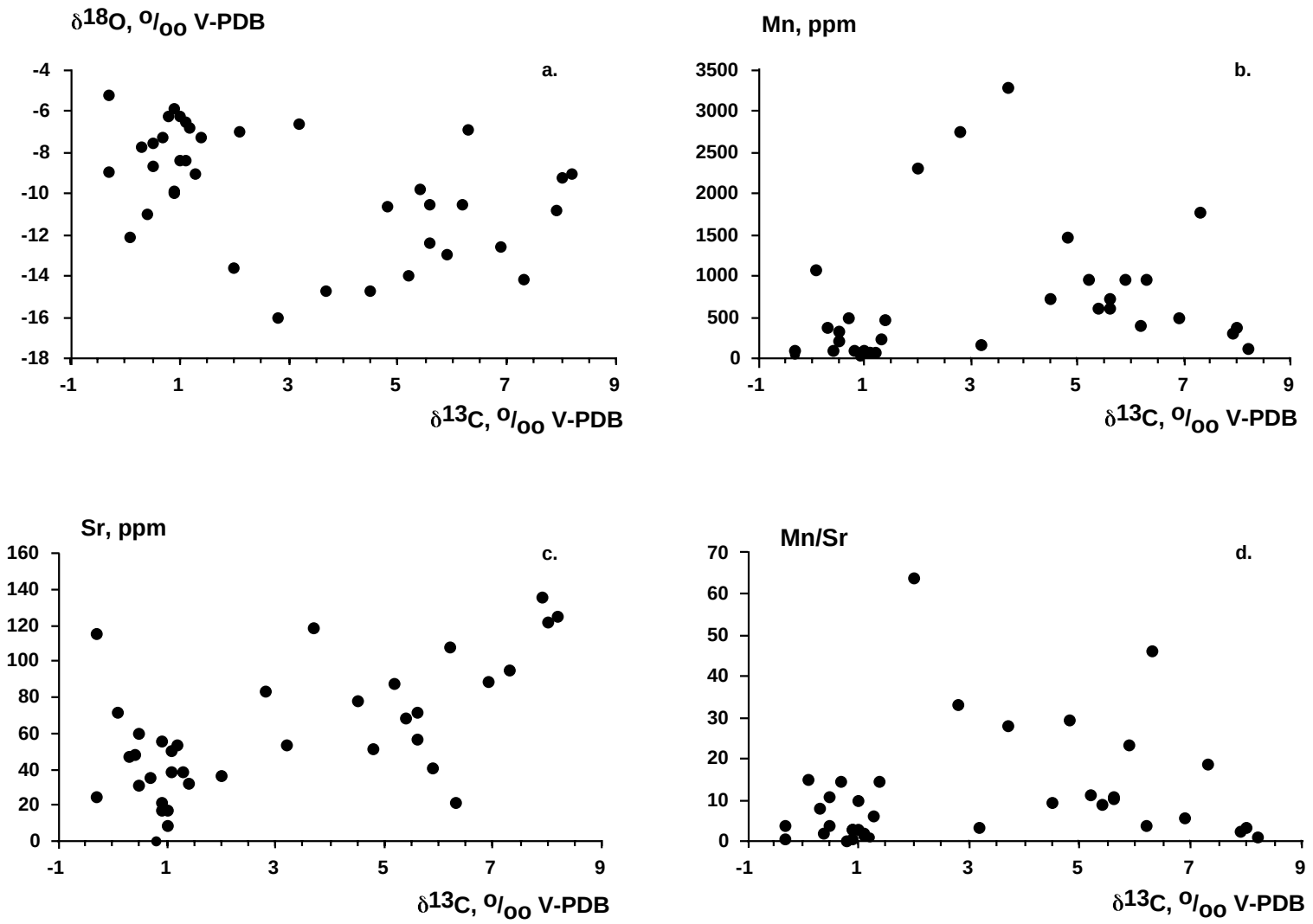

Fig. 4.10. Scatter diagrams for carbonates from the Whalen Group, Hartville Uplift, WY. a - $\delta^{18}O$, ‰ V-PDB vs. $\delta^{13}C$, ‰ V-PDB; b - Mn, ppm vs. $\delta^{13}C$, ‰ V-PDB; c - Sr, ppm vs. $\delta^{13}C$, ‰ V-PDB; d - Mn/Sr vs. $\delta^{13}C$, ‰ V-PDB; e - Mn, ppm vs. $\delta^{18}O$, ‰ V-PDB; f – Sr, ppm. vs. $\delta^{18}O$, ‰ V-PDB; g – Mn/Sr vs. $\delta^{18}O$, ‰ V-PDB.

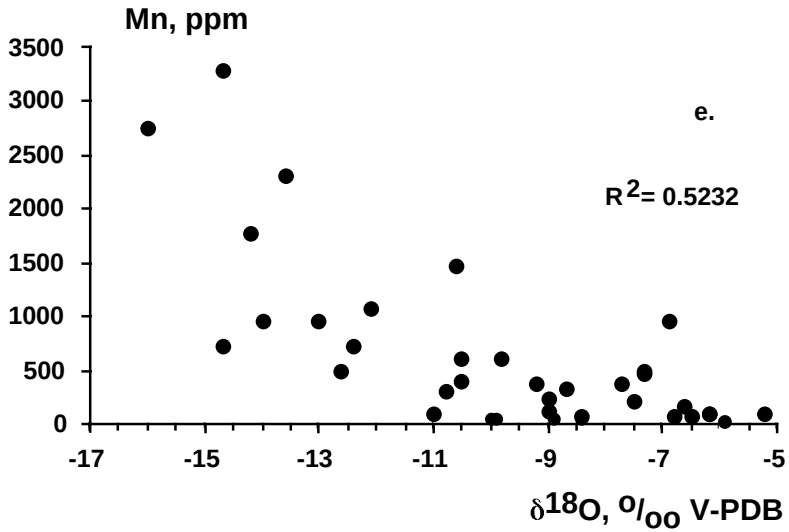
Mn, ppm
e.
R 2= 0.5232
3500
3000
2500
2000
1500
1000
500
0
-17
-15
-13
-11
-9
-7
-5
δ18O, o/oo V-PDB

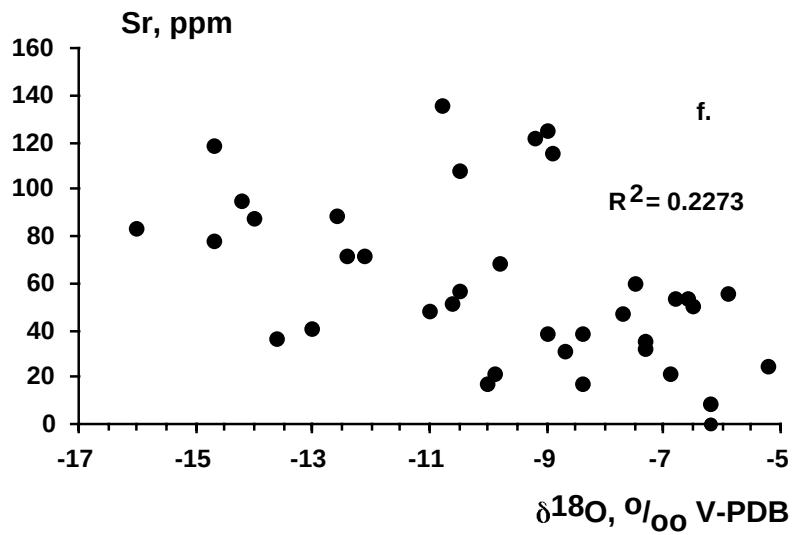
Sr, ppm
f.
R 2= 0.2273
160
140
120
100
80
60
40
20
0
-17
-15
-13
-11
-9
-7
-5
δ18O, o/oo V-PDB

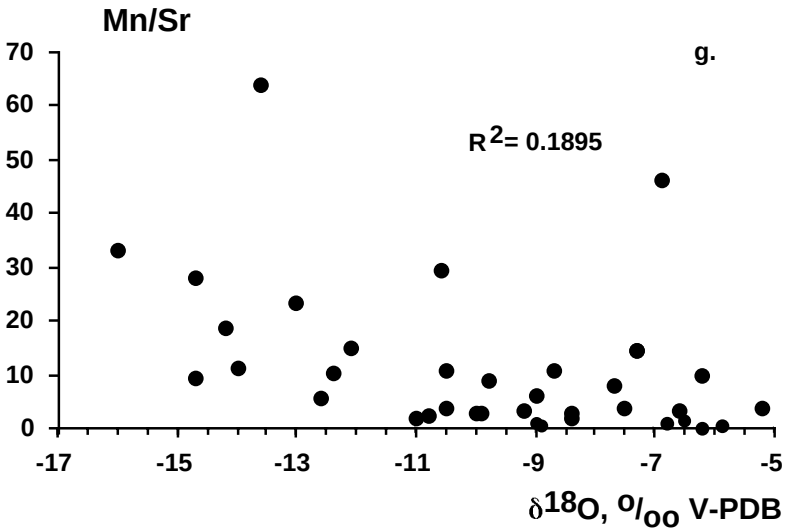
Mn/Sr
g.
R 2= 0.1895
70
60
50
40
30
20
10
0
-17
-15
-13
-11
-9
-7
-5
δ18O, o/oo V-PDB

A cross-plot of $\delta^{13}C$ vs. $\delta^{18}O$ values (Fig. 4.10 a) shows significant correlation for carbonates from the Rawhide Creek area and other localities. Correlation between $\delta^{13}C$ and Mn, Sr and Mn/Sr (Figs. 4.10 b, c, and d) is lacking but, if data from the Rawhide Creek area are considered alone, four samples plots along the alteration trend towards lower $\delta^{13}C$ values and higher Mn contents. These samples (2HV-1, 6, 8 and 14) are silicified or impure and significantly altered. Whereas $\delta^{18}O$ co-varies with Mn, no significant correlation along the expected alteration trend was found between either $\delta^{18}O$ and Sr or $\delta^{18}O$ and Mn/Sr.

In summary, samples characterized by low carbon and oxygen isotope values show evidence for significant alteration including their anomolous values in comparison to other samples from the same sections. In contrast, samples with high $\delta^{13}C$ and $\delta^{18}O$ values likely preserve primary or near primary carbon and, possibly, oxygen isotope signatures since post-depositional processes generally alter carbonates towards lower oxygen and carbon isotope values (e.g. Kaufman and Knoll, 1995). This relatively good preservation is likely related to synsedimentary to early diagenetic dolomitization and the generally pure composition of the Whalen Group dolomites. The level of ^{13}C-enrichment in carbonates of the Rawhide Creek area is similar to that in the lower Nash Fork Formation.

IMPLICATIONS FOR CORRELATION

Correlation between the upper Libby Creek Group in the Medicine Bow Mountains and the other early Paleoproterozoic sedimentary successions of the Wyoming Craton is ambiguous. Based on new chemostratigraphic data presented herein, it is possible to improve age constraints on these units and to suggest correlation between these successions. It is important, however, to review the underlying assumptions about the Paleoproterozoic curve of secular carbon isotope variations that will be applied as a correlation tool. Karhu and Holland (1996) recognized that carbonates with ages between 2.2 and 2.1 Ga have carbon isotope values above +4‰ and compiled a curve of secular carbon isotope variations with a single long-lasting peak between 2.2 and 2.1 Ga. This view was modified with recent discovery of carbonates with carbon isotope values up to +10‰ in the upper part of the Duitschland Formation sandwiched between two Paleoproterozoic glacial diamictites (Buick et al., 1998; Bekker et al., 2001). The view of the two-peak curve of secular carbon isotope variations with one long-lasting peak between 2.2 and 2.1 Ga and another peak of undermined

duration during the Paleoproterozoic glacial epoch was further modified by Melezhik et al. (1999). They presented curve with three to four peaks based on Buick et al. (1998) data for South African successions and their own data from the Pechenga Basin, Kola Peninsula, Russia. The South African data were already discussed in Bekker et al. (2001) and they concluded based on revised stratigraphy and age constraints that South African successions contain evidence only for two carbon isotope excursions. The Kolasjoki Sedimentary Formation in the Pechenga Basin that contains carbonates with $\delta^{13}C$ values close to 0‰ have poor age constraints (Rb/Sr whole rock ages with large error bars) and therefore can not be unequivocally taken as evidence for more than one excursion during the 2.2-2.1 Ga time interval. Based on available data, two-peak curve seems to be the best approximation for the Paleoproterozoic curve of secular carbon variations and will be here applied as a tool for correlation between studied successions.

Houston et al. (1992) suggested that the Nash Fork Formation in the Medicine Bow Mountains and the Slaughterhouse Formation in the Sierra Madre may be correlative. Chemostratigraphic data presented above support correlation between the Slaughterhouse Formation and the lower Nash Fork Formation since carbonates in both units have high $\delta^{13}C$ values including values above +10‰ (Table 4.2). However, it should be noted that the limited number of samples from the Slaughterhouse Formation and poor outcrop of this unit precludes speculation that equivalents of the upper Nash Fork are absent in Sierra Madre.

Carbonates of the Boxelder Formation and BIFs of the Benchmark Iron Formation are unique in terms of their stratigraphic position for the Wyoming Craton and the rest of the North America. Based on evidence for a major time gap at the top of the Benchmark Iron Formation, unconformable position on the Archean rocks and lack of evidence for glacial influence on sedimentation, it is proposed that both units were deposited before the beginning of the glacial epoch and after the initial rifting of Kenorland at ca. 2.45 Ga. Lithostratigraphic and chemostratigraphic data, as well as age constraints permit correlation between the Estes and Roberts Draw formations in the Black Hills, SD and the upper Nash Fork Formation (Table 4.2). Both successions are overlain by mafic volcanics (Towner Greenstone in the Medicine Bow Mountains and unnamed mafic volcanics above the Roberts Draw Formation in the Black Hills, SD) and slates and quartzites (French Slate and Buck Mountain Formation/ Gingrass Draw Slate). The Ellison Formation in the Lead area that is

Table 4.2. Comparative stratigraphy of Early Paleoproterozoic successions (modified and extended from Houston et al., 1992).

	Snowy Pass Supergroup, WY	Snowy Pass Group, Sierra Madre, WY	Nemo Succession, Black Hills, SD	Whalen Group, Hartville Uplift
Fine-grained siliciclastic units with BIFs	French Slate		Gingrass Draw Slate and Buck Mountain Quartzite	
Mafic volcanism with ages ~2.0-1.95 Ga	Towner Greenstone		Unnamed mafic volcanic unit	Muskrat Canyon Metabasalt
Carbonates with $\delta^{13}C$ values close to 0‰	Upper part of the Nash Fork Formation		Estes and Roberts Draw formations	Wildcat Hills Formation
Black organic-rich shales	M1 and M3 members of the Nash Fork Formation	Upper part of the Slaughterhouse Formation		Silver Springs Formation
Carbonates with $\delta^{13}C$ values between +6 and +10‰	Lower part of the Nash Fork Formation except the L1 member	Slaughterhouse Formation except the lower part		Carbonates in the Rawhide Creek area
Carbonates with $\delta^{13}C$ values above +10‰	L1 member of the Nash Fork Formation	Lower part of the Slaughterhouse Formation		
Mature Al-rich hematite bearing quartzites	Medicine Peak Quartzite	Copperton Formation		
Third glacial horizon	Headquarters Formation			
Carbonate above the second glacial horizon	Vagner Formation	Bottle Creek Formation		
Second glacial horizon	Vagner Formation	Bottle Creek Formation		
First glacial horizon	Campbell Lake Formation	Singer Peak Formation		
Pyrite and uraninite-rich mature quartzites	Lindsey Quartzite and Magnolia Formation	Magnolia Formation	Boxelder Formation	

considered correlative with the Buck Mountain Formation and Gingrass Draw Slate of the Nemo area (DeWitt et al., 1986) contains at the base felsic metatuff dated at 1974 ± 8 Ma(U-Pb zircon, Redden et al., 1990). In addition, carbonates in the Roberts Draw, Estes and upper Nash Fork formations have $\delta^{13}C$ values between 0 and 3‰ (Table 4.1). However, the possibility that the Roberts Draw and Estes formations are slightly younger than the Nash Fork Formation cannot be rejected. Carbonates of the Whalen Group in the Rawhide Creek area are likely correlative with the lower Nash Fork Formation based on similar chemostratigraphic characteristics ($\delta^{13}C$ values up to +8‰) as well as similar stromatolite morphologies (Table 4.2). Carbon isotope values up to +8‰ are unknown from well-dated Archean carbonates but typical for Paleoproterozoic carbonates with an age between 2.22 and 2.1 Ga (Karhu and Holland, 1996). Other lithologies of the Whalen Group: carbonates with $\delta^{13}C$ values close to 0‰, mafic volcanic rocks and ferruginous slates might be

correlative with carbonates from the Upper Nash Fork Formation, Towner Greenstone and French Slate, respectively. However, the possibility that some parts of the Whalen Group may be of Archean age cannot be excluded based on available data. Higher metamorphic grade supracrustal rocks in the eastern domain cut by the Archean Flattop Butte granite, supracrustal enclaves in the Archean Rawhide Butte Granite and higher-grade succession near Guernsey (Loc. 1, Fig. 4.8) could well be of Archean age. Additional stratigraphic, geochronologic and chemostratigraphic work is required to resolve remaining questions about the age and stratigraphy of the Whalen Group.

TECTONIC IMPLICATIONS

This study has three implications for the understanding of the Paleoproterozoic tectonic history of the Wyoming Craton: 1) the early Paleoproterozoic passive margin on the southern flank of the Wyoming Craton extended from the Sierra Madre through the Medicine Bow Mountains to the Hartville Uplift; 2) rifting and breakup on the eastern flank of the Wyoming Craton and opening of the Manikewan ocean (sensu Stauffer, 1984) coincided or closely followed the end of the Paleoproterozoic carbon isotope excursion between 2.11 and 2.06 Ga; 3) the rifting and breakup on the eastern flank of the Wyoming Carton dissected and reactivated the mature passive margin on the southern flank of the Wyoming Craton.

The upper part of the Libby Creek Group in the Medicine Bow Mountains was interpreted as a foreland basin succession based on recognition of an upward-deepening trend, presence of a mafic volcanic unit (Towner Greenstone) and its position at the top of the succession (Karlstrom et al., 1983). This interpretation was not confirmed by recent Sm-Nd and REE provenance studies that have shown an Archean source for the Upper Libby Creek Group and no evidence for proximity to the Paleoproterozoic volcanic arc (Ball and Farmer, 1991, Crichton and Condie, 1993). Bekker et al. (submitted) inferred a ~2.17-1.97 Ga age for the Nash Fork Formation based on a chemostratigraphic study; this age conflicts with the foreland basin model since the volcanic arc that collided with the southern flank of the Wyoming Craton was active between 1.74 and 1.78 Ga (Chamberlain, 1998). Consequently, the upper part of the Libby Creek Group is significantly older than the volcanic arc and is considered to have been deposited in a passive margin setting. Lithostratigraphic and chemostratigraphic data permit correlation of passive-margin deposits from the Sierra Madre through the Medicine Bow

Mountains to the Hartville Uplift (Fig. 4.1). The middle part of the Nash Fork Formation contains two carbonaceous shale members that were related to the drowning events associated with the reactivation of this old, mature passive margin on the southern flank of the Wyoming Craton by the rifting and breakup along the eastern flank of the Wyoming Craton (Bekker and Eriksson, submitted).

The age of the rifting and breakup on the eastern flank of the Wyoming Craton is poorly constrained. Mafic intrusives and their felsic differentiates on the southern flank of the Wyoming Craton that are likely related to this rifting and breakup event are between 2.0 and 2.1 Ga in age (Premo and Van Schmus, 1989; Cox et al., 2000). The only exposed area on the eastern flank of the Wyoming Craton is in the Black Hills, SD. Initiation of the younger rift basin in the Black Hills, SD that contains the siliciclastic Estes Formation was likely related to the 2.1-2.0 Ga rifting and breakup of the Kenorland supercontinent (Aspler and Chiarezelli, 1998). The Blue Draw Metagabbro, with an age of 2.17 ± 0.12 Ga (U-Pb zircon; Redden et al., 1990), that intrudes the older rift succession in the Black Hills and is infolded with it, is unconformably overlain by the Estes Formation. The younger rift succession including the Estes Formation is older than mafic volcanics dated at 1974 ± 8 Ma (U-Pb zircon; Redden et al., 1990). Carbonates from the middle part of the Estes Formation have $\delta^{13}C$ values similar to those in the upper Nash Fork Formation suggesting that rifting on the eastern flank of the Wyoming Craton occurred either very late in the carbon isotope excursion or shortly thereafter.

CONCLUSIONS

1. Carbonates of the Slaughterhouse Formation, Sierra Madre and the Whalen Group exposed in the Rawhide Creek area, Hartville Uplift have highly positive $\delta^{13}C$ values, were deposited during the ca. 2.2-2.1 Ga carbon isotope excursion and correlate with the lower and middle Nash Fork Formation in the Medicine Bow Mountains, WY.

2. Following the initial rifting, carbonates of the Whalen Group from other localities in the Hartville Uplift and all carbonate units in the Black Hills, SD have carbon isotope values close to 0‰ PDB and correlate with the upper Nash Fork Formation. Based on carbon isotope systematics and geochronologic and stratigraphic constraints, the Estes and Roberts

Draw formations in the Black Hills and most carbonates of the Whalen Group post-date the ca. 2.2-2.1 Ga carbon isotope excursion.

3. A carbonate, passive margin platform extended along the southern flank of the Wyoming Craton and outcrops in the Sierra Madre, Medicine Bow Mountains and Hartville Uplift. The areal extent of this carbonate platform supports an open-marine depositional setting for these carbonates and thus a global rather than local signature for their highly positive carbon isotope systematics.

4. Later rifting and ocean opening on the eastern flank of the Wyoming Craton was related to the final breakup of the Kenorland supercontinent and succeeded the ca. 2.2-2.1 Ga positive carbon isotope excursion.

5. Similar carbon isotope values in carbonates from the middle part of the Estes Formation, a rift succession on the eastern flank of the Wyoming Craton, and the upper Nash Fork Formation suggest that the two drowning events in the middle Nash Fork Formation can be related to the reactivation of the mature passive margin in response to this rifting event. Since the change in the carbon isotope trend straddles the second drowning event in the Nash Fork Formation, a temporal relationship exists between the final breakup of the Kenorland, relative sealevel rise and the end of the carbon isotope excursion. A similar relationship has been recognized in Fennoscandia.

REFERENCES

Akhmedov, A.M., 1990. Epochs of evaporization in the Paleoproterozoic of the Baltic Shield. Doklady Akademii Nauk 312(3), 698-702.

Amelin, Y.V., Heaman, L.M., Semenov, V.S., 1995. U-Pb geochronology of layered intrusions in the eastern Blatic Shield: implications for the timing and duration of Paleoproterozoic continental rifting. Precambrian Res. 75, 31-46.

Aspler, L.B., Chiarenzelli, J.R., 1998. Two Neoarchean supercontinents? Evidence from the Paleoproterozoic. Sedimentary Geology 120, 75 – 104.

Ball, T.T., Farmer, G.L., 1991. Identification of 2.0 to 2.4 Ga Nd model age crustal material in the Cheyenne belt, northeastern Wyoming: implications for Proterozoic accretionary tectonics at the southern margin of the Wyoming craton. Geology 19, 360 - 363.

Barley, M.E., Pickard, A.L., Sylvester, P.J., 1997. Emplacement of a large igneous province as a possible cause of banded iron formation 2.45 billion years ago. Nature 385, 55-58.

Bekker, A., Karhu, J.A., Eriksson, K.A., Kaufman, A.J., submit. Chemostratigraphy of the early Paleoproterozoic Snowy Pass Supergroup, Wyoming Craton: a record of secular carbon isotope changes.

Bekker, A., Eriksson, K.A., submit. Paleoproterozoic drowned carbonate platform on the southeastern margin of the Wyoming Craton: a record of the Kenorland breakup. Precambrian Res.

Bekker, A., Kaufman, A.J., Karhu, J.A., Beukes, N.J., Swart, Q.D., Coetzee, L.L., Eriksson, K.A., 2001. Chemostratigraphy of the Paleoproterozoic Duitschland Formation, South Africa: Implications for coupled climate change and carbon cycling. Am. J. Sci. 301, 261-285.

Bekker, A., Eriksson, K.A., Kaufman, A.J., Karhu, J.A., Beukes, N.J., 1999. Paleoproterozoic record of biogeochemical events and ice ages, GSA Annual Meeting, Abst. with Programs, v. 31, No. 7, A-487.

Bekker, A., 1998. Chemostratigraphy and climatostratigraphy of the Paleoproterozoic Snowy Pass Supergroup, Wyoming and its application for correlation with other sequences in North America. M.S. Thesis, University of Minnesota, Duluth, 104 pp.

Beukes, N.J., Gutzmer, J., Dorland, H., 1999. Paleoproterozoic laterites, supergene iron and manganese ores and atmospheric oxygen, Geol. Soc. Aust. Abstr., pp. 20-23.

Buick, I.S., Uken, R., Gibson, R.L., Wallmach, T., 1998. High-$\delta^{13}C$ Paleoproterozoic carbonates from the Transvaal Supergroup, South Africa. Geology 26, 875-878.

Chamberlain, K.R., 1998. Medicine Bow orogeny: Timing of deformation and model of crustal structure produced during continent-arc collision, ca. 1.78 Ga, southeastern Wyoming. Rocky Mnt. Geol. 33 (2), 259-277.

Cox, D.M., Frost, C.D., Chamberlain, K.R., 2000. 2.01-Ga Kennedy dike swarm, southeastern Wyoming: Record of a rifted margin along the southern Wyoming province. Rocky Mnt. Geol. 35(1), 7-30.

Crichton, J.G., Condie, K.C., 1993. Trace elements as source indicators in cratonic sediments: A case study from the Paleoproterozoic Libby Creek Group, Southeastern Wyoming. Jour. Geol. 101, 319 - 332.

Dahl, P.S., Holm, D.K., Gardner, E.T., Hubacher, F.A., Foland, K.A., 1999. New constraints on the timing of Early Proterozoic tectonism in the Black Hills (South Dakota), with implications for docking of the Wyoming province with Laurentia. Geol. Soc. Am. Bull. 111(9), 1335-1349.

Day, W.C., Sims, P.K., Snyder, G.L., Wilson, A.B., Klein, T.L., 1999. Geologic Map of Precambrian Rocks, Rawhide Buttes West Quadrangle and Part of Rawhide Buttes East Quadrangle, Hartville Uplift, Goshen and Niobrara Counties, Wyoming *with* a section on Geochronology by Peterman, Z.E., Futa, K. and Zartman, R.E. U.S. Department of the Interior U.S. Geol. Surv. Misc. Invest. Ser. I-2635, pp. 1-14.

DeWitt, E., Redden, J.A., Wilson, A.B., Buscher, D., 1986. Mineral resource potential and geology of the Black Hills National Forest, South Dakota and Wyoming. U.S. Geol. Surv. Bull., 1580, 135 pp.

DeWitt, E., Redden, J.A., Buscher, D., Wilson, A.B., 1989. Geologic map of the Black Hills area, South Dakota and Wyoming. U.S. Department of the Interior U.S. Geol. Surv. Misc. Invest. Series Map I-1910.

Divis, A.F., 1976. Geology and geochemistry of Sierra Madre Range, Wyoming. Quaterly of the Colorado School of Mines, 71 (3), 127 pp.

El Tabakh, M., Grey, K., Pirajno, F., Schreiber, B.C., 1999. Pseudomorphs after evaporitic minerals interbedded with 2.2 Ga strmatolites of the Yerriba basin, Western Australia: Origin and significance. Geology 27(10), 871-874.

Fenton, C.L., Fenton, M.A., 1939. Precambrian and Paleozoic algae. Geol. Soc. Am. Bull. 50, 89 - 126.

Hayes, J.M., Strauss, H., Kaufman, A.J., 1999. The abundance of ^{13}C in marine organic matter and isotopic fractionation in the global biogeochemical cycle of carbon during the past 800 Ma. Chem. Geol. 161, 103-125.

Heaman, L.M., 1997. Global mafic volcanism at 2.45 Ga: Remnants of an ancient large igneous province? Geology 25, 299-302.

Hofmann, H.J., Snyder, G.L., 1985. Archean stromatolites from the Hartville Uplift, eastern Wyoming. Geol. Soc. Am. Bull. 96, 842-849.

Houston, R.S., Graff, P.J., 1995. Geologic map of Precambrian rocks of the Sierra Madre, Carbon County, Wyoming, and Jackson and Routt Counties, Colorado. U.S. Department of the Interior U.S. Geol. Surv., Misc. Invest. Ser. I-2452.

Houston, R.S., 1993. Late Archean and Paleoproterozoic geology of southeastern Wyoming. In: Snoke, A.W., Steidtmann, J. R., and Roberts, S. M. (Ed.), Geology of Wyoming. Geological Survey of Wyoming Memoir 5, pp. 78 - 116.

Houston, R.S., Karlstrom, K.E., Graff, P.J., Flurkey, A.J., 1992. New stratigraphic subdivisions and redefinition of subdivisions of Late Archean and Paleoproterozoic metasedimentary and metavolcanic rocks of the Sierra Madre and Medicine Bow Mountains, southern Wyoming. U. S. Geological Survey Prof. Pap. 1520, 50 pp.

Kah, L.C., 2000. Depositional $\delta^{18}O$ signatures in Proterozoic dolostones: constraints on seawater chemistry and early diagenesis. In: Grotzinger, J.P., James, N.P. (Eds.), Carbonate sedimentation and diagenesis in the evolving Precambrian world. SEPM Spec. Publ. 67, pp. 345-360.

Karhu, J.A., 1993. Paleoproterozoic evolution of the carbon isotope ratios of sedimentary carbonates in the Fennoscandian Shield. Geol. Surv. Finland Bull. 371, Espoo, 87 pp.

Karhu, J.A., Holland, D., 1996. Carbon isotopes and the rise of atmospheric oxygen. Geology 24(10), 867-870.

Karlstrom, K.E., Flurkey, A.J., Houston, R.S., 1983. Stratigraphy and depositional setting of the Proterozoic Snowy Pass Supergroup, southeastern Wyoming: Record of a Paleoproterozoic Atlantic-type cratonic margin. GSA Bul. 94, 1257 - 1274.

Karlstrom, K.E., Houston, R.S., 1984. The Cheyenne belt: Analysis of a Proterozoic suture in southern Wyoming. Precambrian Res. 25, 415-446.

Kaufman, A.J., Knoll, A.H., 1995. Neoproterozoic variations in the C-isotopic composition of seawater: stratigraphic and biogeochemical implications. Precambrian Res. 73, 27-49.

Kirkham, R.V., Roscoe, S.M., 1993. Atmospheric evolution and ore deposit formation. Resource Geol. Spec. Issue No. 15, 1-17.

Kirschvink, J.L., Gaidos, E.J., Bertani, L.E., Beukes, N.J., Gutzmer, J., Maepa, L.N., Steinberger, R.E., 2000. The Paleoproterozoic Snowball Earth: extreme climatic and

geochemical global change and its biological consequences. Proc. Nat. Ac. Sci. 97, 1400-1405.

Krogh, T.E., Kamo, S.L., Bohor, B.F., 1996. Shock metamorphosed zircons with correlated U-Pb discordance and melt rocks with concordant protolith ages indicate an impact origin for the Sudbury structure, Earth Processes: Reading the isotopic code. Geophys. Monograph 95. Am. Geophys. Union, pp. 343-353.

Krogh, T.E., Davis, D.W., Corfu, F., 1984. Precise U-Pb zircon and badelleyite ages for the Sudbury area. In: Pye, E.G., Naldrett, A.J., Giblin, P.E. (Eds.), The geology and ore deposits of the Sudbury structure. Ontario Geol. Surv. Spec. Vol. 1, pp. 431-446.

Kump, L.R., Kasting, J.F., Barley, M.E., 2000. The rise of atmospheric oxygen and the "upside down" Archean mantle. Geochem. Geophys. Geosyst. v.2 Pap. n. 2000GC000114.

Marmo, J.S., 1992. The lower Proterozoic Hokkalampi paleosol in North Karelia, eastern Finland. In: Schidlowski, M., Golubic, S., Kimberly, M.M., Trudinger, P.A. (Eds.), Early Organic Evolution: Implications for Mineral and Energy Resources. Springer, Berlin, Heidelberg, pp. 41-66.

Melezhik, V.A., Fallick, A.E., Medvedev, P.V., Makarikhin, V.V., 1999. Extreme $\delta^{13}C_{carb}$ enrichment in ca. 2.0 Ga magnesite-stromatolite-dolomite-'red beds' association in a global context: a case for the world-wide signal enhanced by a local environment. Earth Sci. Rev. 48, 71-120.

Nesbitt, H.W., Young, G.M., 1982. Early Proterozoic climates and plate motions inferred from major element chemistry of lutites. Nature 299, 715-717.

Premo, W.R., Van Schmus, W.R., 1989. Zircon geocronology of Precambrian rocks in southeastern Wyoming and nothern Colorado. In: Grambling, J.A., Tewksbury, B.J. (Eds.), Proterozoic Geology of the Southern Rocky Mountains. Geol. Soc. Am. Spec. Pap. 235, pp. 1-12.

Redden, J.A., 1980. Geology and uranium resources in Precambrian conglomerates of Nemo area, Black Hills, South Dakota: U.S. DOE Natl. Uranium Resource Evaluation Report GJBX 127(80), pp. 147.

Redden, J.A., 1981. Summary of the geology of the Nemo area. In: Rich, F.J. (Ed.), Geology of the Black Hills, South Dakota and Wyoming. Geol. Soc. Am. Guidebook, Rocky Mountain Section, Annual Meeting, Rapid City, SD, pp. 193-210.

Redden, J.A., Peterman, Z.E., Zartman, R.E., DeWitt, E., 1990. U-Th-Pb geochronology and preliminary interpretation of Precambrian tectonic events in the Black Hills, South Dakota. In: Lewry, J.F., Stauffer, M.R. (Eds.), The Early Proterozoic Trans-Hudson Orogen of North America. Geological Association of Canada, Spec. Pap. 37, pp. 229 - 251.

Sims, P.K., 1995. Archean and Early Proterozoic tectonic framework of north-central United States and adjacent Canada. US Geol. Surv. Bull, 1904-T, 12 pp.

Sims, P.K., Day, W.C., 1999. Geologic map of Precambrian rocks of the Hartville Uplift, southern Wyoming *with* a section on Mineral deposits in the Hartville uplift by Klein, T. U.S. Geol. Surv. Misc. Invest. Ser. Map I-2661, pp. 1-28.

Sims, P.K., Day, W.C., Snyder, G.L., Wilson, A.B., 1997. Geologic map of Precambrian rocks along part of the Hartville Uplift, Guernsey and Casebier Hill quadrangles, Platte and Goshen countries, Wyoming *with* a section on Geochronology of post-tectonic intrusive rocks by Peterman, Z.E. U.S. Department of the Interior U.S. Geol. Surv. Misc. Invest. Series Map I-2567.

Smith, M.D., Heaman, L.M., 1999. Constraints on the timing of felsic magmatism associated with the Matachewan igneous events: preliminary results for the Creighton granite, Ontario, Geol. Ass. Canada, Min. Ass. Canada Joint Ann. Meeting Abstract 24, pp. 119.

Stauffer, M.R., 1984. Manikewan: An Early Proterozoic ocean in Central Canada, its igneous history and orogenic closure. Precambrian Res. 25, 257 -281.

Steyn, M.v.R., Gardyne, W.N., Klop, A.A.C., 1986. The Gopane manganese deposits, Bophuthatswana. Mineral Deposits of Southern Africa, I. Geol. Soc. S. Afr., Johannesburg, 985-989 pp.

Sumner, D.Y., Grotzinger, J.P., 1996. Were the kinetics of calcium carbonate precipitation related to oxygen concentration? Geology 24, 119 - 122.

Young, G.M., 1973. Tillites and aluminous quartzites as possible time markers for middle Precambrian (Aphebian) rocks of North America. In: Young, G.M. (Ed.), Huronian Stratigraphy and Sedimentation. Geol. Assn. Can. Spec. Pap.12, pp. 97-127.

Young, G.M., 1991. The geologic record of glaciation: relevance to the climatic history of Earth. Geoscience Canada 18(3), 100-108.

APPENDIX A

Sample description, locality, and stratigraphic position in respect to the marker beds. Heights of samples in meters above the base of the Duitschland Formation are given for samples collected at Duitschland Farm, as well as estimated heights for correlative sections at Langbaken (KB99.1 series) and de Hoop (KB99.2 series) farms. Samples of the Tongwane Formation were collected in the Tongwane riverbed, just below the Duitschland Formation (see Fig. 1.4).

Sample	Position of sample in unit	Sample description
Tongwane Formation		
TON/4		Argillaceous massive dolomite
TON/5		Argillaceous massive dolomite
TON/6		Argillaceous massive dolomite
TON/7A		Nodule from nodular dolomite
TON/7B		Matrix from nodular dolomite
Duitschland Formation		
Duitschland Farm profile		
Duit/2	280	Flat-laminated light-gray algal limestone
Duit/3	300	Flat-laminated limestone clast within a clay matrix
Duit/6	325	Slightly dolomitized flat-laminated limestone
Duit/9	380	Light-gray massive dolomite with stylolites
Duit/10	390	Light-gray massive dolomite with stylolites and cryptic stromatolites
Duit/15	680	Light-gray limestone with flat laminations and columnar stromatolites
Duit/16	690	Light-gray limestone with flat laminations and columnar stromatolites
Duit/17	700	Flat-laminated gray limestone with slight dolomitization and recrystallization

Duit/18	740	Light-gray oolitic limestone with slight metamorphism
Duit/19	745	Flat-laminated gray limestone with stratiform stromatolites
Duit/20	755	Light-gray oolitic limestone
Duit/21A	765	Gray limestone with pink discolouration due to recrystallization
Duit/21B	765	Gray limestone with pink discolouration due to recrystallization
Duit/24	860	White leached and recrystallized dolomite with domal stromatolites
Duit/25	870	White leached and recrystallized dolomite with domal stromatolites
Duit/26	925	Argillaceous dolomite with stratiform stromatolites
Duit/28	950	Massive recrystallized dolomite with chertification and karst breccia
KB99.3.A	245	Black shale
KB99.3.B	260	Black shale
KB99.3.C	300	Limestone clast within a clay matrix
KB99.3.D	325	Shale
KB99.3.E	345	Black shale
KB99.3.F	360	Black shale
KB99.3.G	375	Black shale
KB99.3.H	400	Gray shale
KB99.3.I	445	Gray shale
KB99.3.J	680	Isopachous sheet cements (limestone). Inorganic precipitates
KB99.3.K	695	Laminated limestone with chert
KB99.3.L	705	Gray shale
KB99.3.M	715	Isopachous sheet cements (limestone). Inorganic precipitates
Langbaken Farm profile		
KB99.1.0.5	280	Interbedded limestone and shale
KB99.1.5.0	285	Laminated limestone
KB99.1.11.0	295	Laminated limestone
KB99.1.19.5	305	Laminated limestone

KB99.1.27.5	325	Laminated limestone
KB99.1.37.5	335	Laminated limestone
KB99.1.60.5	360	Laminated dolomite
KB99.1.83.0	385	Thin dolomite in marly unit
DeHoop Farm profile		
KB99.2.0.5	960	Silicified stromatolitic dolomite
KB99.2.3.0	957	Silicified stromatolitic dolomite
KB99.2.4.0	956	Silicified stromatolitic dolomite
KB99.2.9.0	951	Dolomite
KB99.2.13.5	946	Dolomite
KB99.2.20.0	938	Marl/Dolomite
KB99.2.A	880	Dolomite
KB99.2.B	875	Flat-laminated cherty limestone
KB99.2.C	868	Stromatolitic dolomite above breccia
Lucknow Formation		
Venn/4		Brown/pink fine-grained dolomitic mudstone
Venn/6		Brown/pink fine-grained dolomitic mudstone

Curriculum Vitae
Andrey Bekker

Home address: 7 Vernon St., #3
Brookline, MA, 02445
phone: 617-278-6252 (h)

Work address: 20 Oxford Street
Department of Earth and Planetary Sciences
Harvard University
Cambridge, MA 02445

Personal: Born on August 11, 1967, St. Petersburg, Russia, single
lmmigration status: US citezen, naturalized August 10, 2001

Education:

VPI & SU (Department of Geological Sciences), PhD, 1996-2001
Thesis title: Chemostratigraphy of the Early Paleoproterozoic Carbonate Successions (Kaapvaal and Wyoming Cratons)
Advisor: Eriksson, K. A.
University of Minnesota, Duluth (Department of Geology), M.Sc., 1994-1996
Thesis title: Chemostratigraphy and climatostratigraphy of the Paleoproterozoic Snowy Pass Supergroup, Wyoming and their application for correlation with other sequences in North America
Advisor: Ojakangas, R. W.
Leningrad Mining Institute (Department of Geology), Russia 1984-1989, Diploma
Thesis title: Project of Geological mapping in the Levo-Kedon area, Far East, Magadan district (scale l:50,000). **Independent research chapter**: Geodynamic development of the Omolon massif based on major elements analyses.

Professional Experience

Postdoctoral fellow, Department of Earth and Planetary Sciences, Harvard University, September, 2001-present
Teacher assistant, Department of Geological Sciences, VPI & SU, 1996-2001
Classes tought: Resource Geology, Physical Geology, Historical Geology
Research assistant, Department of Geology, University of Maryland, College Park, summer 1999
Teacher assistant, Department of Geology, University of Minnesota, Duluth, 1994-1996
Classes tought: Sedimentation and Stratigraphy, Introductory Geology, Structural Geology, Environmental Geology, Basic Minerology and Petrology, Minerology and Petrology, 2 (Sedimentary Petrology) and 3 (Metamorphic Petrology)
Teacher assistant, Geophysical department, University of Chicago, Fall 1992
Classes thought: Earth Sciences
Research assistant and translator, Paleogeographical Atlas Group, University of Chicago, 1991-94
Lecturer, Loyola University, Chicago, Spring 1992
Classes thought: Meteorology
Instructor, Truman City College, Chicago, Spring l992
Classes thought: Earth sciences

Geologist, National Institute of Potassium Salts (Leningrad, Russia), Department of Geology, 1991

Field experience

Thesis field work

Snowy Pass Range, WY, summers of 1995, 1996, 1997, 2000

Huronian (ON, Canada) and Animakie (MI & WI) basins, summer 1998

Mistassini basin (Quebec), summer 1997

Field work

Namibia, Damara Orogen, summer 1993

Mojave desert (Turtle Mountains), Middle Proterozoic massive sulfide deposits, 2 weeks, 1992

Magadan district, Russia, Mapping with the Russian Geological Survey, summer 1988

Kasakhstan, Russia, Mapping with the Leningrad Mining lnstitute and the National Geological Institute (VSEGEI), summer 1987

Urals, Russia, with the National Geological Institute (VSEGEI), paleontological and sedimentologic study of the Neoproterozoic successions, summer 1982

Field trips

Adelaide and Amadeus basins, Australia, with IGSP working group, 2 weeks, 1993

Southern Appalachians, with University of Chicago, 2 weeks, 1993

Field camp, geologic and geophysic mapping, Russia, with the Leningrad Mining Institute, 1986

Participation in professional societies: GSA, AGU, Geochemical Society

Language ability: English (second language), Russian (native language), French (beginning level)

Abstracts

2001 - Bekker, A., Eriksson, K. A., Kaufman, A. J.; Karhu, J. A., Early Paleoproterozoic (2.5–2.0 Ga) giant sediment-hosted mineral deposits: a response to environmental changes, GSA Annual Meeting, Abstracts with Programs, v. 33, No. 6, in press.

2001 - Bekker, A., Master, S., Karhu, J. A., & Verhagen, B. Th., Chemostratigraphy of the Paleoproterozoic Magondi Supergroup, Zimbabwe, In Eleventh Annual V. M. Goldschmidt Conference, Abstract #3772. LPI Contribution No. 1088, Lunar and Planetary Institute, Houston (CD-ROM).

2001 - Bekker, A., Karhu, J. A., & Kaufman, A. J., Tectonic implications of a chemostratigraphic study of Early Paleoproterozoic carbonates from the southeastern margin of the Wyoming Craton, Meeting of the Rocky Mountain section of GSA; Abstracts with Programs, v. 33, No. 5, p. A-44.

2001 - Beukes, N. J., Bekker, A., Swart, Q., Dorland, H., Van Niekerk, H.S., Gutzmer, J., Karhu, J. A., Kaufman, J. A., Implications of carbon isotope values of South African carbonates for the Paleoproterozoic secular carbon isotope curve, European Union of Geosciences, Abstract Suppl. No. 1, v. 13, p. 188.

2000 - Bekker, A., Eriksson, K.A., Kaufman, A.J., Karhu, J.A., Krapez, B., Beukes, N.J., Noce, C.M., Response of the Exosphere to the 2.48 – 2.45 Ga superplume event, GSA Annual Meeting, Abstracts with Programs, v. 32, No. 7, A-315.

2000 - Bekker, A., Kaufman, A J., Karhu, J. A., Beukes, N. J., Swart, Q. D., Coetzee, L. L., & Eriksson, K. A., Chemostratigraphy of the Paleoproterozoic Duitschland Formation, South Africa: Implications for coupled climate change and carbon cycling, Second Annual Meeting of the Penn State Astrobiology Research Center.

2000 - Bekker, A., Eriksson, K. A., Kaufman, A. J., Karhu, J. A., & Beukes, N. J., Paleoproterozoic record of biogeochemical events and ice ages, Second Annual Meeting of the Penn State Astrobiology Research Center.

1999 - Bekker, A., Eriksson, K. A., Kaufman, A. J., Karhu, J. A., & Beukes, N. J., Paleoproterozoic record of biogeochemical events and ice ages, GSA Annual Meeting, Abstracts with Programs, v. 31, No. 7, A-487.

1999 - Kaufman, A. J., Hebert, C., Halverson, G. P., Bekker, A., & Strauss, H., The biogeochemical aftermath of Snowball Earth conditions, GSA Annual Meeting, Abstracts with Programs, v. 31, No. 7, A-485.

1999 - Bekker, A., & Karhu, J. A., Secular carbon-isotopic variations and changing environment in the Early Paleoproterozoic, Ninth Annual V. M. Goldschmidt Conference, LPI Contribution No. 971, p. 22-23.

1998 - Bekker, A., Karhu, J. A., Kaufman, A. J., Beukes, N. J., & Swart, Q., Chemostratigraphy of the Duitschland Formation, South Africa: First evidence for multiple Paleoproterozoic carbon isotope excursions, AGU Fall Meeting, Supplement to EOS Transactions, v. 79, No. 45, p. F412-413.

1998 - Bekker, A., Karhu, J. A., Beukes, N. J., Eriksson, K. A., Aspler, L., Swart, Q., Early Paleoproterozoic climate changes in relation to biogeochemical cycling of carbon, Abstracts, International Symposium “Paleoclimates and the evolution of paleogeographic environments in the Earth’s geological history”, Petrozavodsk, Russia, p. 12-14.

1998 - Bekker, A., Karhu, J. A., & Beukes, N. J., Carbon isotope study of Early Paleoproterozoic interglacial carbonates in North America and South Africa: implications for the earliest stages of the carbon isotope excursion, Abstracts of ICOG-9, Chinese Science Bulletin, v. 43 Suppl., p. 7-8.

1998 - Karhu, J. A., Bekker, A., & Kartelainen, N., Paleoproterozoic positive carbon isotope excursion: comparison of $\delta^{13}C$ records in Fennoscandia and North America, Abstracts of ICOG-9, Chinese Science Bulletin, v. 43 Suppl., p. 64.

1998 - Bekker, A., & Karhu, J. A., Paleoenvironmental changes at the end of the Paleoproterozoic carbon isotope excursion, AAPG-98 Annual convention.

1997 - Bekker, A., Karhu, J. A., Eriksson, K. A., Paleoenvironmental changes at the end of the Paleoproterozoic carbon isotope excursion (~2.06 Ga), GSA Annual Meeting, Abstracts with Programs, v. 29, n. 6, p. 467.

1997 - Bekker, A., Karhu, J.A., Eriksson, K. A., Carbon isotope excursion in the Paleoproterozoic ocean and the rise of atmospheric oxygen: temporal and genetic relationship, AGU Spring meeting, EOS Transactions, v. 78, No. 17, S181.

1997 - Bekker, A., Karhu, J.A., Bennett, G., Carbon isotope study of the Gordon Lake Formation, Huronian Supergroup, ON: implication for correlation and temporal relationship to O_2 rise, GAC/MAC Annual Meeting, Abstract Volume 22, p. A-10.

1997 - Bekker, A., & Karhu, J. A., Comparative study of early Proterozoic carbonates (≥2.22 - 2.06 Ga): evidence for a Greenhouse event, AAPG-97 Annual convention, v. 6, p. A10.

1997 - Bekker A., & Karhu, J. A., Bimodality in carbon isotope values of dolomites of the Chocolay Group: possible implication for their age, Meeting of the Northcentral section of GSA; Abstracts with Programs, v. 29, n. 4, p. 4.

1997 - Karhu, J. A., Bekker A., Global evidence for a Major $\delta^{13}C$ excursion in Paleoproterozoic oceans: implications for the rise in atmospheric oxygen, European Union of Geosciences, Abstract Suppl. No. 1, v. 9.

1996 - Bekker, A., Karhu, J. A., Bennett, G., Lomagundi event in North America: application for stratigraphic correlation, Annual Meeting of GSA, Abstracts with Programs, v. 28, No. 7, p. A-229.

1996 - Bekker, A., Karhu, J. A., Study of carbon isotope ratios of the early Proterozoic Snowy Pass Supergroup, WY and its application for correlation with the Chocolay Group, MI and the Huronian Supergroup, ON [abstract], Institute on Lake Superior Geology Proceedings, 42nd Annual Meeting, v. 42, part 1, p. 4-5.

1992 - Bekker, Yu. R., Bekker, A. Yu., The stages of development of the Russian platform in the Precambrian time, Annual Meeting of GSA, Abstracts with Programs, v. 24, n. 7, p. A-115.

1989 - Geodynamic reconstructions on the basis of major element analyses (the Omolon craton), Student conference at the Leningrad Mining Institute.

1987 - Study of flysch deposition (the Crimea Mountains) based on the analysis of trace fossils and sedimentary structures, Student conference at the Leningrad Mining Institute. Award for the best paper.

1986 - Thanatocoenosis in the Devonian deposits on the Russian platform, Student conference at the Leningrad Mining Institute.

Publications

Bekker, A., Kaufman, A J., Karhu, J. A., Beukes, N. J., Swart, Q. D., Coetzee, L. L., and Eriksson, K. A., 2001, Chemostratigraphy of the Paleoproterozoic Duitschland Formation, South Africa: Implications for coupled climate change and carbon cycling, American Journal of Science, v. 301, p. 261-285.

Ziegler, A.M., Rees, P.M., Rowley, D.B., Bekker, A., Qing Li, and Hulver, M.L., 1995, Mesozoic Assembly of Asia: Constraints from fossil Floras, Tectonics and Paleomagnetism, Rubey Volume 9: The Tectonic Evolution of Asia, Cambridge, University Press, p. 371-400.

Ziegler, A.M., Parrish, J.M., Jiping, Y., Gyllenhaal, E.D., Rowley, D.B., Parrish, J.T., Shangyou, N., Bekker, A., and Hulver, M.L., 1994, Early Mesozoic phytogeography and climate, In: Allen, J. R. L., Hoskins, B. J., Sellwood, B. W., Spicer, R. A., Valdes, P. J., Palaeoclimates and their modelling; with special reference to the Mesozoic era, Chapman & Hall, London, U. K., p. 89-97.

Ziegler, A.M., Parrish, J.M., Jiping, Y., Gyllenhaal, E.D., Rowley, D.B., Parrish, J.T., Shangyou, N., Bekker, A., and Hulver, M.L., 1993, Early Mesozoic phytogeography and climate, Phil. Trans. R. Soc. Lond. B 341, 297-305.

Volunteer work

Member of Seminar Committee, 1998-1999

Volunteer for USGS, Summer 1992

Awards

Roy J. Shleman Scholarship Award, 2001
David R. Wones Geoscience Endowed Scholarship, 2000, 1999
Research Grant, Graduate School, VPI & SU, 2000, 1999, 1998, 1997
H. Robinson - R. J. Holden Geoscience Scholarship, 1998, 1997
Research Grant, GSA, 1997, 1998
Research Grant, Southeastern Section of GSA, 1997, 1998, 2000
Ogden Tweto Research Grant, Colorado Scientific Society, 1997
Research Grant, Graduate School, University of Minnesota, Duluth, 1995